COLLEGE SCIENCES DOCTORAL DE LA VIE BRETAGNE ET DE LA SANTE

Université de Rennes

THESE DE DOCTORAT DE

L'UNIVERSITE DE RENNES

ECOLE DOCTORALE N° 637
Sciences de la Vie et de la Santé
Spécialité : *Biologie cellulaire et Biologie du Développement*

Par

« Nourhene AMMAR »

« Communication cellulaire dans le maintien de l'intégrité musculaire chez la *Drosophile* »

Thèse présentée et soutenue à « Rennes », le « 31 Octobre 2025 »
Unité de recherche : UMR6290- Institut de Génétique et du Développement de Rennes

Rapporteurs avant soutenance :

Cédric Soler	Maitre de conférences, iGReD, Université Clermont Auvergne, France
Muriel Boube-Trey	CR, RESTORE, Toulouse, France

Composition du Jury :

Présidente :	Carole Gautier-Courteille	Professeure, IGDR, Université de Rennes, France
Examinateurs :	Bruno Lemaitre	Professeur, Ecole Polytechnique Fédérale de Lausanne, Suisse
	Cédric Soler	Maitre de conférences, iGReD, Université Clermont Auvergne, France
	Michèle Crozatier-Borde	DR, CBI, Toulouse, France
	Muriel Boube-Trey	CR, RESTORE, Toulouse, France
	Véronique Brodu	CR, Institut Jacques Monod, Université Paris Diderot, France
Dir. de thèse :	Hadi Boukhatmi	CR, IGDR, Université de Rennes, France

Remerciements

À toi, Hadi, je tiens à te remercier du fond du cœur, non seulement pour ton accompagnement scientifique inestimable, mais aussi pour ta bienveillance, ta disponibilité - même à 6 heures du matin, quand je t'envoie des images de microscope- et l'inspiration que tu as su m'apporter tout au long de ces années. Je ne te remercierai jamais assez pour ton soutien constant, tes conseils toujours justes, et ta capacité à garder ton calme face à mes "betises un peu trop créatives". En repensant à ces quatre années de thèse à tes côtés, je réalise que tu m'as transmis une leçon essentielle : les erreurs font partie intégrante du chemin scientifique. Tu m'as laissé la liberté d'explorer, de me tromper, et surtout d'apprendre à quel point *"les contrôles"* sont importants , ta voix résonne encore : *"Nourhene, une manip sans contrôle est inexploitable !"* Grâce à toi, venir au labo chaque jour était un véritable plaisir pour expérimenter et construire pas à pas ce travail. Merci d'avoir rendu cette aventure à la fois exigeante, inspirante et franchement amusante. Pour tout cela, je t'en suis profondément reconnaissante.

Je remercie sincèrement Bruno Lemaitre, Carole Gautier, Cédric Soler, Michelle Crozatier, Muriel Boube et Véronique Bordu pour l'honneur qu'ils me font en acceptant d'évaluer mon travail et pour le temps précieux qu'ils y ont accordé.

Merci Laetitia, pour toutes nos discussions et tes idées toujours "out of the box". Tu es devenue ma première référence dès qu'il s'agissait de cellules immunitaires ! Merci aussi d'avoir toujours été présente, à l'écoute, et pour tes conseils qui m'ont tant aidée à avancer.

Aurélien, merci pour ton amitié, tes encouragements et toutes les expressions que tu m'as apprises ! Tes râleries pour que je ferme les robinets de CO_2 ou que je pense à mettre mes mouches dans la collection vont clairement me manquer. Et promis, un jour, les "dettes" seront remboursées…!

Merci à Emma et Olivier d'avoir partagé une partie de ces années avec moi et pour tous les moments mémorables qu'on a vécus ensemble. Emma, la première thésarde arrivée après moi, et très vite devenue un peu notre "maman du labo". Toujours là pour tout organiser, tout contrôler, et surtout essayer de nous calmer quand on rigolait un peu trop fort. Merci pour ta patience face à nos bêtises ! Olivier, quant à toi, d'abord mon stagiaire de M2 puis compagnon de galère en thèse, tu es resté fidèle à toi-même : toujours prêt à rigoler, à faire des expériences douteuses (mais drôles), et à transformer chaque journée au labo en sketch. Merci à vous deux d'avoir rendu ces années bien plus amusantes qu'elles n'auraient dû l'être !

Merci à toi, Cyrille, d'avoir nourri mes mouches pendant toutes ces années -le véritable *chef cuisinier de la flyfood* ! Grâce à toi, elles n'ont jamais manqué de rien.

Merci aux copains pour tous les bons moments partagés ! Imane, je te souhaite une très belle continuation dans ta thèse et dans ta vie. C'est fou comme, en à peine deux ans, j'ai l'impression qu'on a partagé une infinité de souvenirs. Merci pour tous ces moments inoubliables et pour ta présence précieuse. Mathis, bon courage pour ta dernière année ! Et ne t'inquiète pas, j'ai soigneusement noté toutes les expressions que tu m'as apprises dans un petit carnet ,prêtes à être ressorties au bon moment !.

Merci à tous les membres de l'IGDR. Merci à toi Géraldine, toujours là pour résoudre mes petites galères administratives avec le sourire, Merci Catherine et toute l'équipe du service gestion pour votre bienveillance constante !

À mes parents et à toute ma famille ,je vous dois une immense reconnaissance pour votre amour, votre soutien et votre patience tout au long de ces années. Merci de m'avoir toujours encouragée, même quand vous ne compreniez pas exactement ce que je faisais avec mes mouches ! Votre confiance et vos encouragements m'ont portée dans les moments de doute et motivée à aller toujours plus loin. Merci aussi pour votre soutien lors des longues journées, et nuits, passées au labo et votre présence, même à distance. Rien de tout cela n'aurait été possible sans vous. Cette thèse est aussi un peu la vôtre ❤️.

Liste d’abréviations

AMP	Adult Muscle Progenitor
AMP	Anti-Microbial Peptide
ASP	Air Sac Primordium
ATP	Adénosine Tri-Phosphate
Bnl	Branchless
BR-C	Broad-Complex C
Btl	Breathless
CAM	Cell Adhesion Molecule
CCR2	C–C motif chemokine Receptor 2
DAMP	Damage-Associated Molecular Pattern
DLM	Dorsal Longitudinal Muscle
Dpp	Decapentaplegic
dSRF	drosophila Serum Response Factor
Duf	Dumbfounded
DVM	Dorso-Ventral Muscle
EC	Endothelial Cell
ECM	Extracellular Matrix
ECMa	Apical Extracellular Matrix
ECMb	Basal Extracellular Matrix
EGF	Epidermal Growth Factor
FAP	Fibro-Adipogenic Progenitor
FC	Founder Cell
FCM	Fusion-Competent Myoblast
FGF	Fibroblast Growth Factor
Fln	Flightine
Hh	Hedgehog
HIF-1	Hypoxia-Inducible Factor 1
Him	Holes in muscles
Hml	Hemolectine
HRE	Hypoxia Response Enhacer
IFM	Indirect Flight Muscle
IL	Interleukine
Imd	Immune difficiency
LOM	Larval Oblique Muscle
MAPK	Mitogen activated protein kinase
Mef2	Myocyte enhancer factor 2
Mhc	Myosin heavy chain
MMP1	Matrix Metalloproteinase 1
MTJ	Myotendinous Junction
MuSC	Muscle Stem Cell
Naa30A	N-acetyltransferase 30A
NMJ	Neuromuscular Junction
PAMP	Pathogen-Associated Molecular Pattern
PPO	Prophenoloxidase
PPR	Pattern Recognition Receptor
Pxn	Peroxidasin
Pyr	Pyramus

ROS	Reactive Oxygen Species
Salm	Spalt-major
Sima	Similar
Sls	Sallimus
SPARC	Secreted Protein Acidic and Rich in Cysteine
Sr	Stripe
TGF-β1	Transforming Growth Factor Beta 1
Ths	Thisbe
TNF-α	Tumor Necrosis Factor-alpha
TpnC4	Troponin C4
Trh	Trachealess
Tsp	Thrombospondin
TTC	Terminal Tracheal Cell
Twi	Twist
Vg	Vestigial
Vkg	Viking
Wg	Wingless
Zfh1	Zinc finger homeodomain-1

Liste des figures :

Figure 1. Processus de régénération musculaire chez les vertébrés

Figure 2. Le cycle de vie de la *Drosophile* et les vagues successives de myogenèse

Figure 3. La subdivision du mésoderme somatique

Figure 4. Représentation schématique de la structure sarcomérique des muscles somatiques

Figure 5. Organisation musculaire chez la *Drosophile* adulte

Figure 6. Développement des muscles indirects du vol (IFMs)

Figure 7. Ancrage des IFMs et établissement des jonctions myotendineuses (MTJ)

Figure 8. Division des sarcomères au cours de la formation des IFMs

Figure 9. La spécification des cellules souches musculaires (MuSC) au cours de la formation des IFMs

Figure 10. La réponse immunitaire humorale chez la *Drosophile*

Figure 11. La réponse immunitaire cellulaire chez la *Drosophile*

Figure 12. Les fonctions non immunitaires des hémocytes chez la *Drosophile*

Figure 13. Organisation structurale du système trachéal chez la *Drosophile*

Figure 14. Les cellules épithéliales trachéales de la *Drosophile*

Figure 15. Les stades du développement embryonnaire du système trachéal

Figure 16. Représentation schématique du bourgeonnement des branches trachéales

Figure 17. La mise en place du système trachéo-musculaire

Figure 18. L'activation de Similar (HIF1-α) et son impact sur la trachéogenèse

Table des matières

I. Introduction 5

Chapitre I. Mécanismes et médiateurs de la régénération musculaire chez les vertébrés 6

A. Processus et effecteurs cellulaires de la régénération musculaire 6

B. Interactions intercellulaires au cours de la régénération musculaire 8

C. Conclusions 12

Chapitre II. La myogenèse et l'homéostasie musculaire chez la *Drosophile* 13

A. Les différentes phases du développement musculaire 14

B. Le maintien et la réparation des muscles du vol adultes 33

Chapitre III. Le système immunitaire de la *Drosophile* : Organisation et Fonctions 37

A. L'immunité chez la *Drosophile* 37

B. L'hématopoïèse chez la *Drosophile* 41

C. Les fonctions « non immunitaires » des hémocytes 42

Chapitre IV. Le système trachéal de la *Drosophile* : Développement et Fonctions . 48

A. Organisation cellulaire du système trachéal 48

B. Mise en place du système trachéal au cours de l'embryogenèse 50

C. Développement et mise en place du système trachéo-musculaire adulte . 54

D. Les fonctions du système trachéal 57

II. Résultats 62

Article 1. Immune–tracheal intercellular signalling coordinates the muscle injury response in *Drosophila* 62

Article 2. Studying Muscle Transcriptional Dynamics at Single-molecule Scales in *Drosophila* 64

Article 3. Statins Induce Locomotion and Muscular Phenotypes in *Drosophila melanogaster* That Are Reminiscent of Human Myopathy: Evidence for the Role of the Chloride Channel Inhibition in the Muscular Phenotypes 65

Article 4. Fluvastatin-induced myofibrillar damage is associated with elevated ROS, and impaired fatty acid oxidation, and is preceded by mitochondrial morphological changes 65

III. Discussion et perspectives 67

IV. Références bibliographiques 76

I. Introduction

Le muscle squelettique joue un rôle central dans plusieurs fonctions vitales, notamment la réalisation des mouvements volontaires, le maintien de la posture et la régulation du métabolisme (Allen et al. 2024). Toutefois, ce tissu est particulièrement vulnérable à différents types de lésions, qu'elles résultent de traumatismes mécaniques ou d'anomalies génétiques congénitales (Sicherer et al. 2020). En l'absence d'un processus de réparation efficace, ces blessures peuvent conduire à des atrophies musculaires et à des altérations des capacités locomotrices (Tidball 2011). Le maintien de l'intégrité fonctionnelle du muscle squelettique repose sur sa remarquable capacité de régénération, laquelle implique une coordination complexe et finement régulée entre divers types cellulaires présents au sein du tissu musculaire ainsi que dans son microenvironnement (Rodríguez et al. 2024). Ces cellules incluent notamment les cellules souches musculaires (MuSCs, Muscle stem cells), les macrophages, les cellules progénitrices fibro-adipogéniques (FAPs, Fibro-Adipogenic Progenitors) et les cellules endothéliales (ECs, Endothelial Cells) qui constituent les vaisseaux sanguins. Les interactions cellulaires et moléculaires entre ces différentes populations ont été principalement étudiées chez les vertébrés, le plus souvent à l'aide des modèles *ex vivo*, où il a été montré qu'un dérèglement de ces interactions peut conduire à des défauts de régénération musculaire (Rodríguez et al. 2024). Par conséquent, l'étude de ces interactions est indispensable pour approfondir la compréhension des mécanismes fondamentaux de la régénération musculaire, identifier les causes potentielles des déficits de réparation et ouvrir la voie à de nouvelles stratégies thérapeutiques. **C'est précisément dans cette perspective que s'inscrivent les travaux menés au cours de ma thèse, qui visent à explorer, *in vivo*, les dynamiques cellulaires impliquées dans la réponse du muscle squelettique à la blessure, ainsi que les mécanismes régulateurs assurant la coordination entre les différentes populations cellulaires au cours de ce processus.**

Chapitre I. Mécanismes et médiateurs de la régénération musculaire chez les vertébrés

A. Processus et effecteurs cellulaires de la régénération musculaire

La régénération musculaire est décrite comme un enchaînement de cinq phases successives et interconnectées : la dégénérescence, l'inflammation, la réparation, le remodelage et la récupération fonctionnelle (Forcina et al. 2020) **(Figure 1)**.

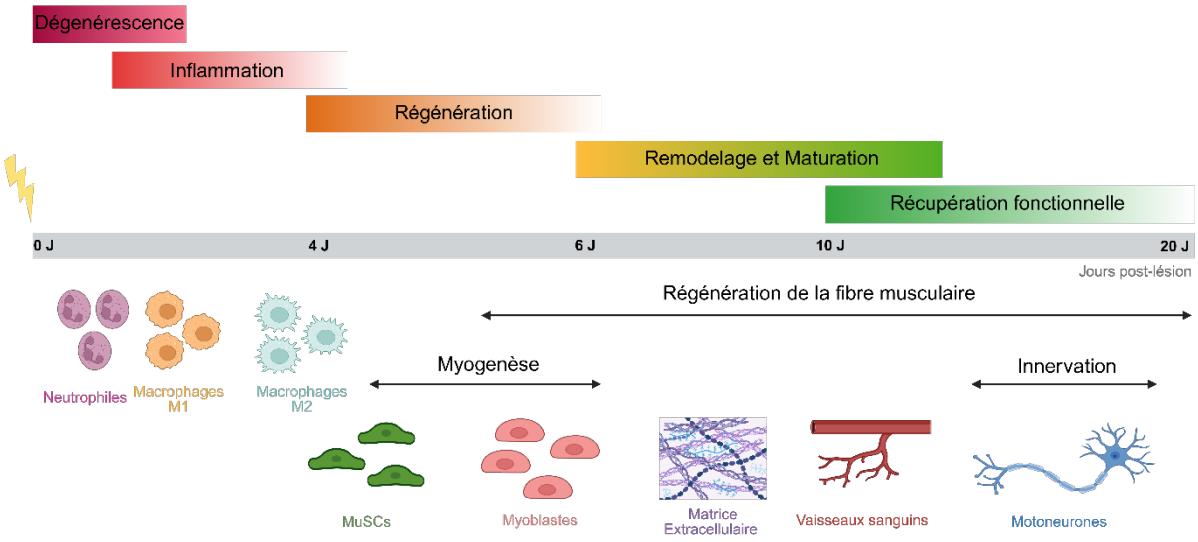

Figure 1. Processus de régénération musculaire chez les vertébrés. La blessure musculaire active une réponse inflammatoire rapide et transitoire, caractérisée par un recrutement des neutrophiles et macrophages. L'inflammation est suivie d'une phase de régénération où les acteurs clés sont les cellules souches musculaires (MuSCs) et leurs progéniteurs nouvellement formés (myoblastes). La fin de ce processus consiste au remodelage de la matrice extracellulaire (ECM), la néovascularisation et l'innervation des myofibres nouvellement régénérées.

La lésion musculaire compromet l'intégrité de la membrane plasmique des myofibres en altérant sa perméabilité, entrainant un dysfonctionnement des organites et une dégradation des protéines musculaires, conduisant ainsi à la nécrose (Hamer et al. 2002). Cette nécrose tissulaire est connue pour induire une réponse inflammatoire appelée "inflammation stérile", en l'absence d'agents infectieux extérieurs (Chen et Nuñez 2010). Lorsque les composants intracellulaires du muscles sont libérés dans le milieu externe, ils agissent comme des signaux d'alarme, connus sous le nom de motifs moléculaires associés aux dommages (DAMPs, Damage-

Associated Molecular Patterns), qui déclenchent l'activation du système immunitaire et la mise en place d'une réponse inflammatoire (Zindel et Kubes 2020). Les neutrophiles, des cellules immunitaires spécialisées dans la détection et l'élimination rapide des débris cellulaires, figurent parmi les premières cellules immunitaires recrutées au cours de la phase pro-inflammatoire. Il a été montré que leur déplétion retarde le processus de régénération (Toumi et al. 2006). À partir du deuxième jour post-lésion, les monocytes, cellules immunitaires circulantes du système inné, infiltrent le tissu musculaire endommagé où ils se différencient en macrophages. Ces derniers deviennent alors les principales cellules effectrices de la réponse immunitaire locale, tandis que le nombre de neutrophiles décroît progressivement (Rigamonti et al. 2014). Ces macrophages passent par deux étapes distinctes d'activation et se répartissent, classiquement, en deux grandes catégories : les macrophages classiquement activés (M1), également appelés macrophages pro-inflammatoires, et les macrophages alternativement activés (M2), qui sont des macrophages anti-inflammatoires (Rigamonti et al. 2014). Au cours des phases précoces, les macrophages pro-inflammatoires (M1) constituent la population prédominante. Leur fonction principale à ce stade est d'éliminer les débris cellulaires issus du traumatisme et empêcher une fusion prématurée des cellules myogéniques (Saclier et al. 2013). Par la suite, ces cellules adoptent un phénotype anti-inflammatoire (M2), nécessaire pour atténuer l'inflammation au site de la lésion et favoriser la régénération musculaire (Rigamonti et al. 2014). La déplétion de ces macrophages M2 entraîne un déficit de différenciation musculaire et de régénération (Tidball et Wehling-Henricks 2007).

La troisième phase du processus de régénération musculaire repose sur l'intervention des MuSCs, aussi appelées cellules satellites, localisées de manière stratégique entre la lame basale et le sarcolemme des myofibres (Motohashi et Asakura 2014; Mauro 1961). En condition homéostatique, ces cellules demeurent quiescentes, mais peuvent être activées en réponse à une blessure. Une fois activées, elles prolifèrent et donnent naissance à une population transitoire de progéniteurs, les myoblastes, qui fusionnent soit entre eux pour former de nouvelles fibres, soit avec des fibres musculaires existantes afin de restaurer le tissu lésé (Motohashi et Asakura 2014). Le comportement de ces cellules au cours de la régénération est finement régulé par des structures appelées "*ghost fibers*". Il s'agit de la matrice extracellulaire (ECM, Extracellular Matrix) résiduelle qui persiste après la lésion musculaire et qui joue le

rôle d'échafaudage architectural en assurant une distribution uniforme des MuSCs le long de la fibre endommagée, condition essentielle à la reconstitution correcte de l'architecture musculaire (Webster et al. 2016). L'importance cruciale des MuSCs dans ce processus est illustrée par l'absence totale de régénération musculaire observée chez les souris génétiquement privées de ces cellules (Fry et al. 2015; Murphy et al. 2011a).

La reconstitution d'un tissu musculaire pleinement fonctionnel nécessite aussi une reconstruction de la ECM, qui joue un rôle essentiel de support en guidant la formation de nouvelles myofibres et de nouvelles jonctions neuromusculaires (NMJs, Neuromuscular Junctions) (Ahmad et al. 2023). Cette phase est assurée - principalement- par l'activité des FAPs (Li et Wang 2011). Une autre composante clé de cette phase de remodelage musculaire est la néovascularisation, indispensable à l'apport en nutriments et en oxygène nécessaires à la survie et à la différenciation cellulaires (Floriano et al. 2022). En effet, les myoblastes ne peuvent ni proliférer ni se différencier s'ils se trouvent à plus de 150 µm d'une source nutritive (Dennis et Kosnik, Ii 2000). Outre la restauration de l'apport en oxygène et nutriments, il a été récemment montré que la néovascularisation établit un environnement permissif nécessaire à l'initiation de la myogenèse au cours de la régénération musculaire (Jacobsen et al. 2023).

Le processus de réparation est considéré comme achevé lorsque les fibres nouvellement formées retrouvent une innervation fonctionnelle (Forcina et al. 2020). Cette récupération se manifeste par l'établissement de nouvelles NMJs, entre les axones restants et les fibres musculaires régénérées. À terme, les muscles réparés deviennent morphologiquement et fonctionnellement comparables aux muscles intacts (Forcina et al. 2020). Ainsi, la succession ordonnée des différentes phases du processus réparateur permet, dans des conditions physiologiques optimales, la restauration complète des propriétés structurelles et fonctionnelles du tissu musculaire.

B. Interactions intercellulaires au cours de la régénération musculaire

Dans la première partie, nous avons décrit les différentes étapes de la régénération musculaire. L'ensemble de ces étapes est coordonné par une diversité de types cellulaires qui interagissent finement afin d'assurer une réparation efficace du muscle

(Rodríguez et al. 2024). Dans cette seconde partie, nous aborderons l'état actuel des connaissances concernant les mécanismes moléculaires sous-jacents à ce dialogue intercellulaire.

1. La dynamique des macrophages et leurs interactions avec les cellules souches musculaires

Bien que leur rôle ait initialement été associé à l'élimination des débris cellulaires et à la limitation de l'inflammation post-lésionnelle, les macrophages sont désormais reconnus comme des acteurs clés dans le maintien de l'intégrité musculaire et la régénération des muscles squelettiques (Wang et Zhou 2022a). Dans ce contexte, de nombreuses études se sont attachées à mieux caractériser leurs fonctions régénératives, notamment leurs interactions avec les MuSCs.

Des études réalisées sur des modèles *in vitro* ont montré que certaines cytokines sécrétées par les macrophages, telles que l'interleukine-1β (IL-1β), l'IL-6 et le facteur de nécrose tumorale alpha (TNF-α, Tumor Necrosis Factor), favorisent la migration, la prolifération et la différenciation des MuSCs (Muñoz-Cánoves et al. 2013; Riera Romo et al. 2016; Al et al. 2023). Par exemple, l'inhibition de l'activité de l'IL-6 bloque le recrutement des macrophages entrainant ainsi une diminution de la différenciation musculaire. Au-delà de cette signalisation médiée par les cytokines, les macrophages présents sur le site de la lésion produisent également des enzymes protéolytiques, telles que la métalloprotéinase-disintégrine ADAMTS1. Cette enzyme est capable d'inhiber la voie de signalisation NOTCH1, un régulateur clé du maintien des MuSCs, contribuant ainsi à leur activation (Du et al. 2017).

Si le rôle essentiel des macrophages dans la préservation de l'intégrité musculaire a été mis en évidence par des approches d'ablation cellulaire, ces stratégies expérimentales ne permettent pas toutefois de discriminer les contributions spécifiques des sous-populations pro- et anti-inflammatoires. Par conséquent, le rôle respectif de ces différentes populations de macrophages reste à élucider, ouvrant la voie à des approches plus ciblées pour mieux comprendre leurs fonctions spécifiques.

2. Les fonctions des progéniteurs fibro-adipogéniques et leurs réseaux d'interactions cellulaires

Les FAPs sont des cellules mésenchymateuses localisées dans le compartiment interstitiel du muscle squelettique, où elles jouent un rôle fondamental dans le maintien de l'homéostasie et la régénération musculaire (Wosczyna et al. 2019a). En condition homéostatique, les FAPs demeurent quiescentes. Toutefois, en réponse à une lésion musculaire, elles s'activent rapidement, entrent en prolifération, et atteignent un pic d'expansion dans les jours qui suivent la blessure. Cette activation s'accompagne d'une production transitoire de ECM (Wosczyna et al. 2019b).

De nombreuses études ont mis en évidence une communication réciproque et fonctionnelle entre les FAPs et les MuSCs. En effet, les FAPs localisées à proximité des fibres musculaires endommagées stimulent la prolifération des MuSCs et contribuent à la formation d'une niche transitoire favorable à leur différenciation (Fiore et al. 2016). En retour, les progéniteurs myogéniques favorisent la prolifération des FAPs via la sécrétion de facteurs solubles activant la voie PI3K/AKT, tout en inhibant leur différenciation en adipocytes par la production de signaux anti-adipogéniques (Uezumi et al. 2010).

Par ailleurs, des travaux récents ont révélé une signalisation croisée entre les FAPs et les macrophages, médiée notamment par la cytokine TGF-β1 (Transforming Growth Factor) (Nawaz et al. 2022a). La suppression spécifique de TGF-β1 dans les macrophages améliore la régénération musculaire, en réduisant la prolifération et la différenciation des FAPs, ces dernières étant impliquées dans la production excessive de ECM et le développement de fibrose musculaire (Nawaz et al. 2022b). En retour, les FAPs influencent la transition phénotypique des macrophages, en facilitant le passage d'un état pro-inflammatoire (M1) vers un état anti-inflammatoire (M2) (Kotsaris et al. 2023).

Ce rôle central des FAPs dans l'homéostasie musculaire a été mis en évidence par des études chez la souris, montrant qu'une déplétion de ces cellules entraine une atrophie musculaire accompagnée d' une réduction du nombre de MuSCs (Roberts et al. 2013). Néanmoins, leur potentiel bi-potent complique leur interprétation fonctionnelle: les FAPs peuvent se différencier soit en fibroblastes, favorisant la

régénération par la production des composants de la ECM, soit en adipocytes, contribuant à la fibrose par l'accumulation de tissu adipeux (Contreras et al. 2021). Ainsi, ce double comportement antagoniste des FAPs complexifie l'analyse de leurs interactions cellulaires.

3. La communication intercellulaire des cellules endothéliales dans le microenvironnement musculaire

Le muscle squelettique constitue le principal réservoir de masse microvasculaire de l'organisme, capable de s'adapter aux variations physiologiques et environnementales (Latroche et al. 2015). Cette micro-vascularisation est assurée par les cellules endothéliales (ECs) qui sont organisées parallèlement aux myofibres (Lo et al. 2003) et sont essentielles à la régulation du tonus vasculaire local ainsi qu'au maintien de l'homéostasie vasculaire. À la suite d'une lésion musculaire, les ECs sont rapidement activées afin de revasculariser le tissu en régénération par un processus d'angiogenèse. Ce mécanisme est indispensable, non seulement pour assurer l'apport en nutriments et en oxygène, mais également pour faciliter le recrutement des cellules immunitaires vers le site lésé (McLennan 1996).

Des expériences de co-culture *in vitro* ont montré que l'angiogenèse est étroitement couplée au processus de myogenèse. En effet, les ECs exercent une activité pro-myogénique via la sécrétion des facteurs paracrines, qui favorisent la migration, la prolifération et la différenciation des cellules progénitrices myogéniques au cours de la réparation musculaire (Latroche et al. 2017). Cette interaction entre les ECs et le tissu musculaire a été davantage confirmée par des études montrant que l'Angiopoïétine-1, un facteur de croissance angiogénique sécrété par les ECs dans le microenvironnement musculaire post-lésionnel, soutient la myogenèse en stimulant la prolifération et la différenciation des myoblastes (Mofarrahi et al. 2015).

L'orchestration du processus de régénération musculaire est aussi régulée par une communication établie entre les ECs et les macrophages. Il a été montré que la protéine chimiotactique des monocytes-1 (MCP-1, Monocyte Chemoattractant Protein 1) et son récepteur CCR2 (C–C motif chemokine Receptor 2), qui sont impliqués dans le recrutement des monocytes/macrophages vers les sites de lésion, sont également essentiels à l'activation des ECs et au soutien de l'angiogenèse (Rowe et al. 2014). En l'absence de CCR2, le muscle en régénération présente des niveaux plus faibles

de facteur angiogénique VEGF (Vascular Endothelial Growth Factor), résultant en une formation réduite de capillaire et une cicatrisation musculaire altérée (Ochoa et al. 2007). Cependant, d'autres études utilisant un modèle de dommage musculaire différent, n'observent aucun effet significatif des macrophages sur la densité vasculaire (Rahat, Hemmerlein et Iragavarapu-Charyulu 2014). Ainsi, ces divergences illustrent les limites actuelles dans l'identification précise des fonctions et des interactions cellulaires au cours de la réparation musculaire, dues à la complexité du microenvironnement musculaire en régénération.

C. Conclusions

La compréhension des mécanismes régissant la coordination des différentes populations cellulaires au sein du muscle squelettique représente un enjeu majeur en recherche biomédicale. L'un des principaux défis réside dans la grande hétérogénéité et la plasticité des types cellulaires impliqués. De plus, la complexité architecturale du muscle en régénération complique l'identification précise des signaux moléculaires échangés entre les cellules. Bien que les modèles *in vitro*, tels que les co-cultures cellulaires et les organoïdes ont permis de comprendre quelques mécanismes fondamentaux, ils ne parviennent pas à reproduire la richesse et la dynamique spatio-temporelle du tissu musculaire *in vivo*. Par conséquent, notre compréhension globale des dialogues intercellulaires demeure encore partielle.

Afin de dépasser certaines de ces limites, nous avons choisi d'explorer les interactions cellulaires impliquées dans la réponse musculaire aux lésions en utilisant un modèle alternatif : la *Drosophile*. Grâce à l'organisation simplifiée de son tissu musculaire et à la présence d'un nombre limité de types cellulaires, ce modèle constitue un outil pertinent pour disséquer avec précision les mécanismes cellulaires et moléculaires déclenchés en réponse aux blessures.

Chapitre II. La myogenèse et l'homéostasie musculaire chez la *Drosophile*

La *Drosophile* est un modèle de choix pour l'étude de la myogenèse (Laurichesse et Soler 2020; Lemke et Schnorrer 2017). Sa musculature présente des similarités structurelles, moléculaires et fonctionnelles remarquables avec celle des vertébrés, permettant d'établir des parallèles inter-espèces pertinents pour mieux comprendre les principes fondamentaux de la biologie musculaire. Ces dernières années, l'intérêt pour ce modèle s'est intensifié grâce à l'émergence de nouvelles technologies permettant une caractérisation fine, à l'échelle cellulaire et moléculaire du lignage musculaire à différents stades du développement. L'émergence des technologies de séquençage unicellulaire a permis de révéler l'hétérogénéité des myoblastes au cours du développement, ainsi que de mieux caractériser leurs interactions avec le microenvironnement (Zappia et al., 2020 ; Everetts et al., 2021). En parallèle, le développement de l'imagerie en temps réel dans les muscles du vol, notamment aux stades avancés du développement, a considérablement enrichi notre compréhension de la dynamique des différents composants musculaires *in vivo* (Segal 2017). Ces avancées technologiques, combinées à la puissance des outils génétiques disponibles chez la *Drosophile*, offrent aujourd'hui la possibilité d'explorer avec une grande précision des processus impliqués dans l'homéostasie ou la réparation musculaire.

Dans ce contexte, et vu leur importance pour la survie de l'insecte en assurant des fonctions vitales telles que l'évasion des prédateurs, la recherche de nourriture ou encore la reproduction, nous avons choisi les muscles du vol comme système modèle pour étudier les réponses cellulaires et moléculaires précoces déclenchées au cours de la réparation musculaire adulte.

Bien que le programme de développement de la musculature de la *Drosophile* ait été largement étudié, les mécanismes assurant leur maintien et leur réparation demeurent encore peu compris, suscitant toutefois un intérêt croissant (Gunage et al. 2017; Chaturvedi et al. 2017; Boukhatmi 2021). **Dans ce chapitre, nous décrirons les mécanismes développementaux responsables de la formation de la musculature adulte, en nous concentrant plus particulièrement sur les muscles**

du vol. Comprendre les programmes qui régissent le développement musculaire permet d'éclairer comment ces tissus sont ensuite maintenus à l'âge adulte. Il est en effet largement reconnu que les mécanismes activés au cours du développement sont fréquemment réutilisés lors des processus de réparation tissulaire ou de régénération chez diverses espèces animales (Musarò 2020; Suzuki et Ochi 2020; Aztekin 2024).

A. Les différentes phases du développement musculaire

Chez la *Drosophile*, la myogenèse s'effectue en deux vagues distinctes au cours du développement : la myogenèse embryonnaire, qui donne naissance aux muscles larvaires, et la myogenèse dite adulte qui a lieu durant la métamorphose et aboutit à la formation des muscles adultes (Laurichesse et Soler 2020) **(Figure 2)**.

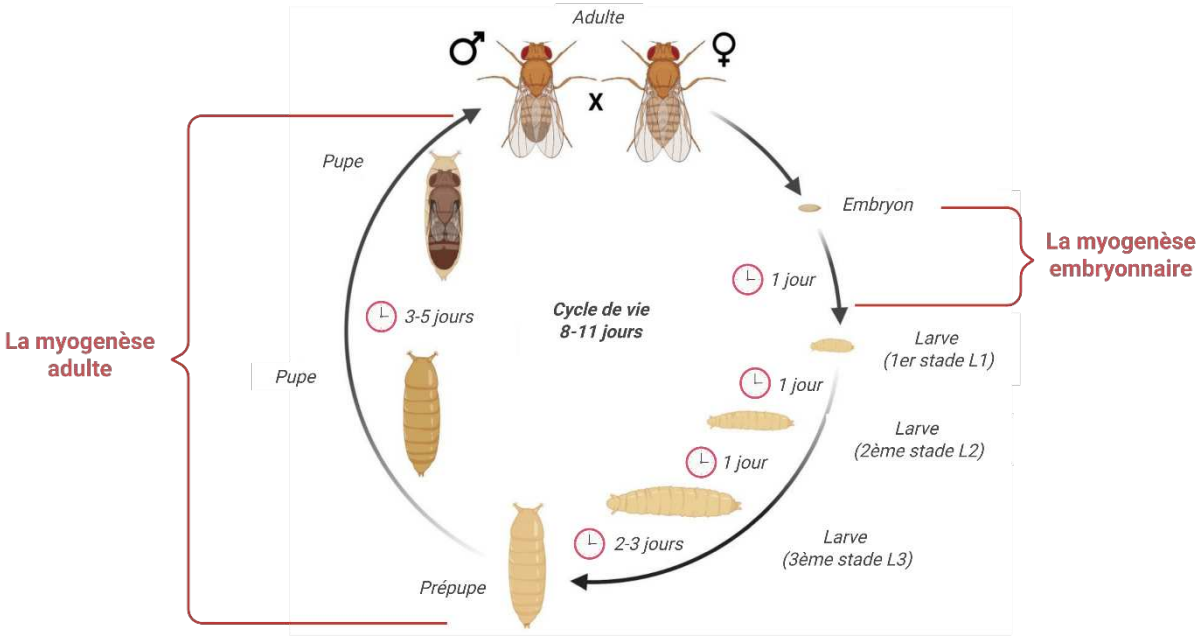

Figure 2. Le cycle de vie de la *Drosophile* et les vagues successives de myogenèse. La myogenèse se déroule en deux phase distinctes : (i) embryonnaire qui établit les muscles larvaires, (ii) adulte, marquée par la formation des muscles adultes à partir des progéniteurs musculaires durant les stades pupaux.

1. La myogenèse embryonnaire

Les muscles somatiques de la larve se forment au cours de la première vague de myogenèse. Grâce à leur agencement segmentaire et leur organisation structurée, ces muscles sont fondamentaux pour permettre l'éclosion ainsi que la locomotion de

la larve (Junion et Jagla 2022). La formation de ces muscles suit un processus à plusieurs étapes clés :

a) La subdivision du mésoderme somatique

Les muscles somatiques proviennent du mésoderme, qui donne également naissance aux muscles viscéraux, au cœur et au corps gras. Cette spécification repose sur une régionalisation précise du mésoderme selon les axes antéro-postérieur et dorso-ventral, régulée par des signaux inducteurs de l'ectoderme, notamment les morphogènes Wingless (Wg), Decapentaplegic (Dpp) et Hedgehog (Hh). L'axe antéro-postérieur est défini par des niveaux d'expression opposés de facteur de transcription Twist (Twi) : un niveau élevé de Twi à l'avant favorise la formation des muscles somatiques et cardiaques, tandis qu'un niveau réduit à l'arrière, oriente vers le mésoderme viscéral et le corps gras. Le gradient dorso-ventral de Dpp précise la formation des territoires mésodermiques destinés au cœur et aux muscles somatiques (Dobi et al. 2015) **(Figure 3)**.

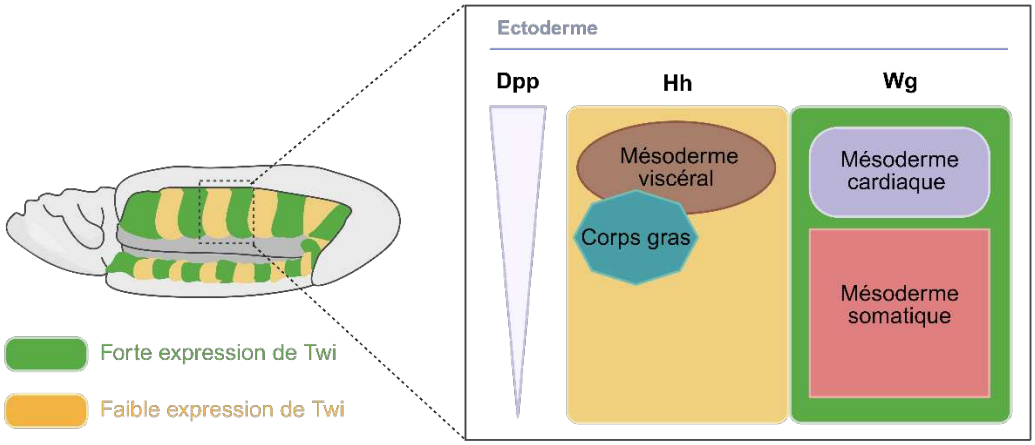

Figure 3. La subdivision du mésoderme somatique. Sous l'influence des signaux Wingless (Wg) et Hedgehog (Hh), le segment se subdivise en deux domaines caractérisés par des niveaux différentiels d'expression de Twist (Twi). Le domaine antérieur (vert) avec une forte expression de Twi, donne naissance au mésoderme somatique et cardiaque. Le domaine postérieur (jaune) exprime un faible niveau de Twi et génère le mésoderme viscéral et le corps gras. Le gradient de diffusion de signal Decapentaplegic (Dpp) permet de distinguer les territoires cardiaques (dorsaux) et somatiques (ventraux). Adapté de (Dobi et al. 2015).

b) La spécification myogénique et formation des myotubes

Dans le mésoderme somatique, les signaux Wg, Dpp et la voie MAPK (Mitogen activated protein kinase) induisent la formation de clusters promusculaires, exprimant

le gène pro-neural *Lethal of scute (l'sc)*, nécessaire à la spécification des progéniteurs musculaires (Carmena et al. 1995). L'activation de la MAPK via les voies FGF (Fibroblast Growth Factor) et EGF (Epidermal Growth Factor) restreint l'expression de *l'sc* à certaines cellules, délimitant ainsi 18 clusters par segment, chacun composé de 4 à 6 cellules pouvant devenir soit une cellule fondatrice (FC, Founder Cell), soit un myoblaste compétent à la fusion (FCM, Fusion-Competent Myoblast) (Ana Carmena et al. 1998).

Par inhibition latérale via la voie Notch, une seule cellule devient progéniteur musculaire (via l'expression de ligand Delta), tandis que les autres deviennent FCMs (Brennan et al. 1999). Le progéniteur musculaire subit ensuite une division asymétrique, générant une FC et un progéniteur musculaire adulte (AMP, Adult Muscle Progenitor), selon une répartition asymétrique des protéines Numb (inhibiteur de Notch) et Inscuteable (A. Carmena et al. 1998).

Ainsi émergent trois types cellulaires : AMPs, FCMs et FCs**.** Les FCs fusionnent ensuite avec des FCMs pour former les myotubes larvaires à noyaux multiples (Beckett et Baylies 2007).

c) Attachement des myotubes

Pour permettre la locomotion larvaire, ces muscles embryonnaires néoformés doivent s'ancrer à des structures appelées apodèmes**,** cellules ectodermiques jouant le rôle de tendons chez la *Drosophile* (Volk 1999). Localisées aux extrémités de l'embryon, ces cellules expriment le facteur de transcription Stripe (et plus précisément son isoforme Stripe-B (Sr-B)), indispensable à leur spécification. En absence de Sr, les muscles ne s'attachent pas correctement, entraînant ainsi une désorganisation musculaire (Vorbrüggen et Jäckle 1997). Les apodèmes sécrètent des signaux attractifs, guidant la migration des myotubes tels que Slit**,** tandis que les myotubes expriment leurs récepteurs Robo1/2, guidant leur migration. Chez les mutants *slit* ou *robo*, les fibres musculaires montrent des défauts d'attachement (Ordan et Volk 2015). Lorsque les myotubes atteignent les apodèmes, une jonction myotendineuse (MTJ, Myotendinous Junction) se forme, composée d'une ECM riche en Thrombospondine (Tsp). Cet ancrage entre muscles et tendons est assuré par les intégrines : αPS1βPS côté tendon interagit avec la laminine musculaire**,** et αPS2βPS

côté muscle interagit avec Tsp et Tiggrin. En absence de ces composants, les jonctions sont instables, entraînant une létalité embryonnaire (Subramanian et al. 2007). Enfin, des études plus récentes ont montré l'implication de la voie FGF dans l'orientation des myotubes. Bien que les ligands Pyramus (Pyr) et Thisbe (Ths) ne soient pas spécifiquement exprimés dans les apodèmes, leur expression étendue dans l'ectoderme semble guider les extrémités des myotubes vers leurs sites d'attachement spécifiques (Yang et al. 2020).

d) Formation de l'appareil contractile : la sarcomérogenèse

La sarcomérogenèse désigne le processus de formation et d'organisation des sarcomères, unités contractiles indispensables à la fonction motrice des muscles. Ces structures répétitives sont responsables de l'aspect strié des fibres musculaires et sont constituées de quatre éléments structuraux principaux : les filaments fins d'actine, les filaments épais de myosine, le disque Z et la ligne M. Un sarcomère s'étend entre deux disques Z successifs, marquants les limites structurales de l'unité (Lemke et Schnorrer 2017) **(Figure 4)**.

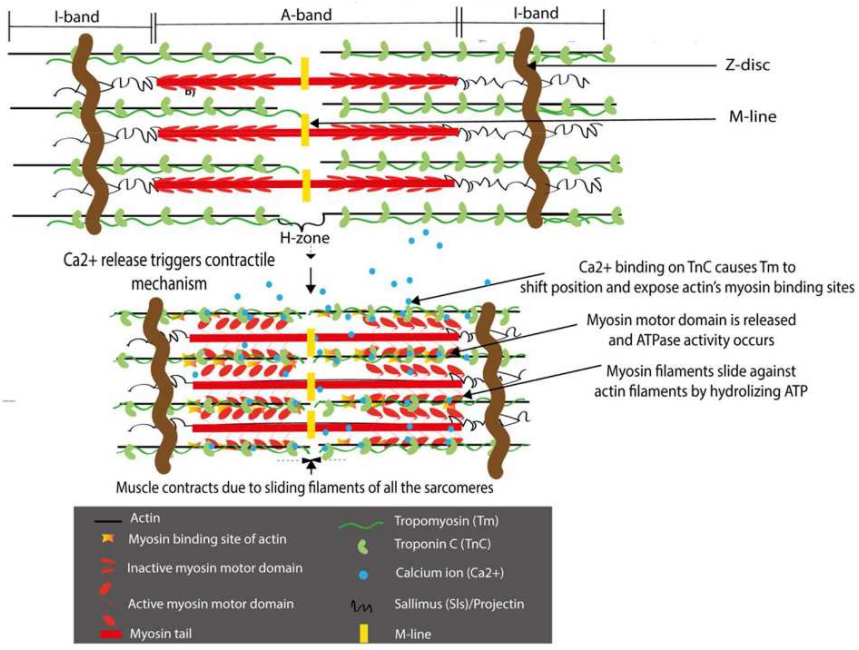

Figure 4. Représentation schématique de la structure sarcomérique des muscles somatiques. Les ions de calcium (Ca2+) libérés lors de la signalisation neurotransmettrice se lient à la Troponine C sur les filaments fins des sarcomères. Cette liaison du Ca2+ provoque un changement de conformation de la Tropomyosine liée à l'actine, exposant les sites de liaison de la myosine à l'actine. Cela permet au domaine moteur de la myosine activée de se lier à l'actine et de glisser contre elle en utilisant l'énergie stockée dans l'Adénosine triphosphate (ATP). Adapté de (Poovathumkadavil et Jagla 2020).

Chez la *Drosophile*, contrairement aux vertébrés, la sarcomérogenèse ne suit pas une séquence rigide d'étapes successives. Elle débute par l'émergence des disques Z, qui servent de points d'ancrage structuraux pour l'assemblage de l'actine polymérisée (F-actine). Des protéines clés telles que la Sallimus (Sls) et l'α-actinine y sont recrutées pour établir une base stable, facilitant l'intégration progressive de la F-actine et la formation du complexe I-Z-I. La Troponine se fixe progressivement aux filaments d'actine en croissance, ce qui permet le recrutement de la Tropomyosine et la stabilisation du filament fin. Les filaments épais de myosine sont ensuite incorporés à cette structure pré-établie, formant ainsi la ligne M au centre du sarcomère. Sls, présente à la fois au niveau de la ligne M et du disque Z, assure une continuité mécanique essentielle en connectant ces deux structures, ce qui permet de préserver l'alignement et l'intégrité du sarcomère lors de la contraction (Schulman et al. 2015).

L'ensemble du processus, ainsi que la stabilité à long terme de la structure sarcomérique, repose sur l'intervention des protéines chaperonnes. Parmi elles, la protéine UNC45 est indispensable à l'intégration de la myosine et son absence perturbe l'organisation du complexe I-Z-I (Karunendiran et al. 2021). En parallèle, Sls assure un contrôle précis de la longueur des filaments de myosine, garantissant ainsi la cohérence architecturale du sarcomère (Loreau et al. 2025).

Une fois les sarcomères correctement assemblés, la fibre musculaire devient contractilement active. L'initiation de la contraction est déclenchée par une élévation du calcium intracellulaire, consécutive à sa libération par le réticulum sarcoplasmique en réponse à une stimulation nerveuse. Ce signal calcique lève l'inhibition exercée par la Troponine, autorisant l'interaction entre l'actine et la myosine**,** et donc la contraction musculaire. A l'inverse, la phase de relaxation repose sur le retrait actif du calcium via des pompes Adénosine triphosphate (ATP)-dépendantes, qui le réinjectent dans le réticulum sarcoplasmique, rétablissant ainsi l'état de repos musculaire (Nongthomba et al. 2004) **(Figure 4)**. Il est important de souligner qu'au fur et à mesure du développement larvaire, ces muscles s'allongent considérablement (Demontis et Perrimon 2009). Cette expansion n'est pas assurée par l'élargissement des sarcomères mais plutôt par l'ajout en série des nouveaux sarcomères. Ce processus repose sur l'intégration progressive des filaments F-actine, médiée par le facteur de dépolymérisation de l'actine : Cofilin (DmCFL). L'inhibition de DmCFL

entraine une accumulation aberrante de la F-actine, accompagnée d'une diminution du nombre de sarcomères formés (Balakrishnan et al. 2020).

e) Innervation musculaire et formation des jonctions neuromusculaires

La contraction musculaire dépend d'une innervation précise par les motoneurones, qui transmettent les potentiels d'action nécessaires à l'activation du processus contractile (Bate et Broadie 1995). Chaque fibre musculaire est ainsi connectée à un ou plusieurs motoneurones issus du système nerveux central. Si la formation des motoneurones est indépendante du développement musculaire (Broadie et Bate 1993), leur trajectoire et la formation des NMJs sont guidées par l'organisation des muscles (Landgraf et al. 1997). Les axones naviguent dans le champ musculaire pour atteindre leurs cibles spécifiques, avec lesquelles ils forment des connexions précises (Jia et al. 1993). Cette spécificité repose sur des interactions entre motoneurones et fibres musculaires, médiées par des molécules d'adhérence cellulaire (CAMs, Cell Adhesion Molecules) et des signaux attractifs ou répulsifs (Fernandes 1995). Les fibres musculaires émettent des prolongements dynamiques, les myopodes, facilitant le contact avec les axones (Ritzenthaler et Chiba 2001). Parmi les CAMs, Fasciclin 2 (Fas2), exprimée dans les motoneurones et faiblement dans les muscles, est cruciale pour la navigation axonale. Certains muscles expriment des facteurs spécifiques qui modulent leur innervation. Par exemple, dans le muscle Ventro-Latéral1 (VL1), le facteur de transcription Teyrha-Meyhra (Tey) définit la spécificité d'innervation neuromusculaire en réprimant le signal répulsif Toll dans le muscle cible, permettant la sélection de la cible synaptique et par conséquent une innervation dirigée (Inaki et al. 2010). Ce processus montre que la précision de l'innervation repose à la fois sur des signaux moléculaires et sur l'identité musculaire. Au-delà de la caractérisation des interactions entre les motoneurones et leurs cibles musculaires via les myopodes, des études plus récentes ont mis en évidence une communication directe entre les progéniteurs musculaires et les motoneurones. Ce dialogue repose sur l'expression, par les progéniteurs, des molécules de guidage Sidestep et Side IV, indispensables à l'attraction des branches nerveuses, notamment segmentaires et intersegmentaires, ainsi que l'établissement de l'innervation musculaire dans le champ latéral. L'ablation des progéniteurs musculaires entraine une absence d'innervation de leur territoires cibles, tandis qu'à l'inverse, la délétion génétique des branches nerveuses

correspondantes induit la disparition spécifiques des progéniteurs qui leur sont associés (Lavergne et al. 2020).

2. La myogenèse adulte : Formation des muscles indirects du vol (IFMs)

À la fin des stades larvaires, la larve entre en pupaison, amorçant le processus de métamorphose. Durant cette phase, la majorité des tissus larvaires, y compris les muscles, sont détruits par histolyse. Une seconde vague de myogenèse devient alors nécessaire pour assurer la formation de la musculature adulte (Laurichesse & Soler, 2020).

a) Structure et organisation fonctionnelle de la musculature adulte

Chez la *Drosophile* adulte, la musculature présente une remarquable diversité morphologique et fonctionnelle, reflétant la spécialisation des muscles selon leurs rôles physiologiques, notamment le vol, la locomotion et la reproduction (Laurichesse et Soler 2020) **(Figure 5)**. Cette musculature se divise en deux grands types : les muscles fibrillaires et les muscles tubulaires (Smith 1961).

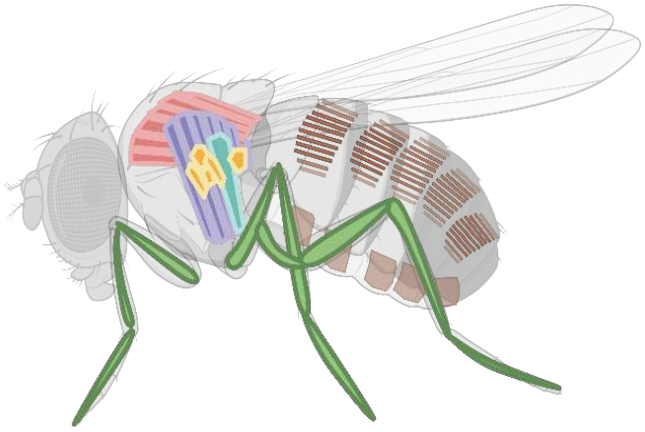

Figure 5. Organisation musculaire chez la *Drosophile* adulte. Les muscles du vol indirects (IFMs) comprennent les DLMs (rose) et les DVMs (violet). Les muscles du vol directs (DFM) sont représentés en jaune. Le muscle du saut (en cyan) est situé entre les DVMs et les DFMs. Des muscles sont également présents dans chaque paire de pattes (en vert) ainsi que dans l'abdomen, où se trouvent les muscles abdominaux (en marron).

Les muscles tubulaires, comme ceux des pattes, se caractérisent par un alignement régulier des myofibrilles et des sarcomères, conférant une architecture classique en faisceaux. À l'inverse, les muscles fibrillaires, représentés notamment par les muscles indirects de vol (IFMs), présentent une organisation désalignée des myofibrilles. Cette configuration permet des contractions très rapides et soutenues, nécessaires aux battements d'ailes (Schönbauer et al. 2011).

Ces muscles du vol constituent les structures les plus massives et les mieux caractérisées, parmi l'ensemble des muscles adultes. Ils sont classés en deux catégories fonctionnelles principales (Dobi et al. 2015):

-Les muscles directs du vol (DFMs, Direct Flight Muscles) : ce groupe comprend huit muscles tubulaires de petite taille attachés directement à la base des ailes. Leur contraction modifie l'orientation des ailes et permet un ajustement fin du mouvement.

-Les muscles indirects du vol (IFMs, Indirect Flight Muscles) : de type fibrillaire, ces muscles occupent la majeure partie du thorax. Fixés entre les parois opposées de l'exosquelette, ils produisent les battements d'ailes par déformation rythmique du thorax. Les IFMs sont subdivisés en deux groupes : les muscles dorso-latéraux (DLMs), composés de six fibres par hémithorax, et les muscles dorso-ventraux (DVMs), au nombre de trois par côté. Le vol est assuré par la contraction asynchrone de ces deux sous-ensembles (Laurichesse et Soler 2020).

Un troisième type de muscle thoracique, appelé **Tergal Depressor of the Trochanter (TDT)** ou « Jump muscles », relie la partie dorsale du thorax à la seconde paire de pattes. Ce groupe de muscles sont essentiels pour déclencher le saut de l'animal permettant ainsi son envol (Jaramillo et al. 2009).

En complément de la musculature thoracique, la *Drosophile* adulte possède également une musculature abdominale, organisée dans chaque hémisegment selon trois positions anatomiques : dorsale, latérale et ventrale (Currie et Bate 1991). Ces muscles interviennent dans divers mouvements corporels, tels que l'expulsion des œufs. La *Drosophile* dispose également des muscles des pattes, leur organisation a été décrite initialement par Miller dans les années 50 puis révisée de manière plus

détaillée par Soler *et al.,* (Soler et al. 2004). De type tubulaire, ces muscles assurent les mouvements articulaires des pattes et jouent un rôle clé dans la locomotion (Schönbauer et al. 2011).

Dans cette section, nous nous sommes concentrés en particulier sur les IFMs, utilisés comme modèle pour étudier le programme de réponse aux blessures chez l'insecte, comme mentionné précédemment.

b) Spécification des IFMs au cours du développement

Les IFMs se développent à partir des progéniteurs musculaires adultes (AMPs), spécifiées dès l'embryogenèse (Fernandes et al. 1991). Ces AMPs, localisées dans le deuxième segment thoracique (T2), s'associent aux disques imaginaux d'aile peu après leur spécification.

Durant les stades larvaires, les cellules épithéliales du disque imaginal d'aile forment une niche spécialisée, sécrétant des signaux moléculaires essentiels au maintien et à la prolifération des AMPs (Boukhatmi et al. 2020; Gunage et al. 2014). Sous l'effet de ces signaux, les AMPs entrent dans un programme de prolifération massive, passant d'environ 250 cellules au stade larvaire L2 à plus de 2500 à la fin du stade L3 (Gunage et al. 2014). Cette expansion repose initialement sur des divisions symétriques qui amplifient la population de progéniteurs, et à partir du stade L3, les AMPs basculent vers des divisions asymétriques, garantissant à la fois leur auto-renouvellement et la production de myoblastes post-mitotiques nécessaires à la formation des myofibres adultes. La régulation de cette transition repose sur des signaux extracellulaires. La voie Notch, activée au cours des premières phases par le ligand Serrate (Ser) exprimé dans l'épithélium adjacent, contrôle les divisions symétriques. Une inhibition de cette voie entraîne une diminution du nombre des progéniteurs en division. Au stade L3, le signal Wg, également produit par l'épithélium, induit une expression asymétrique de la protéine Numb dans les AMPs, marqueur essentiel des divisions asymétriques. L'absence de Numb à ce stade perturbe cette transition, prolongeant indûment les divisions symétriques (Gunage et al. 2014).

Outre les voies Notch et Wg, la signalisation FGF joue également un rôle crucial dans la régulation des AMPs. L'expression localisée des ligands FGF, Ths et Pyr, par l'épithélium, est nécessaire à la régulation de la survie des AMPs (Everetts et al.

2021). Une inhibition spécifique de *pyr* entraîne une diminution du nombre d'AMPs, associée à une augmentation de l'apoptose. Un effet comparable est observé lorsque l'expression de *heartless (htl)*, le récepteur des ligands FGF exprimé dans les AMPs, est perturbée. Ces observations soulignent l'importance de la signalisation FGF entre l'épithélium du disque et les AMPs pour leur maintien au cours du développement. Parallèlement à ces signaux extrinsèques, des mécanismes intrinsèques participent également à la régulation de la prolifération des AMPs. Le suppresseur de tumeur Retinoblastome (pRB), régulateur clé du cycle cellulaire, exerce un contrôle autonome sur la prolifération des AMPs. Sa déplétion induit une augmentation du nombre d'AMPs en division, mettant en évidence son rôle inhibiteur dans l'expansion cellulaire de ces progéniteurs (Zappia et al. 2019).

c) Contrôle de la différenciation des progéniteurs musculaires

Dans les disques imaginaux d'aile, les AMPs constituent une population hétérogène, définie par l'expression différentielle de deux facteurs de transcription : Cut et Vestigial (Vg). La majorité des AMPs expriment fortement *Vg* et faiblement *Cut*, tandis qu'un sous-groupe restreint exprime uniquement *Cut* (Sudarsan et al. 2001). Cette hétérogénéité et l'expression différentielle de ces marqueurs sont régulées par la voie Wg, dont les ligands sont produits par les cellules épithéliales du disque. Wg permet notamment le maintien de *Vg* dans les AMPs adjacentes, préfigurant leur implication dans la formation des IFMs (Vishal et al. 2017; Bernard et al. 2009). *Vg* contribue à spécifier l'identité fibrillaires des IFMs via l'activation de *spalt-major (salm)*, un régulateur essentiel du destin musculaire fibrillaire (Schönbauer et al. 2011). Pendant longtemps, cette régulation différentielle de *vg* constituait la principale démonstration de la diversité fonctionnelle au sein des AMPs. Toutefois, des récentes analyses transcriptomiques à l'échelle unicellulaire (single-cell RNA-seq) ont permis d'élargir cette vision. Elles ont mis en évidence l'existence d'un nouveau facteur clé, Amalgam (Ama), requis pour la formation des IFMs. Sa déplétion conduit à une absence totale de ces muscles, accompagnée d'une létalité, soulignant son rôle indispensable et indépendant de *Vg* (Zappia et al. 2020).

Tout au long des stades larvaires, ces AMPs sont maintenues dans un état indifférencié. Ce maintien repose sur un réseau de facteurs de transcription, tels que Twi, Holes in muscles (Him) et Zinc finger homeodomain-1 (Zfh1), dont l'expression

est régulée en grande partie par la voie de signalisation Notch (Soler et Taylor 2009; Boukhatmi et Bray 2018). La déplétion de *zfh1* dans les AMPs induit une expression prématurée de la *Tropomyosine*, une protéine normalement restreinte aux fibres musculaires différenciées, ce qui souligne son rôle essentiel dans la préservation de l'identité indifférenciée de ces progéniteurs (Boukhatmi et Bray 2018). Il a été montré que ces facteurs de transcription exercent leur fonction en réprimant l'activité de *Myocyte Enhancer Factor 2 (Mef2)*, un acteur central du programme de différenciation musculaire. Enfin, des travaux plus récents issus du laboratoire de Josephine Bageritz indiquent que la voie de signalisation Wg pourrait également intervenir dans la régulation des niveaux de *Mef2* dans les AMPs (Schütze et al. 2025). Cependant, les mécanismes moléculaires précis sous-jacents à cette régulation restent à élucider.

A la fin de stade larvaire L3 et au début de la métamorphose, les AMPs entrent dans une phase de différenciation. À ce stade, l'expression de *twi*, *him* et *zfh1* diminue progressivement, permettant la libération de l'activité transcriptionnelle de *Mef2* et l'initiation du programme de différenciation myogénique (Liotta et al. 2007). L'activation prématurée de *Mef2* suffit d'ailleurs à induire la différenciation des AMPs et l'expression de protéines musculaires telles que la myosine, confirmant son rôle pro-myogénique. Ce phénotype est toutefois réprimé par la surexpression de *Notch*, indiquant que cette voie exerce une inhibition directe ou indirecte sur l'activité de *Mef2* (Caine et al. 2014).

d) Mécanismes de formation des IFMs adultes

Au cours des premières heures suivant la formation de la pupe, les AMPs poursuivent leur prolifération puis migrent vers des régions spécifiques du thorax où elles contribueront à la formation des muscles adultes (Fernandes et al. 1991). Comme mentionné précédemment, les IFMs sont subdivisés en deux groupes : les DLMs et les DVMs, qui se forment de manière parallèle mais selon deux modalités distinctes. Les DVMs résultent d'une fusion *de novo* entre AMPs en cours de différenciation, tandis que les DLMs dérivent de la fusion des AMPs avec un petit nombre de muscles larvaires préexistants qui échappent à l'histolyse **(Figure 6)** (Fernandes et Keshishian 1996).

Durant la métamorphose, l'histolyse entraîne la dégradation de la quasi-totalité des muscles thoraciques, à l'exception de trois muscles obliques dorsaux (LOMs, Larval Oblique Muscles), qui subissent alors des remaniements morphologiques et structuraux importants : ils deviennent plus fins, allongés et adoptent une organisation particulière (Fernandes et Keshishian 1996). L'imagerie en temps réel à partir de 5 heures après la formation de la pupe (APF), montre la migration d'une population d'AMPs dérivés du disque imaginal d'aile en direction des LOMs, qui joue le rôle de cellules fondatrices (Domsch et al. 2017). Ces LOMs expriment la protéine transmembranaire Dumbfounded (Duf), tandis que les AMPs expriment son ligand d'adhésion Stick-and-stones (Sns), favorisant ainsi leur fusion (Dutta et al. 2004; Segal et al. 2016). De façon intéressante, en l'absence des AMPs, les LOMs dégénèrent, et inversement l'ablation des LOMs perturbe la formation d'un nombre correct de fibres musculaires adultes (Dutta et al. 2004). Ces observations suggèrent une dépendance réciproque entre les muscles larvaires et les AMPs pour la mise en place correcte des DLMs.

Une fois fusionnés, les LOMs entrent dans un processus de fragmentation progressive, dit « *Splitting »*, aboutissant à la formation de six fibres musculaires distinctes qui donneront naissance aux DLMs. Cette étape est régulée à la fois par le facteur de transcription myogénique *Salm* (Schönbauer et al. 2011), et le facteur épigénétique la N-acétyl-transférase 30A (Naa30A) (Varland et al. 2023), dont leurs pertes de fonction empêchent le processus de fragmentation, conduisant à la formation de seulement trois fibres musculaires au lieu de six. Contrairement à Salm, dont le rôle dans ce processus est bien caractérisé, le mécanisme par lequel Naa30A régule cette fragmentation musculaire reste encore à déterminer. Par ailleurs, le maintien de l'intégrité des DLMs au cours de la métamorphose est sous le contrôle de l'E3 ubiquitine ligase Mind bomb2 (Mib2), dont la mutation est accompagnée d'une dégénérescence des DLMs naissants (Domsch et al. 2017).

En parallèle, les DVMs sont formés exclusivement à partir des AMPs associés aux disques imaginaux d'aile. Ces AMPs destinés à former les DVMs expriment un fort niveau de *Duf* et migrent vers des régions précises du thorax, correspondant aux futurs sites de formation musculaire. Parmi ces cellules, un sous-ensemble est spécifiquement sélectionné pour adopter un statut de cellule fondatrice, un processus

analogue à celui observé au cours de l'embryogenèse (Atreya et Fernandes 2008). Toutefois, les mécanismes moléculaires sous-jacents à cette sélection et spécification restent à ce jour inconnus.

Enfin, aux alentours de 30 heures APF, la phase de fusion des myoblastes est achevée. Les fibres musculaires entrent alors dans une phase de myofibrillogenèse, caractérisée par l'assemblage progressif des myofibrilles et la mise en place des sarcomères primitifs (Weitkunat et al. 2014), préfigurant ainsi la fonctionnalité contractile des muscles du vol.

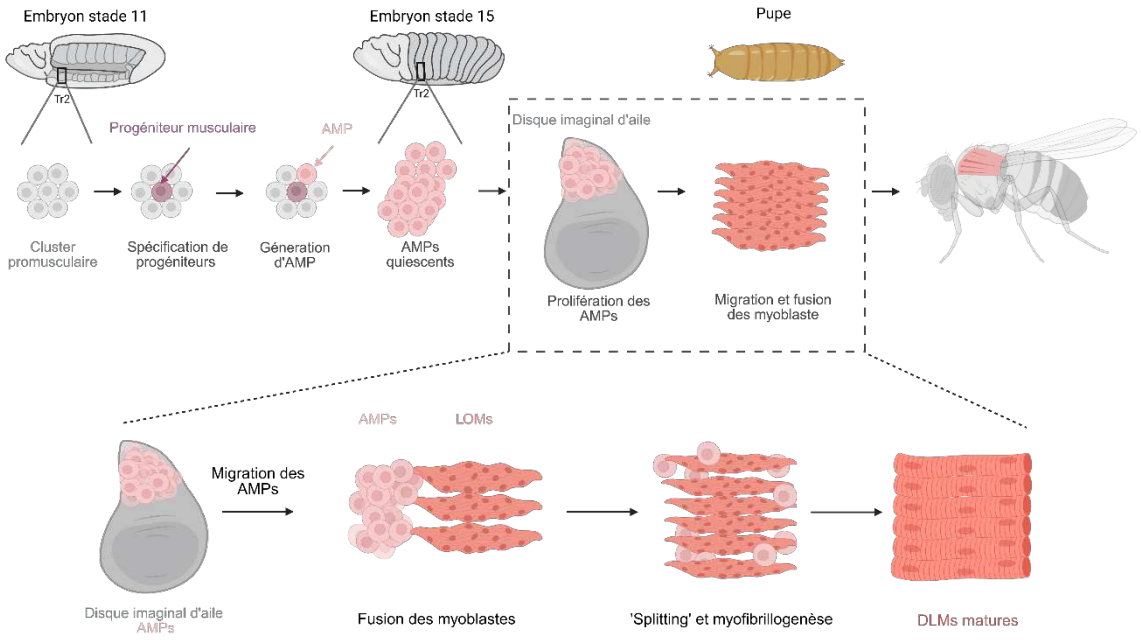

Figure 6. Développement des muscles indirects du vol. Schéma représentant les principales étapes de la formation des IFMs. Les progéniteurs myogéniques adultes (AMPs), spécifiés dans le deuxième segment thoracique (T2) au cours de l'embryogenèse, s'associent aux disques imaginaux de l'aile. Ils prolifèrent durant les stades larvaires, puis entrent en différenciation et migration au début de la métamorphose pupale. Les AMPs fusionnent ensuite avec les muscles larvaires obliques (LOMs), qui servent de matrice pour la formation des muscles dorso-latéraux (DLMs). Ces muscles subissent un processus de splitting donnant naissance à six fibres distinctes, lesquels achèvent leur maturation par la myofibrillogenèse afin d'assurer la formation correcte des DLMs.

e) Ancrage des IFMs et la mise en place des joctions myotendineuses

Afin d'initier le processus de myofibrillogenèse, les muscles doivent d'abord s'ancrer aux tendons pour générer une tension mécanique indispensable à ce processus

(Weitkunat et al. 2014). Des expériences d'ablation laser ciblant les prolongements tendineux ont d'ailleurs altéré la myofibrillogenèse.

Les cellules tendineuses des IFMs sont spécifiées au cours du développement dans le notum des disques d'ailes, et se caractérisent par l'expression de Sr, sous le contrôle des voies de signalisation Wg, Dpp, MAPK et Notch (Fernandes et al. 1996; Ghazi et al. 2003). Par la suite, ces cellules se différencient et expriment la forme active du Sr (Sr-A) (Liu et Geisbrecht 2011). Au cours de la formation des DLMs et une fois la fusion des myoblastes complétée, ces cellules tendineuses émettent de longs filopodes (> 200 µm) en direction des fibres musculaires pour initier le processus d'attachement et la formation des MTJ (Weitkunat et al. 2014) **(Figure 7)**.

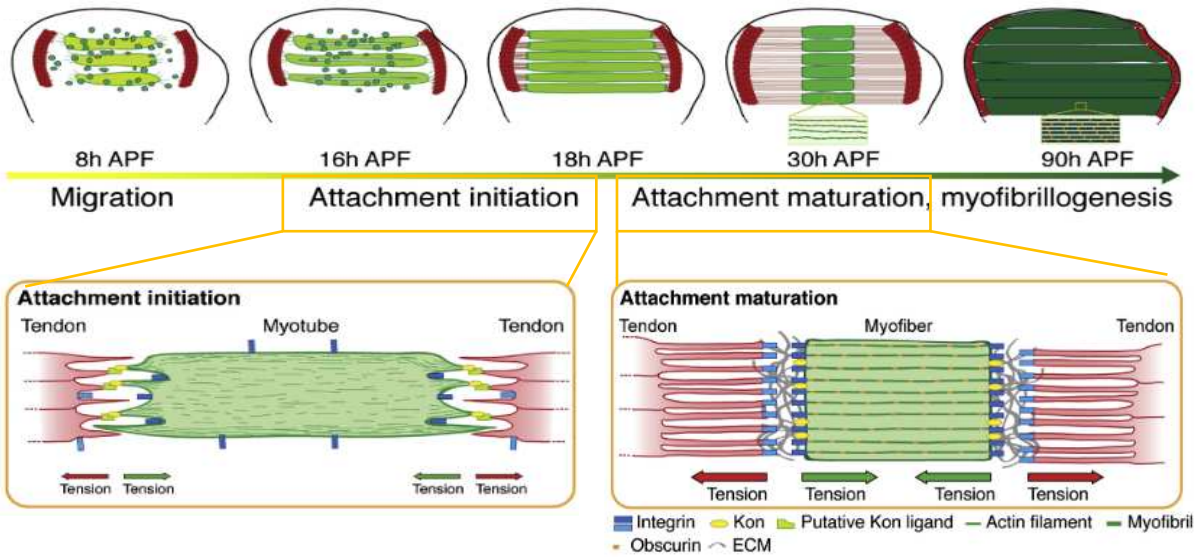

Figure 7. Ancrage des IFMs et établissement des jonctions myotendineuses (MTJ). À partir d'environ 16 heures après la formation de la pupe (APF), les cellules tendineuses (rouge) émettent des filopodes en direction des myotubes (vert). L'ancrage muscle-tendon mobilise plusieurs acteurs, dont des composants de la matrice extracellulaire (ECM), les intégrines et différents récepteurs transmembranaires. Une fois la jonction myo-tendineuse formée, elle entre dans un processus de maturation qui permet sa stabilité et déclenche la myofibrillogenèse nécessaire à la différenciation fonctionnelle des IFMs. Adapté de (Weitkunat et al. 2014).

Bien que la formation de ces MTJs reste encore peu documentée, il est établi qu'elle dépend de l'expression de gènes du complexe Broad-Complex (BR-C). Ce complexe code pour des facteurs de transcription impliqués dans la signalisation hormonale de l'ecdysone, qui initie la métamorphose. Des mutations affectant certaines isoformes de BR-C provoquent des défauts d'ancrage des IFMs, entraînant leur détachement ou leur fixation à des sites ectopiques (Sandstrom et al. 1997; Sandstrom et Restifo

1999). La mise en place de MTJ repose également sur une coordination étroite entre divers composants de la ECM et les intégrines, récepteurs transmembranaires jouant un rôle central dans l'adhérence cellule-matrice. Du côté tendineux, les sous-unités d'intégrines αPS1 et βPS s'associent précocement pour former un hétérodimère fonctionnel, tandis que l'hétérodimère αPS2/βPS s'assemble plus tardivement à la membrane musculaire, contribuant à la stabilisation définitive de la jonction, en interagissant avec des composants de la ECM, notamment la Tsp, qui est sécrétée par les cellules tendineuses et s'accumule au niveau du MTJ (Maartens et Brown 2015; Chanana et al. 2007). L'absence de Tsp provoque un décollement des fibres musculaires de leurs sites d'attachement (Chanana et al. 2007). Une fois la MTJ établie, la cellule tendineuse doit également se connecter à l'exosquelette afin de résister aux contraintes mécaniques induites par la maturation des fibres musculaires. Ce mécanisme repose en partie sur certains composants de la ECM, notamment les protéines Dumpy (Dpy) et Quasimodo (Qsm). Dpy forme des filaments résistants reliant les cellules tendineuses à la cuticule. Qsm, quant à lui, est indispensable à la sécrétion et à la polymérisation de Dpy (Chu et Hayashi 2021).

Ces études soulignent le rôle fondamental des composants de la ECM dans l'établissement et le maintien des MTJ. Une interrogation majeure en découle **: Dans les muscles adultes, les myofibres différenciées conservent-elles la capacité de réactiver les programmes de synthèse de la ECM afin d'assurer la stabilité de l'ancrage muscle-tendon ? Ou bien cette fonction repose-t-elle sur l'intervention d'autres types cellulaires ?**

f) La sarcoromèrogenèse des IFMs :

Afin d'assurer leur fonction motrice, les IFMs doivent développer des sarcomères adaptés aux exigence du vol. Au cours de cette phase, les composants sarcomériques sont progressivement incorporés : Obscurine et Sls se localisent respectivement au niveau des futures lignes M et disques Z. À mesure que les fibres musculaires s'allongent, les sarcomères poursuivent leur maturation en recrutant des protéines supplémentaires telles que la Troponine C4 (TpnC4), la Myofiline et la Flightine (Fln) (Reedy et al. 2000; Spletter et al. 2018). Il est désormais établi que cette organisation repose sur un mécanisme d'auto-assemblage (Kolley et al. 2024). Toutefois, les processus moléculaires permettant une telle précision structurale restent encore

débattus. Une étude récente propose que la formation du motif sarcomérique ne suit pas un programme strictement séquentiel, mais résulte d'un processus d'auto-organisation dynamique : la myosine, Sls et des protéines du disque Z, telles que l'α-actinine, interagissent de manière réversible avec des faisceaux d'actine initialement désorganisés pour établir un motif périodique. Ce n'est qu'ensuite que les filaments d'actine acquièrent leur périodicité (Kolley et al., 2024).

Contrairement à la myogenèse larvaire, où la croissance musculaire s'accompagne d'un ajout progressif de filaments d'actine polymérisée pour former de nouveaux sarcomères (Balakrishnan et al. 2020), la croissance des IFMs au cours de la métamorphose est accompagnée d'une division sarcomérique rapide (Rodier et al. 2025a). Cette division, induite par la tension mécanique générée par l'allongement et les contractions musculaires, implique une rupture de certaines liaisons entre la protéine sarcomérique Sls et le disque Z, ou entre Sls et la myosine, de part et d'autre du sarcomère en division. Cette rupture permet la réorganisation des filaments de myosine bipolaires vers les extrémités opposées, réduisant localement la tension dans la myofibrille. Cette redistribution crée des sites de liaison libres, favorisant le recrutement irréversible de nouvelles protéines sarcomériques. Durant ce processus, l'interaction entre la myosine et les filaments d'actine est maintenue, préservant l'intégrité contractile de la myofibrille. Enfin, la réorganisation centrale des composants Sls, actine et disques Z aboutit à la formation d'un nouveau disque Z **(Figure 8)**. Ce processus permet un allongement rapide des muscles sans compromettre leur fonction contractile. Bien que bien décrit durant le développement, cela soulève une question centrale : ce mécanisme peut-il être réactivé à l'âge adulte ? Autrement dit, les muscles adultes peuvent-ils recourir à la division sarcomérique en réponse à une lésion ? Si tel est le cas, cette plasticité représenterait un mécanisme majeur pour le maintien de la fonction musculaire chez l'adulte. Cette possibilité sera abordée plus en détail dans la section Discussion.

A.

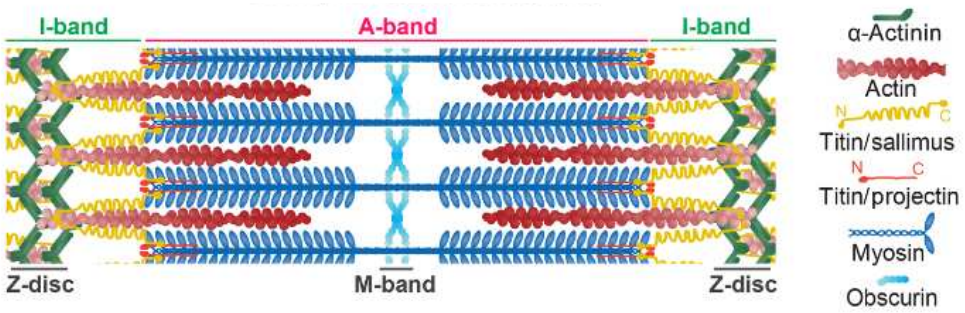

B.

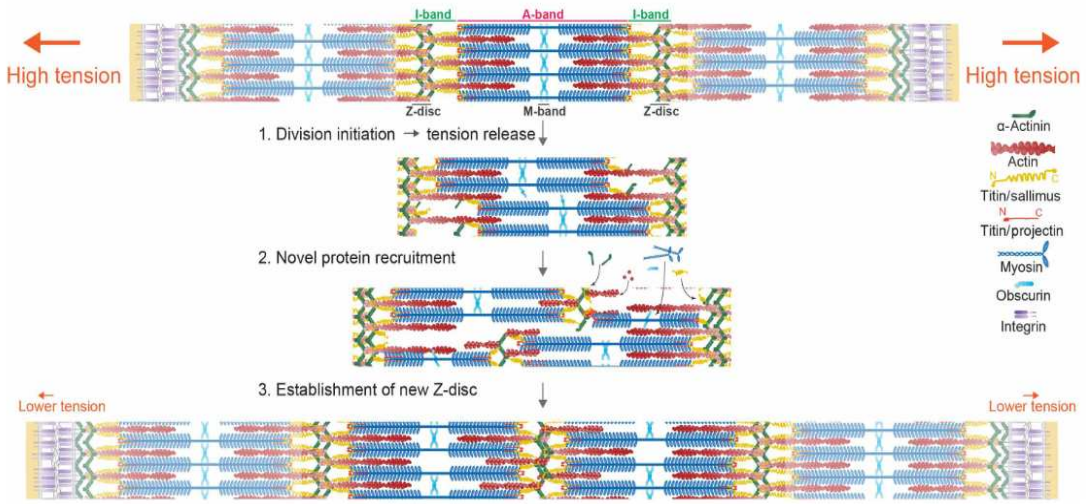

Figure 8. Division des sarcomères au cours de la formation des IFMs. A. La structure d'un sarcomère mature des IFMs. Le sarcomère est délimité par deux disques Z contenant l'α-actinine (en vert), qui relie entre elles les filaments d'actine (en rouge). Au centre, les filaments de myosine (en bleu) sont réticulés par l'Obscurine au niveau de la bande M et constituent la bande A du sarcomère. La zone dépourvue de myosine correspond à la bande I. Sallimus (Sls) (en jaune) relie le disque Z aux filaments de myosine. **B.** La croissance musculaire, marquée par les attachements myotendineux, génère une forte tension qui déclenche la division du sarcomère central (en surbrillance), nécessitant le recrutement des nouvelles protéines sarcomériques et l'établissement des nouveaux disques Z. Le nombre total de sarcomères augmente ainsi de trois à quatre. Adapté de (Rodier et al. 2025a).

À l'âge adulte, les IFMs permettent aux mouches de faire osciller leurs ailes à des fréquences très élevées, pouvant atteindre 1000 Hz, tout en générant des forces mécaniques considérables allant jusqu'à 80 watts par kilogramme de muscle (Götz 1987). Pour répondre à ces exigences, leurs sarcomères présentent une spécialisation particulière au cours du développement. Bien que composés des mêmes éléments de base, leur haute fréquence de contraction repose sur une forme spécifique de Sls, plus courte et rigide et en corrélation avec les bandes I, capable d'ajuster la longueur sarcomérique selon les besoins (Loreau et al. 2023; 2025). L'allongement de cette bande, observé dans les mutants *sls*, altère la performance du vol, indiquant son rôle crucial (Loreau et al. 2025).

Enfin, une fois les sarcomères matures et fonctionnels, leur protection face aux contraintes mécaniques induites par la contraction musculaire devient essentielle. Lors de la contraction, les têtes de myosine situées au niveau de la zone M tirent les filaments d'actine fixés aux disques Z vers le centre du sarcomère, ce qui peut

provoquer des dommages, en particulier la rupture du disque Z le plus fragile. Pour préserver l'intégrité des sarcomères et assurer leur bon fonctionnement, des mécanismes de protection et de réparation sont mis en place. Parmi les acteurs clés de ce mécanisme, la protéine sarcomérique Filamine, liée à l'actine au niveau des disques Z, agit comme un capteur mécanique. Elle détecte les tensions excessives et déclenche des signaux de réparation. En cas de mutation de la Filamine, les disques Z se rompent, entraînant la désorganisation des myofibrilles et des défauts de battement des ailes (Fisher et al. 2024).

g) Acquisition de l'identité fibrillaire des IFMs

Certains composants sarcomériques des IFMs, tels que TpnC4 et Fln, sont également essentiels à l'organisation fibrillaire caractéristique des IFMs. L'expression de ces protéines structurales est contrôlée par le gène déterminant du destin myofibrillaire : *salm* (Schönbauer et al. 2011). *salm* agit en tant que régulateur transcriptionnel en activant les gènes spécifiques aux IFMs tout en réprimant ceux impliqués dans la formation des muscles tubulaires, comme ceux des pattes (Schönbauer et al., 2011). En effet, l'expression ectopique de *salm* dans les muscles des pattes en développement suffit à reprogrammer leur destin musculaire, en induisant une organisation fibrillaire à la place de la structure tubulaire normalement adoptée. L'expression de *salm* est elle-même contrôlée par les protéines à homéodomaine Extradenticle et Homothorax (Bryantsev et al. 2012). *Salm* influence également la morphologie des mitochondries dans les IFMs, en favorisant leurs organisation allongée et intercalée entre les myofibrilles. Cette configuration mitochondriale, est à son tour nécessaire à la mise en place de l'architecture fibrillaire des IFMs. Comme pour la perte de fonction de Salm, une perturbation de cette morphologie des mitochondries conduit à un phénotype musculaire similaire à celui des muscles des pattes accompagné d'une altération de la capacité de vol (Avellaneda et al. 2021). Ces observations suggèrent une coordination fine entre la mise en place du programme myogénique, garant de la structuration mécanique, et l'organisation des structures subcellulaires notamment les mitochondries, l'une des principales sources d'énergie. Cela soulève une question fondamentale : Dans quelle mesure les structures énergétiques s'adaptent à l'architecture musculaire ? Une partie de la réponse réside dans l'organisation du système respiratoire, dont les branches

trachéales atteignent directement les mitochondries des fibres musculaires, optimisant ainsi l'apport en oxygène pour répondre aux exigences métaboliques élevées des muscles du vol (Peterson et Krasnow 2015).

h) Mise en place de l'innervation des IFMs

Contrairement à la myogenèse embryonnaire, dans laquelle l'innervation musculaire survient tardivement, l'établissement des connexions nerveuses dans les IFMs s'effectue de façon précoce et synchronisée avec la formation de la musculature adulte (Fernandes et VijayRaghavan 1993). Les DLMs sont innervés initialement par les nerfs intersegmentaires (ISN) larvaires qui maintiennent transitoirement leurs connexions avec les muscles larvaires persistants (LOMs). Ces motoneurones subissent par la suite des remodelages morphologiques importants afin de s'ajuster à l'émergence de la musculature adulte (J. J. Fernandes and Keshishian 2005).

Si les mécanismes d'innervation des DLMs sont partiellement décrits, l'innervation des DVMs, quant à elle, reste encore peu connue. Les connaissances actuelles à propos cette innervation reposent essentiellement sur des hypothèses suggérant que les motoneurones innervant les DVMs provenaient de motoneurones larvaires re-spécifiés. D'autres hypothèses envisagent qu'ils proviendraient de cellules n'ayant pas de cibles larvaires, et qui se différencieraient tardivement en neurones et émettraient leurs projections axonales au cours de la métamorphose (Fernandes et VijayRaghavan 1993).

À ce jour, la majorité des recherches se sont principalement concentrées sur la mise en place des motoneurones aux stades larvaires, tandis que l'innervation périphérique adulte, en particulier celle des motoneurones innervant les muscles du vol adultes, demeure largement inexplorée. Cela s'explique en partie par le fait que les stades larvaires sont plus accessibles à étudier que les stades adultes. Ce champ de recherche pourrait toutefois connaître un regain d'intérêt, à la faveur des récents progrès technologiques ayant permis de cartographier avec une précision les circuits neuronaux du cerveau de la *Drosophile* (Pospisil et al. 2024).

B. Le maintien et la réparation des muscles du vol adultes

1. Impact du vieillissement sur la structure et le fonctionnement des IFMs

Les muscles indirects du vol (IFMs) subissent, au cours de la vie adulte, des contraintes mécaniques et métaboliques, ainsi que les effets du vieillissement, qui compromettent leur intégrité et leur capacité d'adaptation (Chechenova et al. 2024). Dès les années 1970, il a été montré que l'âge entraîne des altérations morphologiques majeures, avec une désorganisation des fibres et des sarcomères, une réduction de la surface musculaire et des anomalies mitochondriales (Takahashi et al. 1970; Miller et al. 2008). Ces défauts s'accompagnent d'un déclin de l'activité respiratoire et d'une production excessive d'espèces réactives de l'oxygène (ROS), sources de stress oxydatif et de dysfonctionnement contractile (Schwarze et al. 1998; Girardot et al. 2006; Lee et al. 2010) .

En parallèle, le vieillissement perturbe la protéostasie : on observe une accumulation d'agrégats protéiques liée à un défaut des systèmes de contrôle qualité, notamment l'autophagie (Demontis et Perrimon 2010). Le facteur de transcription FOXO joue un rôle central dans ce processus : sa surexpression protège les IFMs du déclin lié à l'âge, tandis que sa perte entraîne des agrégats précoces et une réduction de la longévité. De plus, des mutations affectant la modification post-traductionnelle des protéines, comme Naa30A, conduisent elles aussi à des défauts structuraux et à une altération de l'homéostasie musculaire (Varland et al. 2023).

Ainsi, le vieillissement des IFMs résulte de l'interaction entre altérations structurelles, dysfonctionnement mitochondrial et déséquilibre de la protéostasie, soulignant l'importance des mécanismes de régulation métabolique et protéique dans le maintien de l'intégrité musculaire.

2. Stratégies compensatoires des IFMs face aux dommages musculaires

a) *Remodelage des composants structuraux*

Comme de nombreux organismes dans leur environnement naturel, la *Drosophile* est fréquemment exposée à des blessures (Subasi et al. 2024), ce qui nécessite des mécanismes d'adaptation musculaire efficaces afin de préserver la fonction et

d'assurer la survie de l'animal. Dans le but de de mieux caractériser les voies moléculaires et cellulaires impliquées dans la réponse aux traumatismes musculaires, des stratégies expérimentales ont été développées, consistant à induire de manière contrôlée des lésions physiques dans les muscles thoraciques des mouches adultes. Ces blessures entraînent une réponse transcriptionnelle rapide, marquée notamment par la surexpression de plusieurs gènes de structure musculaire spécifiques des IFMs, tels que *Act88F*, codant pour la seule actine exprimée dans ces muscles, ainsi que *Mlc* (Myosin light chain) et la *troponin C4 (TpnC4)* (Apidianakis et al. 2007).

Cette réponse suggère l'existence d'un processus actif de compensation ou de remodelage visant à restaurer l'intégrité du tissu musculaire lésé. Dans la même perspective, les mouches mutantes pour *Mhc* (Myosin heavy chain), une composante majeure du cytosquelette contractile, présentent une dégénérescence progressive des muscles du vol, accompagnée d'une induction de gènes associés à l'organisation cytosquelettique, tels que *Act88F*, et *Sls* (Montana et Littleton, 2006). Ces observations soutiennent l'hypothèse selon laquelle le remodelage des structures myofibrillaires constitue une réponse adaptative essentielle au maintien de la fonctionnalité musculaire.

b) Mobilisation des cellules souches musculaires

Pendant longtemps, on a supposé que les muscles adultes de la *Drosophile* étaient dépourvus de cellules satellites. Ce n'est qu'en 2017 que le laboratoire de VijayRaghavan a identifié, chez la *Drosophile*, des cellules analogues aux MuSCs et a montré leur rôle essentiel dans le maintien et la réparation des muscles du vol (Chaturvedi et al. 2017). Ces cellules proviennent des AMPs et expriment le facteur de transcription Zfh1, indispensable à leur maintien, une fonction conservée au cours de l'évolution (Siles et al. 2019a). En 2018, le laboratoire de Sarah Bray a élucidé le mécanisme moléculaire permettant à ces cellules de rester dans un état indifférencié au cours du développement **(Figure 9)**. Cette étude a révélé qu'un changement d'isoforme d'ARN du gène *zfh1*, dans un sous-ensemble d'AMPs, est crucial pour leur préservation dans un état indifférencié durant la métamorphose (Boukhatmi et Bray 2018). En effet, la différenciation des AMPs en fibres musculaires fonctionnelles est associée à l'expression du microARN miR-8 (homologue du miR-200 chez les vertébrés), qui cible l'isoforme longue majoritaire de *zfh1* et en diminue les niveaux

protéiques. Sous l'action de la voie de signalisation Notch, un sous-ensemble d'AMPs exprime une isoforme alternative, *zfh1-short*. Ce changement résulte de l'utilisation d'un promoteur alternatif et de sites de polyadénylation précoces, tronquant ainsi la région 3'UTR de l'ARNm et supprimant les sites de fixation de miR-8. Par conséquent, la protéine Zfh1 est spécifiquement maintenue dans ces cellules, leur permettant d'échapper à la différenciation et de persister à l'état indifférencié dans le muscle adulte.

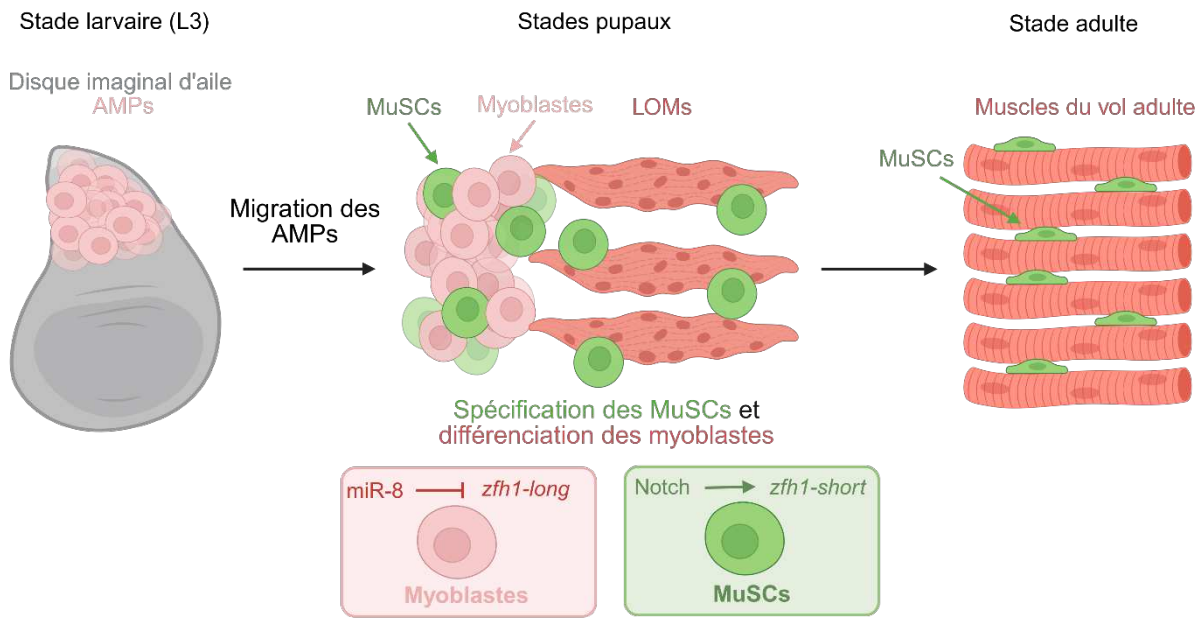

Figure 9. La spécification des cellules souches musculaires (MuSC) au cours de la formation des IFMs. Les progéniteurs musculaires adultes (AMPs) des IFMs sont initialement associés aux disques imaginaux des ailes. Au cours de la métamorphose, pendant les stades pupaux, les AMPs migrent vers les structures larvaires pré-existantes des DLM. L'inhibition de l'isoforme longue de *zfh1(zfh1-long)* par *miR-8* (en rouge) favorise la différenciation des AMPs. L'expression de l'isoforme courte de *zfh1 (zfh1-short)* (en vert) est activée uniquement dans les MuSCs sous le contrôle de la voie Notch. À l'émergence de la mouche adulte, la formation des IFMs et des MuSCs est achevée. L'expression persistante de *zfh1* dans les MuSCs permet le maintien de leur identité. Adapté de (Boukhatmi et Bray 2018).

Depuis ces travaux fondateurs, trois autres études antérieures ont utilisé la *Drosophile* comme modèle pour explorer la régénération musculaire (Catalani et al. 2022; Mitchell-Gee et al. 2024; Goh et al. 2024). Toutefois, malgré ces avancées, notre compréhension des mécanismes moléculaires et cellulaires régissant l'activation, la prolifération et la différenciation des *MuSCs* chez la *Drosophile* demeure très limitée, probablement en raison de la rareté de cette population cellulaire. Par ailleurs, le seul marqueur actuellement identifié, le facteur de transcription Zfh1, est

également exprimé dans une population de cellules immunitaires appelées plasmatocytes (Voir section Résultats), également présentes dans le tissu musculaire, ce qui complique son utilisation comme outil spécifique pour l'étude de la régénération musculaire.

Chapitre III. Le système immunitaire de la *Drosophile* : Organisation et Fonctions

Historiquement, la *Drosophile* a contribué considérablement à la découverte des mécanismes fondamentaux de l'immunité innée, notamment avec l'identification des voies Toll et Imd (Imd, Immune difficiency) (Lemaitre et al. 1996a). Ce modèle s'est ainsi imposé comme un outil puissant pour décrypter l'organisation et le fonctionnement du système immunitaire inné en réponse aux infections (Yu et al. 2022a). En revanche, la question de savoir si, et comment, cet arsenal immunitaire peut être mobilisé en réponse à des lésions musculaires reste largement inexplorée. Avant d'aborder cette problématique, qui constitue une composante centrale de mes travaux de thèse (Voir section Résultats), **ce chapitre présente les grands principes de l'immunité chez la *Drosophile*, en décrivant les étapes clés de sa mise en place au cours du développement, ainsi que ses majeures fonctions.**

A. L'immunité chez la *Drosophile*

1. Le système immunitaire de la *Drosophile*

Le système immunitaire permet à l'organisme de reconnaitre et d'éliminer le « non-soi » assurant ainsi une défense contre diverses agressions, telles que les infections d'origine virale, bactérienne, fongique ou parasitaire, ainsi que contre les cellules tumorales. Il s'organise en deux grandes composantes : l'immunité innée, commune à l'ensemble des métazoaires, et l'immunité adaptative, spécifique des vertébrés (Wang et al. 2024). L'immunité innée constitue la première ligne de défense. Elle repose à la fois sur des barrières physiques, comme l'épiderme et les épithéliums des muqueuses, et sur des mécanismes biologiques rapides et non spécifiques, tels que la phagocytose ou la production de peptides antimicrobiens (AMPs, Antimicrobial peptides). À l'inverse, l'immunité adaptative se distingue par sa capacité à reconnaitre spécifiquement les antigènes via des récepteurs issus d'un remaniement génique somatique. Elle mobilise des cellules spécialisées, notamment les lymphocytes, et confère une mémoire immunitaire permettant une réponse renforcée lors d'expositions ultérieures au même agent pathogène (Wang et al. 2024).

Chez la *Drosophile*, l'immunité repose exclusivement sur des mécanismes innés, en l'absence de système immunitaire adaptatif (Yu et al. 2022b). Cette absence pourrait s'expliquer par sa courte durée de vie qui n'aurait pas favorisé l'évolution de mécanismes de mémoire immunitaire comparables à ceux observés chez les vertébrés.

Cette immunité repose sur deux lignes de défense principales : la réponse humorale et la réponse cellulaire. La réponse humorale est médiée par la production des AMPs, synthétisés principalement par le tissu adipeux en réponse à une infection (Hanson et Lemaitre 2020). Ces peptides ciblent spécifiquement différents types de pathogènes (bactéries à Gram positif ou négatif, champignons). Parallèlement, la réponse cellulaire repose sur l'activité des hémocytes, des cellules sanguines spécialisées capables de phagocyter les agents pathogènes et de les encapsuler (Gold et Brückner 2015). Ces réponses sont rapides, adaptées à la nature de pathogène, et hautement conservées au cours de l'évolution, faisant de la *Drosophile* un modèle de choix pour l'étude des mécanismes cellulaires et moléculaires de l'immunité innée.

2. Les mécanismes de la réponse immunitaire

a) La réponse immunitaire humorale

La réponse immunitaire humorale repose principalement sur la production rapide des AMPs, synthétisés majoritairement par le tissu adipeux, l'équivalent fonctionnel du foie chez les vertébrés, en réponse à une infection (Hanson et Lemaitre 2020). Cette réponse est déclenchée par la détection de motifs moléculaires associés aux pathogènes (PAMPs, Pathogen associated molecular patterns) via des récepteurs de type PRRs (Pattern Recognition Receptors), qui activent deux voies de signalisation majeures : la voie Toll et la voie Imd (Hanson et Lemaitre 2020) **(Figure 10)**.

La voie Toll est principalement activée en réponse à des infections fongiques et des bactéries à Gram positif. Elle conduit à la translocation nucléaire des facteurs de transcription Dorsal-related immunity factor (Dif) ou Dorsal**,** homologues des facteurs de transcription pro-inflammatoires NF-κB des vertébrés, qui stimulent l'expression de plusieurs AMPs tels que la Drosomycine (Hanson et Lemaitre 2020). En parallèle, la voie Imd, est déclenchée par la reconnaissance de peptidoglycanes provenant des

bactéries à Gram négatif. Elle active le facteur de transcription Relish, également de la famille NF-κB, et stimule la production d'AMPs comme la Diptericine, l'Attacine, ou la Cecropine (Hanson et Lemaitre 2020). Ces deux voies de signalisation assurent ainsi une réponse immunitaire spécifique et adaptée à la nature de pathogène (Hanson et al. 2019). Les AMPs ainsi produits sont ensuite sécrétés dans l'hémolymphe, liquide circulant de la *Drosophile* fonctionnellement équivalent au sang, où ils agissent directement sur les agents infectieux. En plus du tissu adipeux, d'autres tissus tels que les voies respiratoires (les trachées), l'intestin ou l'épiderme peuvent également contribuer à la production d'AMPs selon le type d'infection (Tzou et al. 2000; Ferrandon 1998). Cette réponse humorale est généralement transitoire, finement régulée dans le temps et proportionnelle à la charge infectieuse.

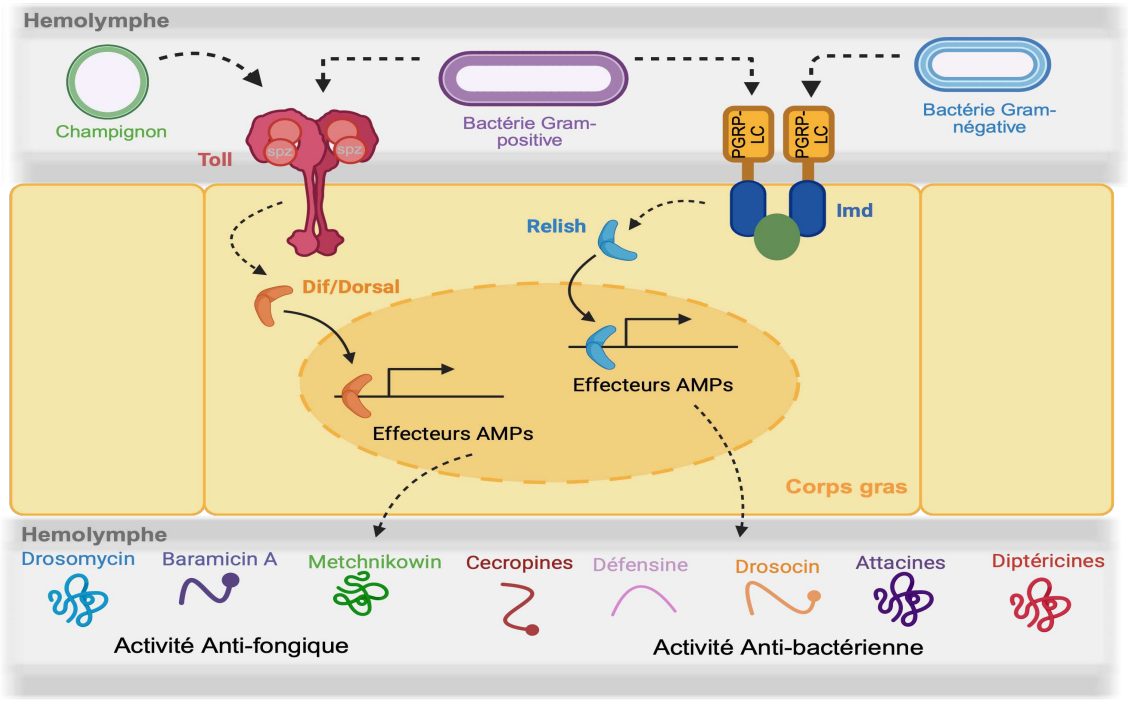

Figure 10. La réponse immunitaire humorale chez la *Drosophile*. Cette réponse est déclenchée principalement dans le tissu adipeux en réponse à la détection de motifs microbiens. L'activation des voies de signalisation Toll (champignons, bactéries Gram+) et Imd (bactéries Gram+ et Gram-) conduit à l'activation des facteurs de transcription : Dif, Dorsal et Relish, induisant l'expression de nombreux peptides antimicrobiens (AMPs) spécifiques sécrétés dans l'hémolymphe. Adapté de (Hanson et Lemaitre 2020).

b) La réponse immunitaire cellulaire

La réponse immunitaire cellulaire chez la *Drosophile* repose principalement sur l'action des hémocytes (Buchon et al. 2014a). Trois grandes catégories d'hémocytes

ont été décrites : les plasmatocytes, les cellules à cristaux et les lamellocytes (Banerjee et al. 2019) **(Figure 11)**.

Les plasmatocytes, qui représentent 90 à 95 % des hémocytes circulants, assurent des fonctions phagocytaires essentielles. Ils reconnaissent et éliminent les pathogènes telles que les bactéries, via des mécanismes d'endocytose (Melcarne et al. 2019). En présence d'agents plus volumineux, comme les œufs de guêpes parasitoïdes ou d'autres corps étrangers, certains plasmatocytes se différencient en lamellocytes (Leitão et Sucena 2015; Anderl et al. 2016). Ces cellules de grande taille sont spécialisées dans l'encapsulation, un processus par lequel elles entourent l'élément étranger d'une matrice cellulaire, l'isolant pour faciliter sa neutralisation (Lanot et al. 2001; Binggeli et al. 2014; Dudzic et al. 2015).

Les cellules à cristaux, bien qu'en nombre plus réduit, jouent toutefois un rôle clé dans la défense de l'organisme. Elles stockent et relarguent des enzymes telles que la prophénoloxydase (PPO), qui initie la cascade de mélanisation. Ce processus permet d'immobiliser, puis de neutraliser les pathogènes, et participe à la cicatrisation des tissus lésés (Nam et al. 2008).

Des études récentes basées sur des approches transcriptomiques à l'échelle unicellulaire, ont révélé que ce système immunitaire est bien plus complexe que ce que suggéraient la classification traditionnelle. En particulier, les plasmatocytes qui ont été considérés longtemps comme un type cellulaire unique, ils se révèlent en réalité très hétérogènes formés d'au moins 12 sous-types distincts. Chacun exprime des profils géniques spécifiques associés à des fonctions variées telles que la réponse au stress oxydatif, la signalisation ou encore le métabolisme (Cattenoz et al. 2020; Hultmark et Andó 2022). Encore plus intéressant, ces plasmatocytes font preuve d'une grande plasticité, capables de changer d'état en fonction des besoins de l'organisme. Ils peuvent notamment se transdifférencier en cellules à cristaux (Marcetteau et al. 2025) ou en lamellocytes en réponse à des signaux immunitaires spécifiques (Shin et al. 2020).

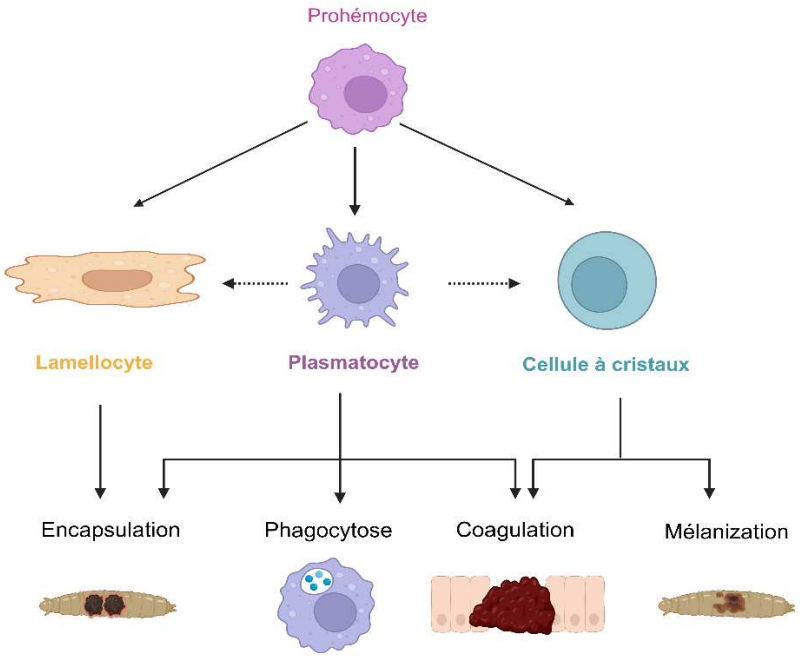

Figure 11. La réponse immunitaire cellulaire chez la *Drosophile*. Elle est assurée par les hémocytes : Les plasmatocytes réalisent majoritairement la phagocytose. Les cellules à cristaux libèrent des enzymes de la voie de la mélanisation, qui entraînent la formation de mélanine au site de l'infection, renforçant la coagulation et exerçant une activité antimicrobienne. Les lamellocytes, forment une capsule cellulaire autour de l'œuf du parasite, menant à son isolement et sa destruction.

B. L'hématopoïèse chez la *Drosophile*

Chez la *Drosophile*, l'hématopoïèse permet de générer les trois types d'hémocytes décrit précédemment. Elle se déroule en deux grandes vagues successives : une première, embryonnaire, et une seconde, larvaire (Banerjee et al. 2019; Crozatier et Meister 2007). La phase embryonnaire débute dans le mésoderme antérieur, où sont produits des plasmatocytes et des cellules à cristaux. Ces cellules colonisent l'ensemble de l'embryon, et persistent tout au long de la vie larvaire, soit en circulation dans l'hémolymphe, soit organisées en agrégats fixés à la face interne de l'épiderme, appelés sites sessiles (Honti et al. 2010; Jung et al. 2005). Malgré leur rôle actif dans l'hématopoïèse, la fonction de ces niches sessiles n'est pas encore pleinement décrite.

La seconde phase d'hématopoïèse se déroule durant le développement larvaire dans un organe spécialisé, la glande lymphatique, localisée dorsalement le long du tube cardiaque. Cette glande contient des cellules progénitrices appelées prohémocytes, qui se différencient majoritairement en plasmatocytes et en cellules à cristaux au cours

du troisième stade larvaire. Au début de la métamorphose, la glande lymphatique se désagrège, libérant dans l'hémolymphe à la fois les hémocytes différenciés et les progéniteurs (Banerjee et al. 2019; Crozatier et Meister 2007).

Chez l'adulte, le nombre d'hémocytes diminue progressivement dès la première semaine suivant l'éclosion. Cette réduction qui s'accélère en cas d'infection (Mackenzie et al. 2011), suggère que les hémocytes sont mobilisés et consommés lors de la réponse immunitaire, sans être remplacés. Toutefois, certaines stimulations bactériennes peuvent induire une surexpression de marqueurs hémocytaires, tels que *Croquemort* (Guillou et al. 2016), traduisant une réponse transcriptionnelle indépendante de toute prolifération cellulaire. Sur la base de ces données, l'absence d'hématopoïèse chez l'adulte a longtemps été considérée comme un dogme. Néanmoins, une étude a proposé l'existence d'une hématopoïèse adulte active (Ghosh et al. 2018), bien que ces résultats aient été récemment remis en question (Sanchez Bosch et al. 2019; Boulet et al. 2021).

C. Les fonctions « non immunitaires » des hémocytes

Les hémocytes sont présents tout au long du développement de la *Drosophile,* depuis l'embryogenèse jusqu'à l'âge adulte. Si certaines de leurs fonctions, telles que la phagocytose des pathogènes en réponse aux infections, sont maintenues tout au long du cycle de vie, d'autres sont spécifiques à certains contextes développementaux ou environnementaux particuliers. En effet, ces dernières années, plusieurs fonctions non immunitaires des hémocytes ont été décrites en réponse à des signaux liés à des stress physiologiques, tels que les lésions tissulaires, le remodelage morphogénétique ou encore les déséquilibres métaboliques (Li et al. 2025). **Cette polyvalence fonctionnelle des hémocytes a suscité un intérêt particulier dans le cadre de mon travail de thèse, centré sur les réponses cellulaires déclenchées par des lésions musculaires.** Ces processus impliquent une interaction complexe entre plusieurs types cellulaires, dont les hémocytes, soulignant leur rôle central au-delà de la simple défense immunitaire (Voir section Résultats).

Dans cette section, je me suis attaché à explorer plusieurs de ces fonctions dites « non immunitaires », telles qu'elles sont rapportées dans la littérature, en mettant en lumière leur diversité, leur spécificité contextuelle et leur pertinence pour la

compréhension globale du rôle des hémocytes dans le développement et l'homéostasie tissulaire chez la *Drosophile* **(Figure 12)**.

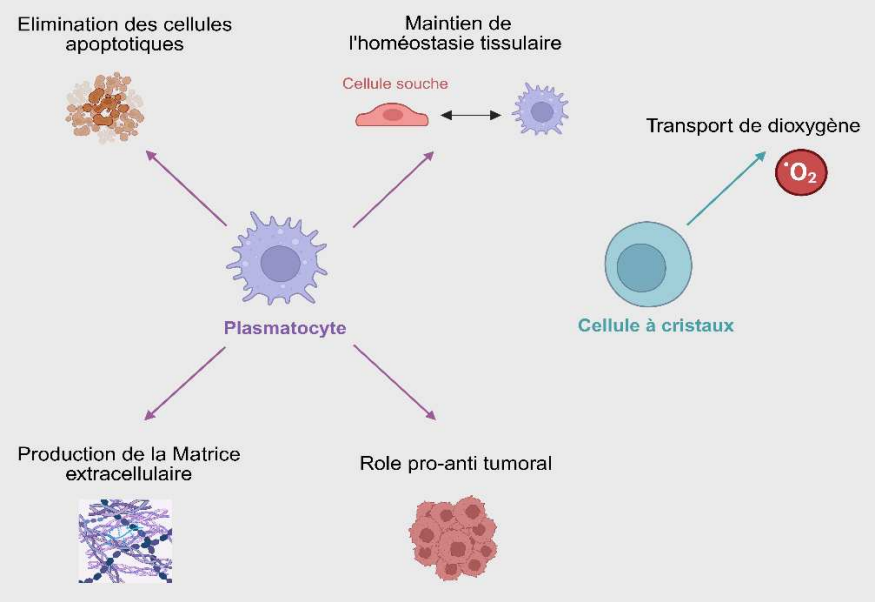

Figure 12. Les fonctions non immunitaires des hémocytes chez la *Drosophile*. Les hémocytes assurent des fonctions essentielles : durant l'embryogenèse, les plasmatocytes phagocytent les cellules apoptotiques et sécrètent des composants matriciels, contribuant à la morphogenèse. Ils produisent aussi des signaux pro- ou anti-inflammatoires. Chez l'adulte, les plasmatocytes soutiennent régénération et homéostasie tissulaire via l'interaction avec les cellules souches. Les cellules à cristaux quant à eux participent à l'oxygénation des tissus larvaires.

1. L'efférocytose : élimination des cellules apoptotiques

Au cours du développement de la *Drosophile*, des phases clés telles que l'embryogenèse et la métamorphose s'accompagnent d'importants remaniements morphogénétiques, générant une accumulation massive de cellules apoptotiques. Leur élimination est essentielle à la formation correcte des structures adultes (Ellis et al. 1991). Ce processus, connu sous le nom d'efférocytose**,** repose principalement sur l'activité phagocytaire des hémocytes.

L'efficience de ce mécanisme dépend de récepteurs phagocytaires conservés exprimés à la surface des hémocytes, tels que Draper**,** Simu et Croquemort**,** capables de reconnaître des signaux de mort cellulaire comme l'exposition de phosphatidylsérine à la surface des cellules apoptotiques (Manaka et al. 2004; Balasubramanian et Schroit 2003). En plus des récepteurs membranaires, l'efférocytose fait également intervenir des facteurs solubles, tels que NimB4**,** une protéine de la famille Nimrod, sécrétée par les plasmatocytes et indispensable à la

maturation des phagosomes. Les mutants pour *NimB4* présentent une accumulation anormale de corps apoptotiques, aussi bien pendant l'embryogenèse que dans le cerveau larvaire (Petrignani et al. 2021). Des travaux récents ont montré que l'efférocytose était assurée par des sous-populations spécifiques de plasmatocytes, régulées par des voies de signalisation distinctes (Brooks et al. 2024).

L'importance physiologique de ce processus est bien illustrée par l'analyse fonctionnelle du gène *draper*. Lors du développement du système nerveux, un excès de neurones est naturellement produit, puis éliminé par apoptose. Chez les mouches mutantes pour *Draper*, l'incapacité à phagocyter ces neurones apoptotiques entraîne leur accumulation dans les cellules gliales, ce qui conduit à une neurodégénérescence progressive liée à l'âge (Etchegaray et al. 2016).

Ce rôle des hémocytes dans l'élimination des débris cellulaires ne se limite pas aux stades précoces du développement. Durant la métamorphose, les hémocytes assurent également le nettoyage des tissus larvaires dégénérés, tels que les muscles larvaires, facilitant ainsi la mise en place des muscles adultes. Bien que le rôle des plasmatocytes dans l'homéostasie musculaire au cours du développement commence à être élucidé, leurs fonctions dans le maintien et la régulation des muscles adultes demeurent encore largement méconnues.

2. Rôle anti- et pro-tumoral des hémocytes

Au-delà de leur rôle dans l'élimination des particules pathogènes, les hémocytes sont requis pour la prévention des tumeurs néoplasiques chez la *Drosophile* via la phagocytose (Pastor-Pareja et al. 2008). L'inhibition des récepteurs phagocytaires dans les plasmatocytes augmente l'occurrence tumorale (Zhang et al. 2020). Toutefois, dans certains contextes, cette activité phagocytaire favorise la croissance tumorale, en amplifiant un signal cytokine exploité par les cellules tumorales dans les disques imaginaux d'aile (Hirooka et al. 2025). Ainsi, les plasmatocytes peuvent exercer des effets ambivalents sur la progression tumorale.

3. Contribution à l'homéostasie tissulaire

Ces dernières années, les cellules immunitaires ont suscité un intérêt croissant dans l'étude du maintien de l'homéostasie tissulaire, notamment à travers leurs interactions avec les cellules souches. Longtemps considérées comme les

principales actrices de la régénération et du renouvellement des tissus, les cellules souches apparaissent désormais comme dépendantes du soutien apporté par les hémocytes (Ayyaz et al. 2015).

Une étude récente a mis en évidence le rôle essentiel des hémocytes dans le maintien de la niche germinale chez les *Drosophiles* mâles âgées. Les plasmatocytes sont essentiels pour préserver le réservoir de cellules souches germinales, et donc pour maintenir la fertilité. Or, avec l'âge, leur nombre diminue progressivement. Ce déclin perturbe la régulation de la niche via une signalisation JAK-STAT altérée, ce qui favorise l'apoptose germinale et compromet la spermatogenèse. Ces résultats mettent en évidence l'importance des interactions entre le système immunitaire et les autres types cellulaires dans le maintien de l'homéostasie tissulaire, indépendamment de toute réponse à une infection (Varga et al. 2025).

Au-delà de ce contexte homéostatique, les plasmatocytes exercent également un rôle immuno-régulateur non canonique lors de la régénération intestinale. En réponse à des lésions du tissu intestinal, ils sont recrutés localement et sécrètent le facteur de croissance Dpp. Ce signal déclenche la prolifération des cellules souches intestinales, un processus crucial pour la survie de l'organisme lors d'infections aiguës (Ayyaz et al. 2015).

Ces découvertes mettent en lumière l'implication active des hémocytes dans les processus homéostatiques régénératifs, et ouvrent des perspectives de recherche sur leur rôle dans d'autres tissus, comme les muscles du vol, qui sont hautement peuplés par les cellules immunitaires (Sanchez Bosch et al. 2019) et pourraient ainsi bénéficier de leur soutien régénératif.

4. Contribution des hémocytes à l'oxygénation tissulaire

L'oxygénation des tissus chez la *Drosophile* a longtemps été considérée comme exclusivement assurée par le système trachéal. Toutefois, des travaux récents ont révélé que les cellules à cristaux, bien que ne constituant qu'une fraction minoritaire des hémocytes, jouent un rôle proactif dans ce processus. En particulier, ces cellules contribuent au transport de l'oxygène en facilitant l'oxydation de la pro-phénoloxydase 2 (PPO2) via un mécanisme de transition de phase protéique. L'importance physiologique de cette fonction a été montrée par l'observation de phénotypes

d’hypoxie chez des larves dépourvues de cellules à cristaux, de PPO2, ou exprimant une forme mutée de cette enzyme (Shin et al. 2024).

Ce rôle des hémocytes dans l’oxygénation a, jusqu’à présent, été documenté uniquement au stade larvaire. Cependant, nos propres observations ont mis en évidence la présence systématique de cellules immunitaires localisées à proximité des structures trachéales dans les muscles du vol de l’adulte (Voir section Résultats Figure 2). Cette distribution spatiale soulève une interrogation fondamentale : Cette proximité morphologique pourrait-elle suggérer une interaction fonctionnelle entre hémocytes et système trachéal au-delà du stade larvaire ?

5. Synthèse des protéines de la matrice extra-cellulaire

Le rôle des hémocytes dans le développement de la *Drosophile* s’exerce notamment à travers leur contribution active à la morphogenèse et à l’organisation tissulaire, via la production d’une grande diversité de composants de la ECM. Ces cellules sécrètent des protéines structurales essentielles telles que Peroxidasin (Pxn), Papiline, Haemolectine (Hml), Laminine**,** ainsi que les deux sous-unités du collagène de type IV : Viking (Vkg) et Cg25C (Shahab et al. 2015; Martinek et al. 2008; Nelson et al. 1994). Un exemple illustratif est leur rôle dans la morphogenèse des tubules rénaux antérieurs, où les hémocytes déposent du collagène IV dans la ECM entourant les tubules en développement. Ce dépôt est crucial pour l’orientation correcte de la croissance cellulaire et l’allongement des structures tubulaires (Bunt et al. 2010). En plus des composants structuraux, les hémocytes sécrètent des protéines chaperonnes comme la glycoprotéine SPARC (Secreted Protein Acidic and Rich in Cysteine), indispensable à la stabilisation et à l’intégration du collagène IV dans la lame basale. L'inhibition spécifique de SPARC dans les hémocytes perturbe l'assemblage de la ECM, provoquant des défauts morphogénétiques sévères et une létalité embryonnaire (Martinek et al. 2008).

Une fonction similaire a été identifiée dans un contexte adulte, au sein des niches de cellules souches. Il a en effet été montré qu’un sous-ensemble spécifique de plasmatocytes, appelés « plasmatocytes compagnons », s’associe aux ovaires dès les stades larvaires et persiste à l’âge adulte. Ces cellules expriment activement du collagène de type IV et contribuent directement à la formation de la membrane basale

entourant la niche des cellules souches germinales. L'ablation spécifique de ces plasmatocytes compagnons, ou l'inhibition ciblée de la production de collagène IV entraîne une désorganisation de la niche et une accumulation anormale de cellules souches germinales chez l'adulte (Van De Bor et al. 2015). À ce jour, cette étude constitue la seule preuve fonctionnelle du rôle direct des hémocytes dans la production de ECM dans un tissu adulte. En dehors de l'ovaire, cette fonction reste encore largement inexplorée dans les autres organes adultes, soulignant l'intérêt d'investigations futures. À noter que jusqu'en 2015, aucune autre étude n'a montré de manière aussi claire cette fonction matricielle des hémocytes adultes.

Comme évoqué précédemment, les IFMs figurent parmi les tissus les plus densément colonisés par les hémocytes (Sanchez Bosch et al. 2019). Ce tissu est également caractérisé par des fibres musculaires enveloppées d'une membrane basale particulièrement riche en composants de la ECM, dont l'intégrité est cruciale pour la stabilité et la fonction musculaire (Zhao et al. 2025). Dans ce contexte, une question centrale émerge : La présence massive de cellules immunitaires dans ce tissu est-elle uniquement liée à leur rôle de sentinelles, ou reflète-t-elle également une implication active dans la synthèse, le maintien ou le remodelage de la ECM ? J'ai abordé cette hypothèse au cours de ma thèse, et j'ai pu proposer de nouvelles perspectives quant à la participation des hémocytes à l'homéostasie structurelle des muscles adultes (Voir section Résultats).

Chapitre IV. Le système trachéal de la *Drosophile* : Développement et Fonctions

Les muscles du vol de la *Drosophile* présentent une activité métabolique exceptionnellement élevée, estimée à environ dix fois celle des muscles squelettiques humains (Chatterjee et Perrimon 2021). Cette exigence énergétique, directement liée à l'intensité du vol, impose une production continue d'ATP et donc une consommation rapide d'oxygène. Contrairement aux vertébrés, la *Drosophile* ne possède pas de système circulatoire spécialisé pour le transport de l'oxygène. Elle repose plutôt sur un réseau trachéal finement ramifié, qui permet une diffusion directe d'oxygène de l'air ambiant vers les cellules (Hayashi et Kondo, 2018). Le système trachéal a été décrit pour la première fois par Wigglesworth en 1930, dans plusieurs insectes dont le moustique de la fièvre jaune *Aedes aegypti* (« A Theory of Tracheal Respiration in Insects » 1930), mais c'est chez la *Drosophile* qu'il a par la suite été le plus étudié et caractérisé (Ghabrial et al. 2003).

Si les mécanismes du développement trachéal ont été largement explorés au cours de l'embryogenèse, le rôle de ce réseau dans le maintien de l'activité physiologique des tissus adultes, en particulier en réponse aux dommages, reste étonnamment peu documenté. Or, l'oxygénation des muscles du vol via la trachée constitue très probablement un paramètre clé de leur réponse au stress ou aux dommages (Voir section Résultats). **Dans ce chapitre, nous décrirons les principales étapes de la formation du système trachéal, ainsi que ses fonctions physiologiques.**

A. Organisation cellulaire du système trachéal

La trachée forme un réseau ramifié de conduits qui transportent l'air depuis les ouvertures externes, appelées spiracles, jusqu'aux structures terminales, les trachéoles ou cellules terminales (TTCs*,*Terminal Tracheal Cells) (Ghabrial et al. 2003). Les plus gros conduits, appelés troncs dorsaux, s'étendent longitudinalement le long du corps et sont reliés entre eux par des branches transversales. De ces troncs primaires émergent des branches secondaires -dorsales, latérales, viscérales et ganglionnaires- qui desservent des régions spécifiques telles que les muscles, le système nerveux ou l'intestin. Ces branches se terminent par des TTCs, en contact direct avec les cellules des tissus environnants et assurent les échanges gazeux

directs : l'oxygène diffuse vers les cellules, tandis que le dioxyde de carbone est expulsé vers l'extérieur (Affolter et Caussinus 2008) **(Figure13)**.

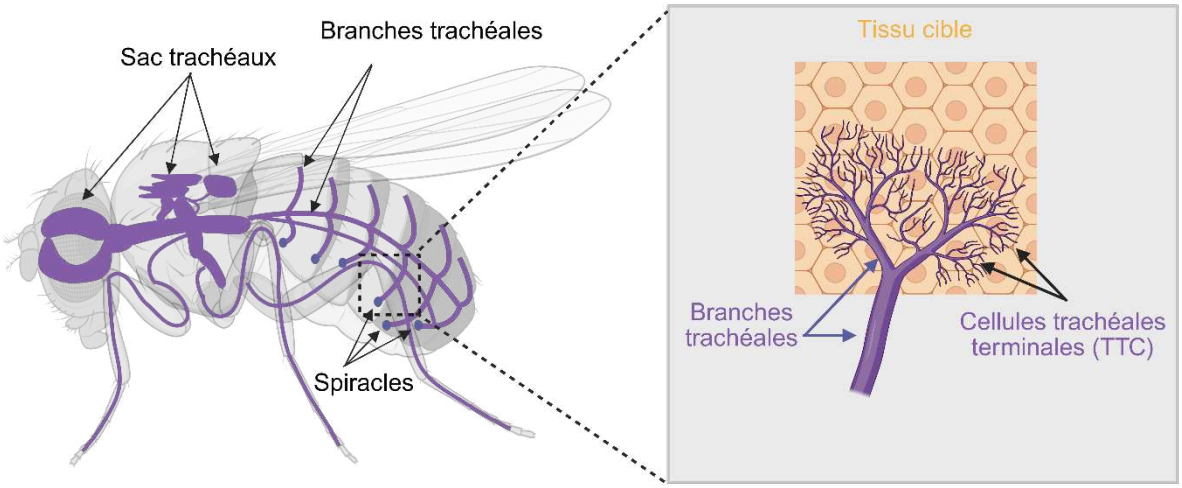

Figure 13. Organisation structurale du système trachéal chez la *Drosophile*. Le schéma de gauche représente l'architecture générale du système respiratoire trachéal adulte (en violet). L'air pénètre les spiracles, situés sur la cuticule. Les spiracles sont connectés à un réseau de branches trachéales tubulaires ramifiées dans tout le corps et assurent l'apport direct d'oxygène aux tissus. Certaines de ces branches sont reliées à des sacs trachéaux, jouant un rôle de réservoir. L'encadré de droite illustre un agrandissement d'une branche trachéale (en violet) au niveau d'un tissu cible (en jaune). Chaque branche principale se subdivise en ramifications de plus en plus fines jusqu'aux cellules trachéales terminales (TTC). Ces cellules émettent de nombreuses protrusions cytoplasmiques qui s'infiltrent profondément entre les cellules du tissu.

Chaque trachée est formée d'un épithélium monostratifié composé de cellules polarisées. La face apicale de ces cellules sécrète une fine cuticule interne, la matrice extracellulaire apicale (ECMa), qui tapisse entièrement la lumière trachéale. Cette ECMa confère au conduit sa rigidité mécanique et son imperméabilité, garantissant ainsi un flux d'air continu (Luschnig et al. 2006). La face basale repose sur une lame basale constituée de matrice extracellulaire basale (ECMb), en contact direct avec les tissus adjacents. Cette ECMb soutient l'architecture épithéliale et permet les échanges avec l'environnement tissulaire. Latéralement, la membrane plasmique des cellules trachéales est organisée en trois domaines distincts suivant un gradient apico-basal : la région sub-apicale (RSA), la jonction adhérente (JA) et la jonction septée (JS). Ces structures sont indispensables au maintien de l'intégrité de la barrière épithéliale, à la cohésion du tissu et au contrôle de la morphologie ainsi que de la position des branches trachéales (Nelson et al. 2010; Wang et al. 2006) (**Figure14**).

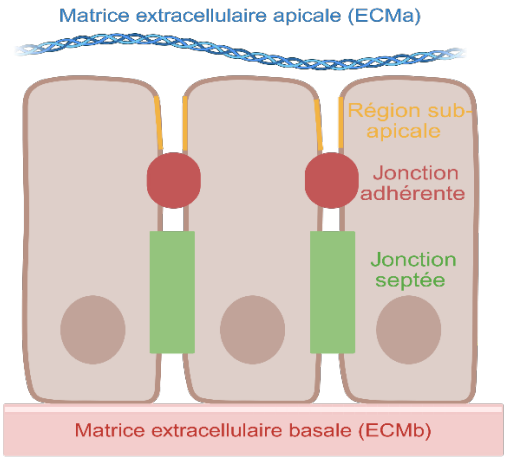

Figure 14. Les cellules épithéliales trachéales de la *Drosophile*. Schéma représentant la structure typique d'une cellule épithéliale trachéale : une région subapicale (jaune) avec jonctions adhérentes (rouge) et jonctions septées (vert). La cellule est en contact apicalement et basalement avec la matrice extracellulaire (ECM-a, et ECM-b respectivement).

B. Mise en place du système trachéal au cours de l'embryogenèse

La formation du système trachéal débute aux alentours du stade 10 du développement embryonnaire et se poursuit jusqu'au stade 17 environ. Ce processus progresse selon une série d'étapes successives, chacune mobilisant des mécanismes génétiques, cellulaires et moléculaires spécifiques. Néanmoins, ces étapes sont génétiquement coordonnées, les gènes impliqués dans la réalisation d'un événement morphologique donné participent également à la régulation des gènes requis pour l'étape suivante (Hayashi et Kondo 2018) **(Figure 15)**.

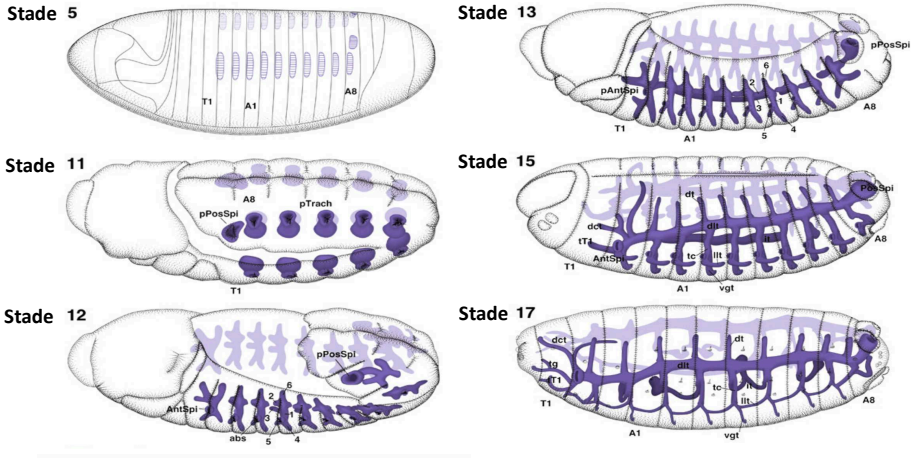

Figure 15. Les stades du développement embryonnaire du système trachéal. Vue latérale du développement trachéal (en violet) chez l'embryon de *Drosophila*. Au stade 11, les placodes trachéales sont visibles de part et d'autre de l'embryon. Au stade 12, les cellules trachéales commencent à migrer dans différentes directions et forment des structures digitiformes appelées branches primaires. Au stade 15, les troncs dorsaux antérieurs et postérieurs de métamères adjacents fusionnent pour former un tronc dorsal continu. Enfin, au stade 17, les branches terminales émergent des branches trachéales interconnectées et se déploient à travers les tissus cibles.

1. Spécification et invagination des placodes trachéales

Aux premiers stades de l'embryogenèse, vingt groupes de cellules ectodermiques, organisés de manière bilatérale et appelés placodes trachéales, sont spécifiés entre le deuxième segment thoracique (T2) et le huitième segment abdominal (A8) (Wilk et al. 1996). La spécification de cette identité cellulaire repose sur l'activation précoce et coordonnée de plusieurs facteurs de transcription. Parmi eux, Trachealess (Trh), un facteur de type bHLH-PAS, constitue le régulateur principal (Wilk et al. 1996). Ventral veinless (Vvl /Drifter), un facteur de type POU, agit en synergie avec Trh pour initier le programme génétique trachéal. L'inactivation de l'un ou l'autre de ces gènes conduit à une absence complète de formation du système trachéal (Boube et al. 2000; Zelzer et Shilo 2000).

Une fois leur identité établie, les placodes trachéales s'invaginent pour former des poches internes, grâce, en partie, à des modifications de la polarité apico-basale et au remodelage du cytosquelette d'actine et de la myosine (Brodu et Casanova 2006).

2. Migration et formation des branches primaires

Après invagination, les précurseurs trachéaux migrent pour former les six branches primaires classiques : le tronc dorsal antérieur (DTa), le tronc dorsal postérieur (DTp), la branche dorsale (DB), la branche latérale (Lt), le tronc latéral antérieur (LTa) et le tronc latéral postérieur, aussi appelé branche ganglionnaire. Chaque branche suit une trajectoire précise vers une cible tissulaire spécifique : par exemple, la branche dorsale se dirige vers l'épiderme dorsal, la branche viscérale vers l'intestin, et la branche ganglionnaire vers la chaîne nerveuse ventrale (Samakovlis et al. 1996).

La spécification de l'identité de chaque branche ainsi que leur migration dirigée sont régulées par des signaux provenant de leur environnement. Trois voies majeures contrôlent spatio-temporellement ce développement : la voie Dpp, Wg et la voie FGF. Dpp agit de manière branche-spécifique en favorisant la migration des branches dorsales, ventrales, latérales et ganglionnaires (Vincent et al. 1997; Myat et al. 2005; Chen et al. 1998). Wg contrôle la migration du tronc dorsal selon l'axe antéro-postérieur et guide la branche dorsale (Llimargas 2000; Chihara et Hayashi 2000). Toutefois, la voie FGF, via Branchless (Bnl)/ Breathless (Btl), constitue le principal moteur du guidage (Sutherland et al. 1996; Dossenbach et al. 2001).

La formation des branches primaires débute dès le stade 11 de l'embryogenèse, lorsque toutes les cellules trachéales expriment Btl, un récepteur tyrosine kinase de la voie FGF, dont l'expression est régulée par le facteur de transcription Trh (Ohshiro et Saigo 1997). Le ligand correspondant, Bnl, est exprimé localement dans les cellules ectodermiques et mésodermiques proches des ébauches trachéales (Sutherland et al. 1996). Bnl agit comme un facteur chimiotactique, guidant l'extension des branches vers leurs tissus cibles **(Figure 15)**. Son rôle a été confirmé par des expériences d'expression ectopique de *bnl* qui induit la formation de branches supplémentaires aux endroits de surexpression (Sutherland et al. 1996). L'activation de Btl par Bnl déclenche la cascade RAS-ERK, essentielle à la migration cellulaire trachéale (Dossenbach et al. 2001).

Bien que la migration des cellules trachéales soit guidée principalement par des voies de signalisation, en particulier la voie FGF qui oriente leur déplacement, elle dépend également d'une expression spécifique de protéines de surface, notamment des intégrines. Dans le cas des branches viscérales, l'intégrine PS1 (αPS1βPS), exprimée dans les cellules trachéales, est indispensable à leur migration effective le long du mésoderme. En parallèle, l'intégrine PS2 (αPS2βPS), exprimée dans le mésoderme viscéral, fournit l'environnement complémentaire nécessaire à cette interaction. Ainsi, PS1 assure l'adhésion des cellules trachéales à leur substrat, tandis que PS2, exprimée dans le mésoderme, contribue à créer le contexte d'interaction et de reconnaissance permettant une migration dirigée et efficace (Boube et al. 2001).

3. Branchement secondaire et ramification terminale du système trachéal

À l'exception du tronc dorsal (DT), des branches secondaires émergent à l'extrémité de toutes les branches primaires. Ces branches secondaires sont initiées par des cellules spécifiques exprimant le facteur de transcription Pointed (Pnt), dont l'activation est déclenchée par la voie de signalisation Bnl/Btl (Myat et al. 2005).

Dès le stade 16 de l'embryogenèse, le développement trachéal entre dans sa phase finale, dite de « branchement terminal », durant laquelle la majorité des branches secondaires produisent des centaines de branches terminales fines et très ramifiées. Ces branches terminales s'étendent dans tout l'embryon pour assurer un apport direct

en oxygène aux tissus à l'éclosion (Harrison 2009). La formation de ces branches terminales repose sur l'expression du facteur de transcription dSRF (Drosophila Serum Response Factor), induite par le signal Bnl (Affolter et al. 1994; Gervais et Casanova 2011), ainsi qu'une expression restreinte de Btl (Ghabrial et Krasnow 2006a) **(Figure 15)**. En effet, l'expression d'une forme constitutivement active de *btl* dans une cellule suffit à lui conférer le rôle de TTC, capable de guider la migration de la branche associée (Sutherland et al. 1996). Ainsi, la restriction spatiale de l'activité de la voie Bnl-Btl permet la spécification de deux types cellulaires distincts : les TTCs, sensibles à Bnl et migrent activement vers sa source pour initier les ramifications terminales, et les cellules de la tige, qui suivent passivement ces 'leaders' pour former le tube trachéal principal (Caussinus et al. 2008).

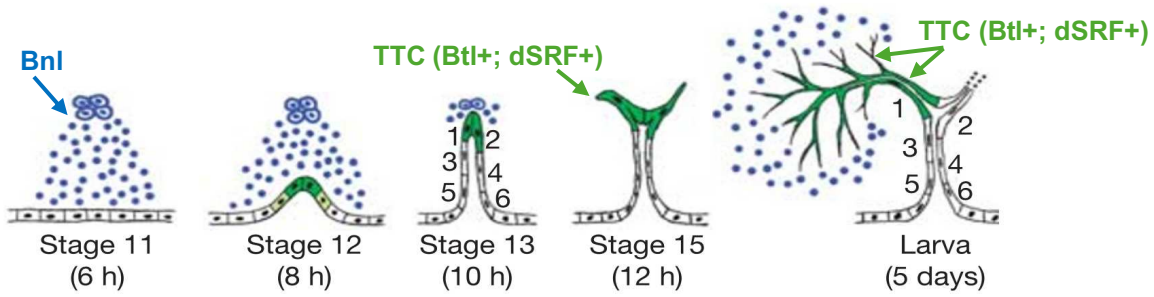

Figure 15. Représentation schématique du bourgeonnement des branches trachéales. Les cellules trachéales (en noire, numérotées de 1 à 6) aux stades et temps de développement indiqués. Les cellules voisines (en bleu) sécrètent Branchless (Bnl) (points bleus), qui active le récepteur Breathless (Btl) sur les cellules trachéales, induisant leur migration et la formation du tube. Le signal Bnl induit également l'expression de gènes de ramification terminale dans certaines cellules (en vert) qui génère des branches terminales en réponse à l'expression de Bnl par les cellules larvaires avoisinantes. Adapté de (Ghabrial et Krasnow 2006b).

Parallèlement, à la fin de l'embryogenèse, alors que la plupart des branches continuent à se ramifier, certaines arrêtent leur croissance pour fusionner avec des branches voisines, assurant ainsi l'interconnexion du réseau respiratoire. Ce processus de fusion est orchestré par une cellule spécialisée à l'extrémité de chaque branche, appelée cellule de fusion. Sa sélection et spécification résultent d'une interaction complexe entre les voies de signalisation Wg, Bnl-Btl, Dpp et Notch (Llimargas 2000; Ikeya et Hayashi 1999; Steneberg et al. 1999; Llimargas 1999). Bnl et Wg, exprimés localement dans les tissus environnants, induisent l'expression du facteur de transcription Escargot, essentiel à l'identité des cellules de fusion,

notamment par l'activation de *Shotgun*, qui code pour l'E-cadhérine, afin d'établir des contacts adhésifs efficaces et garantir la continuité du réseau tubulaire (Jiang et Crews 2006; 2003).

4. Maturation du système trachéal

Avant l'éclosion larvaire, les tubes trachéaux entament une phase de maturation fonctionnelle, indispensable pour transformer les structures primitives en tubes opérationnels, caractérisés par une lumière continue adaptée aux échanges gazeux.

Afin d'assurer une distribution efficace d'oxygène, chaque tube trachéal doit atteindre une longueur et un diamètre précis, régulés par des mécanismes distincts et coordonnés. L'expansion du diamètre dépend notamment de la sécrétion apicale de composants extracellulaires, en particulier la Chitine (Tonning et al. 2005). Cette protéine agit comme un échafaudage provisoire, assurant un arrangement régulier des branches trachéales, avant d'être dégradée par les chitine-désacétylases Serpentine et Vermiform. Des mutations affectants la synthèse ou l'assemblage de la Chitine conduisent à des tubes trachéaux de diamètre et de longueur irréguliers (Öztürk-Çolak et al. 2018).

C. Développement et mise en place du système trachéo-musculaire adulte

1. L'émergence des précurseurs des sacs trachéaux adultes (Air Sac Precursors, ASPs)

Après l'éclosion larvaire, la trachée, déjà fonctionnelle, poursuit sa croissance par la ramification des TTCs, qui étendent leurs filopodes vers les tissus environnants sous le contrôle de la voie de signalisation Bnl-Btl (Jarecki et al. 1999). Parallèlement à cette expansion fonctionnelle, une population de cellules souches trachéales, appelées trachéoblastes, dérivées de l'embryogenèse et résidant dans certains segments thoraciques et abdominaux, s'activent au stade larvaire L3, prolifèrent et se différencient en tubes trachéaux adultes lors de la métamorphose (Pitsouli et Perrimon 2010).

Parmi ces cellules, les précurseurs des sac trachéaux adultes (ASPs) émergent sous forme de bourgeonnement latéral à partir des trachées larvaires du deuxième métamère trachéal (T2), en connexion avec le disque imaginal de l'aile (Sato et Kornberg 2002; Guha et Kornberg 2005) **(Figure 16)**. Le bourgeonnement des ASPs est déclenché en réponse à Bnl, produit par l'épithélium du disque imaginal

d'aile. Dans ces cellules et avant son export, Bnl subit une maturation intracellulaire médiée par la protéine convertase Furin1 (Sohr et al. 2019), indispensable à la ramification des ASPs. Chez les mutants Furin1, les ASPs apparaissent plus petits et peu ramifiés. Seule la forme mature de Bnl est transportée vers l'ASP via les cytonèmes, de fines protrusions membranaires riches en actines et exprimant le récepteur Btl. Dans ce système, les cellules du disque et celles de l'ASP projettent chacune des cytonèmes porteurs de Bnl ou Btl. La liaison spécifique Bnl-Btl constitut un mécanisme de reconnaissance et déclenche des réponses bidirectionnelles (Du et al. 2022). Des analyses à haute résolution ont révélé que les cytonèmes de l'ASP et ceux du disque imaginal établissent des contacts étroits dans la zone source de Bnl (Wood et al. 2021). Une fois lié à son récepteur, Bnl est libéré de la cellule source, assurant un transfert spatialement restreint du signal (Du et al. 2022). Ce mécanisme illustre le rôle central des cytonèmes comme vecteurs de transport et de réception du facteur Bnl.

L'activation de cette voie de signalisation, stimule non seulement la division et la migration des ASPs en induisant la formation d'extensions filopodiales (Sato et Kornberg 2002), mais induit également la production du ligand Vein, qui favorise la prolifération et la survie des ASPs (Cruz et al. 2015; Cabernard et Affolter 2005), qui persistent à travers la métamorphose et constituent les précurseurs spécialisés des sacs trachéaux thoraciques indispensables au vol (Sato et Kornberg 2002; Guha et Kornberg 2005).

2. L'invasion trachéale de muscle du vol

Au cours de la métamorphose, la majorité des cellules trachéales larvaires dégénèrent, à l'exception des ASPs, qui se connectent au réseau trachéal principal et se développent en sacs trachéaux thoraciques adultes alimentant en oxygène les IFMs (Guha et Kornberg 2005). Par la suite, ces sacs trachéaux émettent des ramifications trachéales qui envahissent progressivement les IFMs en développement. Cette invasion trachéale est également régulée par la voie Bnl/Btl. Dans ce système, Bnl agit comme un chemoattractant, guidant les branches trachéales non seulement à l'échelle tissulaire, vers les muscles, mais aussi à une échelle subcellulaire, à travers des microdomaines spécifiques (Peterson et Krasnow 2015) **(Figure 16)**. En effet, Bnl est exprimé initialement de manière diffuse à la surface des fibres musculaires. Par la suite, au moment de l'invasion trachéale, sa

distribution devient restreinte à des structures spécialisées appelées T-tubules, qui sont des invaginations membranaires caractéristiques des muscles. Ces T-tubules forment des 'micro-environnements' qui concentrent localement le signal Bnl afin d'orienter avec précision la croissance des branches terminales trachéales vers l'intérieur des muscles au niveau des T-tubules, ainsi qu'autour de chaque mitochondrie où l'oxygène est utilisé (Peterson et Krasnow 2015). Ces observations illustrent un mécanisme de 'tri intracellulaire' sophistiqué, qui confère à un morphogène diffusible une action localisée et hautement directive. Ce processus connu sous le nom de 'trafic subcellulaire ciblé' assure non seulement une vascularisation efficace, mais permet aussi aux branches trachéales d'atteindre directement les mitochondries, optimisant ainsi l'apport efficace en oxygène.

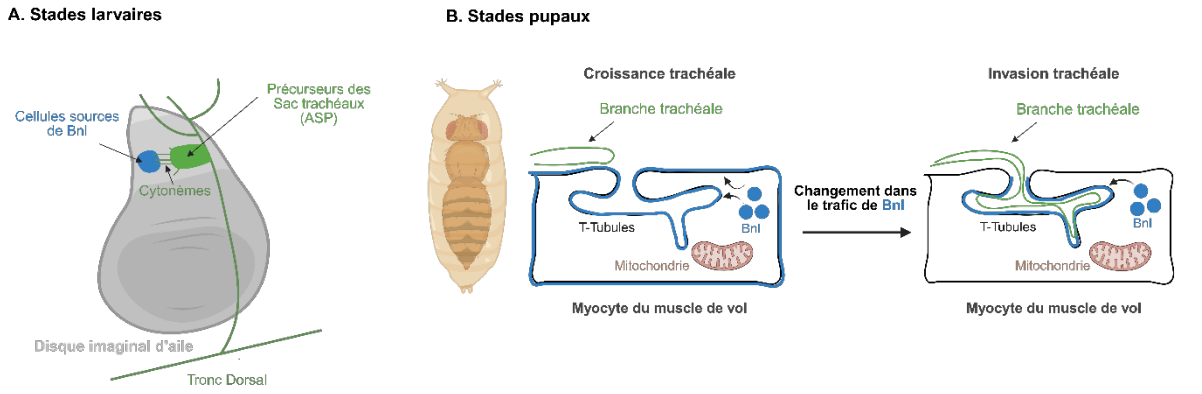

Figure 16. La mise en place du système trachéo-musculaire. A. Au cours du développement larvaire, le système trachéal établit ses bases de formation à partir des précurseurs des sacs trachéaux (ASP, en vert) au niveau de disque imaginal d'aile, et interagissent avec les cellules sources de Brancheless (Bnl, en Bleu) via des cytonèmes afin de former des sacs trachéaux musculaires nécessaires à la respiration chez l'adulte. **B.** Pendant la métamorphose, les branches trachéales issues du primordium trachéal croissent et envahissent progressivement les fibres des muscles de vol en développement. Cette interaction est régulée par la sécrétion du Bnl, produit par les myocytes. Dans un premier temps, les branches trachéales s'orientent vers les fibres musculaires exprimant Bnl à la surface (croissance trachéale). Un changement spatio-temporel dans le trafic intracellulaire de Bnl au sein des myocytes entraîne ensuite une redistribution de ce signal attractif. Ce processus favorise l'invasion trachéale au sein des fibres musculaires, au niveau des tubules en T (T-tubules) à proximité des mitochondries. Cette organisation assure une oxygénation fine et adaptée aux besoins du muscle de vol adulte.

Par ailleurs, cette invasion trachéale dans les IFMs implique également des structures spécialisées situées à l'extrémité des branches trachéales envahissantes, appelées '*growth-cone-like branch tips*' (Sauerwald et al. 2019). Ces structures dynamiques, semblables à des filopodes, jouent un rôle actif dans la pénétration des branches

trachéales dans le tissu musculaire. Un acteur clé dans ce processus est la métalloprotéinase matricielle 1 (MMP1), exprimée par les branches trachéales et facilite leur progression via la dégradation de la protéine matricielle collagène de type IV (Sauerwald et al. 2019).

En conclusion, l'invasion trachéale des IFMs résulte d'une coordination étroite entre la signalisation directionnelle Bnl/Btl (Peterson et Krasnow 2015) et l'activité localisée de MMP1 (Sauerwald et al. 2019), assurant une invasion ciblée et efficace adaptée aux besoins métaboliques des IFMs.

Cependant, si la morphogenèse trachéale au cours du développent musculaire est relativement bien caractérisée, peu de choses sont connues sur la régulation de ce système une fois que la *Drosophile* a atteint le stade adulte. On ignore en grande partie comment les trachées s'adaptent, se maintiennent, ou se renouvellent chez l'adulte, notamment dans des contextes de stress tissulaire tels que le vieillissement ou en réponse aux dommages musculaires.

D. Les fonctions du système trachéal

1. Distribution d'oxygène aux tissus

Comme évoqué précédemment, la fonction principale du système trachéal est d'assurer l'apport en oxygène aux tissus. Les TTCs sont les seules cellules capables de développer de fines extensions cytoplasmiques, permettant une diffusion directe et efficace d'oxygène vers les cellules cibles. Cette capacité morphogénique est régulée par le facteur de transcription dSRF, à la fois marqueur des TTCs et régulateur clé du remodelage cytoplasmique au cours du développement des branches trachéales (Guillemin et al. 1996; Ghabrial et al. 2003).

Au-delà de son rôle dans le transport d'oxygène, le système trachéal est capable de s'adapter aux variations de la disponibilité en oxygène de l'environnement (Centanin et al. 2010). Cette fonction est également assurée par les TTCs qui possèdent la capacité de détecter les variations du taux d'oxygène dans leur environnement et d'y répondre de manière autonome. En effet, l'analyse comparative du développement des branches trachéales sous différentes concentrations d'oxygène a montré que, chez les larves exposées à une hypoxie (5 % d'O_2), les TTCs génèrent un plus grand

nombre de branches, favorisant ainsi une oxygénation optimale des tissus (Jarecki et al. 1999).

En condition d'hypoxie, le ligand Bnl est produit par les cellules hypoxiques et agit comme un signal chimiotactique guidant l'extension des branches terminales déjà existantes vers ces cellules pour apporter localement l'oxygène (Jarecki et al. 1999). Cela soulève toutefois une question fondamentale : Par quels mécanismes les cellules détectent-elles la baisse en oxygène, et comment cette détection déclenche-t-elle l'expression de *bnl* ?

La détection de l'hypoxie repose sur le facteur de transcription Hypoxia-Inducible Factor 1 (HIF-1), dont l'homologue chez la *Drosophile* est Similar (Sima). Ce facteur est considéré comme le régulateur central de la réponse transcriptionnelle à l'hypoxie, dont l'activation entraîne une expansion des TTCs (Henry et Harrison 2004). Chez la *Drosophile*, ce facteur HIF-1 est constitué de deux sous-unités : Sima, l'équivalent de HIF-1α chez les mammifères, et Tango, l'homologue de HIF-1β. En condition normoxique, Sima est rapidement hydroxylée par des prolyl-hydroxylases spécifiques, ce qui entraîne sa dégradation via le système ubiquitine-protéasome. En revanche, en hypoxie, cet hydroxylation est inhibé, permettant ainsi à Sima de s'accumuler, de migrer vers le noyau, puis de s'associer à Tango. Ce complexe actif se fixe alors sur des enhancers de réponse à l'hypoxie (HRE, Hypoxia Response Enhancer), activant ainsi la transcription de gènes cibles impliqués dans l'adaptation aux carences d'oxygène **(Figure 17)**.

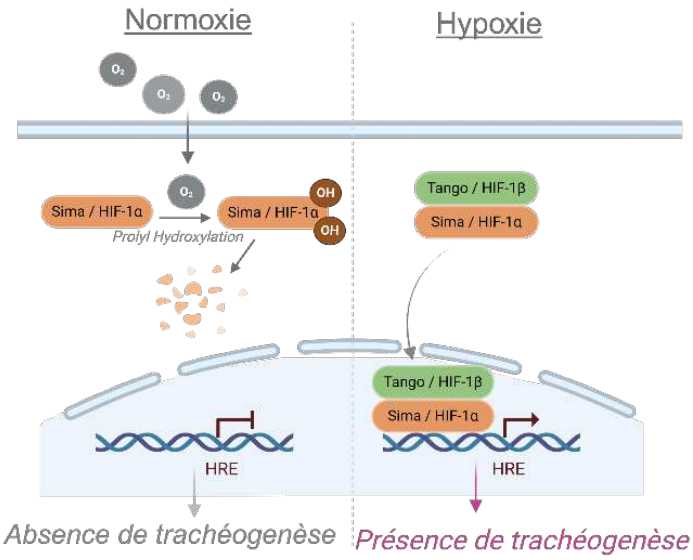

Figure 17. L'activation de Similar (HIF1-α) et son impact sur la trachéogenèse. A gauche, en présence d'oxygène (en normoxie), la sous-unité Sima est hydroxylée au niveau des résidus prolyles par les prolyl-hydroxylases dépendantes d'oxygène. Cette modification marque Sima pour sa dégradation par le protéasome. En conséquence, il ne peut pas se stabiliser ni s'associer à la sous-unité Tango (HIF-1β). L'absence de dimérisation empêche la fixation sur les éléments de réponse à l'hypoxie (HRE, Hypoxia Response Enhancers) au niveau de l'ADN, ce qui bloque l'expression des gènes cibles hypoxie-dépendants. Dans ce contexte, il n'y a pas de trachéogenèse induite. À droite, en condition de faible disponibilité en oxygène (en hypoxie), l'activité des prolyl-hydroxylases est inhibée. La sous-unité Sima échappe alors à l'hydroxylation et à la dégradation, ce qui permet sa stabilisation dans le cytoplasme. Le dimère Sima/HIF-1α–Tango/HIF-1β se fixe sur les HRE présents dans les promoteurs des gènes sensibles à l'hypoxie. Cette activation transcriptionnelle induit l'expression de gènes impliqués dans l'adaptation à l'hypoxie et par conséquent la trachéogenèse.

D'une manière intéressante, l'accumulation de Sima dans les tissus cibles non trachéaux induit l'expression de Bnl, qui s'accumule localement afin de guider l'extension des branches trachéales (Jarecki et al. 1999). En parallèle, dans les cellules trachéales, l'activation de Sima induit l'expression de son récepteur spécifique Btl, le même impliqué dans les étapes précoces du développement trachéal. Cette induction de *btl* en condition hypoxique rend les TTCs plus sensibles au signal Bnl présent dans leur environnement (Centanin et al. 2008). Comme au cours de l'embryogenèse, la liaison de Bnl à son récepteur Btl déclenche des cascades de signalisation intracellulaire qui régulent la migration cellulaire et l'extension des branches (Sutherland et al. 1996).

2. Plasticité nutritionnelle de la trachée : un rôle adaptatif dans l'oxygénation intestinale

Longtemps, le remodelage trachéal induit par l'hypoxie a été considéré comme la seule forme de plasticité de ce système. Cependant, des travaux plus récents ont révélé que la trachée est également capable de s'adapter à l'état nutritionnel de l'organisme (Linneweber et al. 2014). Ainsi, à l'instar de la disponibilité en oxygène, les conditions alimentaires modulent directement la morphologie trachéale : un régime alimentaire riche en calories favorise une ramification accrue de la trachée intestinale, tandis qu'une restriction nutritionnelle entraîne une réduction marquée de la longueur et du nombre de branches. Cette plasticité trachéale précède les ajustements métaboliques, soulignant que la trachée joue un rôle anticipateur**,** en ajustant l'apport en oxygène avant même les réponses métaboliques systémiques. En effet, il a été montré que la réduction de la taille des branches trachéales diminue l'oxygénation intestinale et ralentit le métabolisme global. De manière intéressante, ce remodelage

est contrôlé par des sous-ensembles de neurones sensibles aux nutriments, qui régulent la ramification trachéale via la voie de signalisation de l'insuline, établissant un lien direct entre nutrition, oxygénation intestinale et métabolisme (Linneweber et al. 2014).

3. Rôle structural de la trachée embryonnaire dans le guidage axonal

Avant d'être impliquée dans la respiration, la trachée joue, chez l'embryon, un rôle de support structurel. Elle agit comme un endosquelette contribuant au développement correct des axones sensoriels. Chez le mutant *trh*, dépourvu de système trachéal, la majorité des nerfs sensoriels se forment normalement, mais leur croissance est ralentie et leur morphologie altérée. Ces observations soulignent l'importance de la trachée dans le guidage axonal au cours du développement embryonnaire (Younossi-Hartenstein et Hartenstein 1993).

4. Production des peptides anti-microbiens

a) Fonction anti-infections

Le système trachéal constitue une porte d'entrée potentielle pour divers microbes. Afin de se protéger contre la pénétration des pathogènes, il a développé des réponses immunitaires locales particulièrement efficaces. Chez la *Drosophile*, l'immunité innée trachéale se distingue de l'immunité systémique assurée par les hémocytes. Le système immunitaire systémique détecte les PAMPs via deux voies parallèles : la voie Toll et la voie Imd (Voir chapitre 3). Dans la trachée, la signalisation Toll est généralement inactive, de sorte que l'immunité trachéale repose essentiellement sur la voie Imd (Buchon et al. 2014b). L'activation de cette voie dans le système trachéal déclenche une réponse antimicrobienne particulièrement efficace, principalement médiée par l'expression de gènes codant pour des AMPs (Akhouayri et al. 2011).

b) Fonction anti-tumorale

Au-delà de leur rôle dans la défense antimicrobienne, les AMPs produits par la trachée - en particulier la Défensine - participent activement à l'élimination des cellules tumorales (Parvy et al. 2019). L'induction de cette réponse repose sur l'activation du facteur de nécrose tumorale (TNF, Tumor Necrosis Factor), sécrété par les hémocytes. Le TNF est indispensable à l'exposition de la phosphatidylsérine à la surface des cellules tumorales, rendant celles-ci sensibles à l'action de la Défensine.

Cette dernière se fixe préférentiellement aux membranes enrichies en phosphatidylsérine, induisant la mort des cellules tumorales. Ces résultats mettent en évidence une coopération fonctionnelle entre la trachée et les hémocytes dans la surveillance antitumorale, et soulèvent la possibilité d'une contribution similaire dans d'autres contextes physiologiques, tels que le maintien de l'homéostasie tissulaire après une lésion.

5. Rôle dans la réparation tissulaire

Deux études récentes publiées dans le même journal (Tamamouna et al. 2021; Perochon et al. 2021) ont mis en évidence un rôle de la trachée dans la régénération de l'intestin adulte. Ces travaux montrent qu'à la suite de lésions intestinales, les TTCs subissent une réorganisation morphologique, caractérisée par un allongement et une augmentation de leurs ramifications. Ce remodelage est induit par les ROS produites par l'épithélium lésé, lesquelles activent le facteur HIF-1α/Sima dans les TTCs et déclenchent une signalisation bidirectionnelle Bnl-Btl entre l'intestin et la trachée. Ce remodelage trachéal est nécessaire à la prolifération des cellules souches intestinales, assurant ainsi la réparation du tissu endommagé. Ces résultats suggèrent que la trachée adulte constitue un acteur dynamique, capable de détecter et de répondre aux signaux tissulaires pour soutenir la régénération.

Ces travaux ont largement contribué à la conception de mon projet de recherche. Je me suis donc demandée si le remodelage trachéal est limité à l'intestin, ou pourrait-il également se produire dans d'autres tissus adultes, tels que les IFMs ? Par ailleurs, il a été montré que dans l'intestin adulte, la trachée constitue une niche essentielle pour la régulation des cellules souches intestinales (Perochon et al. 2021), tandis que dans les IFMs, elle sert de réservoir pour les hémocytes (Sanchez Bosch et al. 2019). Ces observations m'ont conduit à formuler l'hypothèse qu'un dialogue fonctionnel pourrait exister entre les hémocytes et les cellules trachéales dans le muscle du vol, analogue à celui observé entre la trachée et les cellules souches intestinales. L'analyse d'une telle interaction dans un tissu aussi métaboliquement actif que le muscle de vol pourrait apporter des informations clés sur le dialogue multicellulaire en réponse aux blessures.

II. Résultats

Article 1. Immune–tracheal intercellular signalling coordinates the muscle injury response in *Drosophila*

Nourhene Ammar, Olivier Josse, Aurélien Guillou, Jessica Perochon, Hadi Boukhatmi (BioRvix 2025, DOI : https://doi.org/10.1101/2025.06.25.661466)

Dans cet article, nous avons étudié la réponse des muscles du vol de la drosophile aux dommages. Nous montrons que ce processus repose sur une coordination multicellulaire impliquant les cellules immunitaires, la trachée et les fibres musculaires elles-mêmes. Les cellules immunitaires occupent une position centrale : elles reconnaissent les fibres lésées et sécrètent des molécules qui permettent à la fois d'attirer le système respiratoire vers la zone endommagée et de consolider le muscle grâce à la production de composants de la matrice extracellulaire.

Bien que les muscles du vol de la drosophile émergent comme un modèle pertinent pour l'étude de la réparation musculaire, aucun marqueur de lésion n'avait été décrit jusqu'à présent. Dans ce travail, nous identifions la myosine lourde (MHC) comme un marqueur inédit des fibres endommagées. En effet, nous montrons que la MHC est systématiquement surexprimée dans les fibres lésées, ce qui permet de les distinguer de manière fiable des fibres intactes **(Figures 1 et S1)**. En utilisant différentes lignées exprimant la GFP fusionnée à des isoformes de la MHC, nous avons pu identifier l'isoforme spécifique associée à cette réponse aux dommages.

Nous avons ensuite montré que les plasmatocytes réagissent rapidement à la lésion musculaire. Dès les premières heures suivant le dommage, ces cellules sont capables d'identifier la fibre endommagée et d'en recouvrir l'ensemble de sa surface. Leur présence et leur dynamique de recrutement ont été mises en évidence grâce à différents marqueurs spécifiques des plasmatocytes, incluant Zfh1, Pxn et Hml **(Figure 1)** Parallèlement, nous avons observé que, dans des conditions normales, les cellules immunitaires sont fréquemment associées au réseau trachéal dans le tissu musculaire. Cette proximité a soulevé deux questions majeures : (1) **La trachée répond-elle aux lésions par une modification de sa plasticité ?** (2) **Existe-t-il une coordination fonctionnelle entre cellules immunitaires et cellules trachéales dans ce processus ?** Nos analyses, basées sur l'utilisation de différents marqueurs fluorescents de la trachée, ont révélé que ce tissu répond effectivement aux

dommages en remodelant ses branches pour enrichir les muscles lésés **(Figure 2)**. De plus, nous avons montré que ce recrutement trachéal dépend de l'action des plasmatocytes. En effet, ces derniers recouvrent la fibre endommagée et y déposent la protéine Branchless (Bnl), ligand du récepteur FGF/FGFR. L'activation de Btl, exprimé à la surface des cellules trachéales, déclenche alors leur remodelage et enrichissement sur la fibre blessée **(Figures 4 et 5).** Nous avons également montré, à l'aide de rapporteurs spécifiques, que les fibres musculaires lésées présentent un état d'hypoxie **(Figure 3)**. Cette observation suggère que le recrutement trachéal est indispensable pour rétablir un apport adéquat en oxygène et préserver la viabilité du muscle endommagé.

Nous nous sommes ensuite interrogés sur la reconstruction de la matrice extracellulaire (MEC) suite aux dommages. Nos résultats montrent que le collagène est effectivement surexprimé dans les fibres endommagées. La stabilisation du collagène dans la MEC nécessite des protéines chaperonnes, telles que SPARC. Nous avons observé une colocalisation du collagène et de SPARC dans les muscles lésés, et montré que la stabilisation du collagène dépend de SPARC, puisque la perte de fonction de cette protéine empêche son dépôt. Nous avons également identifié que ces protéines de la MEC sont spécifiquement produites par les plasmatocytes **(Figure 6)**.

En conclusion, l'ensemble des résultats présentés dans cet article révèle que la réponse musculaire aux lésions repose sur une coordination multicellulaire, où les cellules immunitaires agissent comme des médiateurs centraux, intégrant à la fois des fonctions de signalisation et de soutien structurel, afin de favoriser le maintien des muscles.

Title: Immune–tracheal intercellular signalling coordinates the muscle injury response in *Drosophila*

Authors: Nourhene Ammar[1], Olivier Josse[1], Aurélien Guillou[1], Jessica Perochon[2] and Hadi Boukhatmi[1]*

[1] Institut de Génétique et Développement de Rennes (IGDR), Université de Rennes, CNRS UMR6290, Rennes, France.

[2] Institute of Cancer Sciences−University of Glasgow, Wolfson Wohl Cancer Research Centre, Glasgow, UK.

* Corresponding author: hadi.boukhatmi@univ-rennes.fr

Summary

Effective tissue adaptation to damage requires precise coordination among diverse cell types. In skeletal muscle, injury-responsive cells play a pivotal role in repair, yet the molecular and cellular mechanisms governing their coordinated activity remain incompletely understood. Here, we identify adult *Drosophila* immune cells-hemocytes-as key mediators of the muscle injury response. Following damage, hemocytes are rapidly recruited to affected fibers, where they perform dual functions. First, they promote tracheal (respiratory cell) branching by depositing the FGF ligand Branchless (Bnl) along damaged muscle, which activates its receptor, FGFR/Breathless (Btl), on tracheal cells, stimulating their outgrowth toward the injury and supporting oxygen delivery. Second, hemocytes contribute to structural stabilization by supplying key extracellular matrix (ECM) components, including SPARC and Collagen IV, to the damaged fiber. Together, these findings uncover a coordinated injury response in which immune cells act as central mediators of metabolic and structural adaptation in response to damage.

Introduction

Effective tissue repair relies on a complex interplay requiring precise communication and coordination between cells across multiple tissues and organ systems (Sun and Poss, 2023). Disruption of these interactions can impair regeneration and, in severe cases, threaten organismal survival (Li et al., 2016). In mammals, skeletal muscle regeneration, in particular, depends on a tightly orchestrated collaboration among various cell types, including macrophages, muscle stem cells (MuSCs, also known as satellite cells), and fibro/adipogenic progenitors (FAPs) (Relaix et al., 2021). For example, following muscle injury, macrophages signal to MuSCs to regulate their proliferation and subsequent differentiation to restore damaged muscle fibers (Dort et al., 2019). Simultaneously, the vascular system is mobilized to meet increased metabolic demands and to support the structural remodelling of damaged tissue (Eming et al., 2014). Despite these insights, the signalling events that coordinate cellular recruitment and tissue adaptation in response to muscle damage remains poorly understood.

Like many organisms in the wild, *Drosophila* frequently encounters natural wounding, requiring efficient tissue adaptation mechanisms to maintain function and ensure survival (Subasi et al., 2024). *Drosophila* has long served as a powerful model for studying myogenesis (Laurichesse and Soler, 2020), and more recently, it has emerged as an effective system for investigating adult muscle response to injury (Boukhatmi, 2021; Catalani et al., 2022; Chaturvedi et al., 2017; Goh et al., 2024; Gunage et al., 2017). Although much attention has focused on the role of *Drosophila* MuSCs in regeneration, relatively little is known about how other cell types contribute to muscle adaptation to damage. In particular, the contribution of the immune blood cells-hemocytes-remains largely unexplored. Despite limited hematopoiesis in adults, hemocytes are essential for detecting and responding to bacterial infections (Sanchez Bosch et al., 2019). Approximately 85% of adult hemocytes are plasmatocytes, macrophage-like cells that are distributed throughout the body (Boulet et al., 2021). Studies, including our own, have shown that they can populate the indirect flight muscles (IFMs) under normal conditions (Boukhatmi and Bray, 2018; Sanchez Bosch et al., 2019). However, whether these immune cells engage in active intercellular signalling following muscle damage, and how they coordinate with other cell types, remains an open question.

The tracheal cells -a network of air-filled tubes that functions analogously to the vertebrate vascular and respiratory systems- enwrap and penetrate muscle fibers to oxygenate them (Sauerwald et al., 2019). These connections are established during development through the Branchless (Bnl) FGF pathway (Peterson and Krasnow, 2015). The *Drosophila* FGF ligand Branchless (Bnl), produced by muscle cells, directs tracheal migration by activating the Breathless (Btl) receptor on tracheal cells. For decades, tracheal branching has been well characterized at the morphological, cellular, and genetic levels during *Drosophila* development (Ebner et al., 2002; Ghabrial et al., 2003; Hayashi and Kondo, 2018; Rao et al., 2015). More recently, it has been shown that the adult trachea also undergoes dynamic remodelling to sustain adult gut regeneration (Perochon et al., 2021; Tamamouna et al., 2021), raising the possibility that similar remodelling could contribute to muscle responses following injury. In addition, hemocytes have been shown to closely associate with adult tracheal cells (Sanchez Bosch et al., 2019). However, whether hemocytes and tracheal cells cooperate to mediate a coordinated response to muscle damage remains to be studied.

In this study, we investigated how intercellular communication between muscles, hemocytes, and tracheal cells coordinates the response to muscle injury in adult *Drosophila*. We found that both physical and genetically induced muscle damage trigger the immediate and sustained recruitment of hemocytes to injured fibers. This recruitment is essential for directing tracheal remodeling via Bnl/Btl signaling, enabling the selective identification of damaged fibers over intact ones. Beyond their role in tracheal guidance, hemocytes also contribute to muscle maintenance and repair by producing extracellular matrix (ECM) components. Together, these findings reveal a coordinated injury response in which immune cells act not merely as passive responders, but as central mediators of both signaling and structural adaptation during the early stages of muscle recovery.

Results

Hemocytes are specifically recruited to the injured adult flight muscle

Although *Drosophila* is one model organism for studying muscle repair, it lacks molecular markers that reliably and specifically identify injured muscle fibers. In vertebrates, the re-expression of embryonic myosin heavy chain (MyHC-emb) in damaged fibers is a common marker of muscle injury and regeneration (Murphy et al., 2011). To assess whether Myosin Heavy Chain (Mhc) expression could similarly serve as an indicator of muscle damage in *Drosophila*, we analysed its expression following injury. Our results show that Mhc expression is drastically upregulated in injured muscles and inversely correlated with the downregulation of *Mef2*, providing a robust molecular readout of muscle damage (Figure 1 A-F and G; Figure S1 A-B''). This upregulation persists for at least 20 days post-injury (DPI) (Figure S2 E-N). In *Drosophila*, several Mhc isoforms are generated via alternative splicing of a single *Mhc* gene (Orfanos and Sparrow, 2013). To determine which isoform respond to injury, we analysed the expression of various GFP-tagged Mhc isoforms (Orfanos and Sparrow, 2013; Sarov et al., 2016). Only the shorter adult Mhc isoforms-K, L, and M-were upregulated in response to muscle damage (Figure S1 C-E). To rule out the possibility that Mhc upregulation is an artifact of the injury method used, we examined its expression in *Naa30* mutants, which exhibit developmental defects in flight muscles and spontaneous muscle detachment in eight-day-old adults, along with loss of nuclear *Mef2* expression (Varland et al., 2023). In these mutants, Mhc upregulation coincided with *Mef2* downregulation (Figure 1 I-J'''; Figure S1 F-G''), further supporting Mhc as a reliable marker of muscle damage in *Drosophila*.

To study the hemocytes response to IFMs damage, we started by tracking these cells at various time points after injury using the hemocytes reporters Peroxidasin (*Pxn*) (Figure 1 A-C'') and Hemolectin (*Hml*) (Figure S1 H-I'). Co staining for these markers and Mhc revealed extensive recruitment of hemocytes to the injured muscle fibers (Figure 1 A-C'; Figure S1 H-I'). Notably, while Pxn+ hemocytes persist at the injured muscle for at least 5 DPI, Hml+ hemocytes enrichment declines over time (Figure 1 H'), highlighting the heterogeneity of the adult hemocyte population, consistent with previous findings (Boulet et al., 2021). To further characterize the hemocytes

recruitment dynamics, we examined the transcription factor Zfh1 and its reporter (*Enh3-Gal4 > UAS-mCD8GFP*), another hemocytes marker (Boukhatmi and Bray, 2018; Wu et al., 2019) (Figure 1 D-F''; Figure S2 A-B'). Enh3+ hemocytes exhibited recruitment kinetics similar to Pxn+ cells (Figure 1 H'). Importantly, at 5 DPI all Pxn+ cells were also Enh3+, whereas only a subset of Pxn+ cells were Hml+ (Figure 1 H and Figure S1 H-M'). None of the recruited hemocytes expressed Mef2 (Figure S1 L'-M'). To confirm that hemocytes recruitment is a response to muscle damage, we analyzed *Naa30* mutants. Consistently, we observed a selective recruitment of Enh3+ hemocytes to injured muscle fibers, identified by high Mhc expression and the loss of Mef2 nuclear expression (Figure 1 I-J'''). Altogether, these data show that adult hemocytes are rapidly and specifically recruited to injured muscle fibers, with distinct subpopulations displaying differential persistence over time.

Hemocytes recruitment coordinates with tracheal remodeling following muscle injury

The selective recruitment of hemocytes to damaged fibers suggests a potential role in the muscle damage response. We observed that hemocytes within the indirect flight muscles (IFMs) are closely associated with tracheal cells (Figure 2 A-A'). It has previously been shown that tracheal cells can extend new branches toward damaged regions to support adult gut regeneration (Perochon et al., 2021; Tamamouna et al., 2021). We therefore asked whether tracheal remodelling also occurs in response to IFMs injury and whether it could be functionally linked to hemocyte recruitment. Our analysis revealed that muscle damage, whether caused by physical injury or in *Naa30* mutant animals, leads to a significant increase in tracheal coverage of the injured fiber (Figure 2 B-D and Figure S2 C-D'). The invasion is directed toward the injury site, with the highest branching density near the damaged area and progressively decreasing with distance from the injury (Figure 2 E). We further observed that hemocytes remain spatially close to the tracheal branches, even under injured conditions (Figure 2 C'').

To further investigate the tracheal response to injury, we focused on terminal tracheal cells (TTCs), specialized branches of the tracheal system known for their structural plasticity and ability to invade tissues, including muscle fibers, to deliver oxygen (Ghabrial et al., 2003; Peterson and Krasnow, 2015; Sauerwald et al., 2019). TTCs can be reliably identified by their distinctive morphology and the expression of the

transcription factor Serum Response Factor (dSRF) (Figure 2 F-F' and J-J'). We visualized TTCs by expressing membrane-bound GFP under the control of dSRF-Gal4 (*dSRF-Gal4 > UAS-mCD8GFP*) (Figure 2 G-H'''). We observed a high density of TTCs within injured muscle fibers, with the highest concentration near the injury site (Figure 2 H-H''' and I). Orthogonal views showed that the recruited tracheae are found not only on the muscle surface but also extend branches into the injured fibers (Figure 2 G'''-H'''), consistent with the atypical muscle–tracheal organization optimized to deliver oxygen deep within the muscle, directly to sites of high metabolic demand (Peterson and Krasnow, 2015; Sauerwald et al., 2019). Labelling TTCs nuclei with anti-dSRF confirmed the significant enrichment of dSRF+ nuclei along the injured fibers comparing to the uninjured muscles (Figure 2 K-L'' and M). The tracheal enrichment at the injured muscle results from TTCs branching rather than proliferation, as no PH3+ cells were detected in the muscle trachea cells (Figure 2 K'''-L'''). Altogether, these data indicate that tracheal cells respond to muscle injury and target specifically the damaged fiber.

We found that tracheal remodelling is irreversible, as tracheal enrichment at the injured muscle persists even 20 days post-injury (Figure S2 E-M' and P), a time point when muscle healing is expected to be complete (Catalani et al., 2022; Chaturvedi et al., 2017). A comparison of hemocyte recruitment kinetics with tracheal coverage density revealed that hemocyte recruitment precedes tracheal coverage of the injured fibers (Figure S2 O and P), raising the possibility of an interplay between the two-cell population in supporting the injured muscle fiber.

Tracheal invasion of injured muscle fibers is triggered by local hypoxia

The tracheal recruitment to injured muscle fibers (Figure 2) suggests a critical oxygen demand of the damaged muscle. If this is the case, local hypoxia within injured fibers should serve as a key cue for tracheal attraction and directional growth toward the site of injury, as seen in other physiological contexts (Jarecki et al., 1999). To assess oxygen variations within the injured muscle, we first used the Synthetic HRE (Hypoxia response element) nuclear sensor (SyHREns), a hypoxia reporter that serves as a proxy for evaluating intracellular oxygen fluctuations (Zhao et al., 2024). The SyHREns was found to be expressed in some TTCs, which are identifiable by both their triangular shape and expression of dSRF, in normal conditions (Figure 3 A-A''). Importantly, we

observed a pronounced enrichment of SyHREns-positive cells surrounding injured muscle fibers, in close proximity to the recruited tracheal branches (Figure 3 B-D''). The number of SyHREns+ cells around the injured fibers remained stable for at least 20 DPI (Figure 3 E), indicating that local hypoxia persists in parallel with the sustained tracheal remodelling observed over the same period.

In *Drosophila*, as in mammals, hypoxia-induced tracheogenesis is controlled by the transcription factor Similar (Sima) -the *Drosophila* homolog of hypoxia-inducible factor-1α (HIF-1α)- a central regulator of hypoxic and angiogenic responses (Jarecki et al., 1999)). Accordingly, silencing *sima* in TTCs prevented tracheal expansion towards the injured fibers (Figure 3 F-I). Bnl is a well-established downstream effector of hypoxic signalling, deposited locally on hypoxic tissues to promote tracheal attraction (Jarecki et al., 1999). We therefore hypothesised that if the injured muscle undergoes hypoxia, Bnl should accumulate locally at the damaged fiber to facilitate tracheal remodelling. Analysing the expression of an endogenously tagged *Bnl:GFP^{endo}* allele (Du et al., 2018) revealed marked enrichment of Bnl at injured muscle fibers compared to adjacent intact ones (Figure 3 J-L). Altogether, these data suggest that muscle damage induces local muscle oxygen starvation, which in turn drives tracheal cell recruitment to the injured tissue.

Hemocytes deposit Bnl/FGF at injured muscles to mediate tracheal recruitment

During both embryonic and post-embryonic stages, tracheal guidance is regulated in a dose-dependent manner by local Bnl concentrations (Jarecki et al., 1999). In adult flight muscle development, muscle-tracheal connections are established through the action of Bnl, which is secreted by muscle fibers and acts in a paracrine manner by binding to its receptor, FGFR/Breathless (Btl), expressed on tracheal cells (Peterson and Krasnow, 2015). The observed enrichment of Bnl in injured muscles (Figure 3 J-K) raises two key questions: Is Bnl/Btl signaling functionally involved in directing tracheal recruitment to damaged fibers? If so, what is the source of Bnl enrichment on the injured fibers? To begin addressing these questions, we conditionally overexpressed Bnl in a restricted subset of adult muscle fibers using the flip-out system combined with a regionally expressed driver (Figure S3 A-C and Materials and Methods section). This targeted overexpression was sufficient to recruit tracheal cells to the ectopic Bnl-expressing regions (Figure 4 A–C'), and did so in a dose-dependent

manner: higher levels of Bnl expression (5 days) resulted in more pronounced tracheal remodeling compared to lower expression (24 hours). These findings demonstrate that the adult tracheal system remains responsive to elevated Bnl levels in the IFMs, supporting the hypothesis that Bnl/Btl signaling directs tracheal pathfinding in response to muscle injury.

We next sought to identify the cellular source responsible for Bnl accumulation in injured muscle fibers. Under wild-type conditions, Bnl:GFP^{endo} signal was detected in hemocytes, tracheal cells, and indirect flight muscles (IFMs) (Figure 4 D-D'). However, since Bnl is a diffusible protein, these observations alone cannot distinguish between cells that produce Bnl and those that merely take it up. To address this, we used the *bnl-lacZ* transcriptional reporter, which revealed active *bnl* expression in hemocytes, adult IFMs, and terminal tracheal cells (TTCs), confirming that these cell types are bona fide sources of Bnl under homeostatic conditions (Figure 4 E-F'). Given that canonical Bnl/Btl signaling operates in a paracrine manner, injured muscles and hemocytes emerge as the most plausible sources of injury-induced Bnl accumulation. To distinguish between these two possibilities, we examined *bnl-lacZ* expression following injury. Surprisingly, we found that injured fibers lacked *bnl-lacZ* activity, whereas neighboring uninjured fibers retained its expression (Figure S3 D-E''). These findings indicate that the injured muscle fibers themselves do not contribute to the localized Bnl accumulation after injury and suggest that the source of Bnl is extrinsic to the damaged tissue.

By contrast, we observed a marked enrichment of Bnl:GFP^{endo} signal surrounding Pxn+ hemocytes recruited to the damaged fibers, suggesting that hemocytes might be responsible for Bnl deposition along the injured muscle (Figure 4 G-H''). To functionally assess the contribution of hemocyte-derived Bnl to tracheal invasion, we selectively silenced *bnl* in hemocytes using either the *Enh3-Gal4* or *HmlΔ-Gal4* drivers. While hemocyte recruitment to the injured muscle remained unaffected, *bnl* knockdown significantly impaired tracheal invasion into damaged fibers compared to controls (Figure 4 I-M; Figure S3 F-I). Together, these results show that hemocytes infiltrating injured muscle tissue act as a key source of Bnl, which is essential for tracheal recruitment.

The receptor FGFR/Btl is essential for injury-induced tracheal guided outgrowth

The finding that Bnl orchestrates tracheal morphogenesis in response to muscle damage suggested in turn that it activates its receptor Btl, on tracheal cells, thereby driving guided outgrowth and branching. To investigate this, we examined Btl expression in adult flight muscles using an endogenously tagged *Btl:cherry*^{endo} allele, which faithfully reports Btl expression (Du et al., 2018). Btl:cherry^{endo} was detected along tracheal branches under homeostatic conditions and within tracheal structures invading the injured muscle (Figure 5 A-B''). To complement this approach, we expressed a membrane-tethered GFP (mCD8-GFP) under the control of a *Btl-Gal4* driver (Figure 5 C-E). While Btl:cherry^{endo} reflects consistent endogenous expression, *Btl-Gal4* drives a more heterogeneous pattern across tracheal cells (Figure 5 C-C'). Nevertheless, we observed a striking accumulation of tracheal branches labelled by *Btl-Gal4* at injured muscles, reinforcing that Btl-expressing tracheal cells are actively recruited to damaged fibers (Figure 5 D-E). We then tested whether Btl function is required for proper tracheal pathfinding. To this end, *btl* was specifically silenced in tracheal cells using either *dSRF-Gal4* or *btl-Gal4* drivers (Figure 5 F-I''). In both cases, tracheal invasion into injured fibers was significantly impaired compared to the control (Figure 5 J). Notably, the phenotype was more pronounced when using *dSRF-Gal4*, which is expected given its broader and more uniform expression pattern in terminal tracheal cells (Figure 2 F and G) compared to *Btl-Gal4*. Together, these findings showed that the Bnl/Btl signaling axis plays a pivotal role in guiding tracheal remodeling after muscle damage. While Btl expression is restricted to tracheal cells, localized Bnl secretion from hemocytes at the damaged fiber refines tracheal pathfinding, ensuring precise and targeted tracheal invasion into injured muscle.

Hemocytes supply ECM components to adult muscles

The extracellular matrix (ECM) is critical for muscle repair, providing structural support, mediating cell signalling, and facilitating tissue remodelling (Schuler et al., 2022). Hemocytes are known to be major producers of ECM components during both *Drosophila* development and post-developmental stages (Bunt et al., 2010; Gold and Bruckner, 2015). Based on this, we hypothesized that they might also supply key ECM components in response to adult muscle injury. Collagen IV, a principal structural protein of the muscle ECM, plays a vital role in maintaining muscle integrity in both

Drosophila and vertebrates (Borchiellini et al., 1996). We analysed Collagen IV distribution in adult flight muscles using the Vkg::GFP line (Figure 6 A-B''). Under homeostatic conditions, we detected a basal level of Vkg::GFP surrounding muscle fibers and along tracheal branches (Figure 6 A'). We further found that hemocytes express Collagen IV (Figure 6 A'')**.** Five days after injury, Vkg::GFP is much more abundant in damaged fibers compared to the intact muscles and the controls (Figure 6 A-B and A''-B''). To further assess the relationship between hemocytes and ECM remodeling, we examined Collagen IV distribution at multiple time points post-injury (From 1 to 20DPI) and compared it to the pattern of hemocytes recruitment (Figure 6 C-H). The results show that the more evenly hemocytes are distributed along the injured fiber, the more abundant Vkg::GFP is detected along the same region. These observations show a correlation between Collagen IV accumulation at injured muscles and the presence of newly recruited hemocytes, raising the possibility that hemocytes may contribute to ECM remodelling in response to muscle injury.

Given that the incorporation of Collagen IV into the ECM requires accessory molecules for proper deposition and stabilization, we next investigated whether hemocytes also supply such regulatory components. One such regulator is SPARC, a collagen-binding glycoprotein essential for Collagen IV diffusion, stabilization, and incorporation into basement membranes (Bradshaw, 2009; Chioran et al., 2017). We first examined SPARC localization in hemocytes associated with adult flight muscles. Hemocytes identified using either *Enh3-Gal4* or *HmlΔ-Gal4* drivers were positive for SPARC (Figure 6 I-I' and J–J'). Importantly, when muscle is injured, SPARC was found at higher levels along the injured fiber compared to the controls, mimicking the distribution of Collagen IV (Figure 6 K-K'). These observations suggest that, in adult muscle, SPARC is locally produced by hemocytes. To further confirm the cellular source of SPARC in adult flight muscles, we used the *SPARC-Gal4* driver a Gal4 trap line inserted into the endogenous SPARC locus to drive membrane-targeted RFP (myr-RFP) expression in flies also carrying a BM40-SPARC-GFP fosmid reporter (Figure 6 L-L'). This dual-reporter approach allowed us to simultaneously visualize SPARC (via BM40-SPARC-GFP) and identify the specific SPARC-producing cells (via *SPARC-Gal4 > myr-RFP*), thereby determining whether SPARC is produced by hemocytes at the site of injury. In uninjured muscle, BM40-SPARC-GFP and SPARC-Gal4-driven myr-RFP were co-expressed in hemocytes. Following muscle injury, BM40-SPARC-GFP

was broadly enriched along the damaged fiber, resembling the distribution of endogenous SPARC protein, while *SPARC-Gal4* activity remained restricted to hemocytes and was not detected in muscle nuclei (Figure 6 M-M'). Together, these data show that recruited hemocytes are the primary source of SPARC at the injured muscle fiber.

We then sought to determine whether hemocyte-derived SPARC is required for adult muscle homeostasis. Detailed analysis of hemocytes distribution within the indirect flight muscles revealed that, in addition to their enrichment near tracheal structures, hemocytes are also concentrated at fiber tips (Figure 6 N-N' and (Boukhatmi and Bray, 2018)). Given that the extracellular matrix (ECM) is essential for the development and function of myotendinous junctions (Chu and Hayashi, 2021), we hypothesized that hemocyte enrichment at muscle tips may support muscle attachment through local ECM deposition. To test this, we specifically depleted *sparc* in hemocytes by expressing $Sparc^{RNAi}$ under the control of the *Enh3-Gal4* driver (*Enh3-Gal4 > UAS-*$Sparc^{RNAi}$). Notably, targeted downregulation of *sparc* in hemocytes for seven days resulted in pronounced muscle damage, particularly at the fiber tips adjacent to the myotendinous junctions, as evidenced by increased Mhc expression and muscle architecture disruptions (Figure 6 O-Q). Thus, the morphological defects observed upon *sparc* depletion align with this spatial distribution, supporting a functional role for hemocyte-derived Sparc in maintaining adult muscle structural integrity.

Discussion

Our study provides a compelling example of how the muscle damage response relies on the precise coordination between multiple cell types. While *Drosophila* hemocytes are traditionally recognized for their immunoprotective roles against pathogens and infections (Gold and Bruckner, 2015; Kalra et al., 2018; Sanchez Bosch et al., 2019), our findings reveal that they also play essential roles for preserving adult muscle integrity. We show that hemocytes both signal to the tracheal system to finely regulate its outgrowth toward the injured muscle and directly supply key extracellular matrix (ECM) components to the damaged fiber -two processes that likely support muscle structural maintenance and recovery (Figure 7).

A functional cooperation between immune cells and the respiratory system

Insect respiration has traditionally been viewed as entirely dependent on the tracheal system, operating independently of blood cells. However, this view has been challenged by recent finding showing that a subtype of larval hemocytes, known as crystal cells, can take up oxygen from tracheal cells and contribute to tissue oxygenation (Shin et al., 2024). We found that adult hemocytes are in close proximity with tracheal cells in muscle tissue and contribute indirectly to oxygen delivery by guiding tracheal branches toward sites of muscle injury (Figure 7). Following damage, hemocytes are rapidly recruited and cover the injured muscle. In this context, they secrete key signalling cues-specifically through the FGF/FGFR (Bnl/Btl) pathway-that promote local tracheal outgrowth and precise positioning, thereby supporting oxygenation of the damaged tissue. Interestingly, during development, plasmatocytes have been shown to transdifferentiate into crystal cells in the lymph gland, the primary hematopoietic organ (Marcetteau et al., 2025). Whether a similar transdifferentiation occurs in the adult following muscle injury remains an open question. Finally, the nature of the signals that govern hemocyte recruitment under injury conditions also remains an important avenue for future investigation.

Do Drosophila repair or regenerate their flight muscles?

The IFMs generate the high-frequency wing beats that enable flight -a behavior essential for predator avoidance, foraging, and mating. Given their vital function, IFMs must be maintained in optimal condition to ensure sustained performance throughout the animal's lifespan. This need for resilience is also underscored by the observation that over 30% of wild-caught *Drosophila* exhibit wound injuries, frequently located in the thorax and abdomen (Subasi et al., 2024). Although a rare population of satellite-like cells has been identified in adult flies, the regenerative capacity of adult *Drosophila* muscles remains debated (Chechenova et al., 2024). A major limitation has been the lack of appropriate molecular markers to monitor both muscle regeneration and muscle stem cell (MuSC) activity. In our study, we identified Myosin Heavy Chain (Mhc) as a robust marker that is consistently upregulated in damaged fibers. However, unlike in vertebrates -where MyHC-emb levels return to baseline following regeneration- Mhc expression in *Drosophila* remains elevated even 20 days post-injury (Figure S2). This makes Mhc a sensitive marker for identifying injury, but less useful for assessing

complete muscle recovery. Adult MuSCs have been identified via the transcription factor Zfh1/ZEB and its reporter Enh3 (Boukhatmi and Bray, 2018; Chaturvedi et al., 2017), which currently stands as the only known marker for these cells. An equivalent role of ZEB was recently shown in mice (Siles et al., 2019). Interestingly, both Zfh1 and ZEB are expressed in the muscle associated immune cells (Boukhatmi and Bray, 2018; Siles et al., 2019), underscoring the evolutionary conservation of this transcriptional regulator. In our study, we found that following muscle injury, 100% of the cells recruited to damaged fibers are both $Enh3^{+}$ and Pxn^{+} (a plasmatocytes marker), while being negative for the muscle-specific marker Mef2 (Figure S1 L-M'). This strongly suggests that hemocytes are the predominant -if not exclusive- cell population migrating to injured muscle. These findings suggest that adult *Drosophila* flight muscles possess limited regenerative capacity and may instead rely on compensatory mechanisms-such as increased oxygenation through tracheal remodelling and structural reinforcement via extracellular matrix (ECM) deposition-to cope with muscle damage. This is consistent with the broader idea that short-lived species prioritize immediate survival and reproduction over long-term regenerative investment (Kirkwood, 2005). In such organisms, evolution favors fast and efficient repair mechanisms that support rapid recovery and fitness over complex, energy-intensive regeneration programs.

Functional parallels between Drosophila hemocytes and mammalian FAPs

In mammals, extracellular matrix (ECM) remodeling is essential for maintaining muscle structure and enabling proper tissue repair. Although muscle stem cells (MuSCs) can produce some ECM components (Baghdadi et al., 2018), the primary contributors to ECM production and maintenance during regeneration are fibro-adipogenic progenitors (FAPs) (Molina et al., 2021). *Drosophila* lack dedicated FAPs, raising the question of how flies achieve ECM remodeling and maintain muscle integrity. During development, hemocytes are the primary source of ECM molecule production (Gold and Bruckner, 2015; Mase et al., 2021; Shahab et al., 2015). However, direct functional evidence for their involvement in ECM remodeling in adult tissues—particularly muscle—has remained limited. Here, we showed that adult hemocytes produce at least two key ECM components -Collagen IV and SPARC. This production is particularly enriched around damaged muscle fibers where hemocytes are abundant. We further showed that hemocyte-specific ablation of SPARC led to muscle deffect,

indicating that hemocyte-derived ECM is essential for proper muscle architecture safeguard. We speculate that the ECM produced along the injured muscle by the hemocytes may serve not only to stabilize the tissue but also to restrict the diffusion of key signalling molecules such as Bnl, potentially confining them to the injury site and enhancing their local action. These findings suggest that *Drosophila* hemocytes share functional similarities with mammalian FAPs and may compensate for their absence. This highlights an evolutionarily flexible strategy for achieving tissue repair in organisms with fewer specialized cell types.

Materials and Methods

Drosophila melanogater strains and genetics

All *Drosophila melanogaster* stocks were grown on standard medium at 25°C. The following stains were used: w^{118} as wild type (wt), *Pxn-RFP* (Rodrigues et al., 2021), *HmlΔ-Gal4* (BL#30140), *Enh3-Gal4* (Boukhatmi and Bray, 2018), *Mhc-Iso-K, L, M (fTRG500)* and *Mhc-Iso-A, F, G (fTRG519)* (Sarov et al., 2016), *weeP26* (Orfanos and Sparrow, 2013), *Bnl:GFP*^{endo} *and Btl:cherry*^{endo} (Du et al., 2018), *Bnl-LacZ* (BL#11704), , *dSRF-GAL4* (BL#25753), *Btl-Gal4* (BL#78328), *UAS-Btl*^{RNAi} (BL#435544), *UAS-Bnl*^{RNAi} (BL#34572), *UAS-Bnl::GFP* (Lin, 2009), *Vkg::GFP* (BL#98343), *BM40-SPARC-GFP* (Sarov et al., 2016), *SME-Gal4* (VT 0576871), *UAS-H2B-RFP* (Antonello et al., 2015), *UAS-mCD8GFP* (BL#5137), *UAS-myr-mRFP* (BL#7118), SyHREns (Zhao et al., 2024), *UAS-Sima*^{RNAi} (BL#26207), *SPARC-Gal4* (BL#77473), *UAS-SPARC*^{RNAi} (BL#40885). *Naa30A* deletion males were obtained from crosses between *Naa30A*$^{\Delta 74}$*/FM0* females and either UAS-mCD8GFP; Enh3-Gal4 (Figure 1) or Mhc-Iso-K, L, M (Figure S1) males. RNAi experiments were carried out at 29°C. To achieve temporal control of gene expression in adult tissues, the tubGal80^{ts} was employed, allowing restriction of Gal4 activity to a specific time window. Fly crosses were initially maintained at 18°C, and after adult eclosion, the progenies were transferred to 29°C, where they remained until dissection. An exception was made for the Bnl knockdown experiments shown in Figure 4, which were performed without the tubGal80^{ts} transgene.

Generation of SME-FRT-stop-FRT-Gal4 fly line and flip-out induction procedure.

SME (Shavenbaby Muscle Enhancer) is one of several enhancers of the *shavenbaby* gene (VT057071-Gal4). It is active in larval muscle progenitors (AMPs) (Figure S3 A-A') and remains active in a subpopulation of localized muscle nuclei in the adult indirect flight muscles (IFMs) (Figure S3 B-B'). To generate the SME-FRT-stop-FRT-Gal4 construct, the cis-regulatory element from the original *shavenbaby* enhancer construct was used to replace the *pAct* promoter in the pAct-FRT-stop-FRT3-FRT-FRT3-Gal4 vector (Addgene plasmid #52889). The resulting construct was integrated into the attP site at cytological location 51D on chromosome II via embryo injection into vas-int; attP-51D flies. To induce localized overexpression of Bnl::GFP in adult IFM nuclei, hsflp; FRT-SME-stop-FRT-Gal4/CyO; tubGal80^{ts} females were crossed to UAS-Bnl::GFP males. Progeny were raised at 18°C and subjected to a 2-hour heat shock at 37°C in young adulthood (Figure 4 A-C').

Immunohistochemistry and confocal microscopy

Preparation and immunofluorescence of wing discs and adult muscles were performed as previously described in (Leroux et al., 2023). The following primary antibody were used: Chicken anti-βGal (1:100, Abcam, ab9361), Chicken anti-GFP (1:300, Abcam, ab13970), Mouse anti-Mhc (1:200, DSHB, 3E8-3D3-s) , Mouse anti-dSRF (1:20, a gift from Mark A. Krasnow, Stanford university California , USA), Mouse anti-P1 (1:20, a gift from István Andó, Szeged, Hugary), Rabbit anti-Mef2 (1:500 , DSHB, Mef2-p), Rabbit anti-PH3 (1:100, Cell Signaling Technology, #9713), Rabbit anti-SPARC (1:500, a gift from Maurice Ringuette, University of Toronto, Canada), Rat anti-RFP (1:800, Chromotek, 5F8-20), Rabbit anti-Zfh1 (1:5000, a gift from Ruth Lehmann, New York, USA), Alexa-conjugated Phalloidin (1:200, Thermo fisher scientific life technologies).

Induction of flight muscle injury

Flight muscle injury was induced following previously described protocols (Chakraborty et al., 2018). Young adult flies (2-3 days post-eclosion) were anesthetized and positioned laterally under a stereomicroscope. A single, localized stab wound was inflicted manually using a fine stainless-steel needle (Minutien Pins, 0.1 mm diameter;

#26002–10) to minimize tissue damage and avoid extensive injury. Age-matched, uninjured flies served as controls.

Microscopy and data analysis

Samples were imaged using a Leica SP8 microscope (BIOSIT, University of Rennes) at 20×, 40×, or 63× magnification and a resolution of 1024×1024 pixels. Images were processed with ImageJ and assembled using Adobe Illustrator. To quantify fluorescence intensity, all samples were processed and analyzed in parallel under identical conditions. Confocal images were acquired using the same laser settings across all samples. Sum slice projections were generated from each confocal stack. Regions of interest (ROIs) were manually defined based on protein expression, and mean fluorescence intensities were measured within each ROI. These values were then normalized to background levels measured in comparable areas of the same sample.

Tracheal branches were visualized either by their intrinsic autofluorescence using a 405 nm UV laser (Sauerwald et al., 2019) or by the expression of membrane-bound GFP driven by a tracheal-specific Gal4 driver (UAS-mCD8GFP). Tracheal coverage was quantified as pixel area per muscle fiber from maximum intensity Z-projections acquired at 20× magnification. Quantification was performed using the “Skeletonize” plugin in ImageJ, based on the method described by Perochon et al. (2021), with minor modifications. Briefly, maximum intensity projections were generated from each confocal stack, tracheal branches were segmented by thresholding, and the resulting images were skeletonized. Skeleton pixel intensity was then measured specifically within injured muscle fibers and their corresponding contralateral control fibers. For Figure 2E, square regions of interest (ROIs) were placed at the injury site, as well as in proximal and distal regions, to assess local tracheal enrichment. Hemocyte and dSRF-positive cell numbers were quantified manually using ImageJ.

Graphs and statistical analyses were performed using GraphPad Prism. Pair comparisons were statistically tested with a two-sided Student’s t-test. NS, not significant ($p>0.05$); *$p < 0.05$, **$p < 0.01$, ***$p < 0.001$ ****$p< 0.0001$.

Acknowledgments

We would like to thank Jennifer Zanet, Cedric Polesello, Sougata Roy, Ruth Lehmann, Maurice Ringuette, Jean-Paul Vincent, and Mark A. Krasnow, as well as the Bloomington Drosophila Stock Center, the Vienna Drosophila Resource Center (VDRC), and the Developmental Studies Hybridoma Bank for providing *Drosophila* strains and antibodies. We are grateful to Lucas Waltzer, Laetitia Bataille, Alain Vincent, and Michèle Crozatier for their critical reading of the manuscript, and to other members of H.B's laboratory for valuable discussions. We also thank Emmanuel Gallaud for helpful input during the early phases of the project. We acknowledge Xavier Pinson from the Microscopy Rennes Imaging Center (MRic, BIOSIT, Biogenouest) for technical assistance, and Cyrille Surbled for fly stock maintenance and technical help. Work in the Boukhatmi lab was supported by an AFM-Téléthon Trampoline Grant (#23108), ATIP-Avenir (CNRS), and ANR GenepiMuSC (ANR-23-CE13-0006). N.A. was supported by an AFM-Téléthon PhD fellowship (#23846) and an FRM fellowship (FDT202404018608). Work in the Cordero lab was supported by a Sir Henry Dale Fellowship (Wellcome Trust and Royal Society, 104103/Z/14/Z), a Wellcome ISSF Returner Scheme (204820/Z/16/Z), and a Tenovus Fellowship (Tenovus/S22-28) to J.P.

Competing interest

The authors declare that they have no competing interests.

Reference

Antonello, Z.A., Reiff, T., Ballesta-Illan, E., Dominguez, M., 2015. Robust intestinal homeostasis relies on cellular plasticity in enteroblasts mediated by miR-8-Escargot switch. EMBO J 34, 2025-2041.

Baghdadi, M.B., Castel, D., Machado, L., Fukada, S.I., Birk, D.E., Relaix, F., Tajbakhsh, S., Mourikis, P., 2018. Reciprocal signalling by Notch-Collagen V-CALCR retains muscle stem cells in their niche. Nature 557, 714-718.

Borchiellini, C., Coulon, J., Le Parco, Y., 1996. The function of type IV collagen during Drosophila muscle development. Mech Dev 58, 179-191.

Boukhatmi, H., 2021. Drosophila, an Integrative Model to Study the Features of Muscle Stem Cells in Development and Regeneration. Cells 10.

Boukhatmi, H., Bray, S., 2018. A population of adult satellite-like cells in Drosophila is maintained through a switch in RNA-isoforms. Elife 7.

Boulet, M., Renaud, Y., Lapraz, F., Benmimoun, B., Vandel, L., Waltzer, L., 2021. Characterization of the Drosophila Adult Hematopoietic System Reveals a Rare Cell Population With Differentiation and Proliferation Potential. Front Cell Dev Biol 9, 739357.

Bradshaw, A.D., 2009. The role of SPARC in extracellular matrix assembly. J Cell Commun Signal 3, 239-246.

Bunt, S., Hooley, C., Hu, N., Scahill, C., Weavers, H., Skaer, H., 2010. Hemocyte-secreted type IV collagen enhances BMP signaling to guide renal tubule morphogenesis in Drosophila. Dev Cell 19, 296-306.

Catalani, E., Zecchini, S., Giovarelli, M., Cherubini, A., Del Quondam, S., Brunetti, K., Silvestri, F., Roux-Biejat, P., Napoli, A., Casati, S.R., Ceci, M., Romano, N., Bongiorni, S., Prantera, G., Clementi, E., Perrotta, C., De Palma, C., Cervia, D., 2022. RACK1 is evolutionary conserved in satellite stem cell activation and adult skeletal muscle regeneration. Cell Death Discovery 8, 459.

Chakraborty, K., VijayRaghavan, K., Gunage, R., 2018. A Method to Injure, Dissect and Image Indirect Flight Muscle of Drosophila. Bio Protoc 8, e2860.

Chaturvedi, D., Reichert, H., Gunage, R.D., VijayRaghavan, K., 2017. Identification and functional characterization of muscle satellite cells in Drosophila. Elife 6.

Chechenova, M., McLendon, L., Dallas, B., Stratton, H., Kiani, K., Gerberich, E., Alekseyenko, A., Tamba, N., An, S., Castillo, L., Czajkowski, E., Talley, C., Brown, A., Bryantsev, A.L., 2024. Muscle degeneration in aging Drosophila flies: the role of mechanical stress. Skelet Muscle 14, 20.

Chioran, A., Duncan, S., Catalano, A., Brown, T.J., Ringuette, M.J., 2017. Collagen IV trafficking: The inside-out and beyond story. Dev Biol 431, 124-133.

Chu, W.C., Hayashi, S., 2021. Mechano-chemical enforcement of tendon apical ECM into nano-filaments during Drosophila flight muscle development. Curr Biol 31, 1366-1378 e1367.

Dort, J., Fabre, P., Molina, T., Dumont, N.A., 2019. Macrophages Are Key Regulators of Stem Cells during Skeletal Muscle Regeneration and Diseases. Stem Cells Int 2019, 4761427.

Du, L., Sohr, A., Yan, G., Roy, S., 2018. Feedback regulation of cytoneme-mediated transport shapes a tissue-specific FGF morphogen gradient. Elife 7.

Ebner, A., Kiefer, F.N., Ribeiro, C., Petit, V., Nussbaumer, U., Affolter, M., 2002. Tracheal development in Drosophila melanogaster as a model system for studying the development of a branched organ. Gene 287, 55-66.

Eming, S.A., Martin, P., Tomic-Canic, M., 2014. Wound repair and regeneration: mechanisms, signaling, and translation. Sci Transl Med 6, 265sr266.
Ghabrial, A., Luschnig, S., Metzstein, M.M., Krasnow, M.A., 2003. Branching morphogenesis of the Drosophila tracheal system. Annu Rev Cell Dev Biol 19, 623-647.
Goh, K.Y., Lee, W.X., Choy, S.M., Priyadarshini, G.K., Chua, K., Tan, Q.H., Low, S.Y., Chin, H.S., Wong, C.S., Huang, S.Y., Fu, N.Y., Nishiyama, J., Harmston, N., Tang, H.W., 2024. FOXO-regulated DEAF1 controls muscle regeneration through autophagy. Autophagy 20, 2632-2654.
Gold, K.S., Bruckner, K., 2015. Macrophages and cellular immunity in Drosophila melanogaster. Semin Immunol 27, 357-368.
Gunage, R.D., Dhanyasi, N., Reichert, H., VijayRaghavan, K., 2017. Drosophila adult muscle development and regeneration. Semin Cell Dev Biol 72, 56-66.
Hayashi, S., Kondo, T., 2018. Development and Function of the Drosophila Tracheal System. Genetics 209, 367-380.
Jarecki, J., Johnson, E., Krasnow, M.A., 1999. Oxygen regulation of airway branching in Drosophila is mediated by branchless FGF. Cell 99, 211-220.
Kalra, S., Bahendeka, S., Sahay, R., Ghosh, S., Md, F., Orabi, A., Ramaiya, K., Al Shammari, S., Shrestha, D., Shaikh, K., Abhayaratna, S., Shrestha, P.K., Mahalingam, A., Askheta, M., AA, A.R., Eliana, F., Shrestha, H.K., Chaudhary, S., Ngugi, N., Mbanya, J.C., Aye, T.T., Latt, T.S., Akanov, Z.A., Syed, A.R., Tandon, N., Unnikrishnan, A.G., Madhu, S.V., Jawa, A., Chowdhury, S., Bajaj, S., Das, A.K., 2018. Consensus Recommendations on Sulfonylurea and Sulfonylurea Combinations in the Management of Type 2 Diabetes Mellitus - International Task Force. Indian J Endocrinol Metab 22, 132-157.
Kirkwood, T.B., 2005. Understanding the odd science of aging. Cell 120, 437-447.
Laurichesse, Q., Soler, C., 2020. Muscle development : a view from adult myogenesis in Drosophila. Semin Cell Dev Biol 104, 39-50.
Leroux, E., Ammar, N., Moinet, S., Pecot, T., Boukhatmi, H., 2023. Studying Muscle Transcriptional Dynamics at Single-molecule Scales in Drosophila. J Vis Exp.
Li, J., Zhang, S., Amaya, E., 2016. The cellular and molecular mechanisms of tissue repair and regeneration as revealed by studies in Xenopus. Regeneration (Oxf) 3, 198-208.
Lin, L., 2009. Clonal Analysis of Growth Behaviors During Drosophila Larval Tracheal Development In Doctoral thesis. University of Basel.
Marcetteau, J., Duarte, P., Leitao, A.B., Sucena, E., 2025. Transdifferentiation of plasmatocytes to crystal cells in the lymph gland of Drosophila melanogaster. EMBO Rep 26, 2077-2097.
Mase, A., Augsburger, J., Bruckner, K., 2021. Macrophages and Their Organ Locations Shape Each Other in Development and Homeostasis - A Drosophila Perspective. Front Cell Dev Biol 9, 630272.
Molina, T., Fabre, P., Dumont, N.A., 2021. Fibro-adipogenic progenitors in skeletal muscle homeostasis, regeneration and diseases. Open Biol 11, 210110.
Murphy, M.M., Lawson, J.A., Mathew, S.J., Hutcheson, D.A., Kardon, G., 2011. Satellite cells, connective tissue fibroblasts and their interactions are crucial for muscle regeneration. Development 138, 3625-3637.
Orfanos, Z., Sparrow, J.C., 2013. Myosin isoform switching during assembly of the Drosophila flight muscle thick filament lattice. J Cell Sci 126, 139-148.

Perochon, J., Yu, Y., Aughey, G.N., Medina, A.B., Southall, T.D., Cordero, J.B., 2021. Dynamic adult tracheal plasticity drives stem cell adaptation to changes in intestinal homeostasis in Drosophila. Nat Cell Biol 23, 485-496.
Peterson, S.J., Krasnow, M.A., 2015. Subcellular trafficking of FGF controls tracheal invasion of Drosophila flight muscle. Cell 160, 313-323.
Rao, P.R., Lin, L., Huang, H., Guha, A., Roy, S., Kornberg, T.B., 2015. Developmental compartments in the larval trachea of Drosophila. Elife 4.
Relaix, F., Bencze, M., Borok, M.J., Der Vartanian, A., Gattazzo, F., Mademtzoglou, D., Perez-Diaz, S., Prola, A., Reyes-Fernandez, P.C., Rotini, A., Taglietti, t., 2021. Perspectives on skeletal muscle stem cells. Nature Communications 12, 692.
Rodrigues, D., Renaud, Y., VijayRaghavan, K., Waltzer, L., Inamdar, M.S., 2021. Differential activation of JAK-STAT signaling reveals functional compartmentalization in Drosophila blood progenitors. Elife 10.
Sanchez Bosch, P., Makhijani, K., Herboso, L., Gold, K.S., Baginsky, R., Woodcock, K.J., Alexander, B., Kukar, K., Corcoran, S., Jacobs, T., Ouyang, D., Wong, C., Ramond, E.J.V., Rhiner, C., Moreno, E., Lemaitre, B., Geissmann, F., Bruckner, K., 2019. Adult Drosophila Lack Hematopoiesis but Rely on a Blood Cell Reservoir at the Respiratory Epithelia to Relay Infection Signals to Surrounding Tissues. Dev Cell 51, 787-803 e785.
Sarov, M., Barz, C., Jambor, H., Hein, M.Y., Schmied, C., Suchold, D., Stender, B., Janosch, S., K, J.V., Krishnan, R.T., Krishnamoorthy, A., Ferreira, I.R., Ejsmont, R.K., Finkl, K., Hasse, S., Kampfer, P., Plewka, N., Vinis, E., Schloissnig, S., Knust, E., Hartenstein, V., Mann, M., Ramaswami, M., VijayRaghavan, K., Tomancak, P., Schnorrer, F., 2016. A genome-wide resource for the analysis of protein localisation in Drosophila. Elife 5, e12068.
Sauerwald, J., Backer, W., Matzat, T., Schnorrer, F., Luschnig, S., 2019. Matrix metalloproteinase 1 modulates invasive behavior of tracheal branches during entry into Drosophila flight muscles. Elife 8.
Schuler, S.C., Liu, Y., Dumontier, S., Grandbois, M., Le Moal, E., Cornelison, D., Bentzinger, C.F., 2022. Extracellular matrix: Brick and mortar in the skeletal muscle stem cell niche. Front Cell Dev Biol 10, 1056523.
Shahab, J., Baratta, C., Scuric, B., Godt, D., Venken, K.J., Ringuette, M.J., 2015. Loss of SPARC dysregulates basal lamina assembly to disrupt larval fat body homeostasis in Drosophila melanogaster. Dev Dyn 244, 540-552.
Shin, M., Chang, E., Lee, D., Kim, N., Cho, B., Cha, N., Koranteng, F., Song, J.J., Shim, J., 2024. Drosophila immune cells transport oxygen through PPO2 protein phase transition. Nature 631, 350-359.
Siles, L., Ninfali, C., Cortes, M., Darling, D.S., Postigo, A., 2019. ZEB1 protects skeletal muscle from damage and is required for its regeneration. Nature Communications 10, 1364.
Subasi, B.S., Grabe, V., Kaltenpoth, M., Rolff, J., Armitage, S.A.O., 2024. How frequently are insects wounded in the wild? A case study using Drosophila melanogaster. R Soc Open Sci 11, 240256.
Sun, F., Poss, K.D., 2023. Inter-organ communication during tissue regeneration. Development 150.
Tamamouna, V., Rahman, M.M., Petersson, M., Charalambous, I., Kux, K., Mainor, H., Bolender, V., Isbilir, B., Edgar, B.A., Pitsouli, C., 2021. Remodelling of oxygen-transporting tracheoles drives intestinal regeneration and tumorigenesis in Drosophila. Nat Cell Biol 23, 497-510.

Varland, S., Silva, R.D., Kjosas, I., Faustino, A., Bogaert, A., Billmann, M., Boukhatmi, H., Kellen, B., Costanzo, M., Drazic, A., Osberg, C., Chan, K., Zhang, X., Tong, A.H.Y., Andreazza, S., Lee, J.J., Nedyalkova, L., Usaj, M., Whitworth, A.J., Andrews, B.J., Moffat, J., Myers, C.L., Gevaert, K., Boone, C., Martinho, R.G., Arnesen, T., 2023. N-terminal acetylation shields proteins from degradation and promotes age-dependent motility and longevity. Nat Commun 14, 6774.
Wu, W.H., Kuo, T.H., Kao, C.W., Girardot, C., Hung, S.J., Liu, T., Furlong, E.E.M., Liu, Y.H., 2019. Expanding the mesodermal transcriptional network by genome-wide identification of Zinc finger homeodomain 1 (Zfh1) targets. FEBS Lett 593, 1698-1710.
Zhao, Y., Alexandre, C., Kelly, G., Perez-Mockus, G., Vincent1, J.-P., 2024. Growth-induced physiological hypoxia correlates with growth deceleration during normal development. bioRxiv.

Figure legends

Figure 1. Hemocytes are specifically recruited to the damaged muscle fiber. (A-F). Adult indirect flight muscles (IFMs) imaged under uninjured conditions and at 2- and 5-days post-injury (2DPI and 5DPI) following localized stab injury. Mhc (magenta) marks muscles. Hemocytes (green) are visualized using the following reporters: *Pxn-RFP* in (A-C'') and *Enh3-Gal4; UAS-mCD8GFP* in (D-F''). Dashed yellow outlines indicate injured muscle fibers showing elevated Mhc expression. **(G).** Quantification of normalized Mhc intensity level in uninjured and injured fiber at 2DPI and 5DPI (dashed lines). In each condition light and dark shading indicate data points from three independent replicates (****p<0.0001, Student t-test; *n > 10* heminota per condition). **(H).** Schematic representation of the proportion of recruited hemocytes expressing different reporters. **(H').** Time-course analysis of hemocytes recruitment at 1, 2, 3, 4, and 5DPI reveals heterogeneous kinetics of response to muscle damage. Enh3-positive, Pxn-positive, and Hml-positive hemocytes are represented by light gray, black, and dark gray bars, respectively (****p < 0.0001, Student's t-test; *n ≥ 10* heminota per condition). **(I-J''').** Distribution of hemocytes visualized with *Enh3-Gal4; UAS-mCD8GFP* (green) in control muscles (I-I''') and *Naa30* mutants (J-J'''). Muscles and muscle nuclei are stained with Mhc (magenta) and Mef2 (cyan) respectively. Scale bar: 100µm. Asterisks in panels I''' and J''' mark non-specific signal detected in motoneurons.

Figure 2. Muscle damage induces directed tracheal remodeling. (A-A'). Hemocytes (green/magenta; *Enh3-Gal4, UAS-mCD8GFP; UAS-H2B-RFP*) are associated to the tracheal cells (gray, autofluorescence). Scale bars: 25 µm. **(B-C'').** Distribution of tracheal branches (gray, autofluorescence) and hemocytes (green, *Enh3-Gal4; UAS-mCD8GFP*) in control (B-B'') and at 5DPI (C-C''). Muscles are labeled with Mhc (magenta). **(B'', C'').** Boxed regions from (B and C), magnified 2X. Scale bars: 100 µm. **(D)**. Quantification of tracheal coverage in (B) and (C) (****p < 0.0001, Student's *t*-test; *n = 19* heminota per condition; light, dark, and intermediate shading indicate data points from three independent replicates). **(E).** Quantification of tracheal coverage in (C) at the injury site (orange box), adjacent to the injury site (green box, approximately 135 µm away from the injury site), and at distant regions (blue box, within 300 µm of the lesion border) (*p= 0.0142, Student's *t*-test; *n=19* heminota). **(F-**

F'). *dSRF-Gal4* marks muscle-associated terminal tracheal cells (TTCs). TTC membranes (green) and nuclei (magenta) are indicated by arrowheads and arrows, respectively (*dSRF-Gal4, UAS-mCD8GFP; UAS-H2B-RFP*). *dSRF-Gal4* is inactive in primary tracheal branches (asterisks in F'). Muscles are labeled with Mhc (bleu). Scale bars: 25 µm. **(G-H"').** TTCs distribution in IFMs (green, *dSRF-Gal4, UAS-mCD8GFP*) in control (G-G"') and at 5DPI (H-H"'). Muscles are labeled with Mhc (magenta). **(G", H").** 4.5X magnification of boxed regions in (G') and (H'), respectively. Scale bar: 100 µm. **(G"', H"').** Orthogonal views of (G") and (H"). Arrow in (H"') indicates TTC enrichment at the injured muscle. **(I).** Quantification of TTCs coverage from (G) and (H) (****p < 0.0001, Student's *t*-test; *n = 14* heminota per condition; light, dark, and intermediate shading represent data points from three independent replicates). **(J-J').** dSRF (green) marks TTCs nuclei associated with muscle. Scale bars: 25 µm. **(K-L"').** Distribution of TTCs nuclei (green) in IFMs under control conditions (K-K"') and at 5DPI (L-L"'). Muscles are labeled with phalloidin (blue); tracheae are visualized by autofluorescence (gray). Anti-PH3 (magenta) is used to assess cell division. **(K', L"').** 2X magnification of boxed regions in (K) and (L), respectively. Scale bars: 100 µm. Arrowheads and arrows indicate dSRF expression in the muscle and TTCs nuclei, respectively. **(M).** Proportion of TTCs nuclei located within a selected muscle relative to the total number of TTCs nuclei in the imaged sample ($p = 0.036$, Student's *t*-test; *n = 17* heminota per condition; light, dark, and intermediate shading indicate data points from three independent replicates).

Figure 3. Local hypoxia in response to muscle damage drives tracheal branching. (A-A"). *SyHREns* reporter activity (green) is detected in a subset of TTCs marked by dSRF (magenta, arrows). Scale bars: 25 µm. **(B-D").** Expression of the *SyHREns* reporter (green) in control IFMs (B-B"), at 5DPI (C-C") and 20DPI (D-D"). Muscles are labeled with Mhc (magenta), and tracheal branches are visualized via autofluorescence (gray). **(B", C" and D").** 2X magnification of the boxed regions in B', C' and D'. Scale bars: 100 µm. **(E).** Quantification of SyHREns positive cells (green) per injured muscle fiber (****p < 0.0001, Student's *t*-test; *n > 20* heminota per condition; light, dark and intermediate shading indicate data points from three independent replicates). **(F-H").** *sima* (HIF-1α) downregulation in TTCs (*dSRF-Gal4; UAS-Sima^{RNAi}*) prevents tracheal recruitment at the injured fiber. **(F", G" and H").** 2X

magnification of the boxed regions in E', F' and G'. Scale bars: 100 µm. **(I)**. Quantification of trachea coverage (****p < 0.0001, Student's *t*-test; *n = 13* heminota per condition). **(J-K'').** Detection of Bnl (green, Bnl:GFP^{endo}) in control IFMs (J-J'') and at 5DPI (K-K''). Muscles are labeled with Mhc (magenta), and tracheal cells are visualized via autofluorescence (gray). **(J'', K'').** 4.5X magnification of the boxed regions in J and K. Scale bars: 100 µm. **(J''', K''').** Orthogonal views of (J) and (K). Asterisk in K''' indicates Bnl:GFP^{endo} enrichment at the injured muscle. **(L).** Quantification of normalized Bnl:GFP^{endo} intensity level in uninjured and injured muscle fiber and 5DPI (***p<0.0001, Student *t*-test, *n = 15* heminota per condition from three independent replicates).

Figure 4. Hemocytes provide Bnl ligand to injured muscle to attract tracheal cells. (A-C'). Local overexpression of UAS-Bnl::GFP (green) in adult IFMs under *SME-Gal4* control results in enrichment of terminal tracheal cells (TTCs), marked by dSRF (magenta, B' and C'), and a significant increase in tracheal branching (gray, B and C), compared to untreated controls (A). Scale bars: 100 µm**. (D-D').** Bnl (green, Bnl:GFP^{endo}) is detected in indirect flight muscles (IFMs, labelled with Mhc, blue; arrowheads), tracheal branches (autofluorescence, gray; asterisks), and hemocytes (*Pxn-RFP*, magenta; arrows). Scale bars: 25 µm. **(E-E').** Expression of the *Bnl-LacZ* reporter (green) is observed in terminal tracheal cells (TTCs) marked by dSRF (magenta; asterisks), and in IFMs nuclei (arrowheads). Scale bars: 25 µm. **(F-F').** Bnl-LacZ (green) is detected in IFMs associated hemocytes labelled with *Pxn-RFP* (magenta; arrows). Scale bars: 25 µm. **(G-H'').** Bnl expression (green, Bnl:GFP^{endo}) in control IFMs (D-D'') and at 5DPI (E-E''). Muscles are labeled with Mhc (blue), tracheal cells visualized via autofluorescence (gray), and hemocytes detected with the *Pxn-RFP* reporter (magenta). Arrows in H'' indicate Bnl localization around hemocytes recruited to the injured muscle. Scale bars: 100 µm. **(I-L).** Downregulating *bnl* in the hemocytes (green, *Enh3-Gal4; UAS-mCD8GFP, UAS-Bnl^{RNAi}*) do not alter hemocytes recruitment but decreases tracheal invasion to the damaged fiber as shown in (L'- L'') and quantified in **(M).** (**** p< 0.0001, Student t-test; *n = 16* heminota from two independent replicates). Scale bars: 100 µm.

Figure 5. The FGF receptor Breathless (Btl) is expressed along tracheal branches and is required for tracheal recruitment to the damaged muscle. (A-B''). Btl:cherry^{endo} (magenta) is detected along tracheal branches (gray) associated with indirect flight muscles (IFMs) labelled with Mhc (cyan), in either control A' or injured muscles B'. **(A'', B'').** Boxed regions from (A-B), magnified 4.5X. Scale bars: 100 µm. **(C-C').** The *Btl-GAL4* driver (green and magenta; *Btl-Gal4, UAS-mCD8GFP; UAS-H2B-RFP*) is active in a subset of tracheal branches (arrows, C-C'). Arrowheads in C indicate the tracheal branches that do not express the *Btl-Gal4* driver. Scale bars: 25 µm. **(D-E).** Expression of the Btl-Gal4 driver (green, *Btl-Gal4, UAS-mCD8GFP*) in control (D) and at 5DPI (E). Muscles are labelled with Mhc (magenta). Scale bars: 100 µm. **(F-I'').** Downregulating *btl* in the tracheal cells with either *dSRF-Gal4* driver (*dSRF-Gal4; UAS-Btl^{RNAi},* H-H'') or Btl-Gal4 driver (*Btl-Gal4, UAS- Btl^{RNAi}*, I-I'') prevents tracheal invasion to the damaged fiber. **(J).** Quantification of trachea coverage (****p < 0.0001, **p=0.0053, Student's *t*-test; *n = 7* heminota per condition). Scale bars: 100 µm.

Figure 6. Hemocytes derived extracellular matrix components are required for muscle maintenance. (A-A''). Vkg::GFP (green) is distributed at basal levels around muscle fibers (arrow, A'), tracheal branches (arrowheads, A'), and hemocytes (magenta, *Pxn-RFP*; arrow, A'') in control conditions. **(B-B'').** At 5DPI, Vkg::GFP is strongly enriched on the injured muscle fibers (labelled with Mhc, blue). **(C-H).** Hemocytes recruitment (magenta, *Pxn-RFP*) and Collagen IV (green, *Vkg::GFP*) distribution on the injured muscle, from 1DPI to 20DPI. Scale bars: 100 µm. **(I-J).** SPARC (magenta) is detected in the IFMs associated hemocytes visualized by either *HmlΔ-Gal4* (I-I') or *Enh3-Gal4* (J-J') drivers. **(K-K').** SPARC expression is increased in injured fibers compared to controls (J-J'). **(L-L').** Adult hemocytes (magenta; *SPARC-Gal4*, *UAS-myr-RFP*) express BM40-SPARC-GFP (green). **(M-M').** BM40-SPARC-GFP produced by adult hemocytes is broadly distributed along the injured muscle fibers. **(N-N').** Detection of adult hemocytes expressing *Enh3-Gal4, UAS-mCD8GFP; UAS-H2B-RFP* (green and magenta, arrowheads) at the distal ends of IFMs and in close proximity to the tendons (arrow). TOPRO (blue) labels muscle nuclei. Scale bars: 100 µm. **(O-P').** Downregulation of *Sparc* in adult hemocytes *(using Enh3-Gal4 driver)* induces localized muscle defects at muscle fiber tips, accompanied by upregulation of Mhc **(Q)**.

Figure 7. Coordinated hemocyte–tracheal communication drives the sequential response to muscle injury. A. Drosophila IFMs damage induces an upregulation of *Mhc* expression and is associated with local hypoxia. **B.** In response to this injury, hemocytes are specifically recruited to the damaged muscle fiber, where they: **C.** secrete Branchless (Bnl), which accumulates within the injured fiber to promote tracheal outgrowth via the Bnl/Breathless (Btl) signaling pathway, and **D.** produce extracellular matrix (ECM) components, such as Sparc and Collagen IV, which are essential for maintaining adult muscle integrity.

Extended figure legends.

Figure S1. Mhc upregulation marks the damaged muscle fiber. (A-B''). Wild-type IFMs stained for Mhc (magenta) and Mef2 (cyan) show upregulation of Mhc and downregulation of Mef2 in the injured fiber (asterisks, B'-B'') at 5DPI. **(A', B').** 2X magnification of the boxed regions in A and B. Scale bars: 100 µm. **(C-C'').** Expression of the embryonic Mhc isoform (*weeP26*, green) in uninjured (C) and injured (C'-C'') IFMs. Injury does not alter weeP26 expression (C and C''). **(D-D'').** The shorter Mhc-GFP isoforms (*Mhc-Iso-K, L, M (fTRG500*); green) colocalize with anti-Mhc staining (magenta) and are upregulated in injured muscle (D-D''). **(E-E'').** The longer Mhc-GFP isoforms (*Mhc-Iso-A, F, G (fTRG519*); green) are not expressed in adult IFMs and do not respond to muscle injury (E-E''). Scale bars: 100 µm. **(F-G'').** In *Naa30A* mutant IFMs, defective muscle attachment correlates with increased Mhc expression (magenta, G), upregulation of short Mhc-GFP isoforms (green, G'), and a loss of Mef2 (cyan, G''). **(H-I').** Co-expression of hemocytes markers *HmlΔ-Gal4, UAS-mCD8GFP* (green) and *Pxn-RFP* (magenta) reveals two subsets of hemocytes: $Pxn^{+}Hml^{+}$ (arrows) and $Pxn^{+}Hml^{-}$ (arrowheads). Nuclei are visualized with TO-PRO (blue). Data from *n >10* heminota from two independent replicates. **(J-M').** Co-expression analysis of *Enh3-Gal4; UAS-mcD8GFP* (green) and *Pxn-RFP* (magenta) shows that all $Enh3^{+}$ cells express Pxn (J'-K'). No Mef2 expression (cyan) is observed in these cells, in either undamaged (L') or damaged (M', dashed lines) fibers. Scale bars: 100 µm. Yellow asterisks in panels F', G'' and L' mark non-specific signal detected in motoneurons.

Figure S2. Early recruitment of hemocytes initiates tracheal remodeling after muscle damage. (A-B'). Hemocytes are visualized using an anti-Zfh1 (green) are recruited to the injured fiber exhibiting elevated Mhc expression (magenta). **(C-D').** In

Naa30A mutant flies, defective muscle attachment is associated with tracheal enrichment (gray, D') and increased hemocytes accumulation (green, D') compared to controls (C-C'). **(E-M').** Time-course analysis of tracheal remodeling and hemocytes recruitment in *Enh3-Gal4; UAS-mCD8GFP* adult IFMs following localized stab injury. Tracheal branches are visualized by autofluorescence (gray), and hemocytes are labeled with GFP (green). Muscles are labeled with Mhc (magenta). Time points range from 1-hour post-injury (1HPI) to 20 days post-injury (20DPI). **(N)**. Quantification of normalized Mhc intensity. **(O)**. Quantification of the hemocytes number in the injured fiber shows a significant increase starting at 1HPI which remains elevated until 20DPI. **(P).** Tracheal quantification shows a marked increase in its density from 3DPI and remains sustained until 20 DPI. (****p < 0.0001, ***p < 0.001; Student's t-test; $n \geq 10$ heminota per condition). Scale bars: 100 μm.

Figure S3. Tracheal branching in response to muscle damage requires precise control of Bnl levels and distribution. (A-B'). Expression pattern of the *Shavenbaby* (*Svb*) muscle regulatory enhancer (*SME-Gal4; UAS-mCD8GFP*). *SME-Gal4* drives GFP expression (green) in a subset of larval muscle progenitors located in the posterior region of the wing disc (A-A') and in a subset of adult muscle nuclei (DAPI, blue, B-B') Scale bars: 100 μm. **(C).** Schematic representation of the *Drosophila* FLP-OUT system used for localized overexpression of UAS-Bnl::GFP in muscle nuclei, employing the *Hsflp; FRT-SME-Stop-FRT-Gal4/CyO; tub-Gal80ts* trasgenes. **(D-E'').** Loss of Bnl-LacZ reporter expression (green) is specifically observed in the nuclei of the injured muscle fibers overexpressing Mhc (magenta). **(D', E').** 6X magnification of the boxed regions in D and E, Scale bars: 25 μm. **(F-H).** Targeted downregulation of *bnl* in a subset of hemocytes using *HmlΔ-Gal4* driver significantly reduces tracheal enrichment at the injured fiber, as quantified in **(I)**. (*p < 0.05, Student's t-test; $n \geq 10$ heminota per condition). Scale bars: 100 μm.

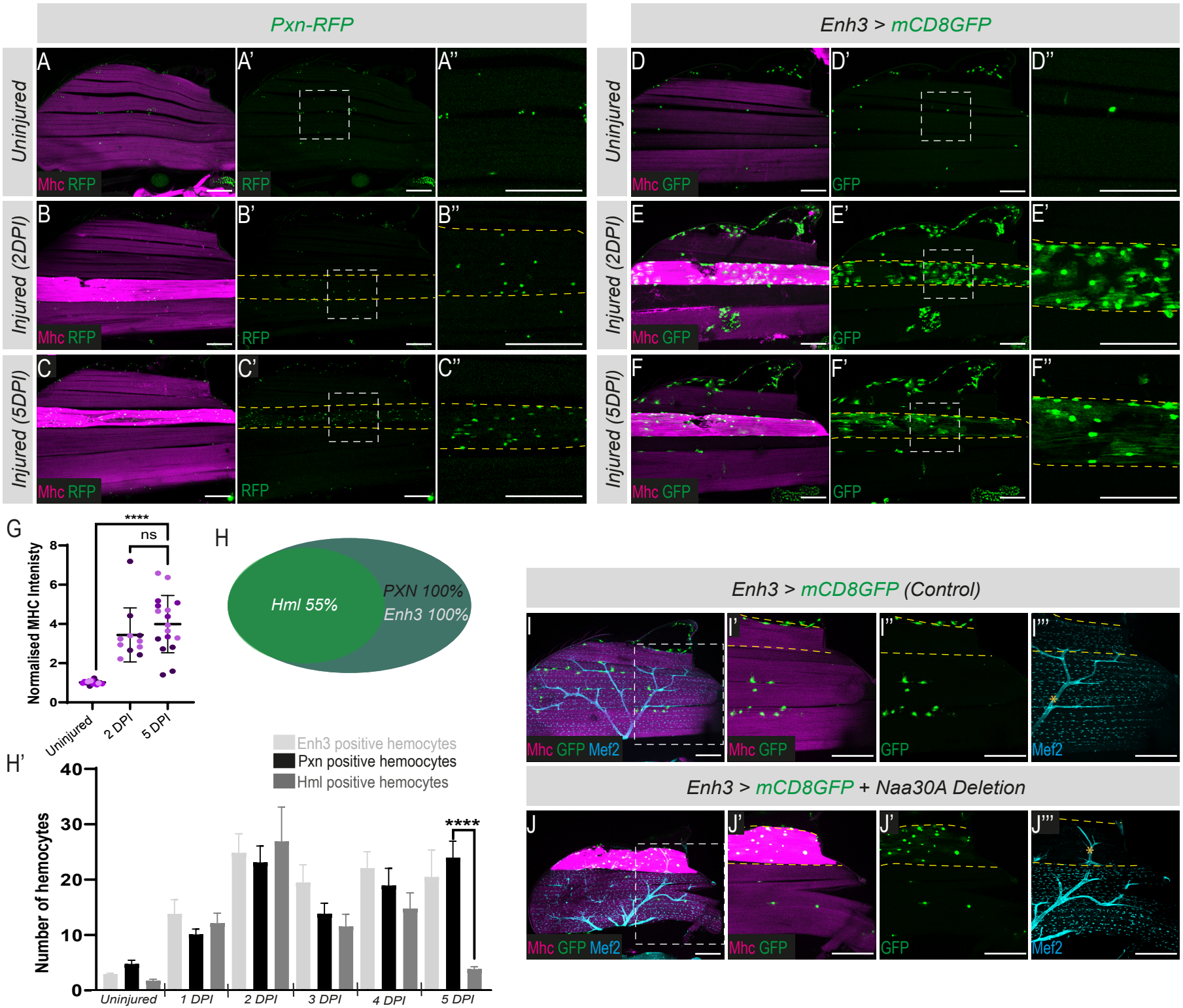
Pxn-RFP
Enh3 > mCD8GFP
Uninjured
Injured (2DPI)
Injured (5DPI)
A
A'
A''
B
B'
B''
C
C'
C''
D
D'
D''
E
E'
E'
F
F'
F''
Mhc RFP
RFP
Mhc GFP
GFP
G
****
ns
Normalised MHC Intenisty
0
2
4
6
8
Uninjured
2 DPI
5 DPI
H
Hml 55%
PXN 100%
Enh3 100%
H'
Enh3 positive hemocytes
Pxn positive hemoocytes
Hml positive hemocytes
Number of hemocytes
0
10
20
30
40
****
Uninjured
1 DPI
2 DPI
3 DPI
4 DPI
5 DPI
Enh3 > mCD8GFP (Control)
I
I'
I''
I'''
Mhc GFP Mef2
Mhc GFP
GFP
Mef2
Enh3 > mCD8GFP + Naa30A Deletion
J
J'
J''
J'''
Mhc GFP Mef2
Mhc GFP
GFP
Mef2

Figure 1

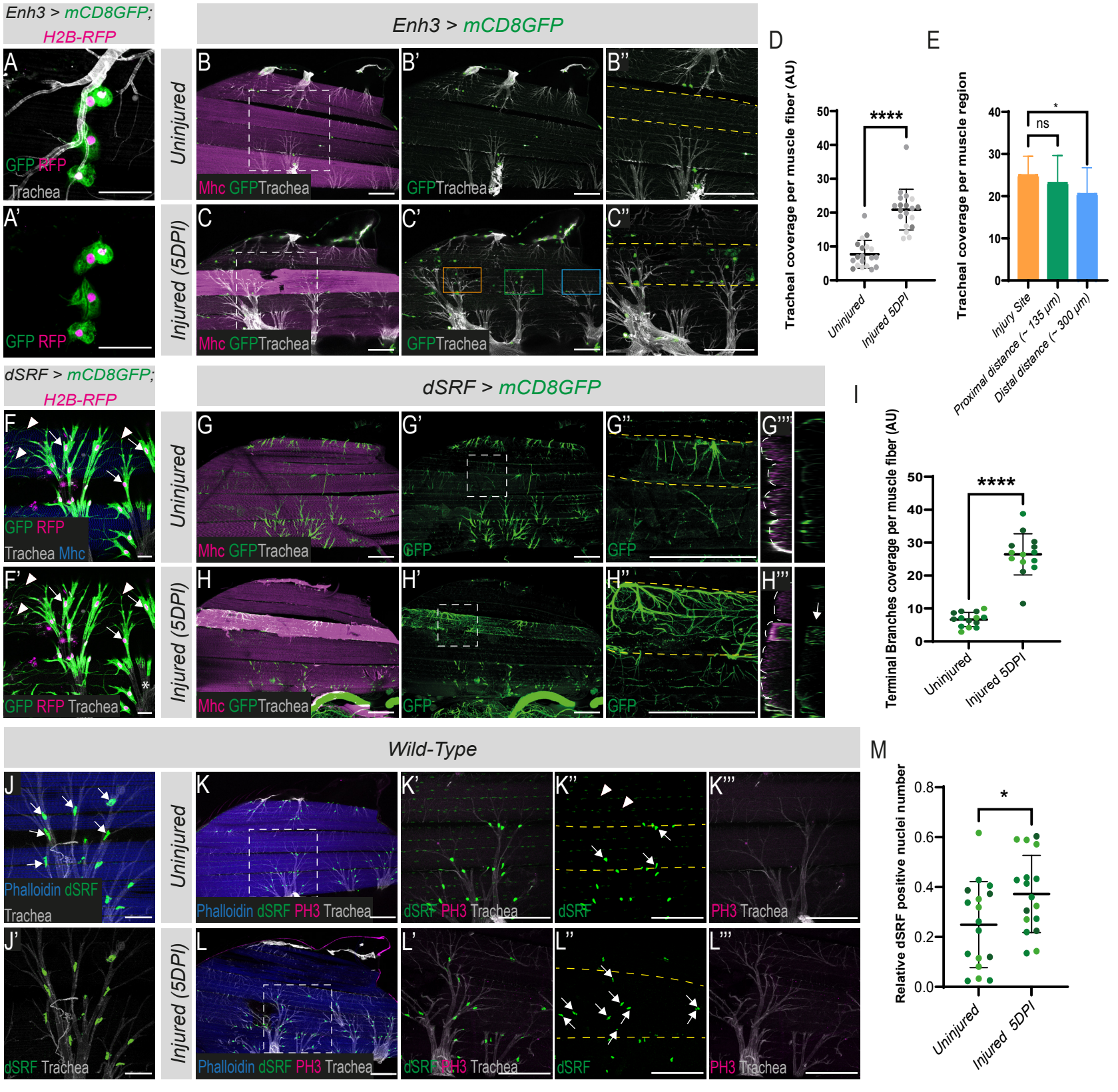
Enh3 > mCD8GFP; H2B-RFP
Enh3 > mCD8GFP
Uninjured
Injured (5DPI)
A
A'
B
B'
B''
C
C'
C''
GFP RFP
Trachea
Mhc GFP Trachea
GFP Trachea
D
Tracheal coverage per muscle fiber (AU)
****
Uninjured
Injured 5DPI
E
Tracheal coverage per muscle region
ns
*
Injury Site
Proximal distance (~ 135 µm)
Distal distance (~ 300 µm)
dSRF > mCD8GFP; H2B-RFP
dSRF > mCD8GFP
F
F'
G
G'
G''
G'''
H
H'
H''
H'''
GFP RFP Trachea Mhc
Mhc GFP Trachea
GFP
I
Terminal Branches coverage per muscle fiber (AU)
****
Uninjured
Injured 5DPI
Wild-Type
J
J'
K
K'
K''
K'''
L
L'
L''
L'''
Phalloidin dSRF Trachea
Phalloidin dSRF PH3 Trachea
dSRF PH3 Trachea
dSRF
PH3 Trachea
M
Relative dSRF positive nuclei number
*
Uninjured
Injured 5DPI

Figure 2

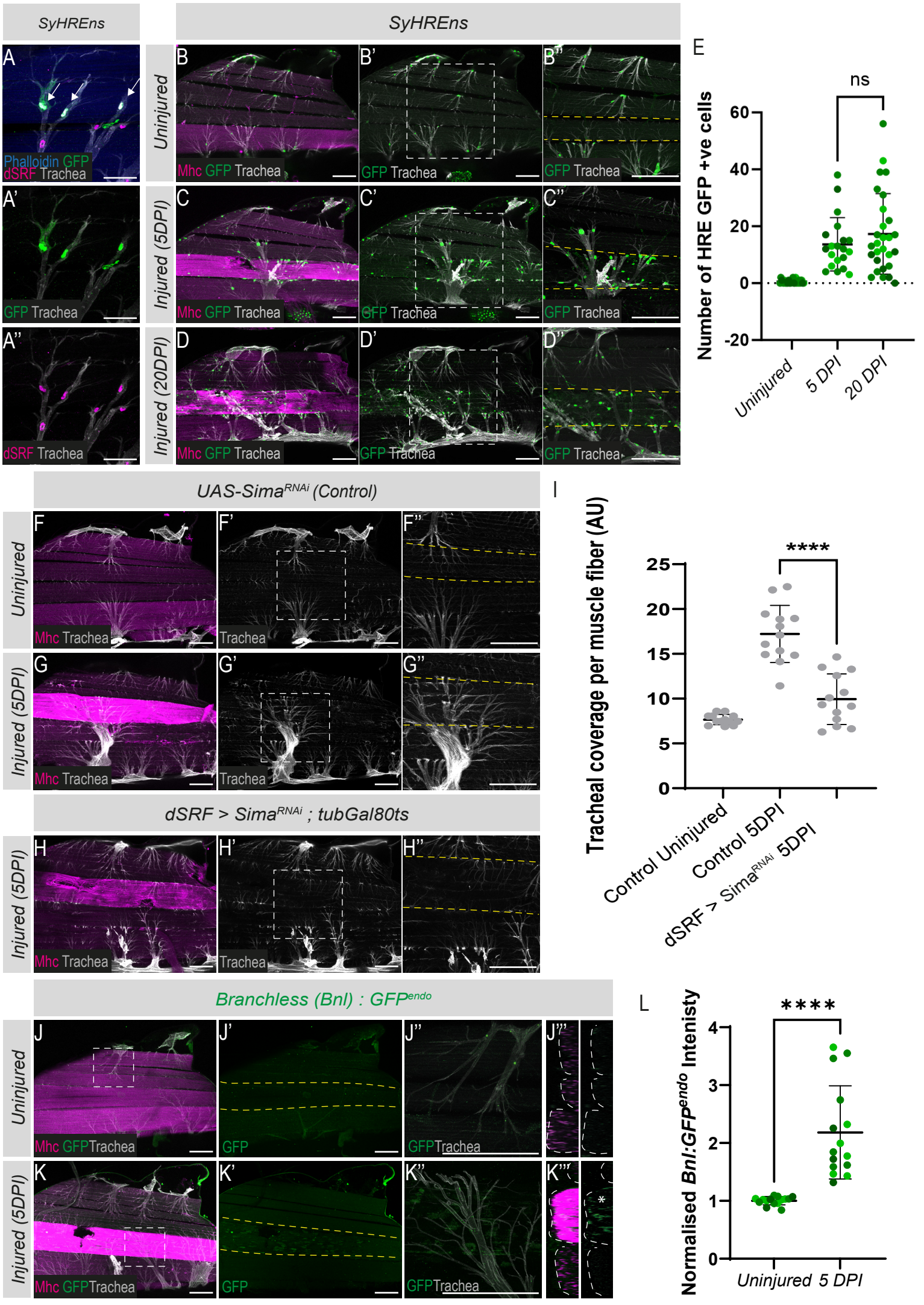
SyHREns
SyHREns
A
Phalloidin GFP
dSRF Trachea
A'
GFP Trachea
A''
dSRF Trachea
Uninjured
Injured (5DPI)
Injured (20DPI)
B
B'
B''
C
C'
C''
D
D'
D''
Mhc GFP Trachea
GFP Trachea
E
ns
Number of HRE GFP +ve cells
60
40
20
0
-20
Uninjured
5 DPI
20 DPI
UAS-Sima^RNAi (Control)
F
F'
F''
G
G'
G''
Mhc Trachea
Trachea
I
****
Tracheal coverage per muscle fiber (AU)
25
20
15
10
5
0
Control Uninjured
Control 5DPI
dSRF > Sima^RNAi 5DPI
dSRF > Sima^RNAi ; tubGal80ts
H
H'
H''
Branchless (Bnl) : GFP^endo
J
J'
J''
J'''
K
K'
K''
K'''
Mhc GFPTrachea
GFP
GFPTrachea
L
****
Normalised Bnl:GFP^endo Intenisty
4
3
2
1
0
Uninjured
5 DPI

Figure 3

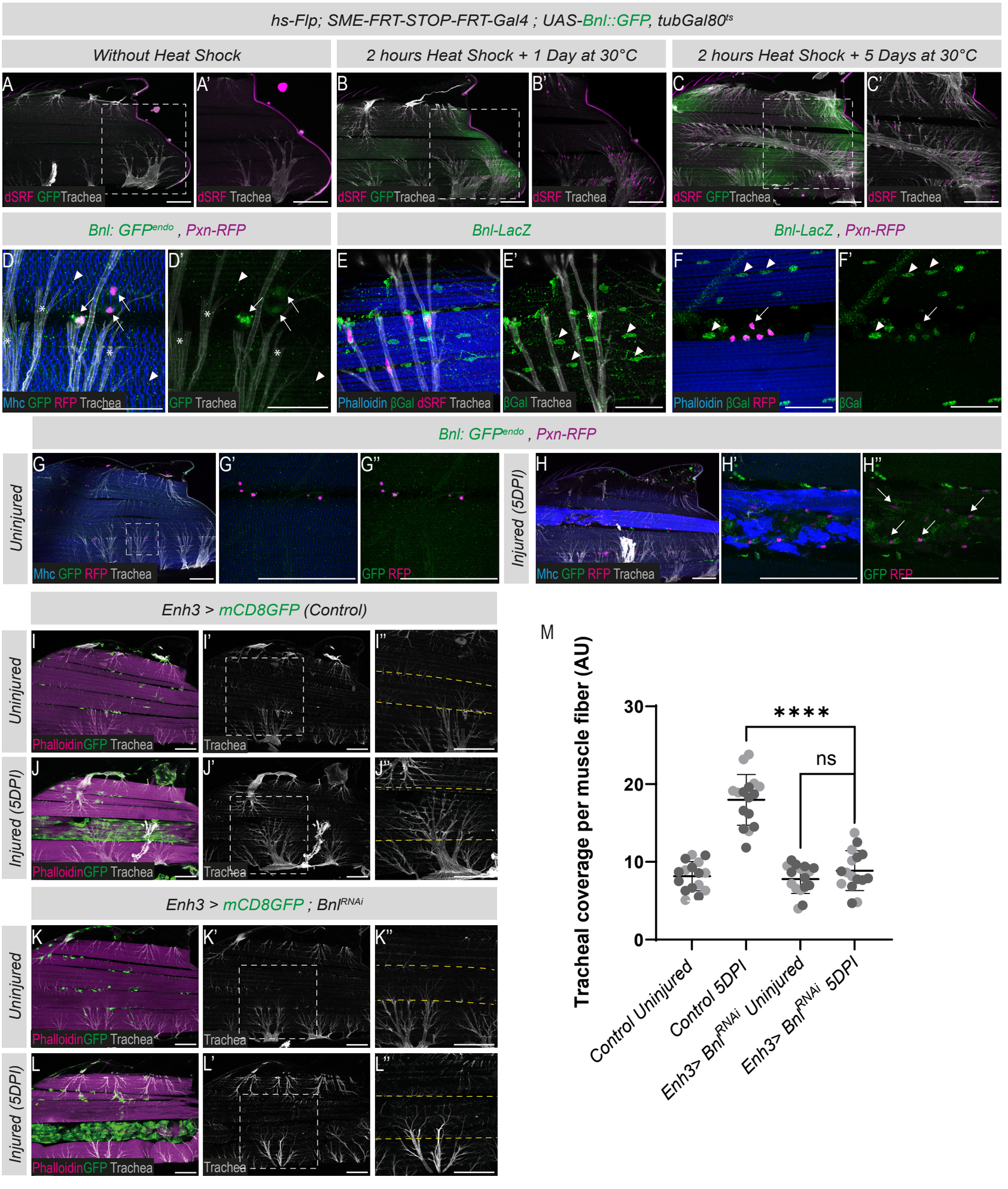
hs-Flp; SME-FRT-STOP-FRT-Gal4 ; UAS-Bnl::GFP, tubGal80ts
Without Heat Shock
2 hours Heat Shock + 1 Day at 30°C
2 hours Heat Shock + 5 Days at 30°C
A
A'
B
B'
C
C'
dSRF GFP Trachea
dSRF Trachea
Bnl: GFPendo , Pxn-RFP
Bnl-LacZ
Bnl-LacZ , Pxn-RFP
D
D'
E
E'
F
F'
Mhc GFP RFP Trachea
GFP Trachea
Phalloidin βGal dSRF Trachea
βGal Trachea
Phalloidin βGal RFP
βGal
Bnl: GFPendo , Pxn-RFP
Uninjured
Injured (5DPI)
G
G'
G''
H
H'
H''
Mhc GFP RFP Trachea
GFP RFP
Enh3 > mCD8GFP (Control)
Enh3 > mCD8GFP ; BnlRNAi
I
I'
I''
J
J'
J''
K
K'
K''
L
L'
L''
PhalloidinGFP Trachea
Trachea
M
Tracheal coverage per muscle fiber (AU)
30
20
10
0
****
ns
Control Uninjured
Control 5DPI
Enh3> BnlRNAi Uninjured
Enh3> BnlRNAi 5DPI

Figure 4

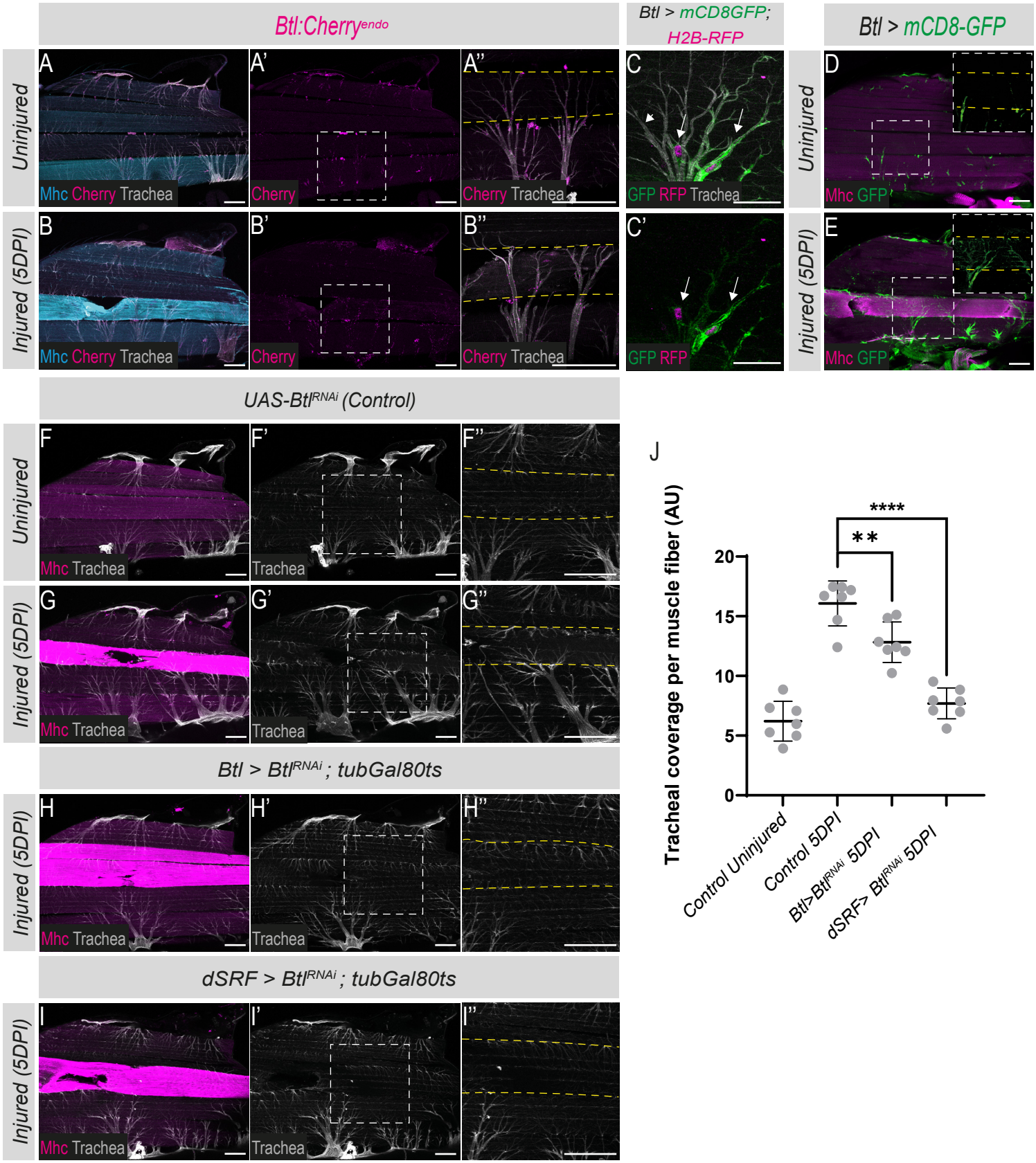
Btl:Cherry^endo
Btl > mCD8GFP; H2B-RFP
Btl > mCD8-GFP
Uninjured
Injured (5DPI)
A
A'
A''
B
B'
B''
C
C'
D
E
Mhc Cherry Trachea
Cherry
Cherry Trachea
GFP RFP Trachea
GFP RFP
Mhc GFP
UAS-Btl^RNAi (Control)
F
F'
F''
G
G'
G''
Mhc Trachea
Trachea
Btl > Btl^RNAi ; tubGal80ts
H
H'
H''
dSRF > Btl^RNAi ; tubGal80ts
I
I'
I''
J
Tracheal coverage per muscle fiber (AU)
****
**
20
15
10
5
0
Control Uninjured
Control 5DPI
Btl>Btl^RNAi 5DPI
dSRF> Btl^RNAi 5DPI

Figure 5

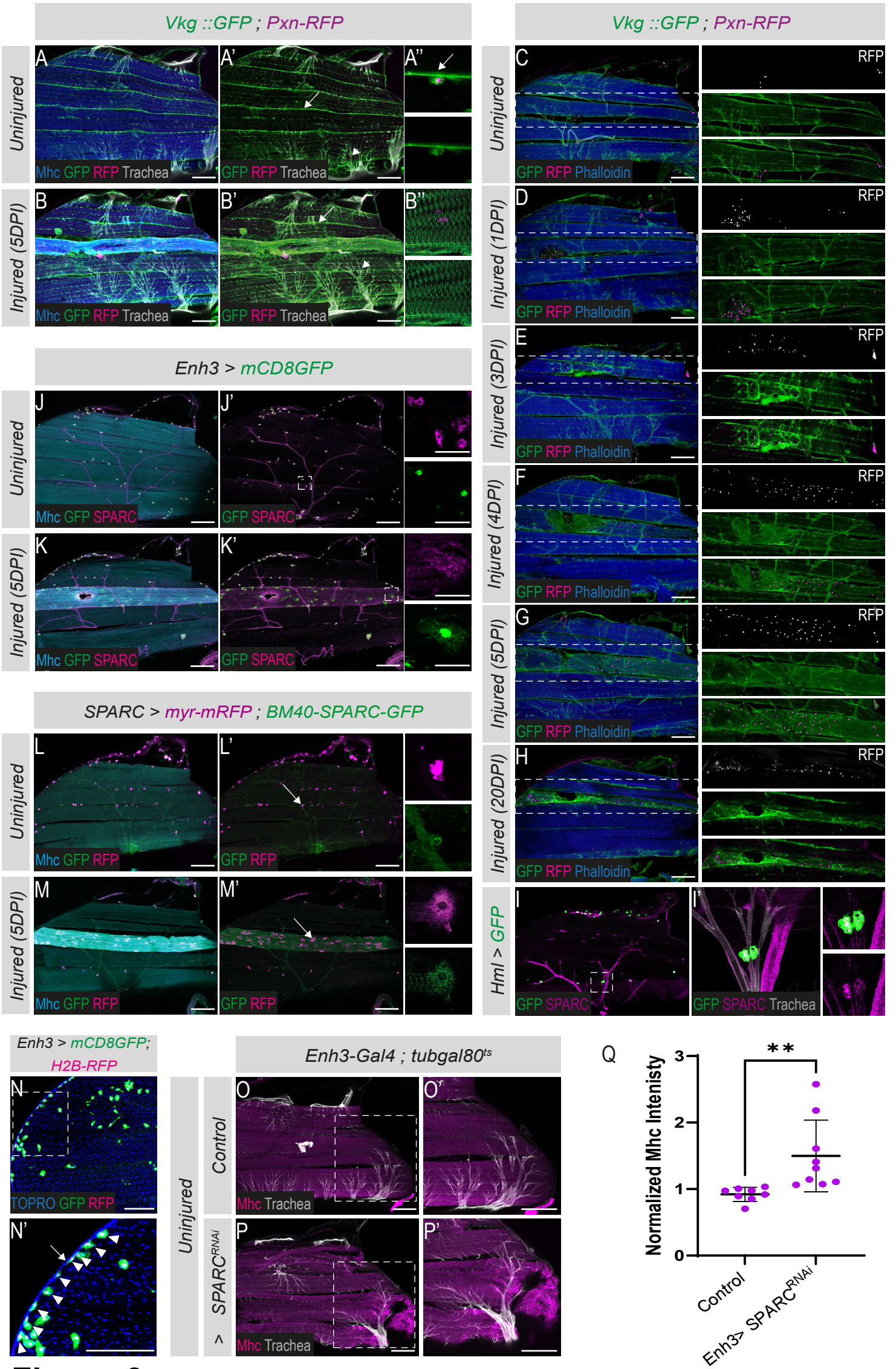
Vkg ::GFP ; Pxn-RFP
Uninjured
Injured (5DPI)
A
A'
A''
B
B'
B''
Mhc GFP RFP Trachea
GFP RFP Trachea
Vkg ::GFP ; Pxn-RFP
Uninjured
Injured (1DPI)
Injured (3DPI)
Injured (4DPI)
Injured (5DPI)
Injured (20DPI)
C
D
E
F
G
H
RFP
GFP RFP Phalloidin
Enh3 > mCD8GFP
Uninjured
Injured (5DPI)
J
J'
K
K'
Mhc GFP SPARC
GFP SPARC
SPARC > myr-mRFP ; BM40-SPARC-GFP
Uninjured
Injured (5DPI)
L
L'
M
M'
Mhc GFP RFP
GFP RFP
Hml > GFP
I
I'
GFP SPARC
GFP SPARC Trachea
Enh3 > mCD8GFP; H2B-RFP
N
N'
TOPRO GFP RFP
Enh3-Gal4 ; tubgal80ts
Uninjured
Control
> SPARCRNAi
O
O'
P
P'
Mhc Trachea
Q
Normalized Mhc Intensity
0
1
2
3
**
Control
Enh3> SPARCRNAi

Figure 6

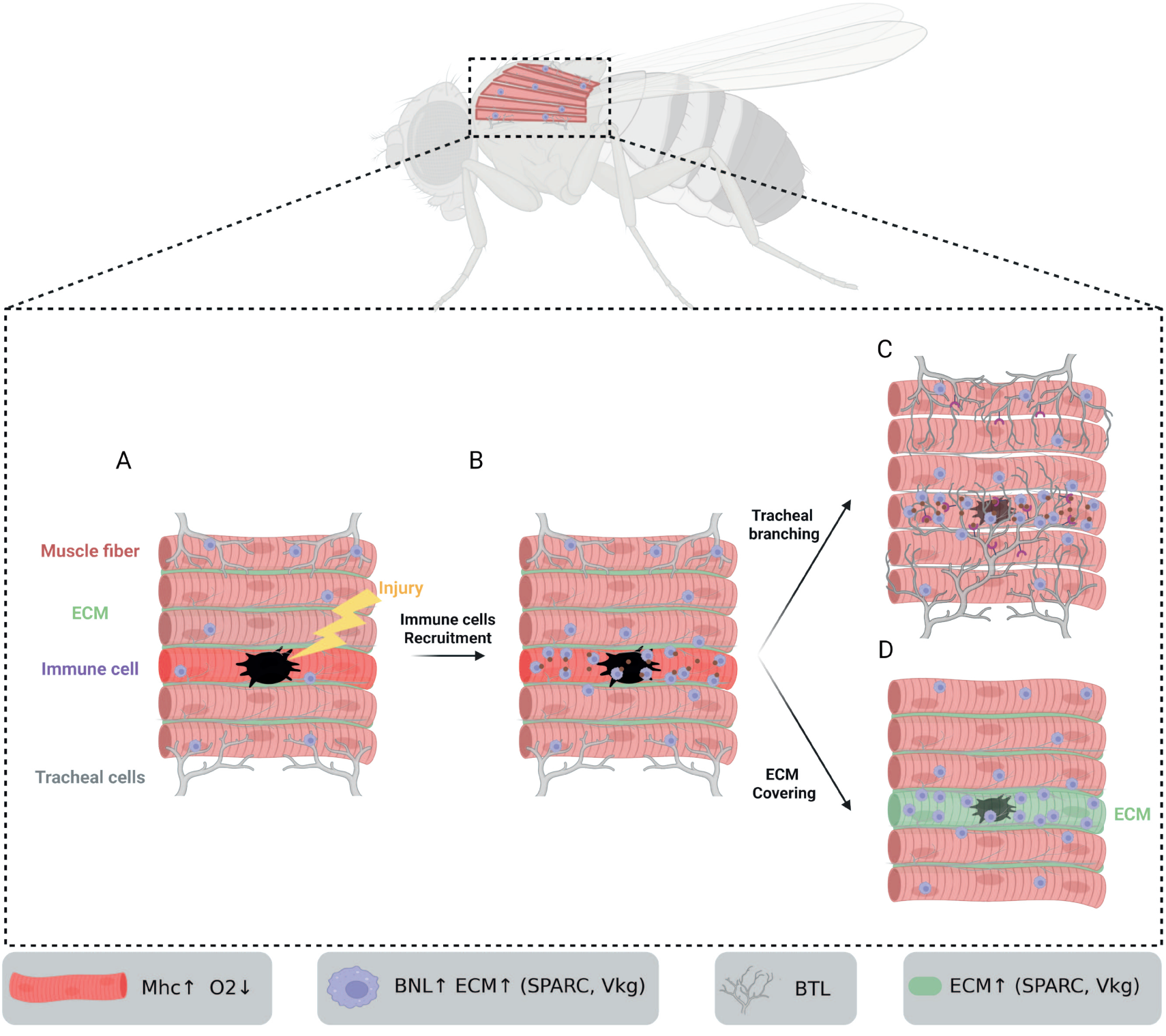
A
B
C
D
Muscle fiber
ECM
Immune cell
Tracheal cells
Injury
Immune cells
Recruitment
Tracheal
branching
ECM
Covering
ECM
Mhc↑ O2↓
BNL↑ ECM↑ (SPARC, Vkg)
BTL
ECM↑ (SPARC, Vkg)

Figure 7

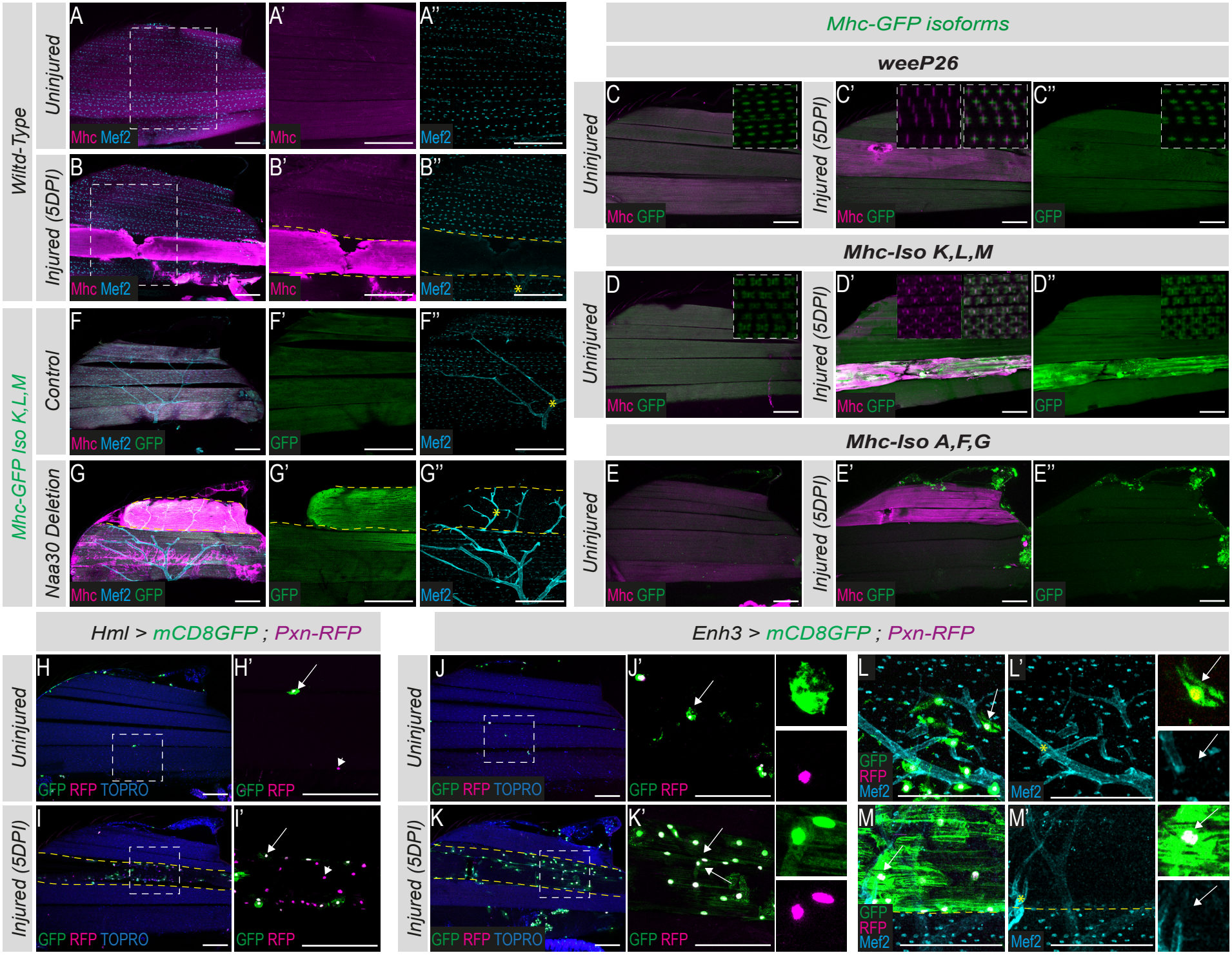
Wiltd-Type
Uninjured
Injured (5DPI)
Mhc-GFP Iso K,L,M
Control
Naa30 Deletion
Mhc-GFP isoforms
weeP26
Mhc-Iso K,L,M
Mhc-Iso A,F,G
Hml > mCD8GFP ; Pxn-RFP
Enh3 > mCD8GFP ; Pxn-RFP
A
A'
A''
B
B'
B''
C
C'
C''
D
D'
D''
E
E'
E''
F
F'
F''
G
G'
G''
H
H'
I
I'
J
J'
K
K'
L
L'
M
M'
Mhc Mef2
Mhc
Mef2
Mhc GFP
GFP
Mhc Mef2 GFP
GFP RFP TOPRO
GFP RFP
RFP
Mef2

Figure S1

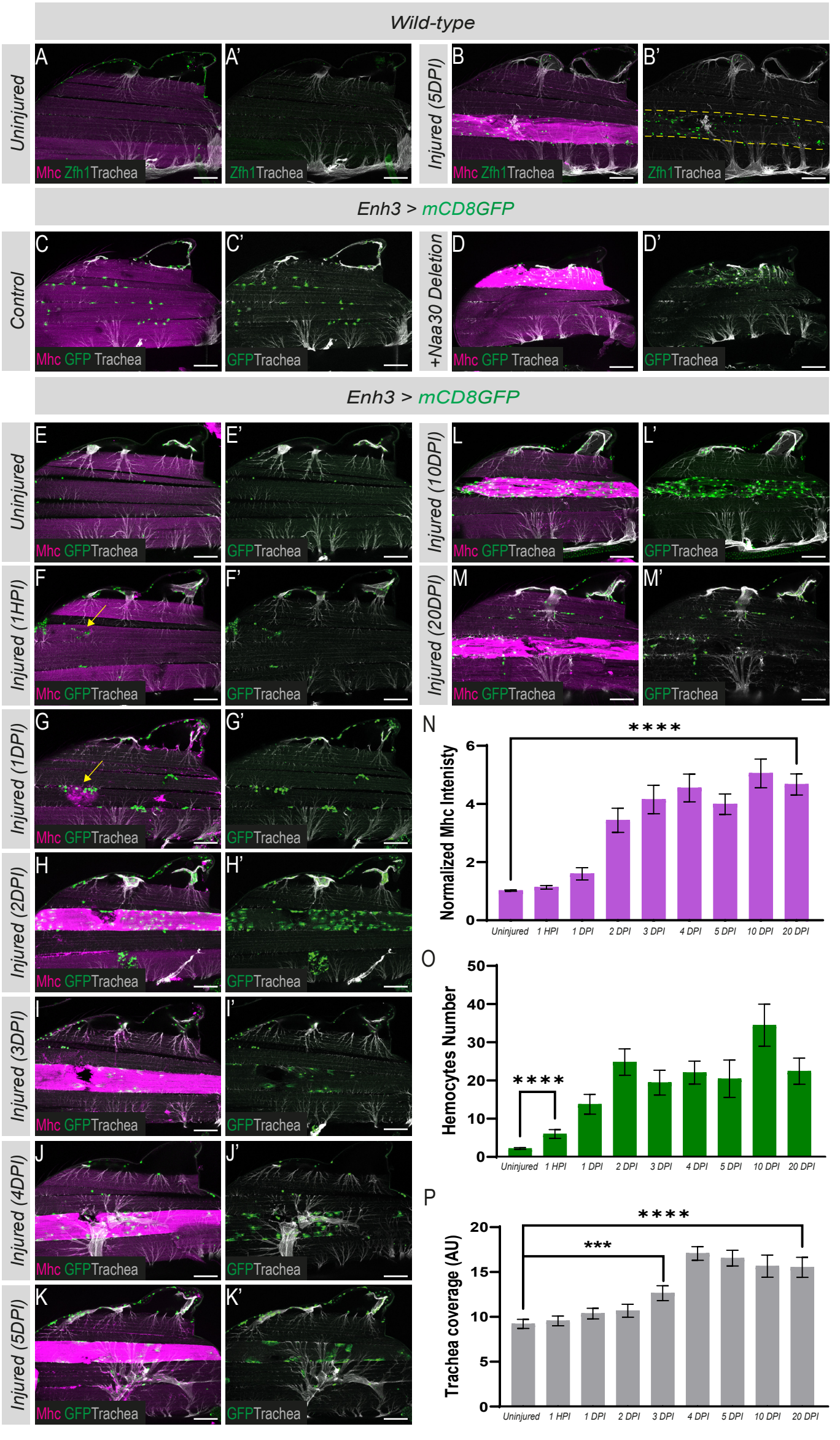
Wild-type
Uninjured
A
A'
Mhc Zfh1 Trachea
Zfh1 Trachea
Injured (5DPI)
B
B'
Mhc Zfh1 Trachea
Zfh1 Trachea
Enh3 > mCD8GFP
Control
C
C'
Mhc GFP Trachea
GFP Trachea
+Naa30 Deletion
D
D'
Mhc GFP Trachea
GFP Trachea
Enh3 > mCD8GFP
Uninjured
E
E'
Mhc GFP Trachea
GFP Trachea
Injured (10DPI)
L
L'
Mhc GFP Trachea
GFP Trachea
Injured (1HPI)
F
F'
Mhc GFP Trachea
GFP Trachea
Injured (20DPI)
M
M'
Mhc GFP Trachea
GFP Trachea
Injured (1DPI)
G
G'
Mhc GFP Trachea
GFP Trachea
Injured (2DPI)
H
H'
Mhc GFP Trachea
GFP Trachea
Injured (3DPI)
I
I'
Mhc GFP Trachea
GFP Trachea
Injured (4DPI)
J
J'
Mhc GFP Trachea
GFP Trachea
Injured (5DPI)
K
K'
Mhc GFP Trachea
GFP Trachea
N
****
Normalized Mhc Intenisty
0
2
4
6
Uninjured
1 HPI
1 DPI
2 DPI
3 DPI
4 DPI
5 DPI
10 DPI
20 DPI
O
****
Hemocytes Number
0
10
20
30
40
50
Uninjured
1 HPI
1 DPI
2 DPI
3 DPI
4 DPI
5 DPI
10 DPI
20 DPI
P
****
***
Trachea coverage (AU)
0
5
10
15
20
Uninjured
1 HPI
1 DPI
2 DPI
3 DPI
4 DPI
5 DPI
10 DPI
20 DPI

Figure S2

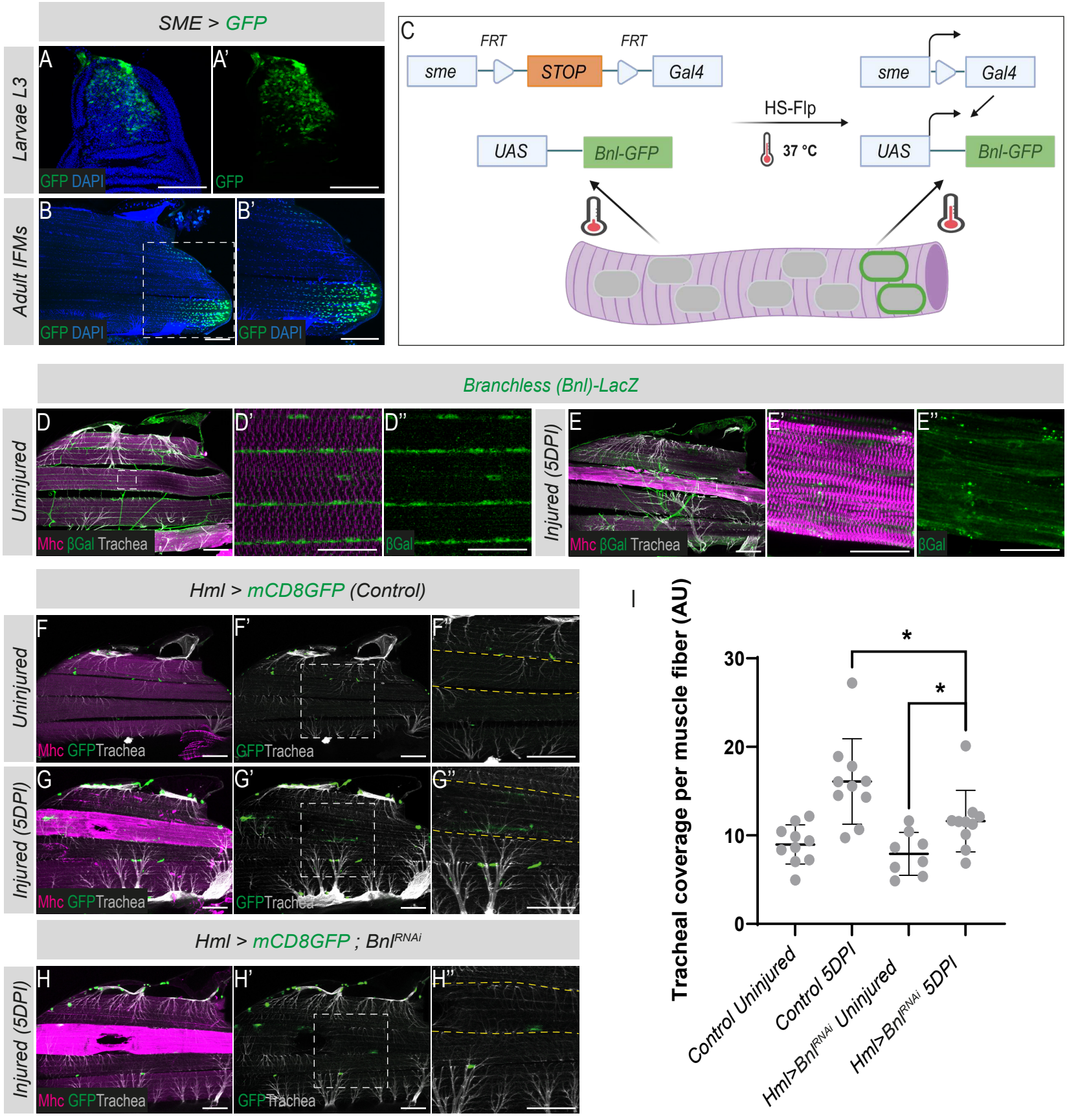
SME > GFP
Larvae L3
Adult IFMs
A
A'
B
B'
GFP DAPI
GFP
C
FRT
FRT
sme
STOP
Gal4
HS-Flp
37 °C
UAS
Bnl-GFP
Branchless (Bnl)-LacZ
Uninjured
Injured (5DPI)
D
D'
D''
E
E'
E''
Mhc βGal Trachea
βGal
Hml > mCD8GFP (Control)
Hml > mCD8GFP ; Bnl^RNAi
F
F'
F''
G
G'
G''
H
H'
H''
Mhc GFP Trachea
GFP Trachea
I
Tracheal coverage per muscle fiber (AU)
30
20
10
0
*
*
Control Uninjured
Control 5DPI
Hml>Bnl^RNAi Uninjured
Hml>Bnl^RNAi 5DPI

Figure S3

Article 2. Studying Muscle Transcriptional Dynamics at Single-molecule Scales in *Drosophila*

Emma Leroux, **Nourhene Ammar**, Savannah Moinet, Thierry Pecot, Hadi Boukhatmi (JoVE Journal, 2023, DOI : 10.3791/65713)

L'un des axes majeurs de recherche développés dans notre laboratoire concerne l'étude de la dynamique transcriptionnelle des gènes impliqués dans la myogenèse. Dans le cadre du projet de thèse d'Emma Leroux (doctorante en 3e année dans notre équipe), nous avons entrepris l'optimisation de la technique de *single-molecule RNA fluorescence in situ hybridization* (smFISH), afin de détecter et de quantifier avec précision les molécules individuelles d'ARN messager (ARNm) dans le lignage musculaire de la *Drosophile*. Cette optimisation a nécessité l'adaptation spécifique du protocole smFISH aux disques imaginaux d'aile et aux IFMs, permettant ainsi une visualisation à haute résolution spatiale des ARNm et rendant possible l'analyse de leur distribution à l'échelle de la cellule individuelle.

Pour valider cette approche, nous nous sommes concentrés sur deux facteurs de transcription fortement impliqués dans la formation des muscles : Mef2 et Zfh1. Nous avons réussi à visualiser, avec une très haute résolution, les transcrits naissants dans les noyaux (*transcriptional starts*), ainsi que les ARNm matures dans le cytoplasme. Nous avons adapté cette méthodologie aux AMPs (dans les disques d'aile), aux IFMs adultes ainsi qu'aux MuSCs associés aux IFMs.

Parallèlement, nous avons, en collaboration avec la plateforme FIAA (Biosite, Rennes), développé un programme automatisé permettant de quantifier avec précision l'abondance et la localisation subcellulaire de ces ARNm, ouvrant la voie à une analyse fine de l'hétérogénéité transcriptionnelle entre noyaux appartenant à un même muscle. Cette méthodologie constitue un outil puissant pour explorer la régulation spatio-temporelle de l'expression génique dans les muscles, offrant ainsi une meilleure compréhension des processus moléculaires qui gouvernent leur développement, leur homéostasie et leur adaptation. De plus, elle pourra être appliquée à l'étude des mécanismes impliqués dans la réparation musculaire.

jove

Studying Muscle Transcriptional Dynamics at Single-molecule Scales in *Drosophila*

Emma Leroux[1], **Nourhene Ammar**[1], **Savannah Moinet**[1], **Thierry Pecot**[2], **Hadi Boukhatmi**[1]

[1] Institut de Génétique et Développement de Rennes (IGDR), UMR6290 CNRS - Université de Rennes [2] BIOSIT, UAR 3480 US 018, Université de Rennes

Corresponding Author

Hadi Boukhatmi
hadi.boukhatmi@univ-rennes1.fr

Citation

Leroux, E., Ammar, N., Moinet, S., Pecot, T., Boukhatmi, H. Studying Muscle Transcriptional Dynamics at Single-molecule Scales in *Drosophila*. *J. Vis. Exp.* (199), e65713, doi:10.3791/65713 (2023).

Date Published

September 8, 2023

DOI

10.3791/65713

URL

jove.com/video/65713

Abstract

Skeletal muscles are large syncytia made up of many bundled myofibers that produce forces and enable body motion. *Drosophila* is a classical model to study muscle biology. The combination of both *Drosophila* genetics and advanced omics approaches led to the identification of key conserved molecules that regulate muscle morphogenesis and regeneration. However, the transcriptional dynamics of these molecules and the spatial distribution of their messenger RNA within the syncytia cannot be assessed by conventional methods. Here we optimized an existing single-molecule RNA fluorescence *in situ* hybridization (smFISH) method to enable the detection and quantification of individual mRNA molecules within adult flight muscles and their muscle stem cells. As a proof of concept, we have analyzed the mRNA expression and distribution of two evolutionary conserved transcription factors, Mef2 and Zfh1/Zeb. We show that this method can efficiently detect and quantify single mRNA molecules for both transcripts in the muscle precursor cells, adult muscles, and muscle stem cells.

Introduction

Adult skeletal muscles are made of differentiated multinucleated myofibers whose contractile properties generate movements. Muscle growth, maintenance, and regeneration rely upon muscle progenitors and muscle stem cells (MuSCs) that are specified during embryonic development[1]. The myogenic program is finely controlled by a set of core myogenic transcription factors (TFs) (e.g., Pax3/7, MYOD, Mef2, and ZEB)[2,3,4]. Deciphering the molecular mechanisms regulating muscle biology is important for elucidating fundamental myology-related questions and for possible therapeutic use in treating muscle-degenerative diseases.

Drosophila has a long history as a genetic model to study myogenesis[5]. It has recently emerged as a new model to investigate muscle regeneration[6,7,8]. The muscle structure and core myogenic programs are highly conserved between flies and mammals. For example, the TFs Mef2 and Zfh1/ZEB have a conserved function in regulating muscle development and regeneration[3,9,10,11]. Adult *Drosophila* muscles, such as the Indirect Flight Muscles (IFMs), are formed from

Copyright © 2023 JoVE Creative Commons Attribution-NonCommercial-NoDerivs 3.0 Unported License

a specific population of MuSCs, known as Adult Muscle Progenitors (AMPs)[12]. These AMPs are specified during embryogenesis and associate with epithelial structures such as wing and leg discs. Throughout embryonic and larval stages, AMPs remain undifferentiated until metamorphosis when they engage in differentiation and fusion to form the IFMs[13,14]. The TF Spalt major (*spalt, salm*) is expressed during flight muscle development and is necessary to determine their structural identity[15]. Mef2 is another important myogenic TF that is essential for adult muscle formation[16,17]. It is expressed in the AMPs and maintained in the adult IFMs[10,18]. While the majority of AMPs differentiate into functional muscles, a subset escapes differentiation and forms the adult MuSCs[11]. Similar to vertebrates, the TF Zfh1/ZEB is required to prevent premature differentiation of the adult MuSCs and to maintain their stemness[9,10].

Gene expression dynamics have been proven to regulate various muscle biological processes[19,20]. The advent of high-throughput single-cell and single-nuclei RNA sequencing techniques has enabled a comprehensive exploration of these transcriptional dynamics[21,22]. One notable limitation of these approaches is their inability to provide the spatial distribution of mRNA molecules in the multinucleated muscle fibers. These features can be investigated by single-molecule fluorescence *in situ* hybridization (smFISH) that reveals two types of mRNA bodies: 1. Individual mRNA molecules spread out in the cytoplasm and representing the mature RNA and 2. A maximum of two bright nuclear foci correspond to the nascent transcript and reveal the transcriptionally active alleles[23]. Therefore, smFISH is a method of choice for individual mRNA molecule quantification, investigating their spatial distribution and providing snapshots of the gene transcriptional dynamics.

The smFISH method relies on a set of short fluorescent oligonucleotide probes specifically designed to be complementary to the target transcript. Upon annealing, it generates high-intensity point sources permitting the detection of mRNA at a single-molecule level using confocal microscopy[24]. This method is increasingly applied for a wide variety of cell types, including mammalian muscle tissues[19,20]. However, in *Drosophila* like other animal models, most of the knowledge about adult muscle gene expression is derived from bulk molecular assays, which lack quantitative information on the spatial location of mRNA molecules. Here we optimized a method for performing smFISH on muscle precursor cells and adult *Drosophila* muscles[23,25]. This protocol includes a fully automated analysis pipeline for nuclei segmentation and mRNA counting and localization.

Protocol

1. Wing disc and adult muscle dissection and preparation

NOTE: Clean up the dissection bench and all the dissection instruments with RNAse inhibitor solution (**Table of Materials**). Laboratory gloves should be worn during the whole experimental procedure.

1. **Wing disc**
    1. Place the L3 staged larvae in cold 1x phosphate-buffered saline (PBS) (**Figure 1A**).
    2. Rinse the larvae 3x with 1x PBS and keep them in this solution for 5 min.

Copyright © 2023 JoVE Creative Commons Attribution-NonCommercial-NoDerivs 3.0 Unported License

3. Using two pairs of sharp forceps, hold the larva from the anterior part and pull and discard the rest of the body tissues (around 2/3).
4. Hold both the first 1/3 of the larva with one pair of forceps and the mouth hooks with the other pair. Retract the mouth hooks inside the larva until it is fully inverted.
   NOTE: Dissect approximately 30 larvae per experiment, to ensure adequate sample size for analysis.
5. Observe that the wing discs are closely associated with the two primary branches of the tracheae, which run along each side of the larva.
6. Remove all the other larval components (leg discs and brain) to obtain a clean inverted larval carcass with a pair of wing discs attached to the trachea (**Figure 1B**).
7. Place the samples in a 1 mL centrifuge tube and fix them in 4% paraformaldehyde (PFA) diluted in 1x PBS for 45 min at room temperature under agitation.
   NOTE: The sample agitation is achieved by an oscillating stirrer (**Table of Materials**).
8. Wash the samples 3 x 5 min with 70% ethanol (EtOH, diluted in RNAse-free water) and store them in the same washing solution at 4 °C for at least 2 days and up to 1 week.

2. **Indirect flight muscles**

1. Anesthetize the adult flies on a CO_2 fly pad and remove the heads, abdomens, legs, and wings.
2. Place the dissected thoraxes in cold 1x PBS and continue doing so until all samples are dissected (**Figure 1D**).
3. Prefix the thoraxes in 4% PFA, (1% Triton) for 20 min at room temperature under agitation.
4. Rinse the samples 3 x 5 min with 1x PBT washing solution (1% Triton in 1x PBS).
5. Position the thoraxes on a double-sided tape (**Table of Materials**) on a glass slide and bisect them with a sharp microtome blade to produce two hemi-thoraces (**Figure 1E,F**).
6. Fix the samples in 4% PFA (1% Triton) for 45 min at room temperature under agitation.
7. Wash 2 x 20 min with 1x PBT washing solution (1% Triton, 1x PBS) at room temperature under agitation.
8. Place the hemi-thoraces in cold 1x PBS and use the forceps to gently isolate the IFMs from the hemi-thorace (**Figure 1G**).
   NOTE: To achieve this, it is important to remove the cuticle as thoroughly as possible.
9. To permeabilize the samples, store the isolated IFMs in 70% EtOH solution for at least 2 days and up to 1 week at 4 °C.
   NOTE: Isolate the IFMs from approximately 10 thoraxes per experiment to ensure adequate sample size for analysis.

2. Hybridization, immunostaining, and mounting

NOTE: Similar hybridization procedure is applied for both wing discs and IFMs samples. It is critical to isolate the wing discs from the larval carcasses and put them in 200 µL of Buffer A prior to starting the hybridization.

1. Resuspend the probes in 400 µL of TE buffer (10 mM Tris-HCl, 1 mM EDTA, pH 8.0) for a final stock solution of 12.5 µM.

Copyright © 2023 JoVE Creative Commons Attribution-NonCommercial-NoDerivs 3.0 Unported License

2. Transfer the samples to a 0.5 mL centrifuge tube containing Buffer A (**Table of Materials**).
   NOTE: By decreasing the volume of the container, it becomes easier to visualize the samples and avoid losing them during the washing process.
3. Wash the samples 2 x 20 min with Buffer A.
4. Aspirate Buffer A, replace it with 400 µL of the hybridization buffer (**Table of Materials**), and prehybridize the samples for 30 min at 37 °C in a thermal mixer (**Table of Materials**).
5. Dilute the probes to a final concentration of 125 nM for wing discs and 200 nM for adult muscles, in the hybridization buffer and add the primary antibody.
   NOTE: The antibody dilution varies depending on the specific antibody being used (**Table of Materials**). Adding antibodies is optional. Users may opt to forego protein staining and instead use a similar smFISH protocol that does not include the addition of antibodies.
6. Aspirate the hybridization buffer and replace it with 100 µL of hybridization buffer containing the probe and the antibody.
7. Incubate the samples in the dark at 37 °C for at least 16 h under 300 rpm agitation in a thermal mixer.
8. Warm up an aliquot of Buffer A at 37 °C.
9. Wash the samples for 3 x 10 min in the thermal mixer at 37 °C under 300 rpm agitation.
10. During the last wash, dilute the secondary antibody (1/200) and DAPI (1/10,000) in Buffer A and incubate the samples in this solution at 37 °C for at least 1 h.
11. Wash the samples for 3 x 20 min with Buffer B (**Table of Materials**).
12. Carefully transfer the samples on a microscope slide, wipe off the residual Buffer B, and add 30 µL of mounting medium, and cover with an 18 x 18 mm coverslip. Use a nail polish to seal the preparation.
13. Store the samples for up to 1 week at 4 °C.
    NOTE: However, it is recommended to perform the imaging as soon as possible to avoid probe signal degradation.

3. Imaging

1. Acquire images with an xyz acquisition mode using a confocal microscope equipped with 40x and 63x oil immersion objectives (**Table of Materials**). The smFISH signal is detected by the HyD detector via a photon counting mode.
2. Locate the samples using the DAPI signal and UV lamp.
3. To image the wing disc-associated muscle progenitors and IFMs (**Figure 2** and **Figure 3**), apply the following setup for laser lines and emission filters: select **DAPI** (excitation (ex.) **405 nm**, emission (em.) **450 nm**), **Alexa Fluor 488** (ex. **496 nm**, em. **519 nm**), and **Quasar 670** for the smFISH probes (ex. **647 nm**, em. **670 nm**).
4. To image the adult MuSCs (**Figure 2D**), apply the following setup for laser lines and emission filters: select **DAPI** (ex. **405 nm**, em. **450 nm**), **Alexa Fluor 488** (ex. **496 nm**, em. **519 nm**), **Alexa Fluor 555** (ex. **555 nm**, em. **565 nm**), and **Quasar 670** for the smFISH probes (ex. **647 nm**, em. **670 nm**).
   NOTE: For the imaging, the wavelengths can be adapted according to the dyes associated with secondary antibodies and probes.
5. Save the confocal images as .TIFF files.

Copyright © 2023 JoVE Creative Commons Attribution-NonCommercial-NoDerivs 3.0 Unported License

4. Post imaging analysis

1. To get started, launch ImageJ and navigate to the **Plugins** menu. From there, select **Macros | Edit** to open the macros source code.
   NOTE: This will enable adjustment of the parameters as needed, and if required, modify the folder directory for each channel within the macro's source code.
2. To follow this protocol and quantify *Mef2* smFISH spots in larvae, use the following settings: **Log_radius = 3.0 and Log_quality = 20.0**. Segement Mef2-positive nuclei with **blur = 2; nucleus_scale_parameter = 30; nucleus_threshold = -8.0; nucleus_size = 300**.
3. In muscle fibers, use the following parameters: **Log_radius = 2.5; Log_quality = 60.0; blur = 2; nucleus_scale_parameter = 100; nucleus_threshold = 0.0; nucleus_size = 300**.
4. To initiate the macro, simply execute the run command and wait for the macro to automatically load all images from the designated folder and quantify them in a sequential manner.
   NOTE: Please note that the duration of this process may vary from a few seconds to several hours, depending on the volume of data being analyzed.
5. Look for the results displayed in two new .csv files: file_FISH_results and file_nuclei_results. The first shows the number of transcriptional spots and their average and maximum intensities. The second one gives both the total number of nuclei and the number of spots inside each nucleus.

Representative Results

In this protocol, we used commercially produced probes targeting *Mef2* and *zfh1* mRNA. We designed the probes with the manufacturer's FISH probes designer (**Table of Materials**). The *Mef2* set targets the exons common to all *Mef2* RNA isoforms (from exon 3 to exon 10). The *zfh1* set targets the third exon common to both *zfh1-RB* and *zfh1-RE* isoforms[10]. Both probes are conjugated to the Quasar 670 fluorescent dye.

We generated a macro in-house that was compatible with ImageJ software to automatically analyze the raw .tif data. The macro allows the 3D segmentation of the nuclei by Cellpose[26] with the Fiji plugin BIOP and the transcriptional spot quantification by a Laplacian of Gaussian as implemented in the Trackmate plugin[27]. MorpholibJ plugin[28] is used for postprocessing (**Supplemental File 1**).

As a first step, we performed smFISH on wing imaginal discs, where *Mef2* and *zfh1* are known to be expressed in the AMPs. These data show that both transcripts are uniformly detected in the AMPs population co-stained with either Mef2 or Zfh1 antibodies (**Figure 2A,B**). Active transcription sites (TS) can be revealed and distinguished from mature mRNA by smFISH as they tend to be larger and have more intense signals than individual cytoplasmic transcripts or mature nuclear transcripts**.** Consistently, higher magnifications of AMPs distinguish between TS foci and mature mRNA scattered in the cytoplasm (**Figure 2A',B'**), validating the sensitivity of this smFISH protocol. It should, however, be mentioned that we observed one active TS per nucleus for both *zfh1* and *Mef2* (**Figure 2A',B'**). These data further validate the accuracy of the probe design since *Mef2* and *zfh1* transcriptional patterns

Copyright © 2023 JoVE Creative Commons Attribution-NonCommercial-NoDerivs 3.0 Unported License

in the AMPs colocalize with the detection of their respective proteins (**Figure 2**).

In a second step, we examined the transcription site and distribution of *Mef2* and *zfh1* mRNAs in differentiated adult IFMs and associated stem cells (**Figure 2C,D**). These data clearly illustrate *Mef2* TSs in the syncytial muscle nuclei and *Mef2* mRNA distribution throughout the cytoplasm (**Figure 2C,C'**). Zfh1 specifically marks the MuSCs population[10,11]. Using this smFISH protocol, we successfully detected *zfh1* transcription in MuSCs marked by Zfh1-Gal4 > GFP expression. Higher magnification illustrates the detection of both *zfh1* TS and cytoplasmic single mRNAs (**Figure 2D'**).

Finally, we used our in-house-built ImageJ macro to quantitatively analyze *Mef2* transcriptional dynamics and spatial distribution. The computational pipeline can efficiently detect and segment *Mef2* spots and muscle nuclei (**Figure 3A-C**). However, due to signal-to-noise ratio issues, some spots may not be detected in certain cases (**Figure 3A',B'**). We used this automated method to investigate whether *Mef2* mRNA abundance varies between muscle precursor cells (AMPs) and differentiated adult IFMs. Our analysis shows that the number of *Mef2* mRNA per nuclei in adult IFMs and the AMPs are not significantly different (**Figure 3D**).

To gain insight into the spatial distribution of *Mef2* transcripts in adult IFM muscles, we quantified the fraction of cytoplasmic versus nuclear *Mef2* mRNA spots (**Figure 3E,F**). Using our program, we counted both the total number of *Mef2* mRNA spots and the number of *Mef2* mRNA spots overlapping with nuclei staining (Mef2). Subtracting the nuclei-associated mRNA from the total mRNA number provides the number of cytoplasmic mRNA spots. Our findings reveal that approximately 92% of *Mef2* mRNA is present in the cytoplasm, while the remaining 8% is associated with muscle nuclei, as shown in **Figure 3E,F**.

Copyright © 2023 JoVE Creative Commons Attribution-NonCommercial-NoDerivs 3.0 Unported License

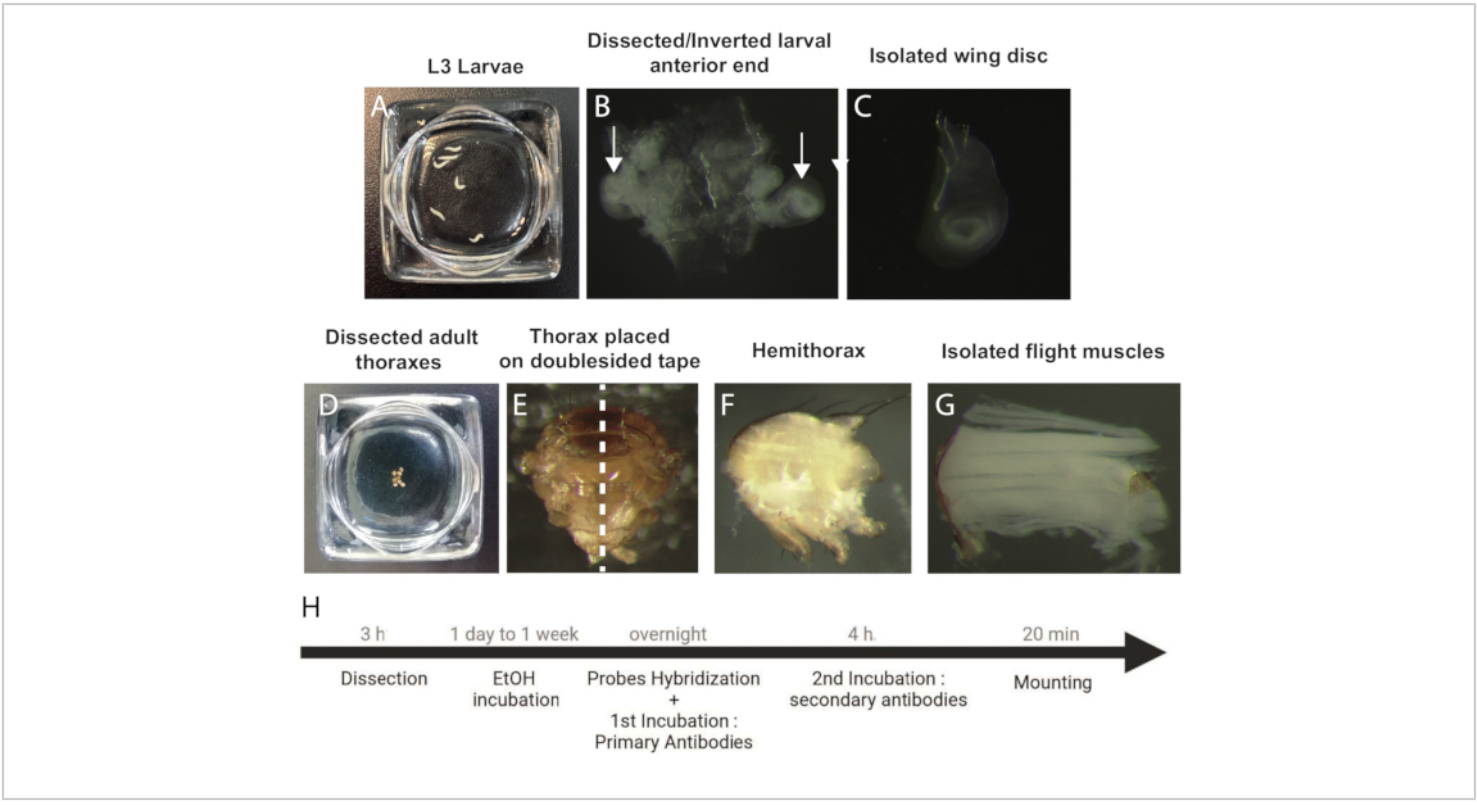

Figure 1: Procedure to dissect and prepare wing discs and IFM samples for smFISH. (**A**) L3 staged larvae. (**B**) Dissected and inverted anterior end of the larva. Arrows indicate the wing discs. (**C**) Isolated wing disc. (**D**) Dissected adult thoraxes. (**E**) Adult thorax oriented on a doublesided tape prior to bisection (dotted line). (**F**) Adult hemithorax. (**G**) Isolated IFMs. (**H**) Workflow of the smFISH protocol**.** Abbreviations: IFMs = indirect flight muscles; smFISH = single-molecule RNA fluorescence *in situ* hybridization; EtOH = ethanol. Please click here to view a larger version of this figure.

Copyright © 2023 JoVE Creative Commons Attribution-NonCommercial-NoDerivs 3.0 Unported License

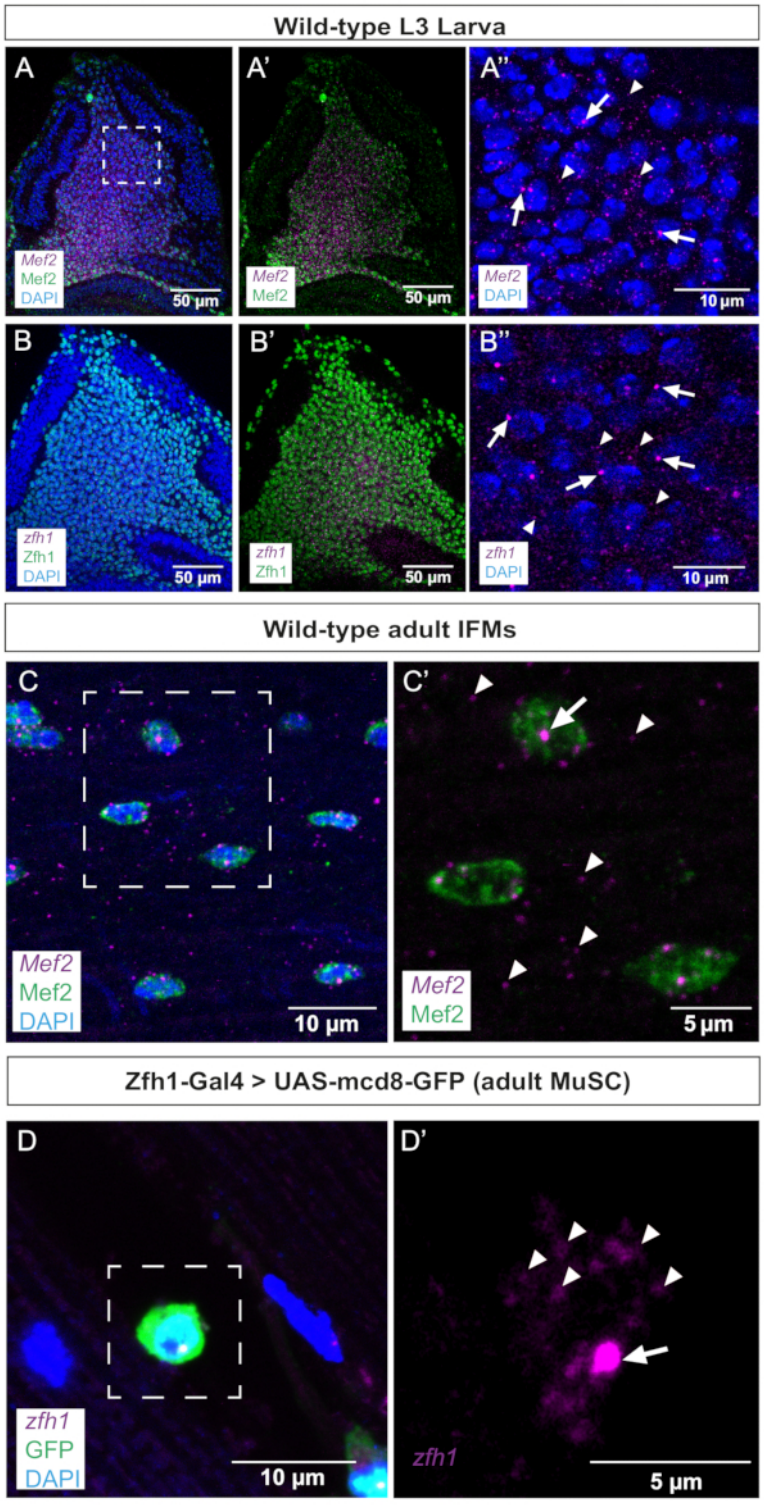

Figure 2: Representative images of *Mef2* and *zfh1* smFISH in wing discs and adult IFMs. (**A**,**B**) *Mef2* and *zfh1* mRNAs (purple) are detected uniformly in AMPs and co-localize with (**A**,**A'**) Mef2 and (**B**,**B'**) Zfh1 proteins (green), respectively.

Copyright © 2023 JoVE Creative Commons Attribution-NonCommercial-NoDerivs 3.0 Unported License

(**A",B"**) Higher magnification of the AMPs. (**C**) *Mef2* mRNAs and Mef2 protein are detected in adult IFMs. (**C'**) Higher magnification of the boxed region in **C**. (**D**) *Zfh1-Gal4 >UAS-mCD8GFP* expression (green) labels adult MuSCs. *zfh1* RNA is detected in adult MuSCs. (**D'**) Higher magnification of the boxed region in **D**. *Zfh1* transcription start sites and single mRNAs are indicated by arrows and arrowheads, respectively. DAPI staining (blue). Scale bars = 50 µm (**A,B,A',B'**), 10 µm (**A",B",C,D**), 5 µm (**C',D'**). Abbreviations: IFMs = indirect flight muscles; smFISH = single-molecule RNA fluorescence *in situ* hybridization; AMPs = adult muscle progenitors; MuSCs = muscle stem cells; DAPI = 4',6-diamidino-2-phenylindole; GFP = green fluorescent protein. Please click here to view a larger version of this figure.

Copyright © 2023 JoVE Creative Commons Attribution-NonCommercial-NoDerivs 3.0 Unported License

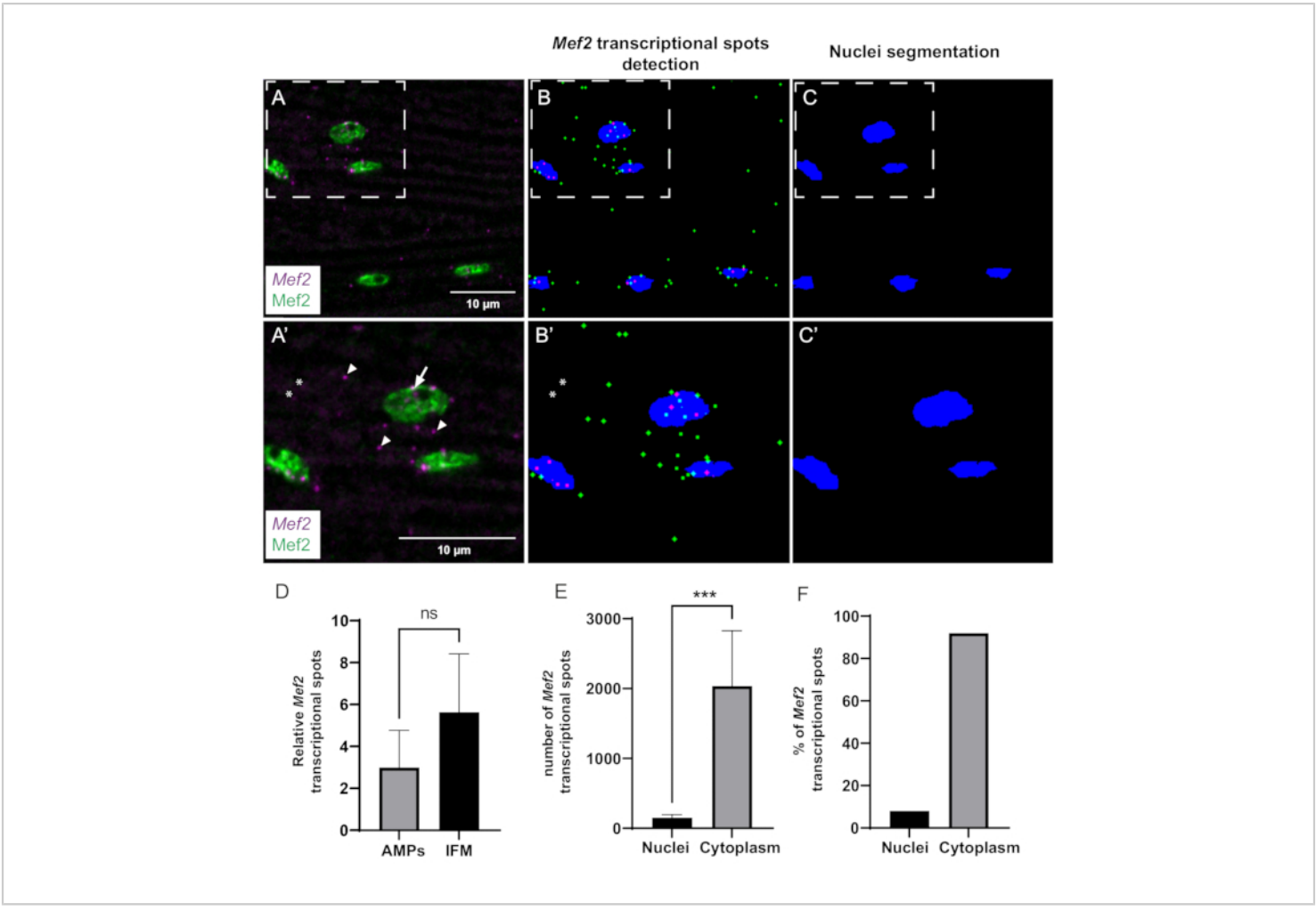

Figure 3: Quantification of *Mef2* transcription and cytoplasmic mRNA accumulation by smFISH. (**A**) Distribution of *Mef2* transcripts (purple) and Mef2 protein (green) in wildtype adult IFMs. (**A'**) Higher magnification of boxed region in **A**. Transcription start sites and single mRNAs are indicated by arrows and arrowheads, respectively. (**B,C**) Automatic *Mef2* spots finding and nuclear segmentation. Cytoplasmic and nuclear *Mef2* mRNAs are indicated in green and magenta, respectively. (**B',C'**) Higher magnifications of boxed regions in **B** and **C**. Asterisks indicate spots that are not counted by the macro. (**D**) Example of *Mef2* spot quantification in AMPs and adult IFMs, relative to the total number of nuclei. (p = 0,0785, Student's *t*-test, wing discs (n = 4), IFMs (n = 11)). (**E**) Example of quantification of *Mef2* spot distribution in adult IFMs. (*** p< 0.0007, Student's *t*-test, n = 5). (**F**) Percentage of *Mef2* mRNA spots detected inside and outside the nuclei (n = 5). Scale bars = 10 µm (**A,A'**). Abbreviations: IFMs = indirect flight muscles; smFISH = single-molecule RNA fluorescence *in situ* hybridization; AMPs = adult muscle progenitors. Please click here to view a larger version of this figure.

Supplemental File 1: Macro used for postprocessing.

Please click here to download this File.

Copyright © 2023 JoVE Creative Commons Attribution-NonCommercial-NoDerivs 3.0 Unported License

Discussion

The application of the smFISH method has gained popularity in recent times, with its use extending to various cell types and model organisms. However, in the case of *Drosophila*, the majority of knowledge about adult muscle gene expression is derived from bulk molecular assays, which fail to provide quantitative information on the precise spatial location of mRNA molecules. To address this gap, we have optimized a method for performing smFISH on muscle precursor cells and adult *Drosophila* muscles. This approach has been adapted from a previously published protocol[23] and optimized for *Drosophila* muscle tissues.

The major obstacle in obtaining high-quality smFISH images is the thickness of adult muscles, which hinders the optimal penetration of probes. Therefore, it is crucial to separate the adult muscles from the other tissues of the animal and carry out the hybridization process with mild agitation. This particular step ensures effective permeabilization of the tissues.

Another critical aspect is that the signal-to-noise ratio can cause the computational pipeline to fail in detecting certain mRNA spots. We found that increasing the signal-to-noise ratio can be achieved by finding the optimal concentration of probes. The optimal dilution may differ depending on the composition of each probe set, including the conjugated dye and oligonucleotide composition. We recommend trying different dilutions; a final dilution of 200 nM yielded the best signal-to-noise ratio for adult tissues in these experiments.

With the smFISH method, it is possible to quantify the number of newly synthesized RNAs at the TS foci. When a gene is actively transcribed, multiple nascent RNAs are produced concurrently at the TS. As a result, the TS's intensity will surpass that of mature cytoplasmic RNA, and this feature, combined with its nuclear localization, can differentiate the TS from individual cytoplasmic RNAs. In the context of muscle biology, TS detection and quantification are particularly important for determining the synchronization of transcription of a specific gene among muscle nuclei within the same syncytium. However, this computational pipeline is not designed to differentiate between cytoplasmic mRNA and TS signals. As an alternative, we suggest combining this smFISH method with other well-established smFISH analysis tools, such as BayFISH or FISH-quant[29,30]. These tools have been proven to facilitate automated segmentation and fluorescence intensity calculations of RNA aggregates with remarkable precision.

Finally, while smFISH detects mRNA molecules with high spatial resolution, it is limited to analyzing a small number of mRNA at the same time. Multiscale methods like merFISH (multiplexed error-robust fluorescence *in situ* hybridization) enable the simultaneous analysis of a large number of different mRNA[31]. By combining oligonucleotide probes and error-correcting codes, this method facilitates the detection of hundreds of RNA species in single cells.

Disclosures

The authors have no conflicts of interest to disclose.

Acknowledgments

We thank Alain Vincent for his critical reading of the manuscript. We thank Ruth Lehmann for providing the Zfh1 antibody. We acknowledge the help of Stephanie Dutertre and Xavier Pinson for confocal microscopy at the MRic Imaging Platform. EL is supported by PhD fellowship from ministère de l'enseignement supérieur et de la recherche scientifique. NA is supported by the AFM-Telethon Ph.D. fellowship 23846. TP is funded by a Chan Zuckerberg

Copyright © 2023 JoVE Creative Commons Attribution-NonCommercial-NoDerivs 3.0 Unported License

Initiative DAF grant to T.P. (2019-198009). HB is supported by CNRS, the Atip Avenir program, and the AFM-Telethon trampoline grant 23108.

References

1. Relaix, F. et al. Perspectives on skeletal muscle stem cells. *Nature Communications.* **12** (1), 692 (2021).
2. Chal, J., & Pourquie, O. Making muscle: skeletal myogenesis in vivo and in vitro. *Development.* **144** (12), 2104-2122 (2017).
3. Taylor, M. V., & Hughes, S. M. Mef2 and the skeletal muscle differentiation program. *Seminars in Cell and Developmental Biology.* **72**, 33-44 (2017).
4. Siles, L. et al. ZEB1 imposes a temporary stage-dependent inhibition of muscle gene expression and differentiation via CtBP-mediated transcriptional repression. *Molecular and Cellular Biology.* **33** (7), 1368-1382 (2013).
5. Weitkunat, M., & Schnorrer, F. A guide to study *Drosophila* muscle biology. *Methods.* **68** (1), 2-14 (2014).
6. Boukhatmi, H. *Drosophila*, an integrative model to study the features of musclestem cells in development and regeneration. *Cells.* **10** (8), 2112 (2021).
7. Bothe, I., & Baylies, M. K. Drosophila myogenesis. *Current Biology.* **26** (17), R786-791 (2016).
8. Catalani, E. et al. RACK1 is evolutionary conserved in satellite stem cell activation and adult skeletal muscle regeneration. *Cell Death Discovery.* **8** (1), 459 (2022).
9. Siles, L., Ninfali, C., Cortes, M., Darling, D. S., Postigo, A. ZEB1 protects skeletal muscle from damage and is required for its regeneration. *Nature Communications.* **10** (1), 1364 (2019).
10. Boukhatmi, H., Bray, S. A population of adult satellite-like cells in *Drosophila* is maintained through a switch in RNA-isoforms. *Elife.* **7**, e35954 (2018).
11. Chaturvedi, D., Reichert, H., Gunage, R. D., VijayRaghavan, K. Identification and functional characterization of muscle satellite cells in *Drosophila. Elife.* **6**, e30107 (2017).
12. Gunage, R. D., Reichert, H., VijayRaghavan, K. Identification of a new stem cell population that generates *Drosophila* flight muscles. *Elife.* **3**, e03126 (2014).
13. Figeac, N., Daczewska, M., Marcelle, C., Jagla, K. Muscle stem cells and model systems for their investigation. *Developmental Dynamics.* **236** (12), 3332-3342 (2007).
14. Aradhya, R., Zmojdzian, M., Da Ponte, J. P., Jagla, K. Muscle niche-driven insulin-Notch-Myc cascade reactivates dormant adult muscle precursors in *Drosophila. Elife.* **4**, e08497 (2015).
15. Schonbauer, C. et al. Spalt mediates an evolutionarily conserved switch to fibrillar muscle fate in insects. *Nature.* **479** (7373), 406-409 (2011).
16. Bryantsev, A. L., Baker, P. W., Lovato, T. L., Jaramillo, M. S., Cripps, R. M. Differential requirements for Myocyte Enhancer Factor-2 during adult myogenesis in *Drosophila. Developmental Biology.* **361** (2), 191-207 (2012).
17. Soler, C., Han, J., Taylor, M. V. The conserved transcription factor Mef2 has multiple roles in adult Drosophila musculature formation. *Development.* **139** (7), 1270-1275 (2012).
18. Soler, C., Taylor, M. V. The Him gene inhibits the development of Drosophila flight muscles during

Copyright © 2023 JoVE Creative Commons Attribution-NonCommercial-NoDerivs 3.0 Unported License

metamorphosis. *Mechanisms of Development.* **126** (7), 595-603 (2009).

19. Pinheiro, H. et al. mRNA distribution in skeletal muscle is associated with mRNA size. *Journal of Cell Science.* **134** (14), jcs256388 (2021).
20. Denes, L. T., Kelley, C. P., Wang, E. T. Microtubule-based transport is essential to distribute RNA and nascent protein in skeletal muscle. *Nature Communications.* **12** (1), 6079 (2021).
21. Li, H. et al. Fly Cell Atlas: A single-nucleus transcriptomic atlas of the adult fruit fly. *Science.* **375** (6584), eabk2432 (2022).
22. Santos, M. D. et al. Extraction and sequencing of single nuclei from murine skeletal muscles. *STAR Protocols.* **2** (3), 100694 (2021).
23. Raj, A., van den Bogaard, P., Rifkin, S. A., van Oudenaarden, A., Tyagi, S. Imaging individual mRNA molecules using multiple singly labeled probes. *Nature Methods.* **5** (10), 877-879 (2008).
24. Femino, A. M., Fay, F. S., Fogarty, K., Singer, R. H. Visualization of single RNA transcripts in situ. *Science.* **280** (5363), 585-590 (1998).
25. Raj, A., Tyagi, S. Detection of individual endogenous RNA transcripts in situ using multiple singly labeled probes. *Methods in Enzymology.* **472**, 365-386 (2010).
26. Stringer, C., Wang, T., Michaelos, M., Pachitariu, M. Cellpose: a generalist algorithm for cellular segmentation. *Nature Methods.* **18** (1), 100-106 (2021).
27. Tinevez, J. Y. et al. TrackMate: An open and extensible platform for single-particle tracking. *Methods.* **115**, 80-90 (2017).
28. Legland, D., Arganda-Carreras, I., Andrey, P. MorphoLibJ: integrated library and plugins for mathematical morphology with ImageJ. *Bioinformatics.* **32** (22), 3532-3534 (2016).
29. Mueller, F. et al. FISH-quant: automatic counting of transcripts in 3D FISH images. *Nature Methods.* **10** (4), 277-278 (2013).
30. Gomez-Schiavon, M., Chen, L. F., West, A. E., Buchler, N. E. BayFish: Bayesian inference of transcription dynamics from population snapshots of single-molecule RNA FISH in single cells. *Genome Biology.* **18** (1), 164 (2017).
31. Chen, K. H., Boettiger, A. N., Moffitt, J. R., Wang, S., Zhuang, X. RNA imaging. Spatially resolved, highly multiplexed RNA profiling in single cells. *Science.* **348** (6233), aaa6090 (2015).

Copyright © 2023 JoVE Creative Commons Attribution-NonCommercial-NoDerivs 3.0 Unported License

Article 3. Statins Induce Locomotion and Muscular Phenotypes in *Drosophila melanogaster* That Are Reminiscent of Human Myopathy: Evidence for the Role of the Chloride Channel Inhibition in the Muscular Phenotypes

Mohamed H. Al-Sabri, Neha Behare, Ahmed M. Alsehli, Samuel Berkins, Aadeya Arora, Eirini Antoniou, Eleni I. Moysiadou, Sowmya Anantha-Krishnan, Patricia D. Cosmen, Johanna Vikner,Thiago C. Moulin, **Nourhene Ammar**, Hadi Boukhatmi, Laura E. Clemensson, Mathias Rask-Andersen, Jessica Mwinyi, Michael J. Williams, Robert Fredriksson and Helgi B. Schiöth (Cells 2022, DOI: 10.3390/cells11223528)

Article 4. Fluvastatin-induced myofibrillar damage is associated with elevated ROS, and impaired fatty acid oxidation, and is preceded by mitochondrial morphological changes

Mohamed H. Al-Sabri, **Nourhane Ammar**, Stanislava Korzh, Ahmed M. Alsehli, Kimia Hosseini, Robert Fredriksson, Jessica Mwinyi, Michael J. Williams, Hadi Boukhatmi, Helgi B. Schiöth (Scientific Reporters 2024, DOI: 10.1038/s41598-024-53446-w)

Les statines sont des médicaments hypolipémiants, définis comme des agents pharmacologiques capables de diminuer les concentrations plasmatiques en lipides, principalement le cholestérol LDL, et ainsi de prévenir les maladies cardiovasculaires. Toutefois, chez certains patients, elles peuvent provoquer des effets secondaires musculaires regroupés sous le terme de myopathies induites par les statines (Statin-Induced Myopathies, SIM). Les mécanismes précis à l'origine de cette toxicité musculaire restent encore partiellement élucidés.

Dans le cadre de travaux réalisés en collaboration avec le laboratoire du Pr Helgi B. Schiöth (Division of Functional Pharmacology and Neuroscience, Biomedical Center, Uppsala University, Suède), nous avons étudié les mécanismes impliqués dans les SIM en utilisant la *Drosophile*, et plus particulièrement ses muscles de vol indirects (IFMs), comme modèle expérimental. Dans ces travaux, nous avons montré qu'un traitement chronique des *Drosophiles* à la fluvastatine entraîne une réduction marquée de leur activité locomotrice. Ce traitement induit également une perturbation du métabolisme lipidique et de la voie de signalisation de l'Insuline. Par ailleurs, nous avons observé une diminution de l'expression du canal chlore musculaire ClC-a, homologue du CLCN1 des vertébrés, un élément clé dans la régulation de l'excitabilité musculaire via le passage rapide des ions chlorure à travers les membranes cellulaires. Ma contribution à ces études a consisté à montrer que ces perturbations métaboliques sont également associées à des altérations phénotypiques des muscles de vol adultes : allongement des sarcomères, désorganisation des lignes Z, ainsi que fragmentation et aspect arrondi des mitochondries. Après cinq jours de traitement, ces

anomalies s’aggravent et s’accompagnent d’une désorganisation sévère des myofibrilles, caractérisée par une augmentation de leur épaisseur, un élargissement des espaces intermyofibrillaires et une altération des myofilaments (Figure 1). Cette désorganisation musculaire est corrélée à une augmentation significative de la production d’espèces réactives de l’oxygène (ROS). En résumé, l’ensemble des données présentées dans ces travaux suggère que la myopathie induite par la fluvastatine résulte d’une cascade d’événements : altérations mitochondriales précoces, augmentation du stress oxydatif, perturbation du métabolisme lipidique, puis dommages myofibrillaires.

cells

MDPI

Article

Statins Induce Locomotion and Muscular Phenotypes in *Drosophila melanogaster* That Are Reminiscent of Human Myopathy: Evidence for the Role of the Chloride Channel Inhibition in the Muscular Phenotypes

Mohamed H. Al-Sabri [1,2], Neha Behare [1], Ahmed M. Alsehli [1,3], Samuel Berkins [1], Aadeya Arora [1], Eirini Antoniou [1], Eleni I. Moysiadou [1], Sowmya Anantha-Krishnan [1], Patricia D. Cosmen [1], Johanna Vikner [1], Thiago C. Moulin [1,4], Nourhene Ammar [5], Hadi Boukhatmi [5], Laura E. Clemensson [1], Mathias Rask-Andersen [6], Jessica Mwinyi [1], Michael J. Williams [1], Robert Fredriksson [2] and Helgi B. Schiöth [1,*]

1 Department of Surgical Sciences, Division of Functional Pharmacology and Neuroscience, Biomedical Center (BMC), Uppsala University, Husargatan 3, 751 24 Uppsala, Sweden
2 Department of Pharmaceutical Biosciences, Uppsala University, 751 24 Uppsala, Sweden
3 Faculty of Medicine, King Abdulaziz University and Hospital, Al Ehtifalat St., Jeddah 21589, Saudi Arabia
4 Faculty of Medicine, Department of Experimental Medical Science, Lund University, Sölvegatan 19, BMC F10, 221 84 Lund, Sweden
5 Institut de Génétique et Développement de Rennes (IGDR), Université de Rennes, CNRS, UMR6290, 35065 Rennes, France
6 Department of Immunology, Genetics and Pathology, Uppsala University, 752 37 Uppsala, Sweden
* Correspondence: helgi.schioth@neuro.uu.se

Abstract: The underlying mechanisms for statin-induced myopathy (SIM) are still equivocal. In this study, we employ *Drosophila melanogaster* to dissect possible underlying mechanisms for SIM. We observe that chronic fluvastatin treatment causes reduced general locomotion activity and climbing ability. In addition, transmission microscopy of dissected skeletal muscles of fluvastatin-treated flies reveals strong myofibrillar damage, including increased sarcomere lengths and Z-line streaming, which are reminiscent of myopathy, along with fragmented mitochondria of larger sizes, most of which are round-like shapes. Furthermore, chronic fluvastatin treatment is associated with impaired lipid metabolism and insulin signalling. Mechanistically, knockdown of the statin-target *Hmgcr* in the skeletal muscles recapitulates fluvastatin-induced mitochondrial phenotypes and lowered general locomotion activity; however, it was not sufficient to alter sarcomere length or elicit myofibrillar damage compared to controls or fluvastatin treatment. Moreover, we found that fluvastatin treatment was associated with reduced expression of the skeletal muscle chloride channel, ClC-a (*Drosophila* homolog of *CLCN1*), while selective knockdown of skeletal muscle ClC-a also recapitulated fluvastatin-induced myofibril damage and increased sarcomere lengths. Surprisingly, exercising fluvastatin-treated flies restored ClC-a expression and normalized sarcomere lengths, suggesting that fluvastatin-induced myofibrillar phenotypes could be linked to lowered ClC-a expression. Taken together, these results may indicate the potential role of ClC-a inhibition in statin-associated muscular phenotypes. This study underlines the importance of *Drosophila melanogaster* as a powerful model system for elucidating the locomotion and muscular phenotypes, promoting a better understanding of the molecular mechanisms underlying SIM.

Keywords: statins; fluvastatin; statin-induced myopathy; Hmgcr; skeletal muscle chloride channel; ClC-a; CLC-1; myopathy; locomotion; sarcomere; mitochondrial dysfunction; lipotoxicity; Pkcdelta (Pkcδ); PKCtheta (PKCθ); chelerythrine; *Drosophila melanogaster*

check for updates

Citation: Al-Sabri, M.H.; Behare, N.; Alsehli, A.M.; Berkins, S.; Arora, A.; Antoniou, E.; Moysiadou, E.I.; Anantha-Krishnan, S.; Cosmen, P.D.; Vikner, J.; et al. Statins Induce Locomotion and Muscular Phenotypes in *Drosophila melanogaster* That Are Reminiscent of Human Myopathy: Evidence for the Role of the Chloride Channel Inhibition in the Muscular Phenotypes. *Cells* **2022**, *11*, 3528. https://doi.org/10.3390/cells11223528

Academic Editor: Yan Burelle

Received: 25 August 2022
Accepted: 1 November 2022
Published: 8 November 2022

Publisher's Note: MDPI stays neutral with regard to jurisdictional claims in published maps and institutional affiliations.

Copyright: © 2022 by the authors. Licensee MDPI, Basel, Switzerland. This article is an open access article distributed under the terms and conditions of the Creative Commons Attribution (CC BY) license (https://creativecommons.org/licenses/by/4.0/).

1. Introduction

Cardiovascular diseases (CVDs) are the leading cause of morbidity and mortality globally, accounting for approximately 17.9 million patients dying each year, with hypercholesteremia as the main risk factor [1,2]. Statins, 3-hydroxy-3-methylglutaryl-CoA reductase (HMGCR) inhibitors, are widely prescribed to lower cholesterol and low-density lipoprotein (LDL) and thus reduce CVDs mortality and morbidity [3–7]. Although relatively safe, multiple reports have shown that due to statin intolerance, more than 30% of patients discontinue statin medications, leading to increased risks for CVD events [8–11]. Statin intolerance is mainly due to muscle problems, including myalgia (without creatine kinase (CK) elevation), myositis (CK 10-fold within the upper limit of normal, ULN), and rhabdomyolysis (CK elevation over 10-fold the ULN along with reddish or brown urine) [12], which are grouped under the term statin-induced myopathy (SIM) [13–15]. In the United States, a recent internet-based survey has indicated that up to 60% of former statin-treated patients have reported an incidence of SIM-related sequelae, with muscle problems as the primary reason for statin discontinuation [10]. More importantly, SIM-related muscle damage has been reported long after the cessation of statins [9,16]. Indeed, statin alternatives do not offer better prevention and treatment for CVDs compared to statins [17]. Therefore, identifying the root cause of SIM is very crucial, and a recent simulation study has shown that improving statin adherence by 50% would lower CVD-related deaths [18,19].

Despite extensive research, the aetiology of SIM remains enigmatic. One theory has attributed SIM to a reduction in muscular membrane sarcolemmal cholesterol levels [20]. Yet, blocking cholesterol synthesis by squalene synthase inhibitors does not cause myopathy [21]. Another hypothesis has linked SIM to isoprenoid depletion, one of the components of the mevalonate pathway which is diminished by the inhibition of HMGCR. Depleted isoprenoid levels result in higher intracellular calcium concentrations, which can trigger cell death in muscles [22–24]. However, a study by Laaksonen et al. has reported that statins do not reduce isoprenoid synthesis in the muscles significantly [25]. Other studies have demonstrated that, due to HMGCR inhibition, statins lead to coenzyme Q10 (CoQ10) depletion and mitochondrial dysfunction, with subsequent muscle problems [26]. Nevertheless, shreds of evidence have indicated that muscular CoQ10 levels are not changed in most statin-treated patients, which could explain why CoQ10 supplementation does not mostly alleviate SIM [25–34]. Moreover, a recent study indicates that statins, except for fluvastatin, induce mitochondrial dysfunctions by binding to mitochondrial Complex III [35]. However, other scholars have pointed out that statins do not cause changes in mitochondrial functions or morphology in muscles of statin-treated patients [36–38] and clinical research has indicated that simvastatin can improve mitochondrial functions in cardiomyocytes [39], which all have questioned the primary role of mitochondrial dysfunction in SIM.

Apart from the mevalonate pathway, a reduction in insulin secretion and sensitivity by statins has been also proposed as an underlying factor for SIM [40–42]. It has been also reported that statin treatment is associated with the inhibition of skeletal muscle chloride channel 1, CLC-1 [43–46], which is the key feature of myotonia [47,48]. Nevertheless, whether statin-associated inhibition of CLC-1 can cause myopathy phenotypes and the mechanistic pathway underlying statin-associated inhibition of CLC-1 are still poorly understood.

Drosophila melanogaster (fruit fly) provides an ideal system to understand muscle disorders, including myopathy with potential application for human conditions and many features of morphology and physiology of skeletal musculature in fruit flies are remarkably similar to humans [49–53]. We hypothesize that statin might induce myopathy phenotypes through direct inhibition of HMGCR or indirect inhibition of skeletal muscle chloride channel or both. Since statin-target HMGCR (in flies, HMGCR is denoted as Hmgcr) is highly conserved in both humans and flies [54–56], we used fruit flies to employ genetic and pharmacological approaches to investigate whether Hmgcr inhibition in skeletal muscles gives rise to myopathy-like phenotypes. Moreover, we examined whether statin

inhibits skeletal muscle chloride channels and whether muscular inhibition of this channel contributes to myopathy phenotypes.

2. Materials and Methods

2.1. Fly Stocks and Maintenance

Fly stocks mentioned in Table 1 were purchased from the Bloomington Stock Center (Bloomington, IN, USA) and used for the experiments. W1118 wild-type flies were used from our in-house stock. The wild-type CSORC flies were obtained by crossing CantonS and OregonR-C flies, both types of flies were ordered from Bloomington Stock centre (Bloomington, IN, USA). All flies, unless otherwise stated, were maintained on enriched Jazz mix standard fly food (Fisher Scientific, Waltham, MA, USA). Flies were maintained at 25 °C in an incubator at 60% humidity on a 12:12 light:dark cycle. Virgin CSORC males aged 1–2 days were used in this study unless otherwise stated. In order to feed flies with drugs, a proper volume of the drug was mixed with warm food in a small plastic vial. Then, we allowed it to cool before we nurtured flies in these plastic vials containing food with/without the drug(s) for five days before experiments.

Table 1. Fly stock purchased from the Bloomington Stock Center and used in this paper.

Bloomington Stock Numbers	Drosophila Line	Referred to as
50652	y[1] v[1]; P{y[+t7.7]v[+t1.8] = TRiP.HMC03053}attP40	*UAS-Hmgcr RNAi*
8176	w[1118]; P{w[+mW.hs] = GawB}EDTP[DJ694]	*EDTP-Gal4*
28355	y[1] v[1]; P{y[+t7.7] v[+t1.8] = TRiP.JF02991}attP2	*UAS-Pkcdelta RNAi*
53337	P{y[+t7.7] v[+t1.8] = TRiP.HMC03566}attP40/CyO	*UAS-ClC-a RNAi*
38464	w[*]; P{w[+mC] = Mhc-RFP.F3-580}2, P{w[+mC] = Mhc-GAL4.F3-580}2/SM6b	*Mhc-Gal4*

2.2. Setting Up the Crosses

To knockdown *Hmgcr* in muscles, virgin female *Mhc-Gal4* was crossed with male *UAS-Hmgcr RNAi* line, referred to as *Mhc-Gal4>UAS-Hmgcr RNAi*, while virgin female *w1118* crossed with male *UAS-Hmgcr RNAi*, referred to as *w1118>UAS-Hmgcr RNAi*, and virgin female *Mhc-GAL4* line crossed with male *w1118*, referred to as *Mhc-Gal4>w1118*, both are used as control groups. Only straight-wing flies were collected and used in the experiments. Most $Hmgcr^{RNAi}$ knockdown flies (*Mhc-Gal4>Hmgcr RNAi*) had a shorter lifespan, less than two days (Supplementary Figure S4B). We tried to overcome this short-life span problem by raising the flies at 25 °C, instead of 27 °C and collecting them immediately for the experiments, but the problem remained. Consequently, we used one-two-day-old flies for the experiments. To knockdown ClC-a in muscles, virgin female *Mhc-Gal4* was crossed with male *UAS-ClC-a RNAi* line, referred to as *Mhc-Gal4>UAS-ClC-a RNAi*, while virgin female *w1118* crossed with male *UAS-ClC-a RNAi*, referred to as *w1118>UAS-ClC-a RNAi*, and virgin female *Mhc-GAL4* line crossed with male *w1118*, referred to as *Mhc-Gal4>w1118*, both are used as control groups. Only straight-wing flies were collected and used in the experiments. To knockdown *Pkcdelta* in the skeletal muscles, virgin female *EDTP-Gal4* was crossed with male *UAS-Pkcdelta RNAi*, referred to as *EDTP-Gal4>UAS-Pkcdelta RNAi*, while virgin female *w1118* crossed with male *UAS-Pkcdelta RNAi*, referred to as *w1118>UAS-Pkcdelta RNAi*, and virgin female *EDTP-GAL4* line crossed with male *w1118*, referred to as *EDTP-Gal4>w1118*, both are used as control groups. Unless otherwise stated, crossed flies were raised at 25 °C until the adults emerged; once collected, adults were raised at 27–29 °C for appropriate times. In all assays, F1 progeny was used.

2.3. Exposure Concentration

For the maximum concentration exposure assessment, we first looked for the fluvastatin concentrations used in the literature. The fluvastatin concentrations used before were

0.05, 0.5 and 1 mM [55] and 5 mg/µL = 11.5 mM [57] without reported toxic effects. Since 0.5 and 1 mM concentrations have been reported to significantly decrease mean activity and enhance sleep duration in *Drosophila* [55], we assessed whether these concentrations are within the reported toxic fluvastatin dose in mice and in relation to humans' mean plasma concentration of 40 mg fluvastatin, the daily recommended dose for adults. According to the literature, the fly adult male weight of 0.88 mg [58] and daily intake of 1.5 µL [59,60]. Next, we selected a range of concentrations of 0.05–40 mM and then calculated how much fluvastatin mg/kg/day in these concentrations corresponded to. After that, we compared them to fluvastatin doses in mg/kg/day used in the toxicity studies in mice (https://www.accessdata.fda.gov/drugsatfda_docs/label/2022/201635s029lbl.pdf, accessed on 1 August 2022). According to our calculations, we found that fluvastatin concentrations of 20 mM (14.7 mg/kg/day) and 40 mM (29.5 mg/kg/day) are equivalent to reported toxic cancerogenic doses in mice (15 and 30 mg/kg/day), which are 2 and 7 times the mean human plasma drug concentration after a 40 mg oral dose. Moreover, the regular fluvastatin dose in humans is 40 mg/day and the maximum dose is 80 mg/day; thus, considering the average human male weight is 70 kg, the daily doses per kg are 0.57 and 1.1 mg/kg/day, respectively. Therefore, we concluded that 0.5 mM (0.3 mg/kg/day) and 1 mM (0.74 mg/kg/day) are within the therapeutic dose range and suitable for our study.

2.4. Quantification of Climbing Ability Using Forced-Climbing System

To examine the effect of fluvastatin on the climbing ability of the flies, we used the Forced-Climbing System as described by Moulin et al. [61]. In short, this system comprises two MultiBeam Activity Monitor, MB, (TriKinetics Inc., Waltham, MA, USA) placed vertically in Vortexer Mounting Plate, VMP, (TriKinetics Inc., Waltham, MA, USA) see Figure 1.

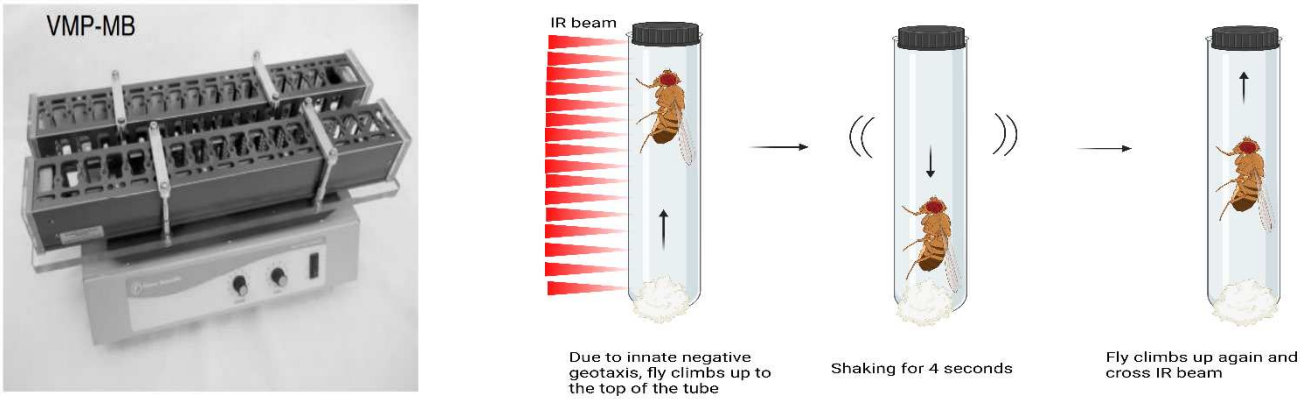

Figure 1. Schematic representation for the Forced-Climbing System. The left image is VMP-MB where the upper portion is two slots of MultiBeam Activity Monitor (MB), each has 16 slots for tubes and each slot is equipped with 17 IR beams and the lower portion is Vortexer Mounting Plate, (VMP) which is used as a shaker. The right picture shows how the Forced-Climbing System works. Simply, an anaesthetized fly was placed inside the tube plugged with cotton from the bottom and with a black cap from the top. Then, the tube was placed inside MB. Each MB consists of 16 slots. The VMP agitates tubes inside MB for 4 s each minute. The fly tends to climb up against gravity due to innate negative geotaxis. Then, after a four-second shaking period, the fly falls to the bottom and climbs up again to the top of the tube and crosses the 17 IR beam. The left image was taken from TriKinetics.com, accessed on 1 August 2022 (with permission) while the right was created with Biorender.com.

Flies were anaesthetised using CO_2 and placed in individual glass tubes covered with cotton on one end and the other end with a black plastic lid. The glass tubes were loaded vertically into the MB5 with the side containing cotton on the bottom. The flies were agitated at a regular interval (4 s per minute) by the VMP for six hours, starting at 13:00 and the light was kept turned on for the entire experiment. After each agitation, flies fell to

the bottom of the tubes and then, due to their natural negative geotaxis, flies climb up the tube against gravity and crossed the 17 IR beams.

We have optimized the Forced-Climbing System to monitor not only fly moves but also speed and positions in the tubes (representing how far can flies climb up). Specifically, we developed a MATLAB routine that allows us to record the flies' average moves per hour, speed per hour and positions. In short, first, we retrieved the raw files from MB5 software after each run. Then, we applied the following equations:

Hourly locomotor movement (moves) is calculated by averaging the hourly beam-to-beam transition recorded generated from the flies' activity in the course of the experimental time

$$\text{Moves per hour} = \frac{\sum Beam\ to\ beam\ transition\ for\ the\ n^{th}\ hour\ in\ EH}{3600 - (x * 60)}$$

The hourly maximum position reached hourly (positions) is determined by averaging the maximum position reached by the flies in each hour

$$\text{Position} = \frac{\sum Position\ of\ fly\ at\ any\ particular\ instant\ for\ the\ n^{th}\ hour\ in\ EH}{3600 - (x * 60)}$$

Hourly locomotory speed (Speeds) is the summation of the difference between the position of fly at y^{th} second and position of fly at x^{th} second divided by n for the entire course of experimental time

$$\text{Speed per hour } = \left(\left[\sum \frac{Fly\ position\ at\ y^{th}\ sec - x^{th}\ sec}{y - x} \right] for\ each\ hour \right) * 3\ mm/sec$$

where

EH—Experimental hours
TSEA—$(EH * 3600) - (EH * x * 60)$
x—Number of seconds VPM agitated
y—User-determined seconds (>x and <60) and by default 10
The length between each IR is 3 mm.

I. Acute and chronic fluvastatin treatment

Fluvastatin sodium hydrate (MW: 433.45, 10 mg, Sigma, Darmstadt, Germany, #SML0038) was dissolved in water to make the stock solution. Generally, unless otherwise stated, we calculated the required volume of the fluvastatin and then mixed it with an appropriate volume of food to make the final concentration.

To determine the chronic and acute effects of fluvastatin on the flies, one–two-day-old virgin male CSORC flies were collected from the stock. For the control group, flies were fed normal food and then on the fifth day, we starved them for one hour before transferring them onto vials in which 3 mm Whatman filter paper immersed with 100 µL 5% (wt/vol) sucrose alone was placed in the bottom for three hours; for the fluvastatin group (five days), we fed flies with 0.5 mM fluvastatin and then on the fifth day, we fed them with 5% (wt/vol) sucrose alone; and for the fluvastatin group (three hours), flies were fed with normal food for five days and then on the fifth day, we fed them with 0.5 mM fluvastatin for three hours (Table 2).

II. Chronic fluvastatin 0.5 and 1 mM treatment

One–two-day-old virgin male CSCOR flies were collected for the experiments. In the control, 0.5 and 1 mM fluvastatin groups, fluvastatin powder was solubilized in water and mixed into the regular fly food, at concentrations of 0 (control), 0.5, or 1 mM. Then, flies were fed with food for five days before the experiments.

Table 2. Acute and chronic feeding pattern for fluvastatin groups and control group.

Experimental Group	Solution	Feeding Period	On the Fifth Day
Control	4.5 mL food and 0.5 mL water	five days	Starved flies for one hour and then transfer to 100 µL of sucrose alone for three hours
0.5 mM Fluvastatin (five days)	4.5 mL food and 0.5 mL of 5 mM fluvastatin	five days	Starved flies for one hour and then transfer to 100 µL of sucrose alone for three hours
0.5 mM Fluvastatin (three hours)	4.5 mL food and 0.5 mL of 5 mM fluvastatin	five days	Starved flies for one hour and then transfer to 100 µL of 0.5 mM fluvastatin for three hours

III. Chelerythrine and fluvastatin treatment

Chelerythrine chloride (CC) was purchased from Sigma, Germany #C2932. Virgin male CSORC flies of one-two day old were used. In the control and the control with CC groups, flies were fed normal food for five days, while in the fluvastatin group and the fluvastatin with CC group, flies were fed food mixed with 0.5 mM fluvastatin for five days. On the fifth day, we starved them for one hour before transferring them onto vials in which 3 mm Whatman filter paper was placed in the bottom. Then, into the filter paper, we applied 100 µL (sucrose alone) for the control group; 100 µL of 100 µM CC for the control with CC group; 100 µL of 0.5 mM for the fluvastatin group; and 100 µL of 100 µM CC for the fluvastatin with CC group. We used 5% (wt/vol) sucrose solution as a vehicle for the CC and fluvastatin feeding on the fifth day (Table 3).

Table 3. Feeding pattern for fluvastatin group, fluvastatin with CC group, control group, and control with CC group.

Experimental Group	Solution	Feeding Period	On the Fifth Day
Control	4.5 mL food and 0.5 mL water	five days	Starved flies for one hour and then transfer to 100 µL of sucrose alone for three hours
Control with 100 µM CC	4.5 mL food and 0.5 mL water	five days	Starve flies for one hour and then transfer to 100 µL of 100 µM CC for three hours
0.5 mM Fluvastatin	4.5 mL food and 0.5 mL 5 mM fluvastatin	five days	Starved flies for one hour and then transfer to 100 µL of 0.5 mM fluvastatin for three hours
0.5 mM Fluvastatin with 100 µM CC	4.5 mL food and 0.5 mL 5 mM fluvastatin	five days	Starved flies for one hour and then transfer to 100 µL of 100 µM CC for three hours.

2.5. Quantification of General Locomotion Activities Using Drosophila Activity Monitoring System (DAMS)

To examine the fluvastatin effect on the general locomotion activity of the flies, we used DAMS (Drosophila Activity Monitoring System) (TriKinetics Inc., Waltham, MA, USA). All crossed flies were fed with normal food unless otherwise stated.

In 0.5 and 1 mM fluvastatin groups, we prepared a stock solution of 5 mM fluvastatin using water as a vehicle. Then, the calculated volume of fluvastatin (1 and 2 mL, respectively) was taken and mixed with food to have a final volume of 10 mL, while in the control group, food was mixed with 1 mL of water. Each Petri dish mixture was kept to cool down and solidify for one hour. Thereafter, for each group, 30 glass 5 mm × 65 mm tube tips were dipped into the corresponding mixture twice and then plugged with plastic black caps. One–two-day-old virgin male CSCOR flies were collected for the experiments. Then, each fly was transferred into each tube using a CO_2 anaesthesia pad and a paintbrush. Finally, the other ends of the tubes were subsequently plugged with cotton, and the tubes were placed in the DAMS monitor horizontally.

For the preparation of the fluvastatin solution and CC solution, we used water as a vehicle. To check the effect of the fluvastatin on flies, we first fed CSORC flies with 1 mM and 0.5 mM fluvastatin and then we run DAMS. To look out whether CC can rescue the

fluvastatin phenotype, we divided CSORC flies into four groups: for the fluvastatin group, we prepared 0.5 mM concentration from the stock concentration mixed with 10 mL hot food in a 12 mL Petri dish so that the total volume of 12 mL is obtained; for the fluvastatin with CC, we prepared 0.5 mM both fluvastatin and cc mixed with 10 mL hot food in a 12 mL Petri dish so that the total volume of 12 mL is obtained. For the CC group, we added only CC and for the control, we added only the food (Table 4). Each Petri dish mixture was kept to cool down and solidify for one hour. Thereafter, for each group, 30 glass 5 mm × 65 mm tube tips were dipped in the corresponding mixture twice and then plugged with plastic black caps.

Table 4. Feeding pattern for fluvastatin group, fluvastatin with CC group, CC group and control groups.

Group	Stock	Volume Taken	Total Volume with Food
1.0 mM Fluvastatin	3 mM fluvastatin	4 mL	12 mL
0.5 mM Fluvastatin	3 mM fluvastatin	2 mL	12 mL
0.5 mM Fluvastatin with 100 µM CC	3 mM fluvastatin 2.9 mM CC	2 mL fluvastatin 413 µL CC	12 mL
100 µM CC	2.9 mM CC	413 µL CC	12 mL
Control	no	no	12 mL

For the chloride channel blockers, 2-(4-chlorophenoxy) propionic acid (CPP) (50 mg, R750298, Sigma, Taufkirchen, Germany) and 9-anthracenecarboxylic acid (A9C) (50 mg, A89405, Sigma, Germany) were obtained from Sigma-Aldrich™. We used 70% ethanol as a vehicle for CPP and A9C. We divided the flies into three groups (control, 1 mM CPP, 1 mM A9C), each group consists of 32 flies (Table 5). CSPRC virgin males were collected and transferred into the tube in the same way mentioned above. We recorded their general activity, mean activity and activity counts/30 min all for five days. For the crossed flies with GAL4, we used normal food and flies aged was 1–5 days before experimentation, unless otherwise mentioned.

Table 5. Flies feeding pattern for the chloride channel blockers groups and control.

Group	Stock	Volume Taken	Total Volume with Food
Control	no	2.4 mL of alcohol	12 mL
1 mM CPP	5 mM CPP in alcohol	2.4 mL of the stock solution	12 mL
1 mM A9C	5 mM CPP in alcohol	2.4 mL of the stock solution	12 mL

Finally, all monitors were placed in the incubator for five days at 25 °C, and 60% humidity on a 12:12 light:dark cycle. On the sixth day, the data for the flies' general activity for five days were collected from the DAMSystem software and analysed using MATLAB, and GraphPad Prism.

2.6. Transmission Electron Microscopy

i. Morphology

Flies were first cool-anaesthetized by chilling in crushed ice until they stop moving to ensure relaxation of the muscles before dissection. Five flies per group taken from vials were cool-anaesthetized by chilling in crushed ice until they stopped moving. Next, the heads of flies were first cut with a sharp razor and then, cross-sections from femur segments of legs were taken and fixed for morphology. The EM preparation was performed by BioVis Core Facility/Electron microscopy at IGP, Uppsala University, Uppsala, Sweden. In short, the legs were dissected and the dissected tissues were Fixed in 2.5% glutaraldehyde and

1% paraformaldehyde in 0.1 M sodium cacodylate buffer (pH 7.6) overnight at 4 °C. Then, we rinsed it in 0.1 M sodium cacodylate buffer (pH 7.6) for 10 min, Post-fix in 1% osmium tetraoxide in 0.1 M sodium cacodylate buffer (pH 7.6) for 1 h, dehydrated in increasing concentrations of EtOH (50%, 70%, 95%, 100%) for 15 min, embedded in LR white and 100% EtOH (1:1) for 60 min, changed to 100% LR white overnight at 4 °C, transferred to gelatine capsules with 100% LR white for 2–3 h, polymerized at 55 °C for 48 h, sectioned ultrathin sections (~60 nm) on an ultramicrotome (Leica EM UC7), placed sections on a cu slot grid (Ted Pella, Redding, CA, USA) coated with Formvar, contrasted with 2% Uranyl acetate for 5 min, washed extensively with water, again contrasted with 3% lead citrate (Reynold's, Merck, Darmstadt, Germany) for 2 min, again washed extensively with water, air dried for 15 min and finally imaged in Technai™ G2 Spirit (ThermoFisher/FEI, Eindhoven, The Netherlands) electron microscope at 80 kV using a Lab6 filament and a Gatan Orius SC200 camera.

ii. Immunogold labelling

In the fluvastatin group, flies were fed with 1.0 mM fluvastatin in the same way mentioned above, while in the control group, flies were fed with normal food, both groups for five days. Five flies per group taken from vials were cool-anaesthetized by chilling in crushed ice until they stopped moving to ensure the relaxation of the muscles before dissection. Next, the heads of flies were first cut with a sharp razor and then, cross-sections from femur and tibia segments of legs were taken and fixed for immunogold labelling. The EM preparation was performed by BioVis Core Facility/Electron microscopy at IGP, Uppsala University. In short: the femur of the legs were dissected and dissected tissue was fixed in 4% paraformaldehyde and 0.05% glutaraldehyde in 0.1 M sodium cacodylate buffer (pH 7.6) O.N. at 4 °C, rinsed in 0.1 M sodium cacodylate buffer (pH 7.6) for 10 min, dehydrated in increasing concentrations of EtOH (50%, 70%, 95%, 100%) for 15 min, embedded in LR white and 100% EtOH (1:1) for 60 min, changed to 100% LR white O.N. at 4 °C, transferred to gelatine capsules with 100% LR white for 2–3 h and polymerized at 55 °C for 48 h. Legs were then sectioned in ultrathin sections (~60 nm) on an ultramicrotome (Leica EM UC7), and placed on a Ni 200-mesh grid (Ted Pella) coated with formvar. Free aldehyde groups were blocked with 50 mM glycine in PBS for 15 min. Grids were transferred to blocking solution for goat secondary reagents (Aurion, Wageningen, The Netherlands) for 30 min, washed in 0.1% BSA-C (Aurion, Wageningen, The Netherlands) 3 × 5 min. Primary antibody Rabbit Anti-ClC-2 Antibody (Abcam, Amsterdam, The Netherlands, #ab192506) (ClC2, 1:500) was then added and sections were incubated O.N. at 4 °C and then washed in 0.1% BSA-C (Aurion, Wageningen, The Netherlands) 6 × 5 min. A secondary antibody (goat anti-rabbit, 12 nm gold colloidal gold particle, Jackson Immuno Research Europe Ltd., Ely, UK) was then added for 60 min. Sections were then washed in 0.1% BSA-C (Aurion, Wageningen, The Netherlands) 6 × 5 min and washed in MQ Water 6 × 5 min. Sections were contrasted with 2% Uranyl acetate for 5 min and again washed extensively with water and air-dried. Pictures of the grids were then taken, and ImageJ was used to quantify immunogold particles.

iii. Chloride channel particles counting

The grid for each group obtained from immunogold labelling TEM was divided into an area of 33×10^6 pixels (8.7×10^9 micron). Next, we quantified the ClC-a gold particle in each area using ImageJ software (version 1.53Ki, National Institutes of Health, Bethesda, MD, USA) and calculated the statistical difference using GraphPad Prism. The type of the test is indicated in the caption of each figure.

iv. Measuring the sarcomere length

TEM micrographs with a scale bar of 2 or 5 µm have been selected randomly from the groups. The length between Z-lines of the sarcomere was measured in µm using ImageJ (version 1.53Ki, National Institutes of Health, Bethesda, MD, USA) from the top, middle and

bottom of the sarcomere. Then, the significant difference was calculated using GraphPad Prism. The type of the test is indicated in the caption of each figure.

v. Measuring the mitochondria area

Measuring mitochondrial areas in TEM micrographs with a scale bar of 1, 2 and 5 µm was carried out using Image J (version 1.53Ki, National Institutes of Health, Bethesda, MD, USA) by manually tracing mitochondria from selected TEM micrograph. Surface area (mitochondrial size) is reported in squared micrometres. The type of the test is indicated in the caption of each figure.

vi. Counting the number of round-like shaped mitochondria

Counting the number of round-like shaped mitochondria in TEM micrographs with a scale bar of 1, 2 and 5 µm was carried out using Image J (version 1.53K, National Institutes of Health, Bethesda, MD, USA). The type of the test is indicated in the caption of each figure.

2.7. Quantification of Genes and Protein Expressions

i. RNA purification and cDNA synthesis

For the crossed flies, male flies were collected and allowed to age for five days at 27–29 °C per group and then stored at −80 °C before extraction. For CSORC flies, for the fluvastatin group, 100 virgin males were transferred onto a vial containing 5 mL of food mixed with a subsequent volume of fluvastatin stock solution sufficient to make 1 mM fluvastatin, and for the control group, another 100 flies were transferred onto a vial containing 5 mL of food mixed with an equivalent volume of water. Having allowed the flies to age for five days at 25 °C in the mixture, we extracted the RNA using the whole body, and then stored them at −80 °C before extraction. We used chloroform (Sigma #67663), isopropanol (Sigma #I9516) and triazole (Thermofisher #15596026), and the protocol was applied according to Williams et al. [62]. The level and purity of the RNA and cDNA were measured by nanodrop in a Multiscan machine (Thermo Scientific™) using µDrop™ Plate. The accepted Absorbance 260/280 for both, RNA and cDNA ranged from 1.9 to 2.1. The cDNA was synthesized by Thermal cyclers using 20 µL total volume: 9 µL of the extracted RNA, 10 µL RT buffer (Thermofisher, High-Capacity RNA-to-cDNA™ Kit #4387406) and 1 µL Reverse Transcriptase Enzyme (Thermofisher, High-Capacity RNA-to-cDNA™ Kit #4387406).

ii. Real-time qPCR

cDNA was diluted in a ratio of 1:30 using Milli-Q® water and the level of genes of interest was measured using quantitative real-time polymerase chain reactions, qPCR. Primers were selected through FlyPrimerBank and ordered from ThermoFisher™ (Table 6).

Relative expression levels of the housekeeping gene (*RpL32*) and the genes of interest were measured using quantitative RT-PCR (qPCR), Bio-Rad iCycler Thermal Cycler Real-Time PCR Detection. Each plate well contained a total volume of 20 µL of the following: 11.52 µL Milli-Q® water, 3.60 µL Taq buffer, 0.20 µL dNTPs, 0.1 µL primers, 1 µL DMSO (1:20), 0.5 µL SYBR Green (1:50,000) and 3 µL of cDNA of the gene of interest as described in Williams et al. [62]. All qPCR experiments were carried out in triplicates. The qPCR data were analysed using MyIQ 1.0 software (Bio-Rad, Hercules, CA, USA) and values of fold changes (ratio of delta CT value) for the samples were normalized with *RpL32*'s values. Outliers of CT ratio were checked out by Grubbs' test and the significant outliers ($p > 0.05$) were excluded. GraphPad Prism was used to calculate the significance. The type of the test is indicated in each figure's caption.

iii. Western Blotting

For fluvastatin groups, 10 virgin-CSORC males of one–two-day-old per each group were transferred onto a vial containing 5 mL of food mixed with a subsequent volume of fluvastatin stock solution sufficient to make 1 mM or 0.5 mM fluvastatin, and for the control group, another 10 virgin-CSORC male flies aged 1–2 days old were transferred onto a vial

containing 5 mL of food mixed with an equivalent volume of water. We grew the flies in the mixture for five days and then stored them at −80 °C. After that, flies were homogenized in RIPA buffer (Thermofisher #89900) mixed with protease and phosphatase inhibitors (Thermofisher #78441), and then we loaded an equal amount of lysate (equivalent to 30 µg) into SDS-PAGE gel and blotted to the PVDF membrane. For measuring the protein expression of CLC-a, we ran a pair-wise sequence comparison to select the antibodies and the following antibodies were applied: for anti-CLC-a antibodies, Rabbit Anti-ClC-2 Antibody (Abcam, The Netherlands, #ab192506) at 1:500 dilution; β-Actin polyclonal Antibody (ThermoFisher #PA5-16914) at 1:1000 dilution. By using the mild stripping protocol from https://www.abcam.com/protocols/western-blot-membrane-stripping-for-restaining-protocol, accessed on 1 August 2022, the blots were stripped and re-probed in the same PVDF membrane. We used the secondary antibody Rabbit IgG (H + L) Cross-Adsorbed Secondary Antibody (ThermoFisher, HRP #A16104) at 1:1000 dilution. Enhanced reagent ECL kits from Biorad were used for detecting the signals. Signal detection was performed using ChemiDoc MP Imaging System, Bio-Rad. Relative intensity was calculated by normalizing the absolute intensity of the experimental group to the absolute intensity of β-actin using Image Lab and GraphPad Prism software. The *p*-value was calculated using GraphPad Prism. The type of the test is indicated in each figure's caption.

Table 6. Sequences for the primers used in the study.

Primer Name	Forward Sequence	Reverse Sequence
Hmgcr	5′GCTGCACTGCCGTACTGTA3′	5′AATGCCCAGCACATATTTGGA3′
CLC-a	5′TGGGCGAGGATTGGGTATTC3′	5′ACTGAACAAAAGGCTGTGACG3′
Pkc98E	5′TCCATTATGCACGACGATGT3′	5′CTCCGGATTTTTGGTGAGAA3′
Pkcdelta	5′GGCACCAAACACCCGTATCT3′	5′CCCATAGAATCTGGCTCGCT3′
RPL32	5′AGCATACAGGCCCAAGATCG3′	5′TGTTGTCGATACCCTTGGGC3′
AMPK ALPHA	5′TACCAGGTCATATCGACGCC3′	5′ACGCCAGAGATAATCTGCTGAA3′
mdy	5′CACAAAGTGTGACTCGTGCTG3′	5′CCAGTTCACCAGTCCAGAAAAA3′
Dgat2	5′CAGATACTGGTCACGGCCTTT3′	5′CGGATTGGGTTTTCTTGTGGTG3′
Hmgcr	5′GCTGCACTGCCGTACTGTA3′	5′GCCACAAGCACCAGGATG3′
Mef2	5′ATATCACGCATCACCGATGAAC3′	5′GGCGTACTGGTACAGCTTGT3′
Mhc	5′CCAAGACGGTCAAAAACGAT3′	5′GATGTTGGCTCCCGAGATAA3′
zfh1	5′CCTCCAAGAAGTGCATCAGCA3′	5′CGAAGTAGCTCATCGGATGTG3′
Hnf4	5′GGCGACGGGCAAACATTATG3′	5′CGCAAATCTCGCAAGTGTACTGAT3′
Bmm	5′GTCTCCTCTGCGATTTGCCAT3′	5′CTG AAG GGA CCC AGG GAG TA3′
lip1	5′GTG AGCCTGGCCTACTTGC3′	5′GGTCGAGGGTGGTGTGATTC3′
Lpin	5′CACACCGACAACACACTGGA3′	5′CTTCTTCTCGCCCTGAAACAG3′
CG1941	5′GTCTACGCGAATCACAAGAGAA3′	5′CGATAATGCCGAAACAGCCAA3′
CG1946	5′CAGACCTGGTACGTCATTC3′	5′CGCCGTAGTACAGCAGGATAG3′
Chico	5′GCGCACTCACCTTATGACCA3′	5′GCACACGAATGTCAGGGATTT3′
Thor	5′CGTCCAGCGGAAAGTTTTCG3′	5′GTTTGGTGCCTCCAGGAGTGG3′

3. Results

3.1. Chronic Fluvastatin Treatment Induces Lowered General Locomotion Activities and Climbing Ability

Statin treatment has been reported to induce myopathy in humans [9,45], and myopathy-like phenotypes in mice [63], rats [64], goats [65] and zebrafish and chicken [66–68]. Thus, we first asked whether statins induce phenotypes reminiscent of myopathy in the fruit

fly. Previous studies showed that fluvastatin is effective in flies and able to inhibit Hmgcr activity in the mevalonate pathway [69,70]. Additionally, we previously demonstrated that fluvastatin treatment for five days reduces the mean activities and promoted sleep duration [55]. Therefore, we examined the effect of fluvastatin on the climbing ability and general locomotion activity using wild-type CSORC flies as they are commonly used in locomotion and climbing assays [61,71]. We employed the *Drosophila* Activity Monitoring System (DAMS) for monitoring general locomotion activities and improved the Forced-Climbing System described by Moulin et al. [61] to record different aspects of fly climbing ability including the hourly average of moves, speed and positions (see Materials and Methods).

First, we tested the chronic effect (5 days) of 0.5 and 1 mM fluvastatin concentrations on the climbing ability and general locomotion activities. In Forced-Climbing activity, compared to the controls, both, 1.0 mM and 0.5 fluvastatin-treated flies showed significantly lowered climbing ability including the average moves and speed. However, the average position was significantly reduced only in 1 mM fluvastatin-treated flies (Figure 2A–C). If we compared both concentrations, 1 mM fluvastatin had a more significant decline in the average speed and position than 0.5 mM (Figure 2B,C). In DAMS, both 1.0 mM and 0.5 fluvastatin-treated flies displayed significantly lowered general locomotion activities (activity count/30 min, and total activity) while the activity while awake was not altered (Figure 2D and Supplementary Figure S1B). However, acute fluvastatin treatment of CSORC flies for three hours did not change the climbing activity, particularly the average moves (Supplementary Figure S1A). In total, these results indicate that chronic fluvastatin treatment impairs climbing and locomotion activities. In line with these results, statin treatment has been reported to markedly reduce zebrafish movement [66] and reduce the running capacity in mice [72].

3.2. Chronic Fluvastatin Treatment Induces Phenotypic Changes in Myofibrils and Mitochondria and Is Associated with Reduced Muscle Regeneration

To determine whether the lowered locomotion and climbing activities associated with fluvastatin treatment were a result of muscle problems, we treated CSORC flies with 1 mM fluvastatin for five days and examined the morphology of the skeletal muscles of the femur segments of legs using transmission electron microscopy (TEM). Interestingly, in most TEM micrographs, compared to the control group, the skeletal muscle ultrastructure of the fluvastatin-treated flies exhibited more remarkable skewing, displacement, or contortion of myofibrils, specifically, misorientation of sarcomeres, Z-line streaming or/and loss of Z-line and distended T-tubules together with a few vacuoles and a rare occasion of myelin figures, which are circular scroll-like myofilaments, that are similar to toxic myopathy in humans [73] (Figure 3A–C).

The sarcomere is the functional contractile unit of myofibril delimited by two Z lines. Thus, sarcomere size correlates with the diameter of myofibrils and muscle fibres and their contraction strength as well [74–79]. In addition, alteration in sarcomere integrity or/and size affects the whole muscles and therefore sarcomere length/myofibril diameter has been taken as a hallmark of myopathy-related diseases [75–80] and in SIM [65,66,68,81–84]. Accordingly, alterations in myofibril ultrastructure and sarcomere length were taken as reminiscent of myopathy in this study. In this context, strikingly, the fluvastatin-treated flies displayed a larger sarcomere length comparable to the control group (Figure 3D). However, at this point, we did not know exactly whether the increased sarcomere length is caused by longer actin and myosin filaments or due to the greater spacing in the I-Band or A band regions. Therefore, it would be interesting to investigate this using immunohistochemistry and confocal microscopy. Paradoxically, when fluvastatin-treated flies were exercised in the Forced-Climbing System for six hours, the sarcomere length was comparable to the control, although the ultrastructure alteration of myofibril was still obvious (Supplementary Figure S2A,B). In agreement with these results, treating rats with a low dose of fluvastatin led to histological alteration at the myofibril and larger fibre

diameters compared to controls [84]. In goats, skeletal muscles treated with lovastatin resulted in longer fibre diameter [65]. In humans, reports have pointed out that statins cause damage to muscle fibres, wider sarcomeres, loss of Z-lines, separation of myofibrils and distended T-tubules [81,82]. However, in Zebrafish, statins have been reported to induce shortened sarcomeres without affecting muscle fibre integrity [68].

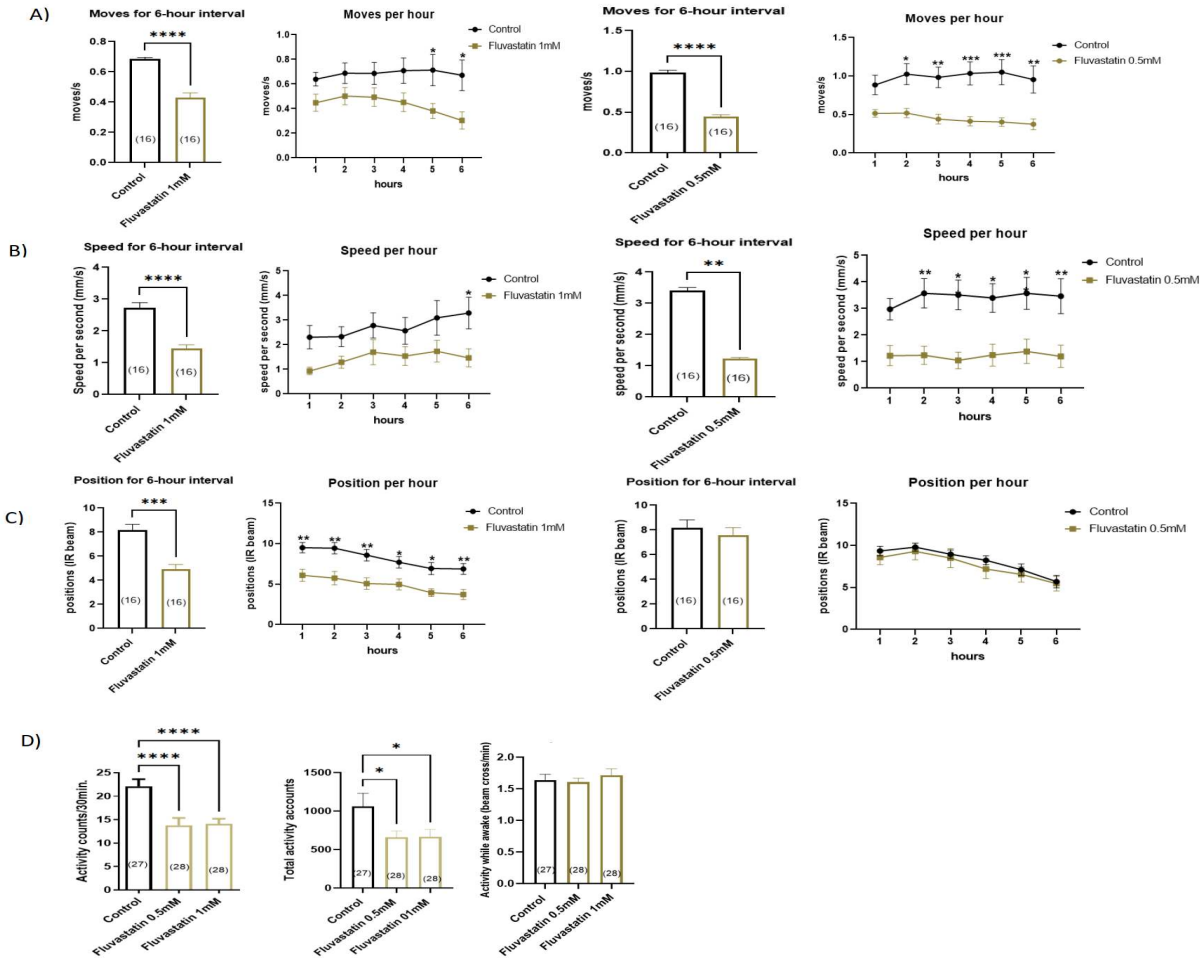

Figure 2. Fluvastatin treatment-induced lower climbing ability and general locomotion activity in CSORC flies. In 0.5 and 1 mM fluvastatin groups, flies were fed with food mixed with a corresponding volume of fluvastatin, while in control groups, flies were fed with food, all for five days before they exercised in the Forced-Climbing System for six hours (**A**) the histograms show the average moves for a combined six-hour interval and per hour, (**B**) the histograms show the average speed for a combined six-hour interval and per hour, and (**C**) the histograms show the average position for a combined six-hour interval and per hour. Using DAMS, flies were treated with 0.5 mM or 1 mM fluvastatin mixed with food in the fluvastatin groups, whereas in the control group, flies were treated with food only, both for five days (**D**) the histograms show the general locomotion activity (activity counts/30 min and total activity) and activity while awake of the flies. The Shapiro–Wilk tests were used to check normality where a parametric test was used for normally distributed data and a non-parametric test for non-normally distributed data. The statistical difference between the three groups was calculated using one-way ANOVA with Bonferroni's multiple comparisons for normally distributed data and Kruskal–Wallis one-way tests for otherwise data. For two groups, except for moves, speed and position per hour where two-way ANOVA with Bonferroni's multiple comparisons test was used, Student's *t*-test or Mann–Whitney test was used to calculate statistical difference according to the normality test whereby * $p \leq 0.05$; ** $p \leq 0.01$; *** $p \leq 0.005$; **** $p \leq 0.0001$. In each histogram, the bars represent the mean values ± SEM and the number of flies is indicated in brackets.

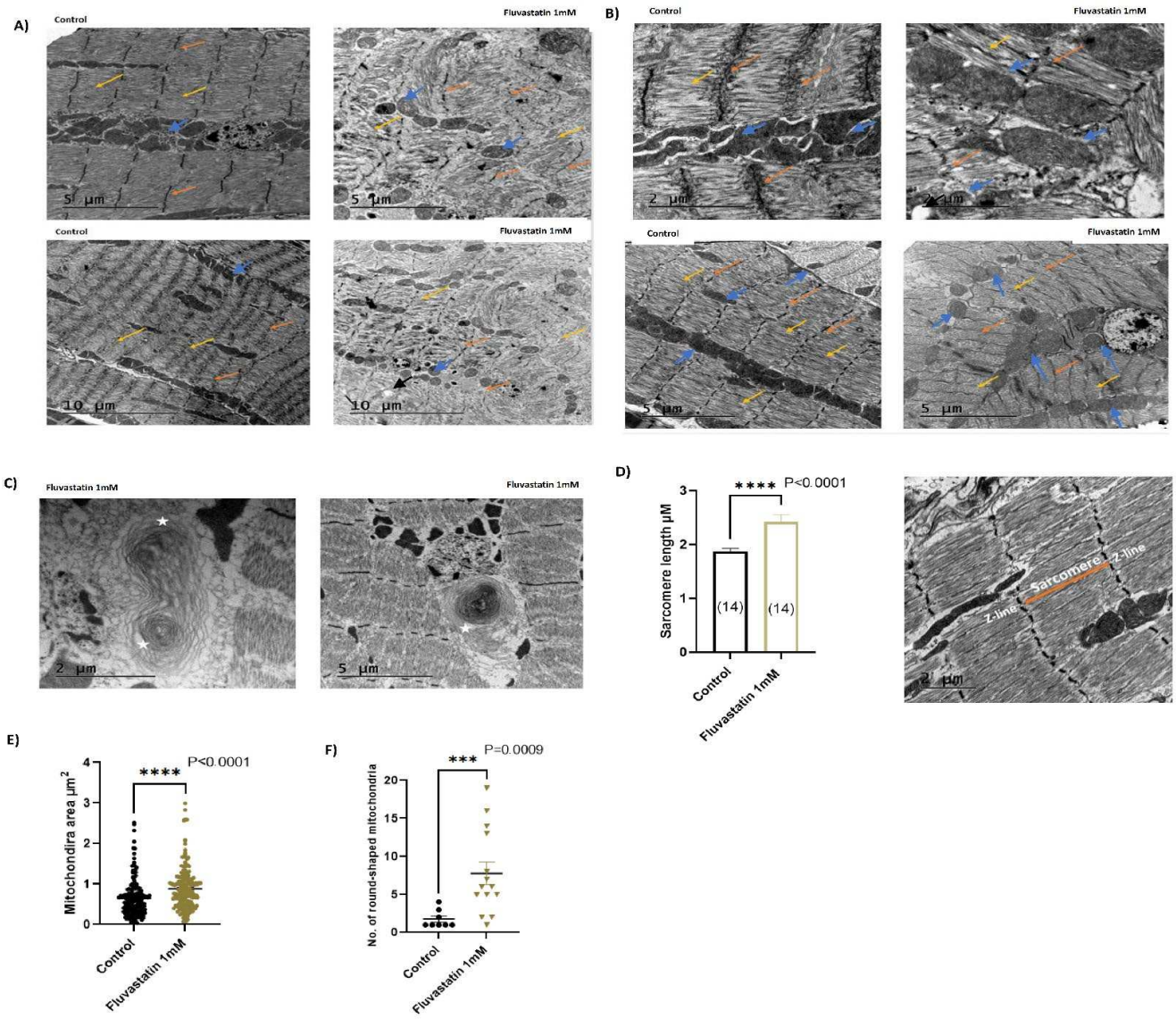

Figure 3. Fluvastatin induces myopathy-like phenotypes in flies. (**A**,**B**) TEM micrographs for the morphology for the longitudinal section of the dissected skeletal muscles of the femur segment of CSORC fly legs, wherein the fluvastatin group, CSORC flies were treated with 1.0 mM fluvastatin while the control group was fed with food, both for five days. Compared to the control group, the muscles of the fluvastatin group showed pronounced abnormal myofibril architecture including distorted sarcomere, Z-line streaming, and very few vacuoles, as well as more fragmented mitochondria with different shapes and sizes. The orange arrow indicates sarcomere, yellow indicates Z line, black indicates vacuoles and blue indicates mitochondria. (**C**) Micrographs show myelinic figures (stars) similar to toxic myopathy in the fluvastatin group. (**D**) Using ImageJ software, we measured the sarcomere length between two adjacent Z-lines. On the left, the histogram shows the sarcomere length in µm which was measured in 14 TEM micrographs for each group (fluvastatin and control). On the right is a representation of the way the sarcomere length was measured. (**E**) Using ImageJ software, we traced the mitochondria area in selected TEM micrographs. The histogram represents the area of mitochondria in μm^2 where the dots represent the number of mitochondria. (**F**) Using ImageJ software, we counted the number of round-like shaped mitochondria in TEM micrographs where the dots represent the number of mitochondria in each micrograph. In each histogram, the bars represent the mean values ± SEM. The Shapiro–Wilk test was used to check normality. Accordingly, for normally distributed data, Student's *t*-test was used to calculate statistical significance and Mann–Whitney test for otherwise data whereby *** $p \leq 0.005$; **** $p \leq 0.0001$.

At mitochondrial levels, in most TEM micrographs, the dissected leg muscles of fluvastatin-fed CSORC flies also exhibited aberrant mitochondrial morphology such as scattered abnormal mitochondria of various shapes, including round-like shapes, and of different sizes, including a few occasions of giant mitochondria (Figure 3A,B). In contrary, in most TEM micrographs, the control group displayed arranged, aggregated and elongated-shaped mitochondria that occasionally isolate neighbouring myofibrils (Figure 3A,B). Given the importance of size and the round shape of the mitochondria in muscle pathologies [85–88], we attempted to quantify surface area (size) and count the number of the round-like shaped mitochondria using ImageJ. Interestingly, in contrast to the control group, the fluvastatin-treated flies showed significantly larger mitochondria sizes (Figure 3E) and the number of round-like shaped mitochondria was remarkably higher (Figure 3F). In line with these results, several publications have pointed out that statins cause enlarged and round-like shaped mitochondria [89–93].

In order to examine the effect of fluvastatin on muscle development and regeneration, we measured the expression of *Mhc* (Myosin heavy chain and *Drosophila* homolog of MHC), *Mef2* (myocyte enhancer factor-2 and Drosophila homolog of *MEF2*) and *zfh1* (Zn finger homeodomain 1 and *Drosophila* homologue of *ZEB2*) due to their importance in muscle development, differentiation, and regeneration and since their disruption gives rise to muscle problems in flies, including myopathy [80,94–101]. We fed CSORC flies with 1mM fluvastatin mixed with food for five days while in the control group, flies were fed with food only. Then, we measured the expression of the genes using qPCR. Notably, CSORC flies treated chronically with 1.0mM fluvastatin showed a significantly reduced expression of *Mhc*, $p = 0.0005$, *Mef2*, $p = 0.0019$, and *zfh1*, $p = 0.0042$, suggesting that fluvastatin may impair muscle development differentiation in flies (Supplementary Figure S1C). Consistent with these effects, recent reports have demonstrated that statins have detrimental effects on the proliferation, differentiation, and regeneration of human skeletal muscle cells [102] and are associated with a considerable reduction in myosin heavy chain 1 protein and mRNA levels [49] and a significant decline in *MEF2* expression in muscle biopsies of statin-treated patients [45]. *zfh1* is essential for skeletal muscle differentiation [103]; thus, it would be interesting to examine the effect of statins on *ZEB2* on muscle biopsy from patients with SIM.

3.3. Chronic Fluvastatin Treatment Is Associated with Impaired Lipid Metabolism and Insulin Signalling

Mitochondrial damage and lipotoxicity are interrelated [104]. Several publications have shown that impaired lipid metabolism contributes to SIM [102,104]. Accordingly, we performed a transcriptome screen for the important genes involved in lipid metabolisms. Interestingly, most genes encoding enzymes that are involved in lipid metabolism were significantly downregulated in fluvastatin-treated flies (Supplementary Figure S3A and Table 7). Of importance, *Lpin* (*Drosophila* homolog of *LPIN1*) was highly downregulated in the fluvastatin group ($p < 0.0001$) (Supplementary Figure S3A and Table 7). *Lpin* encodes a phosphatidate phosphatase, which is responsible for the conversion of phosphatidic acid to diacylglycerol (DAG) during triacylglycerol (TG) biosynthesis. In mice, loss of its homolog in the skeletal muscles induces myopathy while elevating its expression muscles prevents statin-induced myotoxicity [104]. Moreover, in humans, mutation of *LPIN1* causes severe rhabdomyolysis [105,106].

Furthermore, *mdy* (*Drosophila* homolog of *DGAT1*) and *Dgat2* (*Drosophila* homolog of *DGAT2*) were significantly reduced in fluvastatin-treated flies ($p = 0.0056$ and 0.0007, respectively) (Supplementary Figure S3A and Table 7). Similarly, muscle biopsy of the statin-treated patient has shown reduced, *DGAT1* and *DGAT2* [107]. The same study suggests that statin treatment reduces the capacity to couple FA and DAG into TG in the skeletal muscles [107]. Taken together, our data suggest that alteration of key enzymes involved in lipid metabolism in muscles or in the whole body may contribute to myopathy,

most likely through the accumulation/oversupply of toxic lipid intermediates [104,107,108], which ultimately leads to lipotoxicity.

Lipotoxicity has been shown to compromise insulin signalling in human skeletal muscles [109,110]. We, therefore, looked into the effect of fluvastatin on key genes involved in insulin sensitivity and signalling. *chico* (*Drosophila* homolog of *IRS1*), which encodes the only insulin receptor substrate that functions in an insulin/insulin-like growth factor (IGF) signalling pathway [111,112], was very significantly reduced in fluvastatin-treated flies (p = 0.0003) (Supplementary Figure S3B and Table 7). Furthermore, *Thor*, which encodes a eukaryotic translation initiation factor 4E binding protein and is implicated in insulin resistance [113,114], was remarkably reduced (0.0019) (Supplementary Figure S3B and Table 7). *Thor* is also essential for mitochondrial function and synaptic homeostasis in *Drosophila* neuromuscular junctions [114,115]. In total, our data suggest that chronic fluvastatin treatment may disrupt insulin signalling as well.

Table 7. Effects of chronic fluvastatin treatment on the transcription of important genes involved in lipid metabolism and insulin haemostasis.

	Drosophila Gene/ Protein Name	Statin Effect	Human Homolog	Function
1	*Bmm*/brummer	Upregulated Mean fold change (1.58)	*PNPLA2*/Patatin-like phospholipase domain-containing protein 2 [116,117]	Triglyceride lipase in adipose tissue and muscles [116,117]
2	*Lip1*/Lipase 1	Downregulated Mean fold change (0.64)	*LIPF*/Gastric triacylglycerol lipase [116,117]	Triglyceride lipase and expressed in the digestive system, adipose tissue and muscles [116,117]
3	*Lpin* (Lipin)/ Phosphatidate phosphatase	Downregulated Mean fold change (0.55)	*LPIN1*/Phosphatidate phosphatase LPIN3 [116,117]	Conversion of phosphatidic acid to diacylglycerol during triglyceride biosynthesis and required for insulin signalling. Expressed in many tissues including adipose tissue and muscles [116,117]
4	*mdy* (midway)/ Diacylglycerol O-acyltransferase	Downregulated Mean fold change (0.74)	*DGAT1*/Diacylglycerol O-acyltransferase 1 [116,117]	Triglyceride biosynthesis in the muscles [116,117]
5	*Dgat2*/ Diacylglycerol O-acyltransferase 2	Downregulated Mean fold change (0.43)	*DGAT2*/Diacylglycerol O-acyltransferase 2 [116,117]	Triglyceride biosynthesis and expressed in different tissues [116,117]
6	*CG1941*/ Diacylglycerol O-acyltransferase	No change	*DGAT2*/Diacylglycerol O-acyltransferase 2 [116,117]	Triglyceride biosynthesis [116,117]
7	*CG1946*/ Diacylglycerol O-acyltransferase	No change	*DGAT2*/Diacylglycerol O-acyltransferase 2 [116,117]	Triglyceride biosynthesis [116,117]
8	*Hnf4*	Downregulated Mean fold change (0.43)	*HNF4G*/Hepatocyte nuclear factor 4-gamma [116,117]	A transcription factor involves in fatty acid oxidation, and lipid metabolism [118,119]
9	*Chico*/ encodes a substrate insulin receptor.	Downregulated Mean fold change (0.58)	*IRS1*/Insulin receptor substrate 1 [116,117]	Important for insulin signalling and action [116,117]
10	*Thor*/ encodes a eukaryotic translation initiation factor 4E binding protein	Downregulated Mean fold change (0.51)	*EIF4EBP2*/eukaryotic translation initiation factor 4E binding protein 2 [116,117]	Involved in insulin sensitivity [116,117]

The above-mentioned effects might be systemic or specific in the muscles since the whole body of the flies was used in the qPCR. More studies elucidating specific statin effects on key regulators of lipid metabolism specifically in the skeletal muscles are highly warranted.

3.4. Loss of Hmgcr in Skeletal Muscles Results in Phenotypic Changes in Mitochondria and Reduced General Locomotion Activities without Affecting Myofibril Integrity or Climbing Moves and Speeds

Second, we explored possible underlying mechanisms for statin-induced myopathy phenotypes. HMGCR is the main target of statins and many reports have linked SIM to its inhibitory effect on skeletal HMGCR [30,120]. Consequently, we asked whether inhibition of Hmgcr in the skeletal muscles induces locomotion defects and myopathy-like phenotypes similar to fluvastatin treatment. To answer this question, we assessed the impact of Hmgcr knockdown in muscles using the Mhc-Gal4 driver line, as it is specifically expressed in skeletal muscles including the embryonic/larval muscular system and adult flight, legs and labial muscles [121–124] and it is commonly used in muscles studies [125–127]. The knockdown efficiency of *Hmgcr* was confirmed by qPCR (Supplementary Figure S4A). In contrast to both controls, $Hmgcr^{RNAi}$ knockdown flies (*Mhc-Gal4>UAS-Hmgcr RNAi*) exhibited significantly reduced general locomotion (activity counts/30 min. and total activity counts) as well as the activity while awake (Figure 4A and Supplementary Figure S4B). Surprisingly, in terms of climbing measures, the average position of $Hmgcr^{RNAi}$ knockdown flies was higher compared to both controls, while the average moves and speed were not significantly changed compared to both groups (Figure 4(B1–B3)). Unexpectedly, at TEM, the dissected leg muscles of $Hmgcr^{RNAi}$ knockdown flies demonstrated normal myofibril with rare Z-line streaming and the sarcomere length of $Hmgcr^{RNAi}$ knockdown flies was found to be higher than one control group, *Mhc-Gal4>W1118*, but also lower than the another one, *W1118>UAS* $Hmgcr^{RNAi}$ (Figure 4C,D). Vacuolization was present in both $Hmgcr^{RNAi}$ knockdown flies and one control group, *Mhc-Gal4>w1118*, but more conspicuous in $Hmgcr^{RNAi}$ knockdown flies (Figure 4C). Strikingly, at the mitochondrial level, $Hmgcr^{RNAi}$ knockdown flies demonstrated severely fragmented and copious round-liked shaped mitochondria compared to both controls (Figure 4C,F), which may indicate mitochondria dysfunction. However, the mitochondria area of $Hmgcr^{RNAi}$ knockdown flies was significantly reduced compared only to one control group, *Mhc-Gal4>w1118* (Figure 4E). When compared to fluvastatin-treated CSORC flies, the muscles of $Hmgcr^{RNAi}$ knockdown flies showed smaller, but similar round-liked shaped mitochondria with more vacuolization and a few occasions of myofibril changes including Z-line steaming (Figure 4G). Since the sarcomere length and myofibril ultrastructure of the $Hmgcr^{RNAi}$ knockdown flies were not significantly changed compared to both control groups, another mechanism for statin-induced myopathy phenotypes is likely to be involved.

3.5. Chronic Fluvastatin Treatment Is Associated with Reduced Expression of the Skeletal Muscle Chloride Channel, ClC-a

Emerging shreds of evidence have indicated that statins inhibit the skeletal muscle chloride channel, CLC-1 in humans and rats [43–46]. We, thus, hypothesized that fluvastatin may induce myopathy-like phenotypes in flies through inhibition of the skeletal muscle chloride channel as well. To test this hypothesis, first, we looked for a *CLCN1* homolog in *Drosophila*. According to the literature and evolutionary data from PhylomeDB, ClC-a is the closest homolog to *CLCN1* with *a* weighted score, which is obtained by 15 integrative ortholog prediction tools, of 10/15 [117,128,129]. In addition, *CLCN1* is expressed in the muscle fibres and responsible for the Cl^- conductance during muscle contraction [128,130]. Therefore, we fed CSORC flies with 1 mM fluvastatin for 5 days and then examined the effect of 1 mM fluvastatin on the ClC-a channel. We dissected leg muscles and fixed them for immunogold labelling using rabbit anti-ClC-2 antibody and then counted the immunogold particles of ClC-a channels. Intriguingly, compared to the control group, fluvastatin-treated flies had a significantly lower number of ClC-a gold particles ($p = 0.0004$) (Figure 5A,B). To

verify this result, we performed a Western blot analysis to study the protein expression of ClC-a. Similarly, 1 mM fluvastatin-treated flies displayed a significantly reduced protein expression of ClC-a more than 0.5 mM (Figure 5C and Supplementary Figure S5C). As we mentioned previously, compared to 0.5 mM, 1 mM fluvastatin-treated flies showed a more significant decline in the average speed and position (Figure 2B,C), which might be attributed to the significantly lowered protein expression of ClC-a induced by 1 mM. Surprisingly, when we measured the transcripts of the ClC-a gene, no change in the transcriptional expression was observed in the fluvastatin-fed flies compared to the control (Supplementary Figure S5B), suggesting that the effect of the fluvastatin on the ClC-a is mediated post-transcriptionally, perhaps, on channel proteostasis. However, when we exercised 1 mM fluvastatin-treated flies in the Forced-Climbing System for six hours, the number of ClC-a gold particles was not altered in comparison with the control group (Supplementary Figure S5A), suggesting that the exercise improves the expression of the ClC-a in the skeletal muscles. Consistent with this is the observation that the muscle biopsy from patients and rats treated with fluvastatin exhibit manifestations of myopathy in which the skeletal muscles show lowered ClC-1 protein expression and decreased chloride conductance with no change in *ClCN1* transcript levels [44–46]. Additionally, in humans, moderate exercise has been shown to improve the manifestation of SIM, although the data are conflicting [72,131,132]. Hence, future studies investigating the role of the skeletal muscle chloride channel in the exercise-related effects in patients with SIM are highly recommended.

To support this notion, we attempted to mimic the inhibitory effect of fluvastatin on ClC-a by treating flies with two chloride channel blockers, 2-(4-chlorophenoxy) propionic acid (CPP) and 9-anthracene carboxylic acid (A9C), both for five days. Similar to fluvastatin, but to a lesser extent, both chloride channel blockers displayed notably lowered activity counts/30 min and the average activity (CPP $p \leq 0.05$ and A9C $p \leq 0.001$) (Supplementary Figure S6) but the activity while awake was only significantly lower with A9C group ($p \leq 0.045$, Supplementary Figure S6). It is worth mentioning that treating skeletal muscle with ClC-1 blockers has been shown to reduce channel activity and cause myotonia in vitro [46,133].

3.6. Loss of ClC-a in Skeletal Muscles Induces Myofibril Phenotypic Changes and Impairs the Climbing Ability

Nevertheless, at this point, we did not know whether statin-mediated inhibition of ClC-a induces myopathy-like phenotypes. To address this, we examined the effects of the loss of skeletal muscle ClC-a using the Mhc-Gal4 driver, as it is expressed in skeletal muscles including leg, flight and labial muscles [121–123,125,126], and then looked into the myopathy-related phenotypes. The ClC-a knockdown efficiency was confirmed by qPCR (Supplementary Figure S7A). Intriguingly, dissected legs of *ClC-a*^{RNAi} knockdown flies (*Mhc-Gal4>ClC-a RNAi*) displayed severe muscle fibre damage including aberrant sarcomere architecture, distorted myofibrils and Z-line streaming along with severely fragmented mitochondria of different shapes and sizes, in comparison to both controls (Figure 6C). Vacuolization was more abundant in *ClC-a*^{RNAi} knockdown flies than in both controls. Strikingly, similar to fluvastatin-treated flies, *ClC-a*^{RNAi} knockdown flies exhibited noticeably longer sarcomeres and, in a few micrographs, a comparable pattern of myofibril damage including rare occasions of myelin figures (Figure 6F,G). However, in Fluvastatin-treated flies, the myelin figures were bigger and thicker than those in *ClC-a*^{RNAi} knockdown flies. Moreover, in contrast to fluvastatin-treated flies, we observed a very rare occasion of round-like-shaped mitochondria in *ClC-a*^{RNAi} knockdown flies and the mitochondria area for *ClC-a*^{RNAi} knockdown flies was not altered compared to both controls (Figure 6C,F). Furthermore, in terms of climbing ability, similar to the fluvastatin treatment, the average move declined in *ClC-a*^{RNAi} knockdown flies compared to both controls (Figure 6(B1)) while the average speed and position were not significantly changed compared to both controls (Figure 6(B2,B3)). Additionally, the activity while wake for the *ClC-a*^{RNAi} knockdown

flies was also significantly reduced compared to controls, indicating locomotion defects (Figure 6A,B and Supplementary Figure S7B). Astonishingly, the general locomotion activity (activity counts/30 min and total activity counts) was not statistically significantly reduced (Figure 6A).

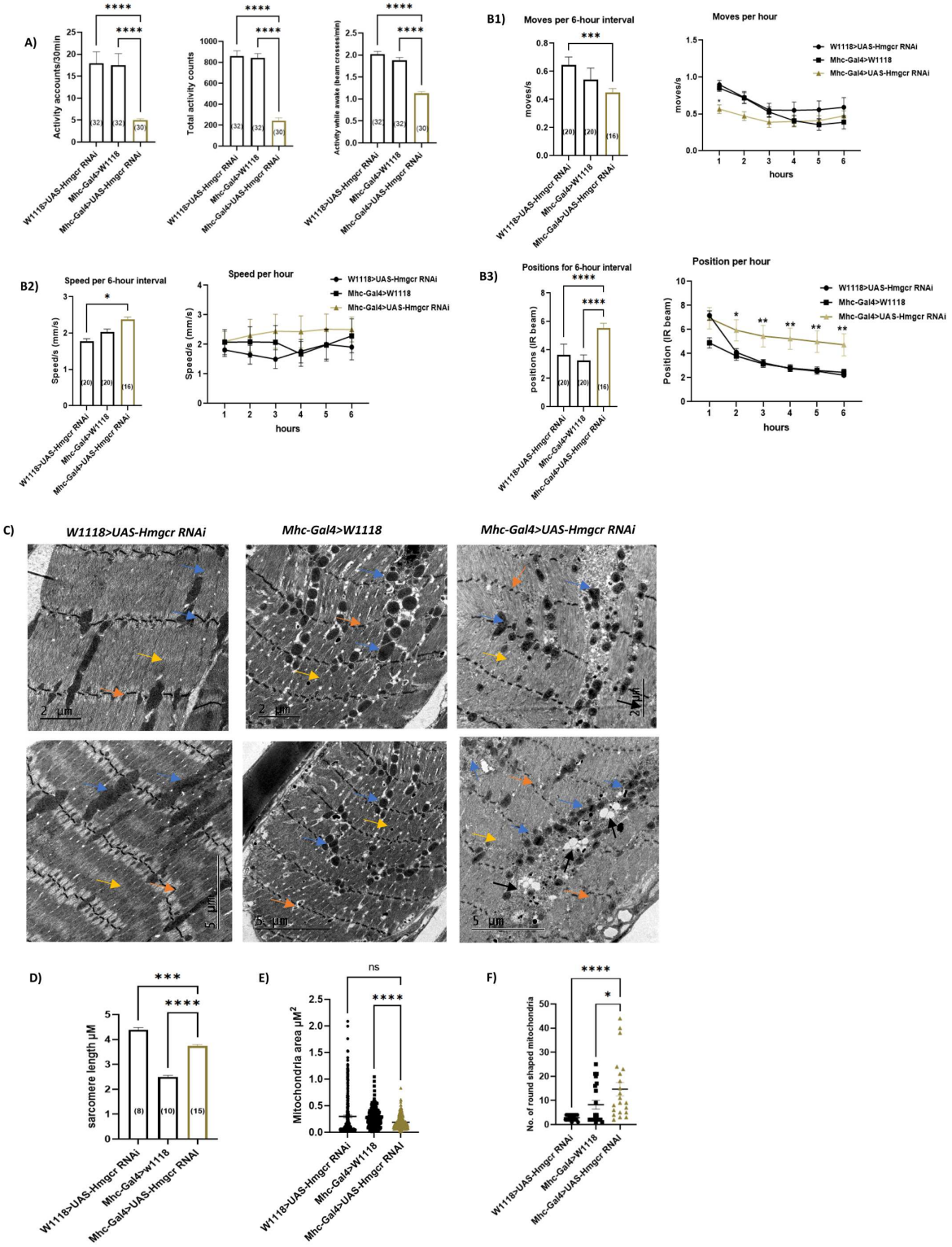

Figure 4. *Cont.*

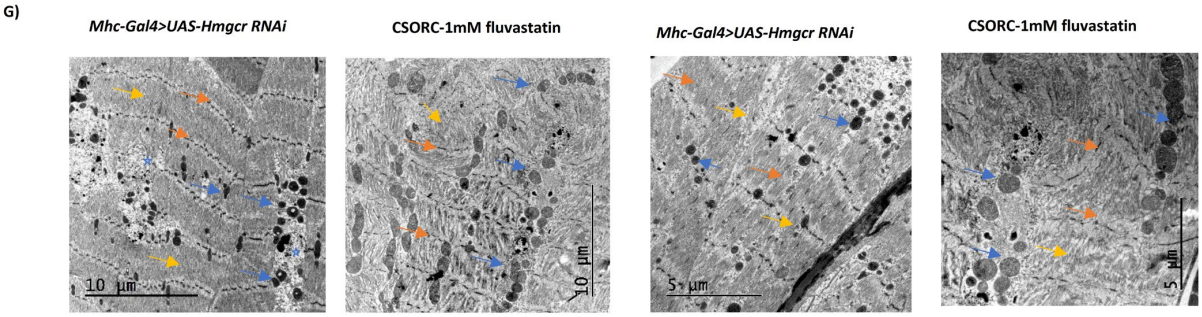

Figure 4. *Hmgcr* knockdown on skeletal muscles results in reduced locomotion activity and mitochondrial phenotypic changes. *Hmgcr* knockdown was carried out by using the Gal4-UAS system, where $Hmgcr^{RNAi}$ knockdown group is *Mhc-Gal4>UAS-Hmgcr RNAi* and control groups are *Mhc-Gal4>w1118* and *w1118>UAS-Hmgcr RNAi*. Male flies, aged 1-2 days after eclosion and fed with normal food, were collected for experiments. (**A**) The histograms show the general locomotion activity (activity counts/30 min and total activity) and activity while awake using DAMs and the number of flies is indicated in the brackets. (**B1**–**B3**) The left histograms indicate the average moves, speed and positions for a total six-hour interval while the right show the same per hour for flies using the force climbing locomotion system and the number of flies is indicated in the brackets. (**C**) TEM micrographs for the morphology of the longitudinal section of leg skeletal muscles show normal sarcomere (orange arrow) architecture and myofibrils and Z-line (yellow arrow) along with more capacious vacuoles (black arrow) in $Hmgcr^{RNAi}$ knockdown flies comparable to both controls. The mitochondria (blue arrows) are more ring-shaped and severely fragmented in $Hmgcr^{RNAi}$ knockdown flies. (**D**) Using ImageJ software, the sarcomere length, in µM, was measured in TEM micrographs (indicated in brackets) in each group. (**E**) Using ImageJ software, we traced the mitochondria area in TEM micrographs. The histogram represents the area of mitochondria in μm^2 where the dots represent the number of mitochondria. (**F**) Using ImageJ software, we counted the number of round-like shaped mitochondria in TEM micrographs where the dots represent the total number of mitochondria in each TEM micrograph. (**G**) TEM micrographs for the morphology of longitudinal sections of leg skeletal muscles for $Hmgcr^{RNAi}$ knockdown flies and CSORC flies treated with 1 mM fluvastatin for five days. Each bar represents the mean value (±SEM). For B 1, 2 and 3, two-way ANOVA with Bonferroni's multiple comparisons was used. For (**A**,**D**–**F**), first, the Shapiro–Wilk test was used to check normality; accordingly, the statistical difference was calculated using one-way ANOVA with Bonferroni's multiple comparisons for normally distributed data and Kruskal–Wallis one-way tests for otherwise data whereby * $p \leq 0.05$; ** $p \leq 0.01$; *** $p \leq 0.005$; **** $p \leq 0.0001$.

3.7. Chronic Fluvastatin Treatment Is Associated with an Upregulation of Pkcdelta and in Contrast to Fluvastatin, Inhibition of Skeletal Muscle Pkcdelta Improves General Locomotion Activities and Climbing Ability

Against the aforementioned data, a pressing question to pose is how fluvastatin inhibits ClC-a in flies. In humans and rats, PKCθ is a negative regulator of CLC-1, which upon activation, phosphorylates and inhibits CLC1 [43,44,134]. We, therefore, looked for a PKCθ homolog in flies. *D. melanogaster Pkcdelta* alignment with human *PRKCQ*, which encodes PKCθ, gives identity 186/328 (57%) and similarity 244/328 (74%) as well as a weighted score, which is obtained by 15 integrative ortholog prediction tools, of 10/15 [117,135]. One of these 15 integrative ortholog prediction tools is the PhylomeDB which indicates, according to its evolutionary data, that the *Pkcdelta* is the closest homolog to *PRKCQ* [129]. Accordingly, we hypothesized that statins mediate inhibition through the activation of *Pkcdelta*. To test this hypothesis, we fed CSORC flies with 1.0 mM fluvastatin for 5 days and examined the expression of *Pkcdelta*. As expected, fluvastatin-treated flies showed a significant upregulated *Pkcdelta* ($p = 0.0025$, Supplementary Figure S1E). Next, since *Pkcdelta* is highly expressed in the muscles [136,137] and is dispensable for the development and survival of flies [138], we decided to explore the impact of *Pkcdelta* loss on the adult skeletal muscles using the *EDTP-Gal4* driver (also known as *DJ694-Gal4*). EDTP-Gal4 is expressed in the skeletal muscles including legs, labial, flight and abdominal

muscles and its expression is restricted solely to the adult stage [125,126,139], making it a specific driver to knockdown *Pkcdelta* in adult skeletal muscles. We confirmed the *Pkcdelta* knockdown efficiency by qPCR (Supplementary Figure S8A). Strikingly, in contrast to both control groups, $Pkcdelta^{RNAi}$ knockdown flies (*EDTP-Gal4>UAS-Pkcdelta RNAi)* exhibited significantly improved climbing activity (the average moves and speed), general locomotion activities (activity count/30 min and total activity) as well as the activity while awake (Figure 7A,B and Supplementary Figure S8B). These results, except for the activity while wake and the position, showed that loss of *Pkcdelta* in the skeletal muscles exhibited improved locomotion and climbing activity that are in contrast to fluvastatin-treated flies. This may support the notion that fluvastatin may activate Pkcdelta in flies, which may, in turn, inhibit ClC-a and induce lowered locomotion and climbing activities.

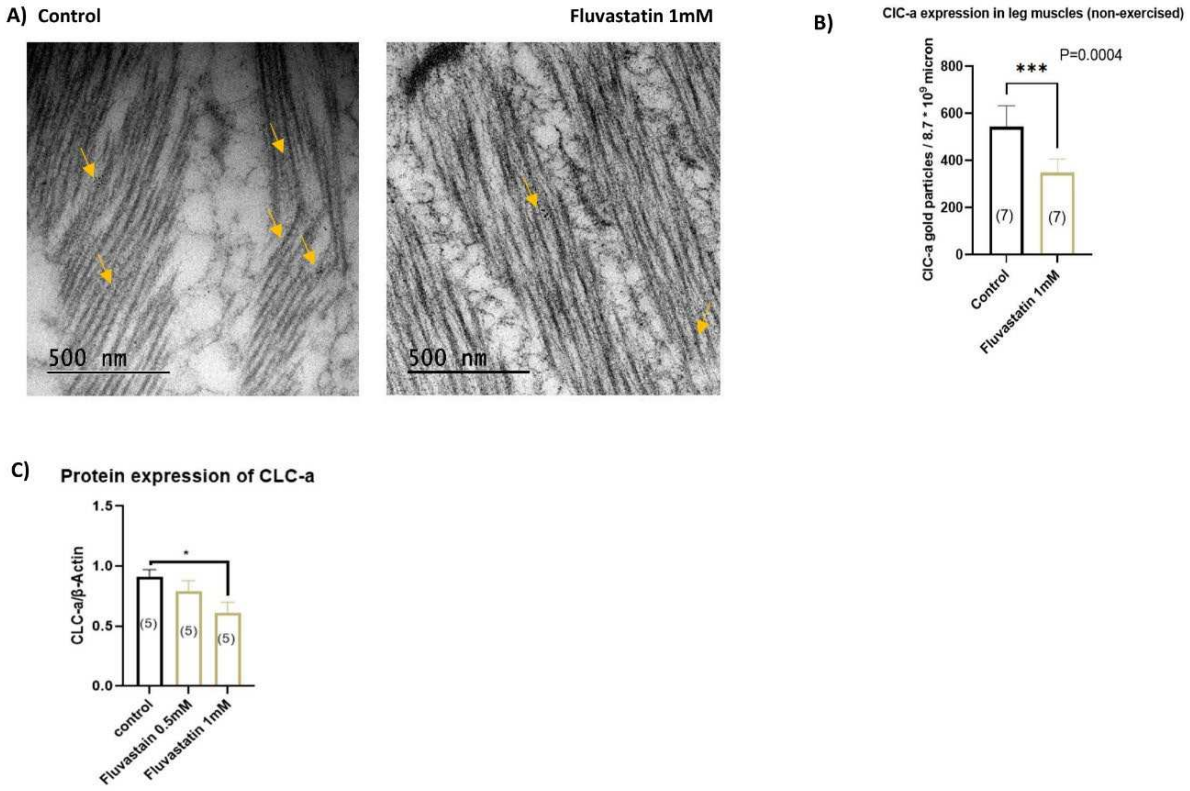

Figure 5. Fluvastatin significantly lowered the expression of the ClC-a channels in the leg's skeletal muscles of CSORC flies. (**A**) TEM micrographs of double labelling using CLC-2 (rabbit anti-ClC-2 antibody) show immunogold particles of ClC-a (yellow arrow) in the femur segment of the legs of CSOCR flies. The morphology of the muscles is poor due to the treatment necessary for immunolocalization. The skeletal chloride channel, ClC-a, is localized along the T-tubules. (**B**) The histogram represents the quantification of ClC-a gold particles in dissected skeletal muscles of femur and tibia segments of CSORC fly legs using ImageJ software. The Shapiro–Wilk test was used to check normality and accordingly, Student's *t*-tests were used to calculate the significant difference between groups. The number of TEM grids in each group is indicated in brackets. (**C**) The histogram represents the quantification of the protein relative levels of ClC-a whereby the relative protein intensity was calculated by normalising the absolute intensity of ClC-a protein with β-Actin. The whole body of 10 flies were used per sample and the number of replicates is indicated with the brackets. The Shapiro–Wilk test was used to check normality and accordingly, one-way ANOVA with Bonferroni's multiple comparisons test was used to calculate statistical significance whereby * $p \leq 0.01$; *** $p \leq 0.005$. Each bar represents the mean value (±SEM).

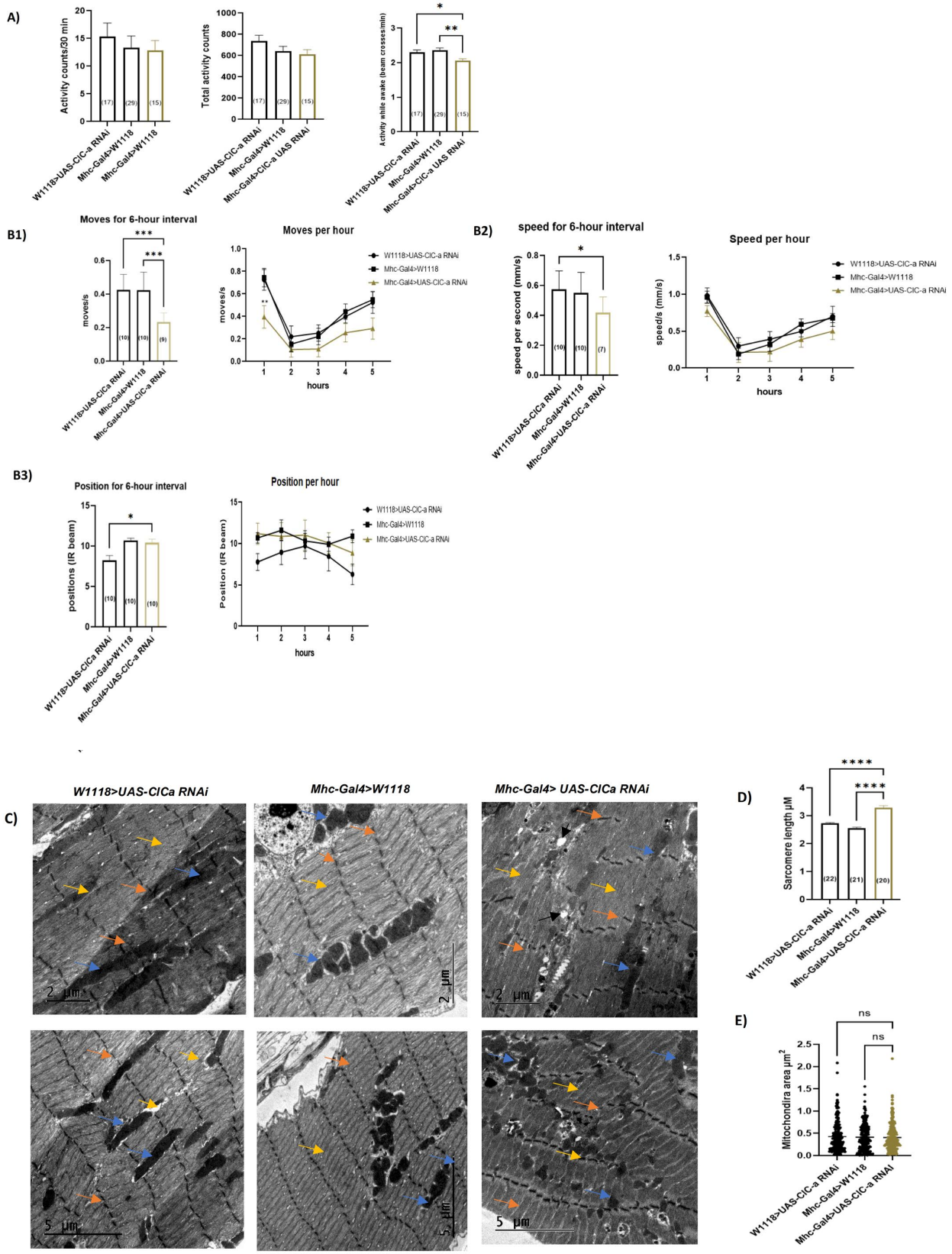

Figure 6. *Cont.*

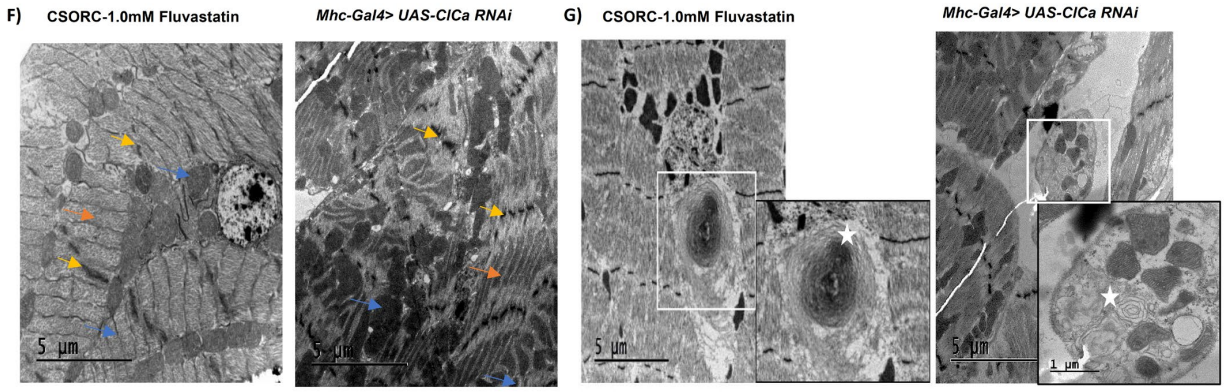

Figure 6. ClC-a knockdown in muscles lowered climbing movement and induced myopathy-like phenotypes in flies. ClC-a knockdown was carried out using the UAS-Gal4 system where *ClC-a*^{RNAi} knockdown group is *Mhc-Gal4>UAS-ClC-a RNAi* and control groups are *Mhc-Gal4>w1118* and *w1118>UAS-ClC-a RNAi*. Male flies, aged for five days after eclosion and fed with food, were collected for the experiments. (**A**) The histograms indicate the activity counts/30 min, total activity accounts and activity while awake using DAMs where the number of flies is indicated in brackets. (**B1**–**B3**) The histograms indicate the average moves, speed and positions for a total six-hour interval on the left and per hour on the right using the Force-Climbing System where the number of flies is indicated in brackets. (**C**) TEM micrographs for the morphology of the longitudinal sections of the skeletal muscles of the femur segment of the legs. *ClC-a*^{RNAi} knockdown flies show abnormal sarcomere architecture, disoriented, distorted myofibrils and Z-line streaming along with severely fragmented mitochondria of different shapes and sizes in comparison to controls. Orange arrow for Z-line, yellow for sarcomere, black for vacuoles, and blue for mitochondria. (**D**) Using ImageJ software, the sarcomere length, in µM, was measured in a selected number of TEM micrographs for each group (indicated in brackets). (**E**) Using ImageJ software, we traced the mitochondria area in selected TEM micrographs. The histogram represents the area of mitochondria in µm^2 where the dots represent the number of mitochondria. (**F**) TEM micrographs illustrate a similar pattern of muscle fibre damage between *ClC-a*^{RNAi} knockdown flies and CSORC flies fed with 1.0 mM fluvastatin for five days while (**G**) shows the myelin figure (star) in both groups. In each histogram, the bars represent the mean values ± SEM. The number of samples is indicated in brackets. The Shapiro–Wilk test was used to check normality wherein (**A**,**D**,**E**) the statistical difference was calculated using one-way ANOVA with Bonferroni's multiple comparisons for normally distributed data and Kruskal–Wallis one-way tests for non-parametric data. For (**B1**–**B3**), two-way ANOVA with Bonferroni correction for multiple comparisons test was used. * $p \leq 0.05$; ** $p \leq 0.01$; *** $p \leq 0.005$; **** $p \leq 0.0001$.

It should be noted that PKCθ suppression has been shown to improve myogenesis in mouse myoblasts [103], enhance healing and regeneration of the muscles in a mouse model of muscular dystrophy [140,141] and protect mice from immobilization-induced muscle atrophy [142].

3.8. Chelerythrine Chloride, CC, a PKC Inhibitor, Rescues the Fluvastatin-Induced Lowered Locomotion and Climbing Ability

To further confirm the notion that fluvastatin mediated inhibition of ClC-a through activation of Pkcdelta, we attempted to rescue the fluvastatin-induced lowered general activities and climbing ability phenotypes using chelerythrine chloride (CC), a potent PKC inhibitor [143]. First, we treated CSOCR flies with 1 mM fluvastatin for five days and then with CC for three hours. After that, we examined their climbing ability. Intriguingly, CC significantly rescued the fluvastatin-induced lower climbing ability including both average moves and positions. (Figure 8A). Next, we examined the chronic exposure of flies to both fluvastatin and CC for five days in DAMS. CC partially, but significantly, improved the fluvastatin-induced lowered activity counts/30 min only while the total activity was not significantly improved (Figure 8B and Supplementary Figure S9).

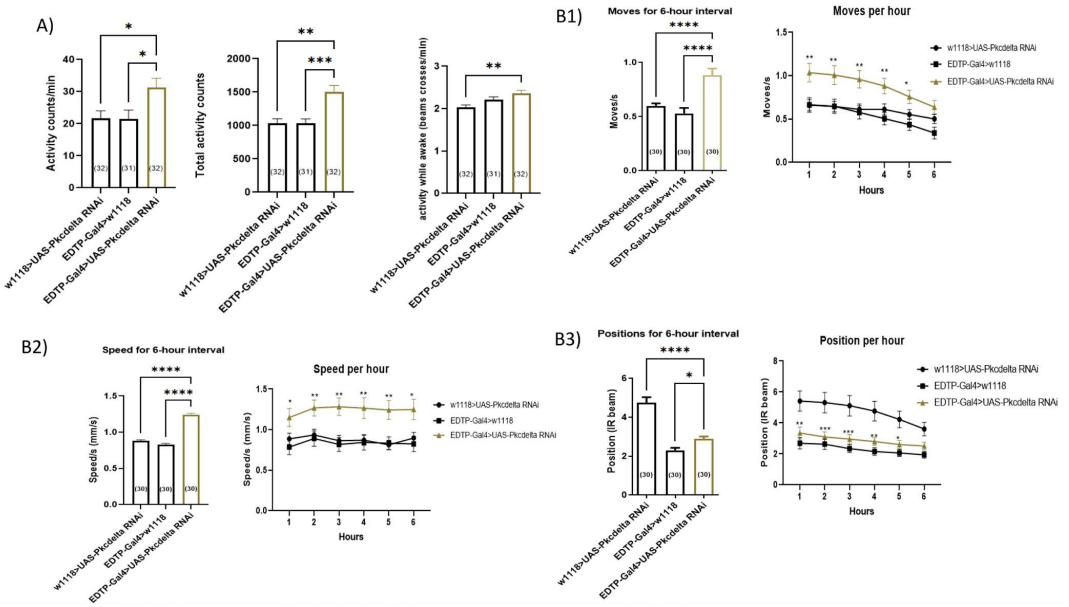

Figure 7. *Pkcdelta* disruption in the skeletal muscles improved general locomotion activity and climbing ability. *Pkcdelta* knockdown was carried out by using the Gal4-UAS system where the *Pkcdelta*^{RNAi} knockdown group is *EDTP-Gal4>UAS-Pkcdelta RNAi* and controls are *EDTP-Gal4>w1118* and *w1118>UAS-Pkcdelta RNAi*. Male flies, aged five days after eclosion, were collected for DAMS and LAMS and all flies were fed with normal food for five days. (**A**) The histograms show the activity counts/30 min, the total activity counts and activity while waking for five days using DAMS. (**B1**–**B3**) The left histograms show the average moves, speed and positions for a six-hour interval while the right histograms show the same per hour using the Forced-Climbing System. Each bar represents the mean value (±SEM) and the number of flies is indicated in the brackets. For (**A**), the Shapiro–Wilk test was used to check the normality test; accordingly, the statistical difference was calculated using one-way ANOVA with Bonferroni's multiple comparisons for normally distributed data and Kruskal–Wallis one-way tests for otherwise data. For (**B1**–**B3**), two-way ANOVA with Bonferroni's multiple comparisons test was used whereby * $p \leq 0.05$; ** $p \leq 0.01$; *** $p \leq 0.005$; **** $p \leq 0.0001$.

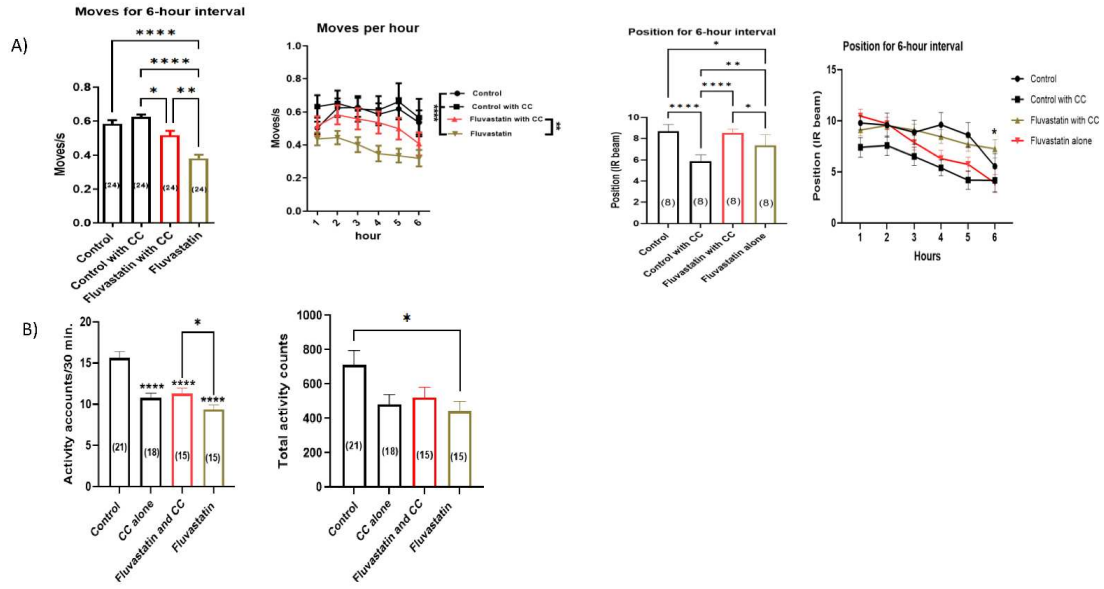

Figure 8. Chelerythrine chloride, CC, partially but significantly rescued the fluvastatin-induced lowered activity counts and climbing ability. Male virgin CSORC flies were used for the experiments.

(**A**) The left histograms show the average moves for six-hour intervals and the moves/s per hour while the right histograms show the same for the average position. In the control group, flies were fed with food for five days; in the CC group, flies were fed with normal food for five days and then on the fifth day, they were fed with 100 µM CC for three hours; in fluvastatin with CC group, flies fed with 0.5 mM fluvastatin for five days and then in the fifth day, they fed with 100 µM CC for three hours; and in fluvastatin group, flies fed with 0.5 mM fluvastatin for five days. Then, flies were exercised for six hours using the force-climbing activity system (**B**) The histograms show the activity counts/30 min and total activity counts in comparison to the control. The control group was fed with normal food alone, the fluvastatin group was fed with 0.5 mM fluvastatin, the fluvastatin and CC group was fed with both 0.5 mM fluvastatin and 100 µM CC, and the CC group was fed with 100 µM CC. For (**A**) two-way ANOVA with the Bonferroni test was used to compare between groups. For (**B**) The Shapiro–Wilk test was used to check normality and accordingly, one-way ANOVA with Kruskal–Wallis test was used for comparing all groups with control, and Mann–Whitney's test was used to calculate the statistical significance between fluvastatin and fluvastatin and CC groups. Each bar represents the mean value (±SEM) and the number of flies is indicated in the brackets where * $p \leq 0.05$; ** $p \leq 0.01$; **** $p \leq 0.0001$.

4. Discussion

Statin medications are the cornerstone for the prevention and treatment of cardiovascular events [144]. Nevertheless, SIM-associated adverse effects hamper patient compliance and subsequently increase the risk for CVD [8–11]. Despite extensive studies, the underlying mechanisms for SIM are still poorly understood. Therefore, we employ both pharmacological and genetic approaches to investigate and understand possible underlying causes of SIM using *Drosophila melanogaster.*

We demonstrate, for the first time, that chronic fluvastatin treatment induces morphological damage in myofibrils in *Drosophila* including longer sarcomeres and Z-line losses/streaming (See Figure 3), which are reminiscent of myopathy, in concert with mitochondrial morphological changes, including fragmented round-like shaped and large-sized mitochondria (See Figure 3). Additionally, chronic fluvastatin treatment is accompanied by a remarkable reduction in key genes involved in muscle regeneration and differentiation (See Supplementary Figure S1C) and impaired lipid metabolism and insulin signalling (See Supplementary Figure S3). Consequently, the general locomotion activities and climbing ability of the flies treated with fluvastatin have been significantly reduced (See Figure 2). Taken together, these findings demonstrate that *D. melanogaster* provides a powerful model system to investigate the SIM phenotypes at multifarious levels.

Mechanistically, we mimicked the statin's inhibitory effect on Hmgcr by selectively knocking down *Hmgcr* in the skeletal muscles. We found that loss of muscular *Hmgcr* was not sufficient to induce muscular phenotypes (myofibril damage or altered sarcomere size) or impair climbing ability in comparison to fluvastatin treatment (See Figures 2A–C, 3A–D and 4B–D,G). In this context, a single study by Yoshinori et al. has reported that skeletal muscle-specific knockout of *HMGCR* in mice displayed myopathy-like phenotypes that were associated with vacuolated myofibers and necrosis [145]. Nevertheless, it is difficult to relate statin-induced muscle phenotypes to a complete deletion of HMGCR in the skeletal muscles since statins inhibit and diminish, rather than abolish, HMGCR enzyme activity [146]. Moreover, knockdown of zebrafish *HMGCR* (*hmgcrb*) or treating zebrafish embryos with statins has been shown to cause strong myofiber damage with shorter myotube diameters [147], but the authors did not investigate the effect of *hmgcrb* knockdown during the adult stage where the muscles are fully developed. This is important since the mevalonate pathway is indispensable for musculoskeletal development in zebrafish embryos [148].

In flies, the mevalonate pathway, in which Hmgcr is the rate-limiting enzyme, is crucial for isoprenoid biosynthesis, including ubiquinone, prenylated proteins, heme A (Cytochrome C oxidase) and dolichol, in the muscles [149]. In humans, ubiquinone,

also called CoQ10, is a crucial node in the electron transfer from mitochondrial Complexes I and II to Complex III in the respiratory transport chains, especially during lipid metabolisms and oxidative stress [150,151]. Consequently, CoQ10deficiency leads to ROS overproduction and impaired FAO [152,153] and ultimately elicits mitochondria dysfunction [154–156]. In this context, our data show that knockdown of muscular *Hmgcr* resulted in reduced general locomotion activities along with phenotypic changes in mitochondria including round-shape mitochondria, that were, to some extent, mimicked by fluvastatin treatment (See Figures 3A,B,F and 4A,C,F,G). In addition, fluvastatin treatment has been associated with an upregulation of AMPKalpha (*Drosophila* homolog of AMPK) (See Supplementary Figure S1D). In humans, muscle biopsy from fluvastatin-treated patients displays a high expression of active AMPK, suggesting a cytoprotective response to oxidative stress [45]. Accordingly, it might be reasonable to propose that the reduced general locomotion activities and mitochondria changes associated with fluvastatin treatment are attributed to CoQ10 depletion and subsequent oxidative stress as a result of statin-inhibition of muscular Hmgcr. Nevertheless, as mentioned previously, the data regarding the role of reduced muscular CoQ10 in SIM is conflicting [27,28,30–34] and above all, whether mitochondrial dysfunction should be considered a frequent hallmark of SIM is still disputed [157,158].

We also demonstrate that chronic fluvastatin treatment has been associated with a reduction in the ClC-a expression (See Figure 5) and loss of ClC-a in skeletal muscles has produced myopathy-like phenotypes similar but stronger, to fluvastatin treatment including myofibril ultrastructure damage and longer sarcomere, as well as impaired climbing activity, in particular, the average moves (See Figure 6B–D,F,G). Moreover, exercising flies for six hours restored the altered sarcomere length and normalized chloride channel expression associated with fluvastatin treatment (See Figures 3D, 5B and Supplementary Figures S2B and S5A), suggesting that exercise may improve the sarcomere length by enhancing the skeletal muscle chloride channel expression. Collectively, the muscular phenotypes (increased sarcomere length and myofibrillar damage) associated with fluvastatin treatment are perhaps a result of the reduction in the skeletal muscle chloride channel ClC-a. This underscores the significance of the skeletal muscle chloride channel in the histopathology of SIM, which is backed up by a recent report which has identified truncating mutations in *CLCN1* (rs55960271) in patients with SIM [159]. These mutations are also the most frequent pathogenetic mutations in myotonia [159]. It is noteworthy that mutation or loss of function of CLC-1 leads to decreased resting conductance and potassium accumulation [160,161]. This, in turn, elicits hyper-excitability, muscle stiffness, and myotonia symptoms [48,160–165]. Furthermore, in humans, moderate exercise has been shown to improve the manifestation of SIM, although the data are conflicting [72,131,132]. Therefore, future studies investigating the role of the skeletal muscle chloride channel in the exercise-related effects in patients with SIM are highly recommended.

It has been reported that through the activation of protein kinase c theta (PKCθ), statins, including fluvastatin, reduce the expression of a skeletal muscle chloride channel, chloride channel 1 (CLC-1), and thereby the chloride resting potential (gCl) [43–46]. As mentioned earlier, PKCθ is a negative modulator of CLC-1 in humans and rats [43,44,134].

Along the same lines, our data show that fluvastatin treatment has been associated with an upregulation of *Pkcdelta* and, contrary to fluvastatin, loss of *Pkcdelta* in the skeletal muscles has led to improved general locomotion activity and climbing measures (See Figures 2 and 7). This leads us to postulate that the statin inhibition ClC-a may be mediated by the activation of Pkcdelta. This possibility is supported by the fact that the locomotion and climbing phenotypes associated with fluvastatin treatment have been partially but significantly rescued by chelerythrine chloride (CC), a potent PKC inhibitor [143], (See Figure 8). It is noteworthy that CC has also been shown to partially restore the declined resting chloride channel conductance (gCl) on the dissected muscle of fluvastatin-treated rats [44] and improves the contraction of the injured skeletal muscle fibres of the rat [166].

So far, evidence for the mechanisms underlying statin-activation of PKCθ in humans is still lacking. It has been suggested that statins induce the mitochondrial release of Ca^{2+} which then activates PKCs [45,46,134]. However, PKCθ, and Pkcdelta, belong to novel PKCs (nPKCs) which are insensitive to Ca^{2+} because their C2 domain lacks the residues for Ca^{2+} binding [167,168]. This could prompt the possibility that statins could mediate the activation of PKCθ through ROS or lipid intermediates, such as FFA and DAG. Regarding ROS, in contrast to fluvastatin-treated flies and the *ClC-a*^{RNAi} knockdown flies, loss of Hmgcr (and maybe the consequent ROS generation) was not enough to elicit myofibril ultrastructure or alter the sarcomere length. Further studies are needed to better understand the role of Hmgcr inhibition or the subsequent decline of its downstream products in the statin-mediated inhibition of ClC-a.

Previous studies have suggested impaired lipid metabolism in patients with SIM [107,110,169]. Furthermore, lipid intermediates, specifically DAG and FFA, have been reported to activate PKC-θ in humans, both, directly and by enhancing its membrane translocation, respectively [170–174]. Consistent with this possibility, in fluvastatin-treated flies, genes regulating TG metabolism have been largely altered (See Supplementary Figure S3A and Table 7), which may result in the accumulation of such toxic lipid intermediates. Since FFA and DAG can also activate other forms of nPKCs [170–174], we examined the effect of the fluvastatin treatment on the expression of *Pkc98E* (*Drosophila* homolog of PRKCE which encodes PKCε), which belongs to the nPKCs and is also expressed in muscles [117,137]. Expectedly, chronic fluvastatin treatment was also associated with an upregulation of *Pkc98E* ($p = 0.0077$, Supplementary Figure S1E). It is therefore reasonable to propose that fluvastatin-induced activation of Pkcdelta could be mediated by accumulated lipid intermediates such as FFA or DAG. This possibility is backed up by data showing that patients with SIM have an elevation of FFA and DAG levels, and activation of PKC and, by the same token, pharmacological inhibition of PKC reverses and restores the statin-induced insulin in the skeletal muscles [107,175]. In this context, in addition to its inhibitory effect on PKC, CC has demonstrated anti-inflammatory and antioxidant effects [176,177] and improved lipid metabolism, particularly fatty acid oxidation, and insulin haemostasis in mice [178] which could suggest additional mechanisms for its rescuing effect on fluvastatin-induced lowered locomotion and climbing phenotypes (See Figure 8). Although impaired lipid metabolism has been reported in SIM [104,107], the underlying mechanisms remain to be elucidated.

Interestingly, our study suggests that depletion of sarcolemma cholesterol is not the main underlying cause of SIM because fruit flies cannot biosynthesize cholesterol de novo and instead obtain it from the food [149,179]. This may exclude the possibility that the locomotion and myopathy phenotypes associated with fluvastatin are caused simply by cholesterol depletion. This possibility is backed up by the fact that, in humans, patients with hereditary cholesterol biosynthetic defects do not show clinical manifestations of skeletal myopathy [120].

A strength of our study is that we have used both genetic and pharmacological approaches to decipher the phenotypes associated with statins treatment using an affordable and easily genetically manipulated platform system, *Drosophila melanogaster*. In addition, we were able to confirm the knockdown efficiency for each flies' crosses, which validated the resulting phenotypes. This study has several limitations. Although we quantified sarcomere lengths using multiple images of the same leg section to robustly detect any differences in sarcomere lengths between control and treated/knockdown flies, we cannot exclude the possibility that different muscle types may have been abundant in the sections that were analysed. This may add to a certain variability in the outcome measurements. Future studies would benefit from examining the differences in the sarcomere lengths within each individual type of femur muscle (tidm, tilm, and tirm) or thorax muscle. In addition, due to the lack of specific antibodies in the market, we could not determine whether fluvastatin activates Pkcdelta which could have been performed with Western blot for its active and inactive form with the appropriate antibodies. Furthermore, we also did

not demonstrate whether Pkcdelta regulates (phosphorylates and inhibits) skeletal muscle ClC-a in flies, as it is outside of the scope of this study and its homologue, PKC-θ, has already been shown to inhibit the skeletal muscle ClC-1 in humans and rats [43,44,134]. Although we demonstrate that CC mechanistically rescued the locomotion and climbing phenotypes accompanied by fluvastatin, we did not show if CC rescued the myofibril or mitochondrial phenotypes caused by fluvastatin. The reason behind this is that we do not know exactly when the muscle or mitochondrial phenotypes started to emerge after statin treatment. Moreover, we did not measure ROS in the fluvastatin-treated flies or *Hmgcr* knockdown flies since this has been studied extensively [180,181]. Finally, we did not test several types of statins, which would help to demonstrate the differential effects of lipophilic and hydrophilic statins on the muscles, which is warranted to be addressed in future studies.

5. Concluding Remarks

This study demonstrates that statins induce locomotion and muscular phenotypes that are reminiscent of the human myopathy in *Drosophila melanogaster*, suggesting that the mechanisms behind the important side effects of statins could be highly evolutionarily conserved. The statins may induce mitochondria phenotypic changes through direct inhibition of muscular Hmgcr and myofibrillar damage reminiscent of myopathy that is associated with inhibition of skeletal muscle ClC-a. The study also underscores the role of skeletal muscle chloride channels for statin muscular phenotypes and its potential, perhaps, as a biomarker for SIM for future clinical studies. Moreover, the study sheds light on a possible mechanistic pathway of the statin-mediated PKC inhibition of skeletal muscle chloride channels as well as the contribution of the impaired lipid metabolism. This study also underlines the potential of chelerythrine as a pharmacological tool for understanding statin myopathy-related phenotypes for future application. Collectively, our findings demonstrate that *D. melanogaster* provides a powerful and affordable model system to elucidate statin myopathy phenotypes in multifaceted aspects.

Supplementary Materials: The following supporting information can be downloaded at: https://www.mdpi.com/article/10.3390/cells11223528/s1, Figure S1: The octogram, average activity and the qPCR for the expression of the genes in the Fluvastatin-treated flies and control; Figure S2: TEM and Sarcomere length for exercised CSORC flies; Figure S3: The effect of Fluvastatin treatment on the key genes involved in lipid metabolism and insulin signalling; Figure S4: The octogram and average activity and qPCR for *Hmgcr* expression for the Hmgcr knockdown flies; Figure S5: ClC-a gold particles in the skeletal muscles of the exercised CSORC flies, ClC-a expression and the blot image for western blotting of protein expression of ClC-a; Figure S6: Chloride channel blockers induced lower activity in CSORC flies; Figure S7: The octogram and average activity and qPCR for the expression of ClC-a for ClC-a Knockdown; Figure S8: The octogram and average activity and qPCR for the expression of *Pkcdelta* for Pkcdelta Knockdown flies; Figure S9: the octogram and the average activity for the CC and Fluvastatin treatment.

Author Contributions: Conceptualization, M.H.A.-S., M.J.W. and H.B.S.; methodology and experiments M.H.A.-S., A.M.A., N.B., A.A., E.A., E.I.M., P.D.C., J.V. and S.B.; software, S.B., T.C.M. and M.H.A.-S.; validation and formal analysis. S.A.-K., A.M.A., N.B., H.B., N.A., A.A., E.A., E.I.M., P.D.C., J.V., R.F. and S.B.; data curation, R.F., M.H.A.-S., S.A.-K., A.M.A., N.B., H.B., N.A., A.A., E.A., E.I.M., P.D.C., J.V. and S.B.; writing the original draft and visualization, M.H.A.-S.; writing—review and editing, H.B.S., R.F., M.R.-A., J.M., M.J.W., H.B., M.H.A.-S. and L.E.C.; supervision, H.B.S., R.F., M.R.-A., J.M. and M.J.W.; project administration, M.H.A.-S. and H.B.S.; funding acquisition, H.B.S., investigation, R.F., M.R.-A., J.M. and M.J.W. All authors discussed the results and commented on the manuscript. All authors have read and agreed to the published version of the manuscript.

Funding: The studies were supported by the Swedish Research Council: 2019-01066. H.B. is also supported by the AFM-Telethon trampoline grant 23108 and ATIP-Avenir. N.A. is supported by the AFM-Telethon PhD fellowship 23846.

Institutional Review Board Statement: Not applicable.

Informed Consent Statement: Not applicable.

Data Availability Statement: Data are contained within the article and Supplementary Materials.

Acknowledgments: The authors acknowledge the assistance of the BioVis Electron Microscopy node staff at the Rudbeck Laboratory, Uppsala University for transmission electron microscopy.

Conflicts of Interest: The authors declare no conflict of interest.

References

1. Roth, G.A.; Mensah, G.A.; Johnson, C.O.; Addolorato, G.; Ammirati, E.; Baddour, L.M.; Barengo, N.C.; Beaton, A.Z.; Benjamin, E.J.; Benziger, C.P.; et al. Global Burden of Cardiovascular Diseases and Risk Factors, 1990–2019: Update from the GBD 2019 Study. *J. Am. Coll. Cardiol.* **2020**, *76*, 2982. [CrossRef] [PubMed]
2. Nelson, R.H. Hyperlipidemia as a Risk Factor for Cardiovascular Disease. *Prim. Care* **2013**, *40*, 195–211. [CrossRef] [PubMed]
3. Taylor, F.; Ward, K.; Moore, T.H.H.M.; Burke, M.; Smith, G.D.; Casas, J.P.; Ebrahim, S.; Huffman, M.D.; Macedo, A.F.; Moore, T.H.H.M.; et al. Statins for the primary prevention of cardiovascular disease. *Cochrane Database Syst. Rev.* **2011**, CD004816. [CrossRef]
4. Zhou, Q.; Liao, J.K. Pleiotropic Effects of Statins—Basic Research and Clinical Perspectives. *Circ. J.* **2010**, *74*, 818–826. [CrossRef]
5. Karmali, K.N.; Lloyd-Jones, D.M.; Berendsen, M.A.; Goff, D.C.; Sanghavi, D.M.; Brown, N.C.; Korenovska, L.; Huffman, M.D. Drugs for Primary Prevention of Atherosclerotic Cardiovascular Disease: An Overview of Systematic Reviews. *JAMA Cardiol.* **2016**, *1*, 341–349. [CrossRef]
6. Wadhera, R.K.; Steen, D.L.; Khan, I.; Giugliano, R.P.; Foody, J.M. A review of low-density lipoprotein cholesterol, treatment strategies, and its impact on cardiovascular disease morbidity and mortality. *J. Clin. Lipidol.* **2016**, *10*, 472–489. [CrossRef]
7. Clark, L.L.; Ikonomidis, J.S.; Crawford, F.A.; Crumbley, A.; Kratz, J.M.; Stroud, M.R.; Woolson, R.F.; Bruce, J.J.; Nicholas, J.S.; Lackland, D.T.; et al. Preoperative statin treatment is associated with reduced postoperative mortality and morbidity in patients undergoing cardiac surgery: An 8-year retrospective cohort study. *J. Thorac. Cardiovasc. Surg.* **2006**, *131*, 679–685. [CrossRef]
8. Tziomalos, K.; Athyros, V.G.; Mikhailidis, D.P. Statin discontinuation: An underestimated risk? *Curr. Med. Res. Opin.* **2008**, *24*, 3059–3062. [CrossRef]
9. Thompson, P.D.; Clarkson, P.; Karas, R.H. Statin-Associated Myopathy. *J. Am. Med. Assoc.* **2003**, *289*, 1681–1690. [CrossRef]
10. Cohen, J.D.; Brinton, E.A.; Ito, M.K.; Jacobson, T.A. Understanding Statin Use in America and Gaps in Patient Education (USAGE): An internet-based survey of 10,138 current and former statin users. *J. Clin. Lipidol.* **2012**, *6*, 208–215. [CrossRef]
11. Gomez Sandoval, Y.-H.; Braganza, M.V.; Daskalopoulou, S.S. Statin Discontinuation in High-Risk Patients: A Systematic Review of the Evidence. *Curr. Pharm. Des.* **2011**, *17*, 3669–3689. [CrossRef] [PubMed]
12. Pasternak, R.C.; Smith, S.C.; Merz, C.N.B.; Grundy, S.M.; Cleeman, J.I.; Lenfant, C. ACC/AHA/NHLBI Clinical Advisory on the Use and Safety of Statins. *Circulation* **2002**, *106*, 1024–1028. [CrossRef] [PubMed]
13. Tomaszewski, M.; Stępień, K.M.; Tomaszewska, J.; Czuczwar, S.J. Statin-induced myopathies. *Pharmacol. Rep.* **2011**, *63*, 859–866. [CrossRef]
14. Klopstock, T. Drug-induced myopathies. *Curr. Opin. Neurol.* **2008**, *21*, 590–595. [CrossRef] [PubMed]
15. Hilton-Jones, D. Statin-related myopathies. *Pract. Neurol.* **2018**, *18*, 97–105. [CrossRef] [PubMed]
16. Needham, M.; Fabian, V.; Knezevic, W.; Panegyres, P.; Zilko, P.; Mastaglia, F.L. Progressive myopathy with up-regulation of MHC-I associated with statin therapy. *Neuromuscul. Disord.* **2007**, *17*, 194–200. [CrossRef]
17. Hadjiphilippou, S.; Ray, K.K. Cholesterol-Lowering Agents Statins—For Everyone? *Circ. Res.* **2019**, *124*, 354–363. [CrossRef]
18. Shroufi, A.; Powles, J.W. Adherence and chemoprevention in major cardiovascular disease: A simulation study of the benefits of additional use of statins. *J. Epidemiol. Community Health* **2010**, *64*, 109–113. [CrossRef]
19. Lotteau, S.; Ivarsson, N.; Yang, Z.; Restagno, D.; Colyer, J.; Hopkins, P.; Weightman, A.; Himori, K.; Yamada, T.; Bruton, J.; et al. A Mechanism for Statin-Induced Susceptibility to Myopathy. *JACC Basic Transl. Sci.* **2019**, *4*, 509–523. [CrossRef]
20. Draeger, A.; Monastyrskaya, K.; Mohaupt, M.; Hoppeler, H.; Savolainen, H.; Allemann, C.; Babiychuk, E. Statin therapy induces ultrastructural damage in skeletal muscle in patients without myalgia. *J. Pathol.* **2006**, *210*, 94–102. [CrossRef]
21. Flint, O.P.; Masters, B.A.; Gregg, R.E.; Durham, S.K. Inhibition of Cholesterol Synthesis by Squalene Synthase Inhibitors Does Not Induce Myotoxicity in Vitro. *Toxicol. Appl. Pharmacol.* **1997**, *145*, 91–98. [CrossRef] [PubMed]
22. Harper, C.R.; Jacobson, T.A. Evidence-Based Management of Statin Myopathy. *Curr. Atheroscler. Rep.* **2010**, *12*, 322–330. [CrossRef] [PubMed]
23. Dirks, A.J.; Jones, K.M. Statin-Induced Apoptosis and Skeletal Myopathy. *Am. J. Physiol.-Cell Physiol.* **2006**, *291*, 1208–1212. [CrossRef] [PubMed]
24. Matzno, S.; Yasuda, S.; Juman, S.; Yamamoto, Y.; Nagareya-Ishida, N.; Nakabayashi, T.; Matsuyama, K.; Tazuya-Murayama, K. Statin-induced apoptosis linked with membrane farnesylated Ras small G protein depletion, rather than geranylated Rho protein. *J. Pharm. Pharmacol.* **2010**, *57*, 1475–1484. [CrossRef] [PubMed]
25. Laaksonen, R.; Jokelainen, K.; Laakso, J.; Sahi, T.; Härkönen, M.; Tikkanen, M.J.; Himberg, J.J. The effect of Simvastatin treatment on natural antioxidants in low-density lipoproteins and high-energy phosphates and ubiquinone in skeletal muscle. *Am. J. Cardiol.* **1996**, *77*, 851–854. [CrossRef]

26. Qu, H.; Guo, M.; Chai, H.; Wang, W.T.; Gao, Z.Y.; Shi, D.Z. Effects of Coenzyme Q10 on Statin-Induced Myopathy: An Updated Meta-Analysis of Randomized Controlled Trials. *J. Am. Heart Assoc.* **2018**, *7*, e009835. [CrossRef]
27. Bookstaver, D.A.; Burkhalter, N.A.; Hatzigeorgiou, C. Effect of Coenzyme Q10 Supplementation on Statin-Induced Myalgias. *Am. J. Cardiol.* **2012**, *110*, 526–529. [CrossRef]
28. Banach, M.; Serban, C.; Sahebkar, A.; Ursoniu, S.; Rysz, J.; Muntner, P.; Toth, P.P.; Jones, S.R.; Rizzo, M.; Glasser, S.P.; et al. Effects of Coenzyme Q10 on Statin-Induced Myopathy: A Meta-Analysis of Randomized Controlled Trials. *Mayo Clin. Proc.* **2015**, *90*, 24–34. [CrossRef]
29. Hodel, C. Myopathy and rhabdomyolysis with lipid-lowering drugs. *Toxicol. Lett.* **2002**, *128*, 159–168. [CrossRef]
30. Marcoff, L.; Thompson, P.D. The Role of Coenzyme Q10 in Statin-Associated Myopathy: A Systematic Review. *J. Am. Coll. Cardiol.* **2007**, *49*, 2231–2237. [CrossRef]
31. Dohlmann, T.L.; Morville, T.; Kuhlman, A.B.; Chrøis, K.M.; Helge, J.W.; Dela, F.; Larsen, S. Statin Treatment Decreases Mitochondrial Respiration But Muscle Coenzyme Q10 Levels Are Unaltered: The LIFESTAT Study. *J. Clin. Endocrinol. Metab.* **2019**, *104*, 2501–2508. [CrossRef] [PubMed]
32. Urbano, F.; Bugliani, M.; Filippello, A.; Scamporrino, A.; Di Mauro, S.; Di Pino, A.; Scicali, R.; Noto, D.; Rabuazzo, A.M.; Averna, M.; et al. Atorvastatin but Not Pravastatin Impairs Mitochondrial Function in Human Pancreatic Islets and Rat β-Cells. Direct Effect of Oxidative Stress. *Sci. Rep.* **2017**, *7*, 11863. [CrossRef] [PubMed]
33. Taylor, B.A.; Lorson, L.; White, C.M.; Thompson, P.D. A randomized trial of coenzyme Q10 in patients with confirmed Statin Myopathy. *Atherosclerosis* **2015**, *238*, 329–335. [CrossRef] [PubMed]
34. Young, J.M.; Florkowski, C.M.; Molyneux, S.L.; McEwan, R.G.; Frampton, C.M.; George, P.M.; Scott, R.S. Effect of Coenzyme Q10 Supplementation on Simvastatin-Induced Myalgia. *Am. J. Cardiol.* **2007**, *100*, 1400–1403. [CrossRef]
35. Schirris, T.J.J.; Renkema, G.H.; Ritschel, T.; Voermans, N.C.; Bilos, A.; van Engelen, B.G.M.; Brandt, U.; Koopman, W.J.H.; Beyrath, J.D.; Rodenburg, R.J.; et al. Statin-Induced Myopathy Is Associated with Mitochondrial Complex III Inhibition. *Cell Metab.* **2015**, *22*, 399–407. [CrossRef]
36. Schaefer, W.H.; Lawrence, J.W.; Loughlin, A.F.; Stoffregen, D.A.; Mixson, L.A.; Dean, D.C.; Raab, C.E.; Yu, N.X.; Lankas, G.R.; Frederick, C.B. Evaluation of ubiquinone concentration and mitochondrial function relative to cerivastatin-induced skeletal myopathy in rats. *Toxicol. Appl. Pharmacol.* **2004**, *194*, 10–23. [CrossRef]
37. Lamperti, C.; Naini, A.B.; Lucchini, V.; Prelle, A.; Bresolin, N.; Moggio, M.; Sciacco, M.; Kaufmann, P.; DiMauro, S. Muscle Coenzyme Q10 Level in Statin-Related Myopathy. *Arch. Neurol.* **2005**, *62*, 1709–1712. [CrossRef]
38. Bitzur, R.; Cohen, H.; Kamari, Y.; Harats, D. Intolerance to Statins: Mechanisms and Management. *Diabetes Care* **2013**, *36*, S325–S330. [CrossRef]
39. Jones, S.P.; Teshima, Y.; Akao, M.; Marbán, E. Simvastatin Attenuates Oxidant-Induced Mitochondrial Dysfunction in Cardiac Myocytes. *Circ. Res.* **2003**, *93*, 697–699. [CrossRef]
40. Sanvee, G.M.; Bouitbir, J.; Krähenbühl, S. Insulin prevents and reverts simvastatin-induced toxicity in C2C12 skeletal muscle cells. *Sci. Rep.* **2019**, *9*, 7409. [CrossRef]
41. Agarwala, A.; Kulkarni, S.; Maddox, T. The Association of Statin Therapy with Incident Diabetes: Evidence, Mechanisms, and Recommendations. *Curr. Cardiol. Rep.* **2018**, *20*, 50. [CrossRef] [PubMed]
42. Betteridge, D.J.; Carmena, R. The diabetogenic action of statins—Mechanisms and clinical implications. *Nat. Rev. Endocrinol.* **2015**, *12*, 99–110. [CrossRef] [PubMed]
43. Zdebik, A.A. Statins and fibrate target ClC-1—From side effects to CLC pharmacology. *Br. J. Pharmacol.* **2009**, *156*, 1204–1205. [CrossRef] [PubMed]
44. Pierno, S.; Camerino, G.M.G.; Cippone, V.; Rolland, J.-F.F.; Desaphy, J.-F.F.; De Luca, A.; Liantonio, A.; Bianco, G.; Kunic, J.D.J.; George, A.G., Jr.; et al. Statins and fenofibrate affect skeletal muscle chloride conductance in rats by differently impairing ClC-1 channel regulation and expression. *Br. J. Pharmacol.* **2009**, *156*, 1206–1215. [CrossRef]
45. Camerino, G.M.; Musumeci, O.; Conte, E.; Musaraj, K.; Fonzino, A.; Barca, E.; Marino, M.; Rodolico, C.; Tricarico, D.; Camerino, C.; et al. Risk of Myopathy in Patients in Therapy with Statins: Identification of Biological Markers in a Pilot Study. *Front. Pharmacol.* **2017**, *8*, 500. [CrossRef]
46. Camerino, G.M.; Tarantino, N.; Canfora, I.; De Bellis, M.; Musumeci, O.; Pierno, S. Statin-Induced Myopathy: Translational Studies from Preclinical to Clinical Evidence. *Int. J. Mol. Sci.* **2021**, *22*, 2070. [CrossRef]
47. Charlet-B., N.; Savkur, R.S.; Singh, G.; Philips, A.V.; Grice, E.A.; Cooper, T.A. Loss of the Muscle-Specific Chloride Channel in Type 1 Myotonic Dystrophy Due to Misregulated Alternative Splicing. *Mol. Cell* **2002**, *10*, 45–53. [CrossRef]
48. Koch, M.C.; Steinmeyer, K.; Lorenz, C.; Ricker, K.; Wolf, F.; Otto, M.; Zoll, B.; Lehmann-Horn, F.; Grzeschik, K.H.; Jentsch, T.J. The Skeletal Muscle Chloride Channel in Dominant and Recessive Human Myotonia. *Science* **1992**, *257*, 797–800. [CrossRef]
49. Dahl-Halvarsson, M.; Olive, M.; Pokrzywa, M.; Norum, M.; Ejeskär, K.; Tajsharghi, H. Impaired muscle morphology in a Drosophila model of myosin storage myopathy was supressed by overexpression of an E3 ubiquitin ligase. *Dis. Models Mech.* **2021**, *13*, dmm047886. [CrossRef]
50. Plantié, E.; Migocka-Patrzałek, M.; Daczewska, M.; Jagla, K. Model Organisms in the Fight against Muscular Dystrophy: Lessons from Drosophila and Zebrafish. *Molecules* **2015**, *20*, 6237–6253. [CrossRef]

51. Suggs, J.A.; Melkani, G.C.; Glasheen, B.M.; Detor, M.M.; Melkani, A.; Marsan, N.P.; Swank, D.M.; Bernstein, S.I. A *Drosophila* model of dominant inclusion body myopathy Type 3 shows diminished myosin kinetics that reduce muscle power and yield myofibrillar defects. *Dis. Models Mech.* **2017**, *10*, 761–771. [CrossRef]
52. Taylor, M.V. Comparison of Muscle Development in Drosophila and Vertebrates. In *Madame Curie Bioscience Database 2000–2013*; Landes Bioscience: Austin, TX, USA, 2006. Available online: https://www.ncbi.nlm.nih.gov/books/NBK6226/ (accessed on 31 October 2022).
53. Piccirillo, R.; Demontis, F.; Perrimon, N.; Goldberg, A.L. Mechanisms of muscle growth and atrophy in mammals and *Drosophila*. *Dev. Dyn.* **2014**, *243*, 201–215. [CrossRef] [PubMed]
54. Santos, A.C.; Lehmann, R. Isoprenoids Control Germ Cell Migration Downstream of HMGCoA Reductase. *Dev. Cell* **2004**, *6*, 283–293. [CrossRef]
55. Alsehli, A.M.; Liao, S.; Al-Sabri, M.H.; Vasionis, L.; Purohit, A.; Behare, N.; Clemensson, L.E.; Williams, M.J.; Schiöth, H.B. The Statin Target HMG-Coenzyme a Reductase (Hmgcr) Regulates Sleep Homeostasis in *Drosophila*. *Pharmaceuticals* **2022**, *15*, 79. [CrossRef]
56. Belgacem, Y.H.; Martin, J.-R.R. Hmgcr in the Corpus Allatum Controls Sexual Dimorphism of Locomotor Activity and Body Size via the Insulin Pathway in Drosophila. *PLoS ONE* **2007**, *2*, e187. [CrossRef] [PubMed]
57. Belgacem, Y.H.; Martin, J.-R. Neuroendocrine control of a sexually dimorphic behavior by a few neurons of the pars intercerebralis in *Drosophila*. *Proc. Natl. Acad. Sci. USA* **2002**, *99*, 15154–15158. [CrossRef]
58. Kucera, W.G. Oxygen Consumption in the Male and Female Fly, Drosophila melanogaster. *Physiol. Zool.* **1934**, *7*, 449–458. [CrossRef]
59. Ja, W.W.; Carvalho, G.B.; Mak, E.M.; de la Rosa, N.N.; Fang, A.Y.; Liong, J.C.; Brummel, T.; Benzer, S. Prandiology of *Drosophila* and the CAFE assay. *Proc. Natl. Acad. Sci. USA* **2007**, *104*, 8253–8256. [CrossRef]
60. The Effects of a Human Food Additive, Titanium Dioxide Nanoparticles E171, on Drosophila Melanogaster—A 20 Generation Dietary Exposure Experiment | Scientific Reports. Available online: https://www.nature.com/articles/s41598-018-36174-w (accessed on 14 September 2022).
61. Moulin, T.C.; Ferro, F.; Hoyer, A.; Cheung, P.; Williams, M.J.; Schiöth, H.B. The Drosophila melanogaster Levodopa-Induced Depression Model Exhibits Negative Geotaxis Deficits and Differential Gene Expression in Males and Females. *Front. Neurosci.* **2021**, *15*, 560. [CrossRef]
62. Williams, M.J.; Alsehli, A.M.; Gartner, S.N.; Clemensson, L.E.; Liao, S.; Eriksson, A.; Isgrove, K.; Thelander, L.; Khan, Z.; Itskov, P.M.; et al. The Statin Target Hmgcr Regulates Energy Metabolism and Food Intake through Central Mechanisms. *Cells* **2022**, *11*, 970. [CrossRef]
63. Singh, F.; Zoll, J.; Duthaler, U.; Charles, A.L.; Panajatovic, M.V.; Laverny, G.; McWilliams, T.G.; Metzger, D.; Geny, B.; Krähenbühl, S.; et al. PGC-1β modulates statin-associated myotoxicity in mice. *Arch. Toxicol.* **2019**, *93*, 487–504. [CrossRef] [PubMed]
64. Sidaway, J.; Wang, Y.; Marsden, A.M.; Orton, T.C.; Westwood, F.R.; Azuma, C.T.; Scott, R.C. Statin-induced myopathy in the rat: Relationship between systemic exposure, muscle exposure and myopathy. *Xenobiotica* **2009**, *39*, 90–98. [CrossRef] [PubMed]
65. Leo, T.K.; Garba, S.; Abubakar, D.; Sazili, A.Q.; Candyrine, S.C.L.; Jahromi, M.F.; Goh, Y.M.; Ronimus, R.; Muetzel, S.; Liang, J.B. Naturally Produced Lovastatin Modifies the Histology and Proteome Profile of Goat Skeletal Muscle. *Animals* **2020**, *10*, 72. [CrossRef] [PubMed]
66. Campos, L.M.; Guapyassu, L.; Gomes, C.; Midlej, V.; Benchimol, M.; Mermelstein, C.; Costa, M.L. Simvastatin and Muscle: Zebrafish and Chicken Show that the Benefits are not Worth the Damage. *Front. Cell Dev. Biol.* **2022**, *10*, 488. [CrossRef]
67. Dubińska-Magiera, M.; Migocka-Patrzałek, M.; Lewandowski, D.; Daczewska, M.; Jagla, K. Zebrafish as a Model for the Study of Lipid-Lowering Drug-Induced Myopathies. *Int. J. Mol. Sci.* **2021**, *22*, 5654. [CrossRef]
68. Huang, S.H.; Hsiao, C.D.; Lin, D.S.; Chow, C.Y.; Chang, C.J.; Liau, I. Imaging of Zebrafish In Vivo with Second-Harmonic Generation Reveals Shortened Sarcomeres Associated with Myopathy Induced by Statin. *PLoS ONE* **2011**, *6*, e24764. [CrossRef]
69. Levine, B.D.; Cagan, R.L. Drosophila Lung Cancer Models Identify Trametinib plus Statin as Candidate Therapeutic. *Cell Rep.* **2016**, *14*, 1477–1487. [CrossRef]
70. Yi, P.; Han, Z.; Li, X.; Olson, E.H. The Mevalonate Pathway Controls Heart Formation in *Drosophila* by Isoprenylation of Gγ1. *Science* **2006**, *313*, 1301–1303. [CrossRef]
71. Moulin, T.C.; Ferro, F.; Berkins, S.; Hoyer, A.; Williams, M.J.; Schiöth, H.B. Transient Administration of Dopaminergic Precursor Causes Inheritable Overfeeding Behavior in Young *Drosophila melanogaster* Adults. *Brain Sci.* **2020**, *10*, 487. [CrossRef]
72. Chung, H.R.; Vakil, M.; Munroe, M.; Parikh, A.; Meador, B.M.; Wu, P.T.; Jeong, J.H.; Woods, J.A.; Wilund, K.R.; Boppart, M.D. The Impact of Exercise on Statin-Associated Skeletal Muscle Myopathy. *PLoS ONE* **2016**, *11*, e0168065. [CrossRef]
73. Reyes-Lugo, M.; Sánchez, T.; Finol, H.J.; Sánchez, E.E.; Suárez, J.A.; Guerreiro, B.; Rodríguez-Acosta, A. Neurotoxic activity and ultrastructural changes in muscles caused by the brown widow spider Latrodectus geometricus venom. *Rev. Inst. Med. Trop. Sao Paulo* **2009**, *51*, 95–101. [CrossRef] [PubMed]
74. Leite, F.D.S.; Rassier, D.E. Sarcomere Length Nonuniformity and Force Regulation in Myofibrils and Sarcomeres. *Biophys. J.* **2020**, *119*, 2372–2377. [CrossRef] [PubMed]
75. de Winter, J.M.; Ottenheijm, C.A.C. Sarcomere Dysfunction in Nemaline Myopathy. *J. Neuromuscul. Dis.* **2017**, *4*, 99–113. [CrossRef] [PubMed]

76. González-Morales, N.; Xiao, Y.S.; Schilling, M.A.; Marescal, O.; Liao, K.A.; Schöck, F. Myofibril diameter is set by a finely tuned mechanism of protein oligomerization in Drosophila. *eLife* **2019**, *8*, e50496. [CrossRef]
77. Joureau, B.; de Winter, J.M.; Conijn, S.; Bogaards, S.J.P.; Kovacevic, I.; Kalganov, A.; Persson, M.; Lindqvist, J.; Stienen, G.J.M.; Irving, T.C.; et al. Dysfunctional sarcomere contractility contributes to muscle weakness in *ACTA1*—Related nemaline myopathy (NEM3). *Ann. Neurol.* **2018**, *83*, 269–282. [CrossRef]
78. Liu, J.; Puolanne, E.; Schwartzkopf, M.; Arner, A. Altered Sarcomeric Structure and Function in Woody Breast Myopathy of Avian Pectoralis Major Muscle. *Front. Physiol.* **2020**, *11*, 287. [CrossRef]
79. Unger, A.; Beckendorf, L.; Böhme, P.; Kley, R.; Von Frieling-Salewsky, M.; Lochmüller, H.; Schröder, R.; Fürst, D.O.; Vorgerd, M.; Linke, W.A. Translocation of molecular chaperones to the titin springs is common in skeletal myopathy patients and affects sarcomere function. *Acta Neuropathol. Commun.* **2017**, *5*, 72. [CrossRef]
80. Dahl-Halvarsson, M.; Olive, M.; Pokrzywa, M.; Ejeskär, K.; Palmer, R.H.; Uv, A.E.; Tajsharghi, H. *Drosophila* model of myosin myopathy rescued by overexpression of a TRIM-protein family member. *Proc. Natl. Acad. Sci. USA* **2018**, *115*, E6566–E6575. [CrossRef]
81. Baher, W.; Abo Zeid, A.A.; Mohamed Fahmy, B.; Mohamed Hashem, A.; Ashraf Sakr, R.; Ahmed Mohamed, F.; Ali Mohamed, N.; Mounir Halem, M. The effect of low dose statin combined with grapefruit on muscle structure and the possible protective role of mesenchymal stem cells. *QJM Int. J. Med.* **2018**, *111*, hcy200-221. [CrossRef]
82. Voigt, T.; Sebald, H.J.; Schoenauer, R.; Levano, S.; Girard, T.; Hoppeler, H.H.; Babiychuk, E.B.; Draeger, A. Annexin A1 is a biomarker of T-tubular repair in skeletal muscle of nonmyopathic patients undergoing statin therapy. *FASEB J.* **2013**, *27*, 2156–2164. [CrossRef]
83. Campos, L.M.; Rios, E.A.; Midlej, V.; Atella, G.C.; Herculano-Houzel, S.; Benchimol, M.; Mermelstein, C.; Costa, M.L. Structural Analysis of Alterations in Zebrafish Muscle Differentiation Induced by Simvastatin and Their Recovery with Cholesterol. *J. Histochem. Cytochem.* **2015**, *63*, 427–437. [CrossRef] [PubMed]
84. Pierno, S.; Didonna, M.P.; Cippone, V.; De Luca, A.; Pisoni, M.; Frigeri, A.; Nicchia, G.P.; Svelto, M.; Chiesa, G.; Sirtori, C.; et al. Effects of chronic treatment with statins and fenofibrate on rat skeletal muscle: A biochemical, histological and electrophysiological study. *Br. J. Pharmacol.* **2006**, *149*, 909–919. [CrossRef] [PubMed]
85. Cantó-Santos, J.; Grau-Junyent, J.M.; Garrabou, G. The Impact of Mitochondrial Deficiencies in Neuromuscular Diseases. *Antioxidants* **2020**, *9*, 964. [CrossRef]
86. Wredenberg, A.; Wibom, R.; Wilhelmsson, H.; Graff, C.; Wiener, H.H.; Burden, S.J.; Oldfors, A.; Westerblad, H.; Larsson, N.G. Increased Mitochondrial Mass in Mitochondrial Myopathy Mice. *Proc. Natl. Acad. Sci. USA* **2002**, *99*, 15066–15071. [CrossRef] [PubMed]
87. Aksu-Menges, E.; Eylem, C.C.; Nemutlu, E.; Gizer, M.; Korkusuz, P.; Topaloglu, H.; Talim, B.; Balci-Hayta, B. Reduced mitochondrial fission and impaired energy metabolism in human primary skeletal muscle cells of Megaconial Congenital Muscular Dystrophy. *Sci. Rep.* **2021**, *11*, 18161. [CrossRef] [PubMed]
88. Moore, T.M.; Lin, A.J.; Strumwasser, A.R.; Cory, K.; Whitney, K.; Ho, T.; Ho, T.; Lee, J.L.; Rucker, D.H.; Nguyen, C.Q.; et al. Mitochondrial Dysfunction Is an Early Consequence of Partial or Complete Dystrophin Loss in mdx Mice. *Front. Physiol.* **2020**, *11*, 690. [CrossRef]
89. Houston, B.A.; Judge, D.P.; Brown, E.; Halushka, M.; Barouch, L.A. Giant Ring Mitochondria in a Patient with Heart Failure and Cerebral White Matter Disease Resulting From an MT-TL1 Mitochondrial Gene Mutation. *J. Card. Fail.* **2017**, *23*, 652–655. [CrossRef]
90. Miettinen, T.P.; Björklund, M. Cellular Allometry of Mitochondrial Functionality Establishes the Optimal Cell Size. *Dev. Cell* **2016**, *39*, 370–382. [CrossRef]
91. Corsetti, G.; D'Antona, G.; Ruocco, C.; Stacchiotti, A.; Romano, C.; Tedesco, L.; Dioguardi, F.; Rezzani, R.; Nisoli, E. Dietary supplementation with essential amino acids boosts the beneficial effects of rosuvastatin on mouse kidney. *Amino Acids* **2014**, *46*, 2189–2203. [CrossRef]
92. Díaz-Zagoya, J.C.; Marín-Medina, A.; Zetina-Esquivel, A.M.; Blé-Castillo, J.L.; Castell-Rodríguez, A.E.; Juárez-Rojop, I.E.; Miranda-Zamora, R. Effects of high rosuvastatin doses on hepatocyte mitochondria of hypercholesterolemic mice. *Sci. Rep.* **2021**, *11*, 15809. [CrossRef]
93. Christie, C.F.; Fang, D.; Hunt, E.G.; Morris, M.E.; Rovini, A.; Heslop, K.A.; Beeson, G.C.; Beeson, C.C.; Maldonado, E.N. Statin-dependent modulation of mitochondrial metabolism in cancer cells is independent of cholesterol content. *FASEB J.* **2019**, *33*, 8186–8201. [CrossRef] [PubMed]
94. Das, S.; Kumar, P.; Verma, A.; Maiti, T.K.; Mathew, S.J. Myosin heavy chain mutations that cause Freeman-Sheldon syndrome lead to muscle structural and functional defects in Drosophila. *Dev. Biol.* **2019**, *449*, 90–98. [CrossRef]
95. Bour, B.A.; O'Brien, M.A.; Lockwood, W.L.; Goldstein, E.S.; Bodmer, R.; Taghert, P.H.; Abmayr, S.M.; Nguyen, H.T. Drosophila MEF2, a transcription factor that is essential for myogenesis. *Genes Dev.* **1995**, *9*, 730–741. [CrossRef]
96. Nongthomba, U.; Cummins, M.; Clark, S.; Vigoreaux, J.O.; Sparrow, J.C. Suppression of Muscle Hypercontraction by Mutations in the Myosin Heavy Chain Gene of *Drosophila melanogaster*. *Genetics* **2003**, *164*, 209–222. [CrossRef] [PubMed]
97. Bernstein, S.I.; Mogami, K.; Donady, J.J.; Emerson, C.P. Drosophila muscle myosin heavy chain encoded by a single gene in a cluster of muscle mutations. *Nature* **1983**, *302*, 393–397. [CrossRef] [PubMed]

98. Chaturvedi, D.; Reichert, H.; Gunage, R.D.; VijayRaghavan, K. Identification and functional characterization of muscle satellite cells in Drosophila. *eLife* **2017**, *6*, e30107. [CrossRef]
99. Postigo, A.A.; Ward, E.; Skeath, J.B.; Dean, D.C. zfh-1, the *Drosophila* Homologue of ZEB, Is a Transcriptional Repressor That Regulates Somatic Myogenesis. *Mol. Cell. Biol.* **1999**, *19*, 7255–7263. [CrossRef]
100. Caine, C.; Kasherov, P.; Silber, J.; Lalouette, A. Mef2 Interacts with the Notch Pathway during Adult Muscle Development in Drosophila melanogaster. *PLoS ONE* **2014**, *9*, e108149. [CrossRef]
101. Postigo, A.A.; Dean, D.C. ZEB, a vertebrate homolog of Drosophila Zfh-1, is a negative regulator of muscle differentiation. *EMBO J.* **1997**, *16*, 3935–3943. [CrossRef]
102. Grunwald, S.A.; Popp, O.; Haafke, S.; Jedraszczak, N.; Grieben, U.; Saar, K.; Patone, G.; Kress, W.; Steinhagen-Thiessen, E.; Dittmar, G.; et al. Statin-induced myopathic changes in primary human muscle cells and reversal by a prostaglandin F2 alpha analogue. *Sci. Rep.* **2020**, *10*, 2158. [CrossRef]
103. Marino, J.S.; Hinds, T.D.; Potter, R.A.; Ondrus, E.; Onion, J.L.; Dowling, A.; McLoughlin, T.J.; Sanchez, E.R.; Hill, J.W. Suppression of protein kinase C theta contributes to enhanced myogenesis In vitro via IRS1 and ERK1/2 phosphorylation. *BMC Cell Biol.* **2013**, *14*, 39. [CrossRef] [PubMed]
104. Zhang, P.; Verity, M.A.; Reue, K. Lipin-1 Regulates Autophagy Clearance and Intersects with Statin Drug Effects in Skeletal Muscle. *Cell Metab.* **2014**, *20*, 267–279. [CrossRef] [PubMed]
105. Michot, C.; Hubert, L.; Romero, N.B.; Gouda, A.; Mamoune, A.; Mathew, S.; Kirk, E.; Viollet, L.; Rahman, S.; Bekri, S.; et al. Study of LPIN1, LPIN2 and LPIN3 in rhabdomyolysis and exercise-induced myalgia. *J. Inherit. Metab. Dis.* **2012**, *35*, 1119–1128. [CrossRef]
106. Bergounioux, J.; Brassier, A.; Rambaud, C.; Bustarret, O.; Michot, C.; Hubert, L.; Arnoux, J.B.; Laquerriere, A.; Bekri, S.; Galene-Gromez, S.; et al. Fatal Rhabdomyolysis in 2 Children with LPIN1 Mutations. *J. Pediatr.* **2012**, *160*, 1052–1054. [CrossRef] [PubMed]
107. Larsen, S.; Vigelsø, A.; Dandanell, S.; Prats, C.; Dela, F.; Helge, J.W. Simvastatin-Induced Insulin Resistance May Be Linked to Decreased Lipid Uptake and Lipid Synthesis in Human Skeletal Muscle: The LIFESTAT Study. *J. Diabetes Res.* **2018**, *2018*, 9257874. [CrossRef]
108. Pennisi, E.M.; Garibaldi, M.; Antonini, G. Lipid Myopathies. *J. Clin. Med.* **2018**, *7*, 472. [CrossRef]
109. Meex, R.C.R.; Blaak, E.E.; Van Loon, L.J.C. Lipotoxicity plays a key role in the development of both insulin resistance and muscle atrophy in patients with type 2 diabetes. *Obes. Rev.* **2019**, *20*, 1205–1217. [CrossRef]
110. Morales, P.E.; Bucarey, J.L.; Espinosa, A. Muscle Lipid Metabolism: Role of Lipid Droplets and Perilipins. *J. Diabetes Res.* **2017**, *2017*, 1789395. [CrossRef]
111. Cheng, C.-L.; Gao, T.-Q.; Wang, Z.; Li, D.-D. Role of insulin/insulin-like growth factor 1 signaling pathway in longevity. *World J. Gastroenterol.* **2005**, *11*, 1891–1895. [CrossRef]
112. Clancy, D.J.; Gems, D.; Harshman, L.G.; Oldham, S.; Stocker, H.; Hafen, E.; Leevers, S.J.; Partridge, L. Extension of Life-Span by Loss of CHICO, a *Drosophila* Insulin Receptor Substrate Protein. *Science* **2001**, *292*, 104–106. [CrossRef]
113. Miron, M.; Lasko, P.; Sonenberg, N. Signaling from Akt to FRAP/TOR Targets both 4E-BP and S6K in *Drosophila melanogaster*. *Mol. Cell. Biol.* **2003**, *23*, 9117–9126. [CrossRef] [PubMed]
114. Kauwe, G.; Tsurudome, K.; Penney, J.; Mori, M.; Gray, L.; Calderon, M.R.; Elazouzzi, F.; Chicoine, N.; Sonenberg, N.; Haghighi, A.P. Acute Fasting Regulates Retrograde Synaptic Enhancement through a 4E-BP-Dependent Mechanism. *Neuron* **2016**, *92*, 1204–1212. [CrossRef] [PubMed]
115. Zid, B.M.; Rogers, A.N.; Katewa, S.D.; Vargas, M.A.; Kolipinski, M.C.; Lu, T.A.; Benzer, S.; Kapahi, P. 4E-BP Extends Lifespan upon Dietary Restriction by Enhancing Mitochondrial Activity in Drosophila. *Cell* **2009**, *139*, 149–160. [CrossRef] [PubMed]
116. Pichler, K.; Warner, K.; Magrane, M. SPIN: Submitting Sequences Determined at Protein Level to UniProt. *Curr. Protoc. Bioinform.* **2018**, *62*, e52. [CrossRef] [PubMed]
117. Thurmond, J.; Goodman, J.L.; Strelets, V.B.; Attrill, H.; Gramates, L.S.; Marygold, S.J.; Matthews, B.B.; Millburn, G.; Antonazzo, G.; Trovisco, V.; et al. FlyBase 2.0: The next generation. *Nucleic Acids Res.* **2019**, *47*, D759–D765. [CrossRef] [PubMed]
118. Palanker, L.; Tennessen, J.M.; Lam, G.; Thummel, C.S. Drosophila HNF4 Regulates Lipid Mobilization and β-Oxidation. *Cell Metab.* **2009**, *9*, 228–239. [CrossRef]
119. Girard, R.; Tremblay, S.; Noll, C.; St.-Jean, S.; Jones, C.; Gélinas, Y.; Maloum-Rami, F.; Perreault, N.; Laplante, M.; Carpentier, A.C.; et al. The transcription factor hepatocyte nuclear factor 4A acts in the intestine to promote white adipose tissue energy storage. *Nat. Commun.* **2022**, *13*, 224. [CrossRef]
120. Baker, S.K. Molecular clues into the pathogenesis of statin-mediated muscle toxicity. *Muscle Nerve* **2005**, *31*, 572–580. [CrossRef]
121. Weaver, L.N.; Ma, T.; Drummond-Barbosa, D. Analysis of Gal4 Expression Patterns in Adult *Drosophila* Females. *G3 Genes Genomes Genet.* **2020**, *10*, 4147–4158. [CrossRef]
122. Weaver, L.N.; Drummond-Barbosa, D. The nuclear receptor seven up functions in adipocytes and oenocytes to control distinct steps of Drosophila oogenesis. *Dev. Biol.* **2019**, *456*, 179–189. [CrossRef]
123. Schuster, C.M.; Davis, G.W.; Fetter, R.D.; Goodman, C.S. Genetic Dissection of Structural and Functional Components of Synaptic Plasticity. I. Fasciclin II Controls Synaptic Stabilization and Growth. *Neuron* **1996**, *17*, 641–654. [CrossRef]

124. Viswanathan, M.C.; Blice-Baum, A.C.; Schmidt, W.; Foster, D.B.; Cammarato, A. Pseudo-acetylation of K326 and K328 of actin disrupts Drosophila melanogaster indirect flight muscle structure and performance. *Front. Physiol.* **2015**, *6*, 116. [CrossRef] [PubMed]
125. Poirier, L.; Shane, A.; Zheng, J.; Seroude, L. Characterization of the *Drosophila* Gene-Switch system in aging studies: A cautionary tale. *Aging Cell* **2008**, *7*, 758–770. [CrossRef] [PubMed]
126. Barwell, T.; DeVeale, B.; Poirier, L.; Zheng, J.; Seroude, F.; Seroude, L. Regulating the UAS/GAL4 system in adult *Drosophila* with Tet-off GAL80 transgenes. *PeerJ* **2017**, *5*, e4167. [CrossRef] [PubMed]
127. Hatfield, I.; Harvey, I.; Yates, E.R.; Redd, J.R.; Reiter, L.T.; Bridges, D. The role of TORC1 in muscle development in Drosophila. *Sci. Rep.* **2015**, *5*, 9676. [CrossRef] [PubMed]
128. Rose, U.; Derst, C.; Wanischeck, M.; Marinc, C.; Walther, C. Properties and possible function of a hyperpolarisation-activated chloride current in *Drosophila*. *J. Exp. Biol.* **2007**, *210*, 2489–2500. [CrossRef] [PubMed]
129. Huerta-Cepas, J.; Capella-Gutiérrez, S.; Pryszcz, L.P.; Marcet-Houben, M.; Gabaldón, T. PhylomeDB v4: Zooming into the plurality of evolutionary histories of a genome. *Nucleic Acids Res.* **2014**, *42*, D897–D902. [CrossRef]
130. Flores, C.A.; Niemeyer, M.I.; Sepúlveda, F.V.; Cid, L.P. Two splice variants derived from a Drosophila melanogaster candidate ClC gene generate ClC-2-type Cl− channels. *Mol. Membr. Biol.* **2006**, *23*, 149–156. [CrossRef]
131. Parker, B.A.; Thompson, P.D. Effect of Statins on Skeletal Muscle: Exercise, Myopathy, and Muscle Outcomes. *Exerc. Sport Sci. Rev.* **2012**, *40*, 188–194. [CrossRef]
132. Allard, N.A.E.; Janssen, L.; Aussieker, T.; Stoffels, A.A.F.; Rodenburg, R.J.; Assendelft, W.J.J.; Thompson, P.D.; Snijders, T.; Hopman, M.T.E.; Timmers, S. Moderate Intensity Exercise Training Improves Skeletal Muscle Performance in Symptomatic and Asymptomatic Statin Users. *J. Am. Coll. Cardiol.* **2021**, *78*, 2023–2037. [CrossRef]
133. Altamura, C.; Mangiatordi, G.F.; Nicolotti, O.; Sahbani, D.; Farinato, A.; Leonetti, F.; Carratù, M.R.; Conte, D.; Desaphy, J.F.; Imbrici, P. Mapping ligand binding pockets in chloride ClC-1 channels through an integrated in silico and experimental approach using anthracene-9-carboxylic acid and niflumic acid. *Br. J. Pharmacol.* **2018**, *175*, 1770–1780. [CrossRef] [PubMed]
134. Camerino, G.M.; Bouchè, M.; De Bellis, M.; Cannone, M.; Liantonio, A.; Musaraj, K.; Romano, R.; Smeriglio, P.; Madaro, L.; Giustino, A.; et al. Protein kinase C theta (PKCθ) modulates the ClC-1 chloride channel activity and skeletal muscle phenotype: A biophysical and gene expression study in mouse models lacking the PKCθ. *Pflug. Arch. Eur. J. Physiol.* **2014**, *466*, 2215–2228. [CrossRef] [PubMed]
135. Zirin, J.; Hu, Y.; Liu, L.; Yang-Zhou, D.; Colbeth, R.; Yan, D.; Ewen-Campen, B.; Tao, R.; Vogt, E.; VanNest, S.; et al. Large-Scale Transgenic *Drosophila* Resource Collections for Loss- and Gain-of-Function Studies. *Genetics* **2020**, *214*, 755–767. [CrossRef] [PubMed]
136. Vaziri, P.; Ryan, D.; Johnston, C.A.; Cripps, R.M. A Novel Mechanism for Activation of Myosin Regulatory Light Chain by Protein Kinase C-Delta in Drosophila. *Genetics* **2020**, *216*, 177–190. [CrossRef]
137. Hruz, T.; Laule, O.; Szabo, G.; Wessendorp, F.; Bleuler, S.; Oertle, L.; Widmayer, P.; Gruissem, W.; Zimmermann, P. Resource Review Genevestigator V3: A Reference Expression Database for the Meta-Analysis of Transcriptomes. *Adv. Bioinform.* **2008**, *2008*, 420747. [CrossRef]
138. Maier, D.; Nagel, A.C.; Kelp, A.; Preiss, A. Protein Kinase D Is Dispensable for Development and Survival of Drosophila melanogaster. *G3 Genes Genomes Genet.* **2019**, *9*, 2477–2487. [CrossRef]
139. Seroude, L.; Brummel, T.; Kapahi, P.; Benzer, S. Spatio-temporal analysis of gene expression during aging in *Drosophila melanogaster*. *Aging Cell* **2002**, *1*, 47–56. [CrossRef]
140. Madaro, L.; Pelle, A.; Nicoletti, C.; Crupi, A.; Marrocco, V.; Bossi, G.; Soddu, S.; Bouché, M. PKC Theta Ablation Improves Healing in a Mouse Model of Muscular Dystrophy. *PLoS ONE* **2012**, *7*, e31515. [CrossRef]
141. Marrocco, V.; Fiore, P.; Benedetti, A.; Pisu, S.; Rizzuto, E.; Musarò, A.; Madaro, L.; Lozanoska-Ochser, B.; Bouché, M. Pharmacological Inhibition of PKCθ Counteracts Muscle Disease in a Mouse Model of Duchenne Muscular Dystrophy. *eBioMedicine* **2017**, *16*, 150–161. [CrossRef]
142. Madaro, L.; Marrocco, V.; Carnio, S.; Sandri, M.; Bouché, M. Intracellular signaling in ER stress-induced autophagy in skeletal muscle cells. *FASEB J.* **2013**, *27*, 1990–2000. [CrossRef]
143. Herbert, J.M.; Augereau, J.M.; Gleye, J.; Maffrand, J.P. Chelerythrine is a potent and specific inhibitor of protein kinase C. *Biochem. Biophys. Res. Commun.* **1990**, *172*, 993–999. [CrossRef]
144. Jones, P.H. Statins as the cornerstone of drug therapy for dyslipidemia: Monotherapy and combination therapy options. *Am. Heart J.* **2004**, *148*, S9–S13. [CrossRef] [PubMed]
145. Osaki, Y.; Nakagawa, Y.; Miyahara, S.; Iwasaki, H.; Ishii, A.; Matsuzaka, T.; Kobayashi, K.; Yatoh, S.; Takahashi, A.; Yahagi, N.; et al. Skeletal muscle-specific HMG-CoA reductase knockout mice exhibit rhabdomyolysis: A model for statin-induced myopathy. *Biochem. Biophys. Res. Commun.* **2015**, *466*, 536–540. [CrossRef] [PubMed]
146. Bansal, A.B.; Cassagnol, M. HMG-CoA Reductase Inhibitors. In *StatPearls*; StatPearls Publishing: Treasure Island, FL, USA, 2022. Available online: https://www.ncbi.nlm.nih.gov/books/NBK542212/ (accessed on 4 July 2022).
147. Hanai, J.; Cao, P.; Tanksale, P.; Imamura, S.; Koshimizu, E.; Zhao, J.; Kishi, S.; Yamashita, M.; Phillips, P.S.; Sukhatme, V.P.; et al. The muscle-specific ubiquitin ligase atrogin-1/MAFbx mediates statin-induced muscle toxicity. *J. Clin. Investig.* **2007**, *117*, 3940–3951. [CrossRef] [PubMed]

148. Chen, J.W.; Niu, X.; King, M.J.; Noedl, M.T.; Tabin, C.J.; Galloway, J.L. The mevalonate pathway is a critical regulator of tendon cell specification. *Development* **2020**, *147*, dev185389. [CrossRef]
149. Spindler, S.R.; Li, R.; Dhahbi, J.M.; Yamakawa, A.; Mote, P.; Bodmer, R.; Ocorr, K.; Williams, R.T.; Wang, Y.; Ablao, K.P. Statin Treatment Increases Lifespan and Improves Cardiac Health in Drosophila by Decreasing Specific Protein Prenylation. *PLoS ONE* **2012**, *7*, e39581. [CrossRef]
150. Alcázar-Fabra, M.; Navas, P.; Brea-Calvo, G. Coenzyme Q biosynthesis and its role in the respiratory chain structure. *Biochim. Biophys. Acta Bioenerg.* **2016**, *1857*, 1073–1078. [CrossRef]
151. Shults, C.W.; Haas, R.H.; Passov, D.; Beal, M.F. Coenzyme Q10 levels correlate with the activities of complexes I and II/III in mitochondria from parkinsonian and nonparkinsonian subjects. *Ann. Neurol.* **1997**, *42*, 261–264. [CrossRef]
152. Cornelius, N.; Byron, C.; Hargreaves, I.; Guerra, P.F.; Furdek, A.K.; Land, J.; Radford, W.W.; Frerman, F.; Corydon, T.J.; Gregersen, N.; et al. Secondary coenzyme Q10 deficiency and oxidative stress in cultured fibroblasts from patients with riboflavin responsive multiple Acyl-CoA dehydrogenation deficiency. *Hum. Mol. Genet.* **2013**, *22*, 3819–3827. [CrossRef]
153. Quinzii, C.M.; López, L.C.; Gilkerson, R.W.; Dorado, B.; Coku, J.; Naini, A.B.; Lagier-Tourenne, C.; Schuelke, M.; Salviati, L.; Carrozzo, R.; et al. Reactive oxygen species, oxidative stress, and cell death correlate with level of CoQ_{10} deficiency. *FASEB J.* **2010**, *24*, 3733–3743. [CrossRef]
154. Lalani, S.R.; Vladutiu, G.D.; Plunkett, K.; Lotze, T.E.; Adesina, A.M.; Scaglia, F. Isolated Mitochondrial Myopathy Associated with Muscle Coenzyme Q10 Deficiency. *Arch. Neurol.* **2005**, *62*, 317–320. [CrossRef] [PubMed]
155. Woerner, A.C.; Vockley, J. Mitochondrial Disease and Coenzyme Q10 Deficiency: Commentary. *J. Pediatr.* **2021**, *228*, 14–15.e1. [CrossRef] [PubMed]
156. Neergheen, V.; Chalasani, A.; Wainwright, L.; Yubero, D.; Montero, R.; Artuch, R.; Hargreaves, I. Coenzyme Q_{10} in the Treatment of Mitochondrial Disease. *J. Inborn Errors Metab. Screen.* **2017**, *5*, 232640981770777. [CrossRef]
157. Mollazadeh, H.; Tavana, E.; Fanni, G.; Bo, S.; Banach, M.; Pirro, M.; von Haehling, S.; Jamialahmadi, T.; Sahebkar, A. Effects of statins on mitochondrial pathways. *J. Cachexia Sarcopenia Muscle* **2021**, *12*, 237–251. [CrossRef] [PubMed]
158. Hou, T.; Li, Y.; Chen, W.; Heffner, R.R.; Vladutiu, G.D. Histopathologic and Biochemical Evidence for Mitochondrial Disease Among 279 Patients with Severe Statin Myopathy. *J. Neuromuscul. Dis.* **2017**, *4*, 77–87. [CrossRef]
159. Neřoldová, M.; Stránecký, V.; Hodaňová, K.; Hartmannová, H.; Piherová, L.; Přistoupilová, A.; Mrázová, L.; Vrablík, M.; Adámková, V.; Hubáček, J.A.; et al. Rare Variants in Known and Novel Candidate Genes Predisposing to Statin-Associated Myopathy. *Pharmacogenomics* **2016**, *17*, 1405–1414. [CrossRef] [PubMed]
160. Imbrici, P.; Altamura, C.; Pessia, M.; Mantegazza, R.; Desaphy, J.F.; Camerino, D.C. ClC-1 chloride channels: State-of-the-art research and future challenges. *Front. Cell. Neurosci.* **2015**, *9*, 156. [CrossRef]
161. Adrian, R.H.; Bryant, S.H. On the repetitive discharge in myotonic muscle fibres. *J. Physiol.* **1974**, *240*, 505–515. [CrossRef]
162. Pierno, S.; Liantonio, A.; Camerino, G.M.; De Bellis, M.; Cannone, M.; Dinardo, M.M.; Scaramuzzi, A.; Madaro, L.; Bouchè, M.; Desaphy, J.-F.; et al. Characterization of the Role of PKC-Theta in the Modulation of ClC-1 Chloride Channel Function and Calcium Homeostasis in Fast- and Slow-Twitch Skeletal Muscle by using PKC-Theta Null Mice. *Biophys. J.* **2012**, *102*, 332a–333a. [CrossRef]
163. Steinmeyer, K.; Ortland, C.; Jentsch, T.J. Primary structure and functional expression of a developmentally regulated skeletal muscle chloride channel. *Nature* **1991**, *354*, 301–304. [CrossRef]
164. Imbrici, P.; Altamura, C.; Camerino, G.M.; Mangiatordi, G.F.; Conte, E.; Maggi, L.; Brugnoni, R.; Musaraj, K.; Caloiero, R.; Alberga, D.; et al. Multidisciplinary study of a new CIC-1 mutation causing myotonia congenita: A paradigm to understand and treat ion channelopathies. *FASEB J.* **2016**, *30*, 3285–3295. [CrossRef]
165. Desaphy, J.F.; Gramegna, G.; Altamura, C.; Dinardo, M.M.; Imbrici, P.; George, A.L.; Modoni, A.; LoMonaco, M.; Camerino, D.C. Functional characterization of ClC-1 mutations from patients affected by recessive myotonia congenita presenting with different clinical phenotypes. *Exp. Neurol.* **2013**, *248*, 530–540. [CrossRef] [PubMed]
166. Han, R.; Bakker, A.J. The effect of chelerythrine on depolarization-induced force responses in skinned fast skeletal muscle fibres of the rat. *Br. J. Pharmacol.* **2003**, *138*, 417–426. [CrossRef] [PubMed]
167. Dekker, L.V.; Parker, P.J. Protein kinase C—A question of specificity. *Trends Biochem. Sci.* **1994**, *19*, 73–77. [CrossRef]
168. Newton, A.C.; Johnson, J.E. Protein kinase C: A paradigm for regulation of protein function by two membrane-targeting modules. *Biochim. Biophys. Acta Rev. Biomembr.* **1998**, *1376*, 155–172. [CrossRef]
169. Phillips, P.S.; Haas, R.H.; Bannykh, S.; Hathaway, S.; Gray, N.L.; Kimura, B.J.; Vladutiu, G.D.; England, J.D.F.; Scripps Mercy Clinical Research Center. Statin-Associated Myopathy with Normal Creatine Kinase Levels. *Ann. Intern. Med.* **2002**, *137*, 581–585. [CrossRef]
170. Ragheb, R.; Shanab, G.M.L.; Medhat, A.M.; Seoudi, D.M.; Adeli, K.; Fantus, I.G. Free fatty acid-induced muscle insulin resistance and glucose uptake dysfunction: Evidence for PKC activation and oxidative stress-activated signaling pathways. *Biochem. Biophys. Res. Commun.* **2009**, *389*, 211–216. [CrossRef]
171. Abplanalp, W.; Clegg, D.J. Translocation of PKC theta by fatty acids causes hypothalamic insulin resistance. *Appetite* **2007**, *49*, 274. [CrossRef]
172. Boden, G. Obesity and Free Fatty Acids. *Endocrinol. Metab. Clin. N. Am.* **2008**, *37*, 635–646. [CrossRef]
173. Itani, S.I.; Ruderman, N.B.; Schmieder, F.; Boden, G. Lipid-Induced Insulin Resistance in Human Muscle Is Associated with Changes in Diacylglycerol, Protein Kinase C, and IκB-α. *Diabetes* **2002**, *51*, 2005–2011. [CrossRef]

174. Griffin, M.E.; Marcucci, M.J.; Cline, G.W.; Bell, K.; Barucci, N.; Lee, D.; Goodyear, L.J.; Kraegen, E.W.; White, M.F.; Shulman, G.I. Free fatty acid-induced insulin resistance is associated with activation of protein kinase C theta and alterations in the insulin signaling cascade. *Diabetes* **2000**, *48*, 1270–1274. [CrossRef] [PubMed]
175. Kain, V.; Kapadia, B.; Misra, P.; Saxena, U. Simvastatin may induce insulin resistance through a novel fatty acid mediated cholesterol independent mechanism. *Sci. Rep.* **2015**, *5*, 13823. [CrossRef] [PubMed]
176. Fan, L.; Fan, Y.; Liu, L.; Tao, W.; Shan, X.; Dong, Y.; Li, L.; Zhang, S.; Wang, H. Chelerythrine Attenuates the Inflammation of Lipopolysaccharide-Induced Acute Lung Inflammation through NF-KB Signaling Pathway Mediated by Nrf2. *Front. Pharmacol.* **2018**, *9*, 1047. [CrossRef] [PubMed]
177. Vrba, J.; Dvořák, Z.; Ulrichová, J.; Modrianský, M. Conventional protein kinase C isoenzymes undergo dephosphorylation in neutrophil-like HL-60 cells treated by chelerythrine or sanguinarine. *Cell Biol. Toxicol.* **2008**, *24*, 39–53. [CrossRef]
178. Zheng, W.; Qiu, L.; Wang, R.; Feng, X.; Han, Y.; Zhu, Y.; Chen, D.; Liu, Y.; Jin, L.; Li, Y. Selective targeting of PPARγ by the natural product chelerythrine with a unique binding mode and improved antidiabetic potency. *Sci. Rep.* **2015**, *5*, 12222. [CrossRef]
179. Niwa, R.; Niwa, Y.S. The Fruit Fly *Drosophila melanogaster* as a Model System to Study Cholesterol Metabolism and Homeostasis. *Cholesterol* **2011**, *2011*, 176802. [CrossRef]
180. Bouitbir, J.; Singh, F.; Charles, A.-L.; Schlagowski, A.-I.; Bonifacio, A.; Echaniz-Laguna, A.; Geny, B.; Krähenbühl, S.; Zoll, J. Statins Trigger Mitochondrial Reactive Oxygen Species-Induced Apoptosis in Glycolytic Skeletal Muscle. *Antioxid. Redox Signal.* **2016**, *24*, 84–98. [CrossRef]
181. Bouitbir, J.; Charles, A.L.; Echaniz-Laguna, A.; Kindo, M.; Daussin, F.; Auwerx, J.; Piquard, F.; Geny, B.; Zoll, J. Opposite effects of statins on mitochondria of cardiac and skeletal muscles: A 'mitohormesis' mechanism involving reactive oxygen species and PGC-1. *Eur. Heart J.* **2012**, *33*, 1397–1407. [CrossRef]

scientific reports

Check for updates

OPEN

Fluvastatin-induced myofibrillar damage is associated with elevated ROS, and impaired fatty acid oxidation, and is preceded by mitochondrial morphological changes

Mohamed H. Al-Sabri[1,2]✉, Nourhane Ammar[3,6], Stanislava Korzh[4,6], Ahmed M. Alsehli[1,5], Kimia Hosseini[2], Robert Fredriksson[2], Jessica Mwinyi[1], Michael J. Williams[1], Hadi Boukhatmi[3] & Helgi B. Schiöth[1]✉

Previously, we showed that fluvastatin treatment induces myofibrillar damage and mitochondrial phenotypes in the skeletal muscles of *Drosophila*. However, the sequential occurrence of mitochondrial phenotypes and myofibril damage remains elusive. To address this, we treated flies with fluvastatin for two and five days and examined their thorax flight muscles using confocal microscopy. In the two-day fluvastatin group, compared to the control, thorax flight muscles exhibited mitochondrial morphological changes, including fragmentation, rounding up and reduced content, while myofibrils remained organized in parallel. In the five-day fluvastatin treatment, not only did mitochondrial morphological changes become more pronounced, but myofibrils became severely disorganized with significantly increased thickness and spacing, along with myofilament abnormalities, suggesting myofibril damage. These findings suggest that fluvastatin-induced mitochondrial changes precede myofibril damage. Moreover, in the five-day fluvastatin group, the mitochondria demonstrated elevated H_2O_2 and impaired fatty acid oxidation compared to the control group, indicating potential mitochondrial dysfunction. Surprisingly, knocking down *Hmgcr* (*Drosophila* homolog of *HMGCR*) showed normal mitochondrial respiration in all parameters compared to controls or five-day fluvastatin treatment, which suggests that fluvastatin-induced mitochondrial dysfunction might be independent of Hmgcr inhibition. These results provide insights into the sequential occurrence of mitochondria and myofibril damage in statin-induced myopathy for future studies.

Cardiovascular diseases (CVDs) are the leading causes of mortality globally, accounting for 20.5 million deaths in 2021, with hypercholesteremia as the major risk factor[1,2]. Statins reduce low-density lipoprotein (LDL) cholesterol levels by inhibiting HMG-CoA reductase (HMGCR), the rate-limiting enzyme in the cholesterol biosynthesis pathway in many tissues, including the liver, muscles and brain; therefore, they are the gold standard for the management of CVDs[3–6]. Inhibition of intracellular cholesterogenesis enhances the expression of LDL receptors in hepatocytes, leading to increased clearance of cholesterol from the blood[3]. Despite their beneficial therapeutic effects on the management of CVDs, statins are associated with certain side effects, including muscle damage[7,8], an increased risk for diabetes[9,10], cognitive impairment[11,12], and sleep disturbance[13]. Statin-associated muscle

[1]Department of Surgical Sciences, Division of Functional Pharmacology and Neuroscience, Biomedical Center (BMC), Uppsala University, Husargatan 3, 751 24 Uppsala, Sweden. [2]Department of Pharmaceutical Biosciences, Uppsala University, 751 24 Uppsala, Sweden. [3]Institut de Génétique Et Développement de Rennes (IGDR), Université de Rennes, CNRS, UMR6290, 35065 Rennes, France. [4]Latvian Institute of Organic Synthesis, Aizkraukles 21, Riga 1006, Latvia. [5]Faculty of Medicine, King Abdulaziz University and Hospital, Al Ehtifalat St., 21589 Jeddah, Saudi Arabia. [6]These authors contributed equally: Nourhane Ammar and Stanislava Korzh. ✉email: mohamed.alsabri@uu.se; helgi.schioth@neuro.uu.se

symptoms, otherwise known as statin-induced myopathy (SIM), are the most common side effects of statins, with an incidence of 27.8%, ranging from myalgia to rare muscle necrosis called rhabdomyolysis[14]. SIM compromises patients' adherence to statin therapy, leading to an elevated risk of developing cardiovascular events[15–17].

Recent reports have underscored the crucial role of mitochondrial impairment in SIM[7,8,18]. Mitochondrial dysfunction leads to energy depletion and reduced oxidative phosphorylation capacity[7], diminished mitochondrial membrane potential, activation of apoptosis and ultimately muscle weakness, fatigue and cramps[19–21]. Nevertheless, the role of mitochondrial dysfunction in SIM is still under debate[8,18,22,23]. The exact mechanisms by which statins induce mitochondrial impairment are not fully understood. Studies have indicated potential mechanisms by which statins impact mitochondrial morphology and function[18,24]. For instance, reports have suggested that, due to inhibition of HMGCR, statin treatment leads to a reduced muscular level of coenzyme Q10 (CoQ10), which is a crucial node in the mitochondrial respiratory chain, causing depletion of energy, mitochondrial dysfunction and muscle damage[21,25]. Other studies have shown that statins cause mitochondrial dysfunction through the inhibition of mitochondrial Complexes I, II, and III, which leads to the overproduction of reactive oxygen species (ROS) and cytotoxicity[7]. The inhibition of carnitine-palmitoyltransferase-2 (CPT2) and impairment of fatty acid oxidation (FAO) have also been reported as an underlying cause for statin-induced mitochondrial dysfunction and SIM[7,26]. However, the temporal relationship between mitochondrial dysfunction and muscular damage has not been fully elucidated.

We previously revealed that chronic fluvastatin treatment for five days induced a mitochondrial morphological phenotype (fragmented and round shape) and myofibrillar damage in the skeletal muscles of *Drosophila*[8]. We also demonstrated that targeted knockdown of *Hmgcr* (*Drosophila* homolog of *HMGCR*) in skeletal muscle induced a similar pattern of mitochondrial morphological phenotype (round shape) but was not sufficient to elicit myofibrillar damage[8]. However, the chronic effect of fluvastatin and the role of Hmgcr on mitochondrial respiration function in skeletal muscle are still elusive.

In this study, we used *Drosophila* as a model system to examine whether the fluvastatin-induced mitochondrial phenotype in the skeletal muscles precedes myofibrillar damage and examined the effect of chronic fluvastatin treatment on mitochondrial respiration. To mimic the effect of fluvastatin on its known target, HMGCR, we also investigated whether selective knockdown of *Hmgcr* in skeletal muscles recapitulates fluvastatin's effect on mitochondrial respiration, aiming to expand our understanding of the underlying mechanisms for SIM.

Results

Fluvastatin-induced myofibril phenotypes are preceded by mitochondrial morphological changes.

In our previous study, we showed that chronic fluvastatin treatment for five days induced myofibrillar damage and mitochondrial phenotypes (fragmented and round shape) in the skeletal muscles of fly legs[8]. Nevertheless, the sequence of events of mitochondrial alteration and muscle damage remains unknown. To investigate this, we treated adult *Mef2-Gal4 > UAS-mitoGFP* flies with 1.0 mM fluvastatin for two and five days and used confocal microscopy to examine the morphology of thorax flight muscles. In the control group, the myofibrils were organized in parallel, with normal diameter and spacing and mitochondria (Fig. 1A–C) adopted a filamentous shape, forming an elongated structure along the myofibrils. Interestingly, after two days of fluvastatin treatment, we observed noticeable mitochondrial morphological changes. These changes included a fragmented network of mitochondria with varying sizes and round-like shapes (arrowheads Fig. 1A',D). Additionally, there was a significant decrease in overall mitochondrial content, as indicated by a reduced ratio of mitochondrial area to actin area (Fig. 1E). However, the myofibrils maintained an organized, parallel pattern, with unaffected diameter and spacing when compared to control flies (Fig. 1B',C',F,G).

In chronic five-day fluvastatin treatment, compared to the control, the mitochondria displayed more pronounced fragmentation, with a higher number of round-like shapes, particularly in areas where the myofibrils were more separated (Fig. 1A",C",D,E). Additionally, chronic fluvastatin-treated flies showed a more significant reduction in mitochondrial content than both the control and the two-day fluvastatin groups (Fig. 1 E). Intriguingly, the myofibrils exhibited disorganization and separation, characterized by a thicker diameter, significant spacing between individual myofibrils, and abnormal myofilaments, when compared to both the two-day fluvastatin treatment and untreated flies (Fig. 1 arrows, B", F & G). These observations suggest damage to the myofibrils. Collectively, these findings suggest that fluvastatin treatment induced mitochondrial morphological changes in a time-dependent manner and that these changes preceded myofibril damage in the thorax flight muscles of *Drosophila*.

Chronic Fluvastatin treatment for five days impairs mitochondrial respiration

Abnormal mitochondrial morphology, as well as content, are associated with impairment of mitochondrial respiration[27,28]. Previous studies have reported that acute fluvastatin treatment for 24 h impairs mitochondrial respiration in myoblast[7]. Since the mitochondria morphological changes including reduced content were dramatically obvious along with severe myofibril damage after chronic fluvastatin treatment (Fig. 1), and studies have linked myofibril damage to excessive production of reactive oxygen species, ROS, and reduced mitochondrial content[29–31], we sought here to determine whether chronic fluvastatin treatment for five days is also associated with impairment of mitochondrial respiration. To answer this question, we first fed CSORC flies with 1 mM fluvastatin for five days and then dissected thorax skeletal muscles and examined different parameters of mitochondrial respiration using High-Resolution FluoRespirometry[32,33]. Next, we measured mitochondrial respiratory control, specifically the efficiency of the different complexes in the mitochondrial electron transfer system (ETS), using the Substrate-Uncoupler-Inhibitor Titration (SUIT) protocol mentioned in the Methods section of this study. Fluvastatin treatment significantly increased the respiration rate at all measured pathway-linked

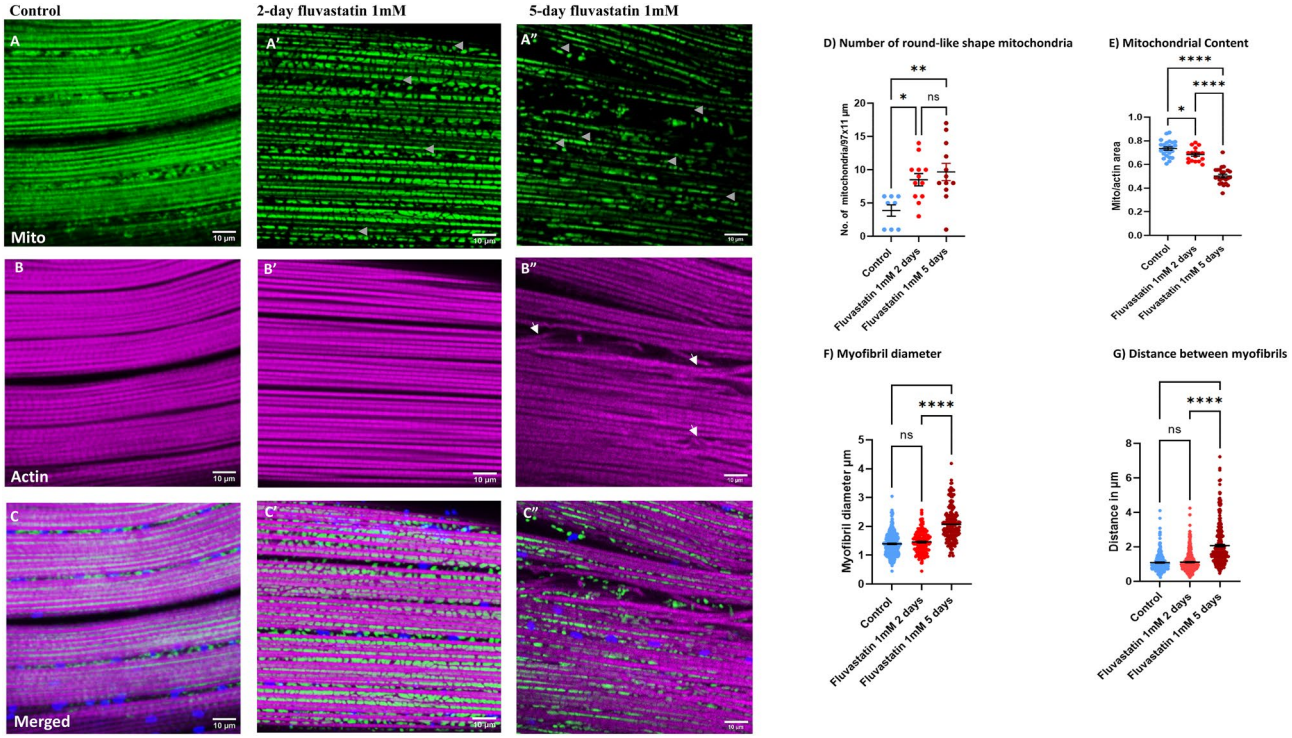

Figure 1. Fluvastatin induces altered mitochondrial morphology that precedes the myofibril abnormalities. *Mef2-GAL4 > UAS-mitoGFP* thorax flight muscles were stained with phalloidin to visualize actin (magenta), Mef2 labels muscle nuclei (red) and expresses mito-GFP to visualize the mitochondrial matrix (green) under confocal microscopy. In the fluvastatin group, flies were treated with 1 mM fluvastatin in fly food for two or five days while in the control group, flies were fed normal fly food for five days. In the control group, dissected thorax skeletal muscles showed a regular myofibril arrangement along with aggregated and elongated-shaped mitochondria distributed parallel to the myofibril direction (**A**,**B**,**C**). After two days of 1 mM fluvastatin, compared to the control group, skeletal muscles exhibited fragmented mitochondria of different sizes, most of which were round in shape (arrowheads **A'**,**D**) along with organized and parallel myofibrils, which showed normal diameter and spacing (**B'**,**C'**,**F**,**G**). After five days, compared to the control, the skeletal muscles displayed severely aberrant and fragmented mitochondria of small sizes with capacious round shapes (arrowheads **A"**,**D**), and the mitochondria were absent in areas where myofibrils were more disorganized and separated (**A"**,**C"**). The myofibrils also showed abnormal myofilament (arrows **B"**) with longer spacing and thicker diameter compared to the control group (**B"**,**C"**,**B**,**C**,**E**,**F**). The relative mitochondrial content (ratio of mitochondrial area to actin area) was also significantly reduced in the fluvastatin groups in a time-dependent manner. The scale bar is indicated at the bottom of each image. The magnification was 40 megapixels. Each bar represents the mean value (± SEM). *, $P \leq 0.05$; **, $P \leq 0.01$**** $P \leq 0.0001$. The type of the statistical test and number of images used are mentioned in the Method section.

OXPHOS states and at the NSProDHGp-linked ET state (Fig. 2A), while calculated flux control factors remained unchanged, indicating that treatment with fluvastatin did not affect the activity/capacity of electron transfer system complexes (Fig. 2B). In the fluvastatin-treated group, an increase in the H_2O_2 production rate was observed (Fig. 2C), while the H_2O_2/O ratio remained comparable to that of the control group (Fig. 2D), suggesting that the observed increase in the respiration rate in the statin-treated group is more likely a result of an increased H_2O_2 production rate. Overall, these results indicate that fluvastatin treatment increases ROS production without affecting individual complexes of the electron transfer system.

We previously showed that chronic fluvastatin treatment is associated with lipotoxicity through disruption of the key genes involved in lipid metabolism[8]. Thus, we sought to determine whether chronic fluvastatin treatment for five days impairs the mitochondrial fatty acid of the thorax muscles. Interestingly, in the fluvastatin-treated group, FAO-dependent respiration at LEAK and OXPHOS states (Fig. 3A), as well as FAO-dependent OXPHOS coupling efficiency (Fig. 3B), were significantly decreased when compared with the control. A lower respiration rate was also observed at the FN-pathway-linked OXPHOS state, while afterwards, the respiration rate of the fluvastatin-treated group was comparable with control values (Fig. 3A). Flux control factors were higher for pyruvate and proline input in the fluvastatin group compared with the control group (Fig. 3B), indicating that fluvastatin-induced stimulation of pyruvate and proline-related metabolism compensates for the reduction in FAO (CPT2-dependent) for ATP production. In addition, an increase in the H_2O_2/O ratio was observed after treatment with fluvastatin when compared with the control (Fig. 3C), suggesting that part of the consumed oxygen is wasted for ROS production. Overall, these results suggest that treatment with fluvastatin induces a decrease in CPT2-dependent FAO, with a concomitant increase in pyruvate and proline pathways, while electron

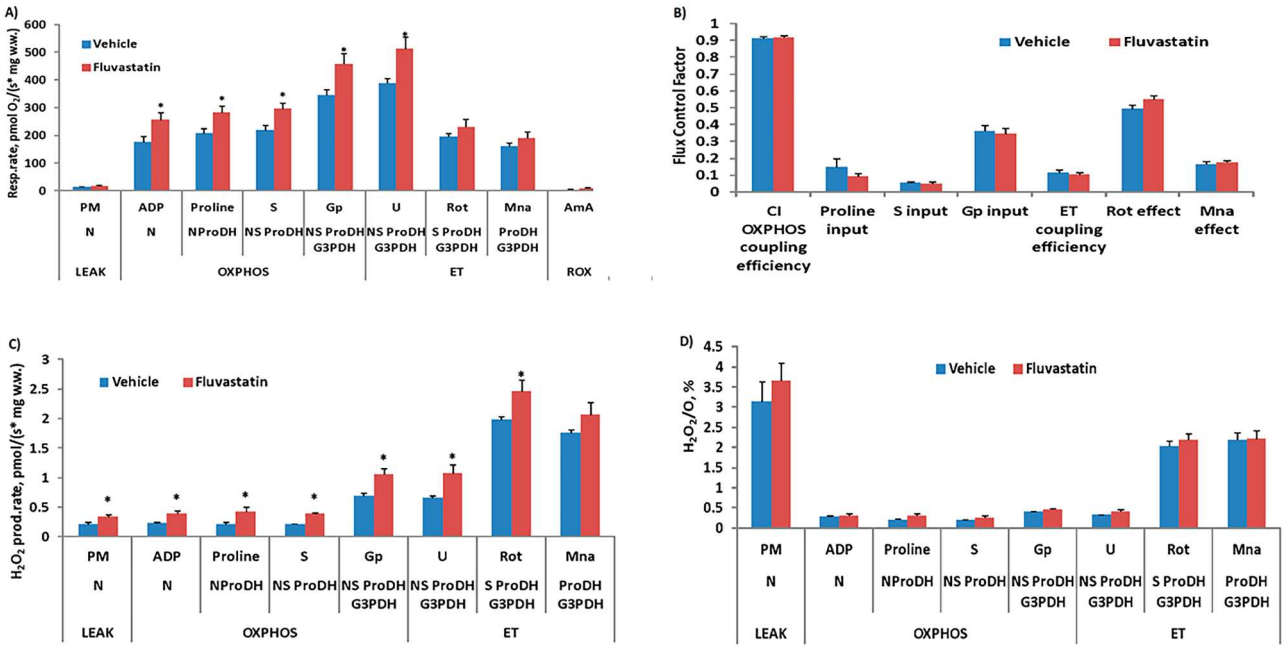

Figure 2. Fluvastatin treatment is associated with increased ROS production. In the fluvastatin group, flies were treated with 1 mM fluvastatin, and then the muscles of the thorax were dissected for the respirometry assay, while in the control group, flies were treated with normal food, both for five days. Each bar represents the mean ± SEM, and the statistical significance was calculated using Student's t-test whereby *, $P \leq 0.05$. N = 5. PM, pyruvate and malate; ADP, adenosine diphosphate; P, pyruvate; S, succinate; Gp, gycerol-3-phosphate; U, uncoupler; Rot, rotenone; AmA, antimycin A; F, fatty acid oxidation-dependent pathway; N, NADH pathway; LEAK, substrate-dependent state; OXPHOS, oxidative phosphorylation-dependent state; ROX, residual oxygen consumption; H2O2, hydrogen peroxide; G3PDH, glyceraldehyde-3-phosphate dehydrogenase; FNS, FAO, NADH and succinate.

transfer system efficiency was altered. In agreement with these results, fluvastatin has been shown to reduce the activity of Complexes I & II without affecting the activity of Complex III[7]. Other reports have also revealed that the inhibition of CPT2 and impairment of FAO are also associated with SIM[7,26].

Hmgcr knockdown in skeletal muscles does not alter mitochondrial respiration

The statin's main target is HMGCR. Thus, we asked whether fluvastatin-induced mitochondrial dysfunction resulted from the inhibition of HMGCR. To mimic the statin inhibitory effect on HMGCR enzyme activity, we performed a specific knockdown of *Drosophila Hmgcr* in the skeletal muscles using the *Mhc-Gal4* driver. Then, we dissected thorax skeletal muscles and examined different parameters of respiration using High-Resolution FluoRespirometry. Surprisingly, compared with both controls (*Mhc-Gal4 > w^{1118}* & *w^{1118} > UAS-GAL4 RNAi*), *Hmgcr* knockdown flies (*Mhc-Gal4 > UAS Hmgcr RNAi*) showed a normal respiration rate at all measured pathway-linked OXPHOS states and at the NSProDHGp-linked ET state (Supplementary Fig. 1A), as well as flux control factors remained unchanged (Supplementary Fig. 1B). This indicates that knockdown of *Hmgcr* in skeletal muscles may not affect the mitochondrial activity/capacity of any electron transfer system complexes (Supplementary Fig. 1B). In addition, no changes in the H_2O_2 production rate (Supplementary Fig. 1C) or the H_2O_2/O ratio (Supplementary Fig. 1D) were observed compared with controls. Overall, these results suggest that the inhibition of Hmgcr in skeletal muscles does not affect the respiration rate, ROS production or individual complexes of the electron transfer system of *Drosophila* mitochondria.

In terms of fatty acid oxidation, we noticed that in *Hmgcr* knockdown flies, FAO-dependent respiration at LEAK and OXPHOS states (Supplementary Fig. 2A), as well as FAO-dependent OXPHOS coupling efficiency (Supplementary Fig. 2B), were not changed compared with both controls. A normal respiration rate was also observed at FN-pathway linked OXPHOS state, and the respiration rate in the fluvastatin-treated group was comparable to the control values (Supplementary Fig. 2A). Flux control factors were also normal for pyruvate and proline input in the *Hmgcr* knockdown flies compared with controls (Supplementary Fig. 2B). In addition, no change in the H_2O_2/O ratio was observed in the *Hmgcr* knockdown flies (Supplementary Fig. 2C). Altogether, these results suggest that *Hmgcr* knockdown in skeletal muscles did not alter CPT2-dependent FAO or result in changes in electron transfer system efficiency.

Discussion

In *Drosophila* skeletal muscles, compared with the control, acute fluvastatin treatment for two days, mitochondria were fragmented with a higher number of round-like shapes and their content was significantly reduced, all without noticeable alterations in myofibrils. With chronic fluvastatin treatment for five days, the mitochondria

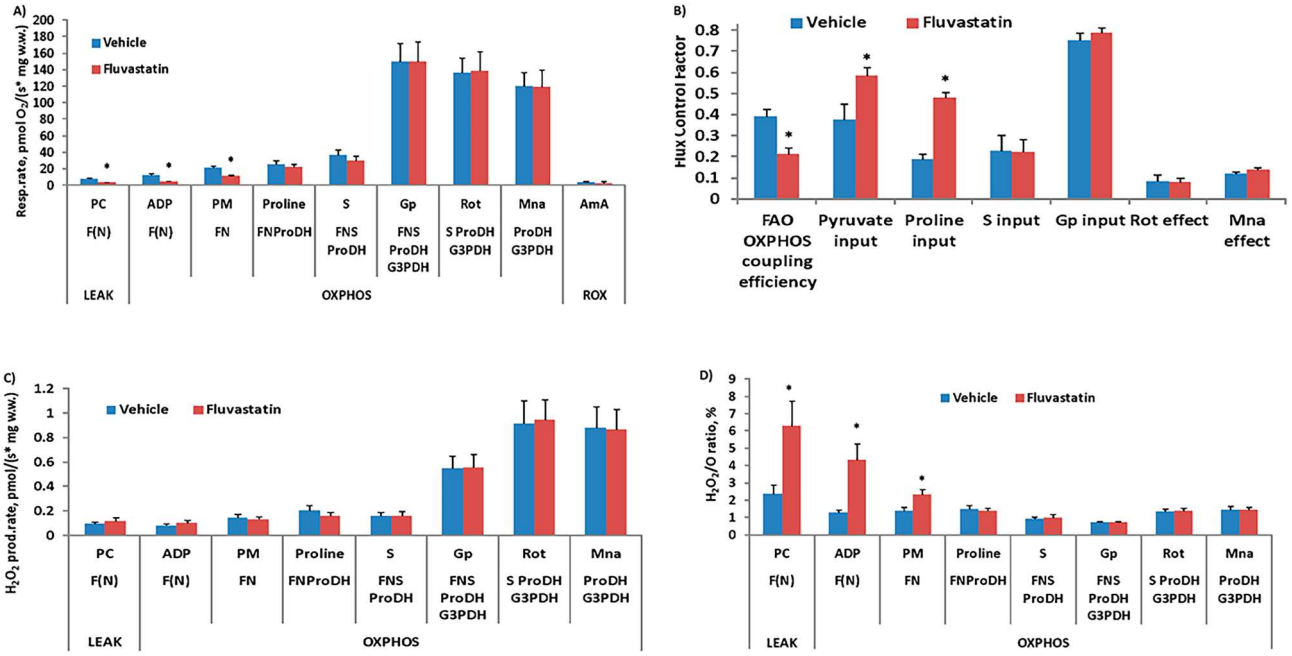

Figure 3. Fluvastatin treatment is associated with decreased CPT2-dependent fatty acid oxidation. In the fluvastatin group, flies were treated with 1 mM fluvastatin-supplemented food, and then the muscles of the thorax were dissected for the respirometry assay, while in the control group, flies were treated with normal food, both for five days. Each bar represents the mean ± SEM, and the statistical significance was calculated using Student's t-test whereby *, $P \leq 0.05$. N = 5. PC, palmitoylcarnitine; ADP, adenosine diphosphate; PM, pyruvate and malate; P, pyruvate; S, succinate; Gp, Glycerol-3-phosphate; U, uncoupler; Rot, rotenone; AmA, antimycin A; F, fatty acid oxidation-dependent pathway; N, NADH pathway; LEAK, substrate-dependent state; OXPHOS, oxidative phosphorylation-dependent state; ROX, residual oxygen consumption; H2O2, hydrogen peroxide; G3PDH, glyceraldehyde-3-phosphate dehydrogenase; FNS, FAO, NADH and Succinate.

exhibited extensive fragmentation, notable rounding up and a more significant reduction in the mitochondria content. However, these mitochondrial phenotypic changes were accompanied by a noticeable disorganization of myofibrils, characterized by a thicker diameter and greater spacing between them along with myofilament abnormalities. These findings may suggest that fluvastatin-induced myofibril damage is proceeded by mitochondrial morphological phenotypes.

A recent study has indicated coordination between mitochondrial shape and myofibril tension in *Drosophila* flight thorax muscles[34]. The same study has shown that in normal muscles, the area where the myofibrils are intact, the mitochondria adopt an elongated shape oriented in the direction of the myofibrils[34]. On the other hand, in the area where the myofibrils are mechanically severed, mitochondria exhibit rounded shapes, especially when the connection between the mitochondria and myofibril is lost[34]. In this context, we demonstrated here that mitochondria displayed fragmentation and rounding up which became more pronounced over time with fluvastatin treatment, especially in the area where the connection between myofibrils and mitochondria was lost, suggesting a temporal relation between mitochondrial morphological alteration and myofibril damage. Given this, two possibilities are proposed: There is a bidirectional feedback mechanical cue, or a default of one cell component (mitochondria) may cause a morphological defect to the other (myofibril). This can be a subject of future investigations.

Mitochondrial content refers to the amount of mitochondrial proteins and DNA and reflects the number of mitochondria in the muscle fibres[34,35]. This is crucial to allow the muscles to generate more ATP to meet energy demand, as mitochondrial respiration is contingent upon mitochondrial content[27,28]. Acute exposure to fluvastatin for 24 h has been reported to impair mitochondrial respiration[7] and induce apoptosis[36] in different cell types. Muscle fibre damage can lead to excessive ROS production, which, in turn, triggers further degradation of mitochondrial content, including mitochondrial proteins, enzymes and genetic materials[29–31]. Consistent with this, we reported here that chronic fluvastatin treatment for five days caused excessive ROS production (see Fig. 2), which may consequently exacerbate mitochondrial degradation and content reduction (see Fig. 1 E). This may explain the reduced locomotion and climbing activity associated with chronic fluvastatin treatment in flies reported previously[8]. In humans, several statins have been shown to alter mitochondrial respiration acutely and chronically[7], inducing ROS overproduction and subsequent oxidative stress in skeletal muscle[18,19,37], and reducing mitochondrial content[24,38,39].

Mitochondria and myofibrils are connected through the sarcoplasmic reticulum (SR), which serves as a calcium store[40,41]. Intriguingly, statins have been demonstrated to alter SR calcium ATPases and cause disconnection of the stabilizing protein FK506 binding protein (FKBP12) from the calcium release channel, Ryanodine Receptor (RyR), in the SR, which is accompanied by ROS[42,43]. Interestingly, these proteins are

regulated by mitochondrial ROS[44]. Here, we noted that chronic fluvastatin treatment was accompanied by elevated ROS levels. Although chronic fluvastatin has been reported to impair the SR/mitochondria calcium store in rat skeletal muscle[45], it would be interesting to examine the acute effect of fluvastatin on SR proteins at different time points and thus understand whether SR damage causes or is initiated by mitochondrial dysfunction and leads to subsequent separation of myofibrils and mitochondria.

We previously demonstrated that *Hmgcr* knockdown in skeletal muscles in *Drosophila* induces rounding up of mitochondria similar to chronic five-day fluvastatin treatment, but it was not sufficient to trigger myofibril damage[8]. Accordingly, we hypothesized that fluvastatin treatment induced mitochondrial dysfunction through the inhibition of Hmgcr in skeletal muscles, leading to subsequent ROS overproduction. To investigate this hypothesis, we measured and compared mitochondrial respiration for chronic fluvastatin treatment and selective *Hmgcr* knockdown in thorax flight muscles. Contrary to our initial hypothesis, *Hmgcr* knockdown did not alter the respiration rate at any of the measured pathways, nor did it lead to changes in ROS production or CPT2-dependent FAO compared to controls or chronic fluvastatin treatment (See Fig. 2 & 3 and Supplementary Fig. 1 & 2). This may indicate that fluvastatin-induced mitochondrial dysfunction is likely independent of Hmgcr inhibition. It is plausible to suggest that the depletion of CoQ10, which is one of the downstream products of the mevalonate pathway, may not be the primary underlying cause of statin-induced mitochondrial dysfunction and subsequent ROS overproduction. In support of this possibility, several publications have indicated that statins cause myopathy through inhibition of mitochondrial repatriation without altering the muscular CoQ10[46,47]. This may explain why CoQ10 does not improve the mitochondrial alteration in cell models treated with statins[48], and CoQ10 supplementation in statin-treated patients has been shown to not improve myopathy-related symptoms[46,49]. However, this does not necessarily exclude the possibility that Hmgcr inhibition in the muscles contributes to the rounded shape phenotype of mitochondria, as we previously showed[8]. Instead, it suggests that the round-up phenotype of mitochondria may be mediated independently of mitochondrial respiration.

We also previously reported that in *Drosophila*, fluvastatin-induced muscular damage is mediated by the inhibition of the muscular chloride channel and is independent of muscular Hmgcr inhibition in skeletal muscles[8]. In the same study, we indicated that chronic fluvastatin treatment was associated with the disruption of key genes involved in lipid metabolism[8]. In our mechanistic model, we suggested that fluvastatin activation of Pkcdelta (*Drosophila* homolog of PKCθ, which upon activation inhibits the chloride channel of skeletal muscles in humans and rats[50,51]) is mediated through both ROS and free fatty acids, FFAs[8]. Here, we demonstrated that chronic fluvastatin treatment led to elevated ROS in skeletal muscles and impaired CPT2-dependent FAO in skeletal muscles. CPT2 is a crucial enzyme for mitochondrial uptake of FFAs from the cytosol into mitochondria and converts fatty acylcarnitines to acyl-CoA for β-oxidation[7,52]. Impairment of CPT2 activity has been reported to accumulate intramuscular and serum-free fatty acids and acylcarnitines[53–55]. Several statins have been associated with the inhibition of CPT2[18,56] and increased levels of both FFAs and acylcarnitines[10,57]. FFA and acylcarnitine are strong activators of PKCθ in the muscles[58,59]. Based on this, fluvastatin-induced impairment of CPT2-dependent FAO in the skeletal muscles may lead to elevated FFAs and acylcarnitines, which, in addition to ROS, contribute to activated Pkcdelta-mediated inhibition of skeletal muscle chloride channels and subsequent myopathy-like phenotypes.

The question that remains is how fluvastatin elicits mitochondrial dysfunction. Two potential mechanisms have been proposed in the literature. First, direct inhibition of mitochondrial complexes has been reported with several statins, including fluvastatin, in humans[7,60] although this has not been investigated in flies yet. A study by Schirris et al. has indicated that most of the statin-lactone forms reduce the mitochondrial respiration capacity and are associated with inhibition of mitochondrial Complex I, II, and III. The same study showed that the activity of mitochondrial Complex III was reduced in C2C12 myoblast where the Q_o binding site of mitochondrial Complex III was identified as off-target of the statin lactones[7]. However, fluvastatin demonstrated a strong inhibitory effect on Complex I and II with no effect on Complex III, which was attributed to the intermediate lipophilicity of fluvastatin, although other hydrophilic statins showed to inhibit Complex III[7]. Taken together with our findings, fluvastatin might impair mitochondrial respiration through inhibition of Complex I and II.

Another possibility is that fluvastatin-induced mitochondrial dysfunction is mediated by lipotoxicity. Here, we demonstrated that fluvastatin treatment was associated with impairment of CPT2 which may result in reduced uptake and accumulation of FFA. In addition, in our previous study, we demonstrated that fluvastatin treatment is associated with disruption of key genes involved in lipid metabolism, which may also exacerbate the accumulation of toxic lipid intermediates such as FFA and diacylglycerides (DAGs) in the muscles. Of interest, we previously found that Lipn (*Drosophila* homolog of *LPIN1* which encodes lipin-1 enzymes, responsible for the dephosphorylation of phosphatidic acid into DAGs) was highly significantly downregulated in fluvastatin-treated flies[8]. In support of this, statins have been shown to reduce the expression of LIPN1 in the skeletal muscles of mice. The same study indicated that loss of LIPN1 in the skeletal muscles leads to aberrant lipid storage, impaired mitochondrial function and ultimately myopathy[61].

This is the first study using *Mef2-Gal4 > UAS-mitoGFP*, which helped visualize and analyse phenotypic changes in the mitochondria in a time-dependent manner under confocal microscopy. This line can be used further to investigate mitochondrial phenotypes associated with other types of statins. Additionally, we quantified the mitochondrial and myofibril phenotypes, which strengthened our findings. We measured and compared respiration functions for both fluvastatin-treated and selective skeletal muscular *Hmgcr* knockdown flies, allowing us to elucidate the known statin-target effect of Hmgcr on muscular mitochondria. Nevertheless, there are certain limitations in our study. Although Acute exposure for 24 h to fluvastatin has been shown to impair mitochondrial respiration[7] and induce apoptosis[36] in different cell types, it would be interesting to investigate the effect of fluvastatin on mitochondrial respiration functions after two days in *Drosophila*. Although all statins share a common target, HMGCR and studies showed that both, lipophilic and hydrophilic statins can penetrate mitochondria and impair mitochondrial respiration[7,18], we could not generalize the effect of the fluvastatin (which

is moderately lipophilic) on temporal dynamics of mitochondrial and myofibril damage on other hydrophilic statins. Despite the fact that fluvastatin induces apoptosis in different study models[7,36,62,63], measuring apoptotic markers, such as caspase activation, and cytochrome C release, in the skeletal muscles of *Drosophila* would enhance our understanding of whether the mitochondrial phenotypes associated with fluvastatin represent the initiation of cell death cascades, subsequently resulting in myofibril damage. Also, we did not examine the effect of fluvastatin at different time points on the sarcoplasmic reticulum (SR) and its proteins involved in calcium regulation, such as SERCA (Sarco(endo)plasmic Reticulum Calcium ATPase) and RyR. Finally, we did not rescue the mitochondrial phenotypes associated with fluvastatin treatment or assess whether CoQ10 or mevalonate can rescue statin-associated mitochondrial dysfunction, although specific Hmgcr inhibition in skeletal muscles provides us with relevant information regarding the depletion of mevalonate and CoQ10.

Conclusion

To our knowledge, this is the first study providing insights into the sequential occurrence of fluvastatin-induced mitochondrial morphological changes and myofibril damage in *Drosophila*. We demonstrate that fluvastatin reduces mitochondrial content in a time-dependent manner and that fluvastatin-induced mitochondrial phenotypes precede myofibril damage. Furthermore, we show that chronic fluvastatin treatment impairs mitochondrial respiration, particularly by inducing elevated ROS and impaired FAO, while skeletal muscle Hmgcr knockdown does not lead to altered mitochondrial respiration. Further investigations are warranted to explore the effect of the statins on the sarcoplasmic reticulum at different time points which may link early mitochondrial alteration to later myofibril damage.

Materials and methods

Drosophila work

To characterize the effect of fluvastatin on mitochondrial morphology, we first decorated actin and mitochondria in skeletal muscles by expressing GFP fused to a mitochondrial matrix targeting signal (*UAS-mito-GFP*, Bloomington #8442) with the *Mef2-GAL4* driver (Bloomington #25756) to generate *Mef2-Gal4 > UAS-mitoGFP* fly lines. Previous publications have shown that fluvastatin treatment is effective in flies and able to inhibit Hmgcr[8,64–67]. In our previous study, we showed that 1.0Mm fluvastatin, which is within the therapeutic range of fluvastatin used in humans and able to induce mitochondrial phenotypic changes[8]. Therefore, we used 1.0 mM fluvastatin (Sigma, Darmstadt, Germany, #SML0038) in this study as well. Accordingly, we treated *Mef2-Gal4 > UAS-mitoGFP* flies with 1.0 mM fluvastatin mixed with standard fly food medium (treated group), while in the control, flies were fed with normal standard fly food medium mixed with an equivalent volume of water for two and five days.

Immunohistochemistry and microscopy

For the imaging experiments, we did not observe any sex-based difference in measurements, therefore we used both male and female *Mef2-Gal4 > UAS-mitoGFP* flies, which is aligned with a previous study that used the same line[34]. *Mef2-Gal4 > UAS-mitoGFP* flies (both male and females) were anaesthetized by CO2, and their adult thorax muscles, which are commonly used in examining mitochondrial morphology and respiration[32,34], were dissected and stained as described in Hunt and Demontis[68]. We used rabbit anti-Mef2 (1:200, Eileen Furlong, Heidelberg, Allemagne), Alexa-conjugated phalloidin (1:200, Thermo Fisher, Waltham/Massachusetts) and goat anti-GFP (1:200, Abcam, ab6673). Samples were acquired on Leica SP5 microscopes (Biosit, IGDR-Rennes) at 40X magnification and 1024/1024-pixel resolution. Images were processed with ImageJ software.

Quantification of mitochondrial content

The quantification of mitochondrial content was carried out according to Avellaneda et al.[34]. The total areas of flight muscle (phalloidin) and mitochondria (mito-GFP) were quantified via Otsu thresholding in ImageJ Fiji for each acquisition channel. This was performed for the same Z-stack number for each condition. The significant difference between groups was calculated using one-way ANOVA with Bonferroni's multiple comparisons. The number of images used is 15 for the control, 17 for the two-day fluvastatin group and 23 for the five-day fluvastatin group.

Quantification of the number of round-like shaped mitochondria

Three confocal images of the dissected thorax flight muscles were selected randomly per group. Next, using ImageJ Fiji, the mitochondria channel (mito-GFP) was selected, followed by segmenting the image into six slices using the "Plugins" and "Macros" menu, "StartUp Macros" option. We applied the following script:

```
N = 6;
w = getWidth;
h = getHeight;
id = getImageID;
for(i = 0; i < N; i + +){
  selectImage(id);
  makeRectangle(0, i*h/N, w, h/N);
  name = "" + (i + 1);
  run("Duplicate…", "title = " + name);
```

}

Afterwards, we counted the round-like mitochondria in each slice using the multipoint tool. Slices where no round-like shapes were found were excluded from the analysis. Subsequently, we used GraphPad Prism to check the normality of the data and select an appropriate test to calculate the significance.

Measuring the distance between myofibrils

Six random confocal images of dissected thorax flight muscles were selected for each group. Using ImageJ Fiji, actin (phalloidin) and mitochondria channels (mito-GFP) were selected, and then the distance between myofibrils was measured manually. In cases where myofibrils were not consistently aligned or parallel, we measured the distance between myofibrils three times: at the beginning, in the middle, and at the end of the individual pair of myofibrils. Areas where mitochondria were absent or where nuclei between individual pairs of myofibrils were present were excluded from the analysis. We used GraphPad Prism to check the normality of the data and select an appropriate test to calculate the significance.

Measuring the thickness of myofibrils

Five random confocal images of dissected thorax flight muscles were chosen randomly for each group. Then, we measured the thickness of individual myofibrils using ImageJ Fiji. In cases where the myofibril thickness exhibited variation across the image, we conducted measurements in both the thicker and thinner sections of each myofibril. Subsequently, we used GraphPad Prism to check the normality of the data and select an appropriate test to calculate the significance.

High-resolution FluoRespirometry

To assess the influence of fluvastatin on mitochondrial respiration, we used wild-type male CSORC flies that were generated by crossing CantonS and OregonR-C flies, both of which were ordered from Bloomington Stock Centre (Bloomington, IN, USA). We first fed CSORC flies with 1.0 mM fluvastatin for five days as described in our previous study[8] and then dissected the thorax muscles. The knockdown of *Hmgcr* was carried out by the UAS-Gal4 System as described in our previous study[8] in which *Mhc-Gal4 > UAS-Hmgcr RANi* is the *Hmgcr* knockdown flies, while *w1118 > UAS-Hmgcr RNAi* & *Mhc-Gal4 > w1118* are the control groups[8]. The *Hmgcr* knockdown efficiency of the line was also determined in our previous study[8]. Only male flies were collected and used in this study and the life span of most *Hmgcr* knockdown flies was short, less than 2 days, which is consistent with our previous study[8]. The lines used for knockdown were obtained from Bloomington Stock Center as follows: Mhc-Gal4 (BN 38,464):w[*]; P{w[+ mC] = Mhc-RFP.F3-580}2, P{w[+ mC] = Mhc-GAL4.F3-580}2/SM6b and UAS-Hmgcr RNAi (BN 50,652): y[1] v[1]; P{y[+ t7.7]v[+ t1.8] = TRiP.HMC03053}attP40.

As described in a previous study, permeabilized thoraxes were prepared from four to five flies with slight modifications[69]. Briefly, dissected thoraxes were permeabilized with 62.5 µg/mL saponin at 4 °C for 15 min in preservation buffer (20 mM imidazole, 0.5 mM dithiothreitol, 20 mM taurine, 7.1 mM $MgCl_2$, 50 mM MES, 5 mM ATP, 15 mM phosphocreatine, 2.6 mM CaK_2EGTA, 7.4 mM K_2EGTA, pH 7.0 at 0 °C). Then, permeabilized thoraxes were washed once for 10 min in MiR05 medium (110 mM sucrose, 60 mM K-lactobionate, 0.5 mM K_2EGTA, 3 mM $MgCl_2$, 20 mM taurine, 10 mM KH_2PO_4, 20 mM HEPES, pH 7.1, 0.1% BSA (FA-free), pH 7.1 at 30 °C). Approximately 1 mg of tissue was used for one experimental run. Mitochondrial respiration and H_2O_2 production measurements were performed at 25 °C using Oxygraph-2k (O2k; Oroboros Instruments, Innsbruck, Austria) with O2k-Fluo-Modules in MiR05 medium, oxygenated to 400–450 µM to avoid any potential oxygen limitation to respiration. H_2O_2 flux was measured simultaneously with respirometry in the O2k-Fluorometer using the H_2O_2-sensitive probe Ampliflu™ Red (AmR) as previously described[58]. The H_2O_2/O flux ratio [%] was calculated as the H_2O_2 flux/(0.5 O_2 flux).

Substrate-Uncoupler-Inhibitor Titration

Pyruvate and malate (10 mM and 2 mM, respectively) were used to determine the NADH (N)-pathway and Complex I (CI)-linked LEAK respiration. Adenosine diphosphate (ADP) was added at a 5 mM concentration to determine oxidative phosphorylation-dependent respiration (OXPHOS state). Then, proline (5 mM, proline dehydrogenase substrate, ProDH-pathway) was added to measure NProDH-pathway-linked respiration. Next, succinate (10 mM, Complex II (CII) substrate, S-pathway) was added to reconstitute convergent NSProDh-pathway, CI-&CII- (CIII-linked) and ProDH-linked respiration. Glycerol-3-phosphate (15 mM, glycerol-3-phosphate dehydrogenase substrate, Gp-pathway) was then added to measure NSProDHGp pathway-linked respiration in the OXPHOS state. Titration with the uncoupler carbonyl cyanide m-chlorophenyl hydrazine (CCCP) (0.5 µM steps) was performed to determine the electron transfer system (ETS) capacity. Next, rotenone (0.5 µM, inhibitor of Complex I) and malonate (5 mM, inhibitor of Complex II) were subsequently added to determine SProDHGp- and ProDHGp-linked ETS capacity. Finally, antimycin A (2.5 µM, inhibitor of Complex III) was added to measure nonmitochondrial residual oxygen consumption (ROX).

Fatty acid oxidation

FAO-dependent mitochondrial respiration in fibres was measured using palmitoylcarnitine (10 µM) and 0.1 mM malate as substrates. ADP was added to a concentration of 5 mM to assess respiration in the OXPHOS state. Pyruvate (5 mM, CI substrate, NADH (N)-pathway) and additional malate (to a final concentration of 2 mM) were then added to reconstitute FN pathway-linked respiration. Then, proline (5mM), succinate (10 mM) and glycerol-3-phosphate (15 mM) were subsequently added to the chamber to measure FNProDH-, FNSProDH- and FNSProDHGp-pathway-linked respiration rates. Next, the inhibitors rotenone and malonate were added to

determine SProDHGp- and ProDHGp-linked respiration rates in the OXPHOS state. Antimycin A was added to determine non-mitochondrial residual oxygen consumption (ROX).

To determine the contribution of each substrate to the respiration rate as well as the OXPHOS and ET coupling efficiencies, the flux control factor was calculated as follows:

$$1 - \frac{Resp.rate\ before\ the\ addition}{Resp.rate\ after\ the\ addition}.$$

Statistical analysis

Data obtained from each experiment was first checked for normality using the Shapiro–Wilk test. If the data is normally distributed, a parametric test was used. If the data is not normally distributed, a non-parametric test is used. Accordingly, for non-normally distributed data the statistical significance was calculated with a nonparametric analysis using the Kruskal—Wallis test followed by the Dunn test for multiple comparisons in Figs. 1D,F,G. For normally distributed data, one-way ANOVA with Bonferroni's multiple comparisons test was used in Fig. 1E and supplementary Figs. 1 and 2. A Student t-test was used in Figs. 2 and 3 to calculate the significance difference.

Data availability

All data are contained within the article and supplementary data.

Received: 5 December 2023; Accepted: 31 January 2024
Published online: 09 February 2024

References

1. Peters, S. A. E., Singhateh, Y., Mackay, D., Huxley, R. R. & Woodward, M. Total cholesterol as a risk factor for coronary heart disease and stroke in women compared with men: A systematic review and meta-analysis. *Atherosclerosis* **248**, 123–131 (2016).
2. Deaths from cardiovascular disease surged 60% globally over the last 30 years: Report. *World Heart Federation* https://world-heart-federation.org/news/deaths-from-cardiovascular-disease-surged-60-globally-over-the-last-30-years-report/.
3. Goldstein, J. L. & Brown, M. S. Regulation of the mevalonate pathway. *Nature* **343**, 425–430 (1990).
4. Baigent, C. *et al.* Efficacy and safety of more intensive lowering of LDL cholesterol: A meta-analysis of data from 170 000 participants in 26 randomised trials. *Lancet* **376**, 1670–1681 (2010).
5. Musunuru, K. Treating coronary artery disease: Beyond statins, ezetimibe, and PCSK9 inhibition. *Ann. Rev. Med.* **72**, 447–458 (2021).
6. Galicia-Garcia, U. *et al.* Statin treatment-induced development of type 2 diabetes: From clinical evidence to mechanistic insights. *Int. J. Mol. Sci.* **21**, 1–25 (2020).
7. Schirris, T. J. J. *et al.* Statin-induced myopathy is associated with mitochondrial complex III inhibition. *Cell Metab.* https://doi.org/10.1016/j.cmet.2015.08.002 (2015).
8. Al-Sabri, M. H. *et al.* Statins induce locomotion and muscular phenotypes in drosophila melanogaster that are reminiscent of human myopathy: Evidence for the role of the chloride channel inhibition in the muscular phenotypes. *Cells* **11**, 3528 (2022).
9. Urbano, F. *et al.* Atorvastatin but not pravastatin impairs mitochondrial function in human pancreatic islets and rat β-cells. Direct effect of oxidative stress. *Sci. Rep.* https://doi.org/10.1038/s41598-017-11070-x (2017).
10. Kain, V., Kapadia, B., Misra, P. & Saxena, U. Simvastatin may induce insulin resistance through a novel fatty acid mediated cholesterol independent mechanism. *Sci. Rep.* **5**, 13823–13823 (2015).
11. Alsehli, A. M., Olivo, G., Clemensson, L. E., Williams, M. J. & Schiöth, H. B. The cognitive effects of statins are modified by age. *Sci. Rep.* **10**, 1–14 (2020).
12. Jamshidnejad-Tosaramandani, T. *et al.* Statins and cognition: Modifying factors and possible underlying mechanisms. *Front. Aging Neurosci. 14* (2022).
13. Alsehli, A. M. *et al.* Differential associations of statin treatment and polymorphism in genes coding for HMGCR and PCSK9 to risk for insomnia. *Front. Biosci. Landm.* **26**, 1453–1463 (2021).
14. Abed, W., Abujbara, M., Batieha, A. & Ajlouni, K. Statin induced myopathy among patients attending the National Center for diabetes, endocrinology, & genetics. *Ann. Med. Surg. (Lond.)* **74**, 103304 (2022).
15. null, null. Influence of pravastatin and plasma lipids on clinical events in the west of Scotland coronary prevention study (WOSCOPS). *Circulation* **97**, 1440–1445 (1998)
16. Nielsen, S. F. & Nordestgaard, B. G. Negative statin-related news stories decrease statin persistence and increase myocardial infarction and cardiovascular mortality: A nationwide prospective cohort study. *Eur. Heart J.* **37**, 908–916 (2016).
17. Ward, N. C., Watts, G. F. & Eckel, R. H. Statin toxicity: Mechanistic insights and clinical implications. *Circ. Res.* https://doi.org/10.1161/CIRCRESAHA.118.312782 (2019).
18. Mollazadeh, H. *et al.* Effects of statins on mitochondrial pathways. *J. Cachexia Sarcopenia Muscle* **12**, 237–251 (2021).
19. Bouitbir, J. *et al.* Opposite effects of statins on mitochondria of cardiac and skeletal muscles: A 'mitohormesis' mechanism involving reactive oxygen species and PGC-1. *Eur. Heart J.* **33**, 1397–1407 (2012).
20. Caffario, P., Dammacco, F., Gernone, A. & Silvestris, F. Statins activate the mitochondrial pathway of apoptosis in human lymphoblasts and myeloma cells. *Carcinogenesis* **26**, 883–891 (2005).
21. Apostolopoulou, M., Corsini, A. & Roden, M. The role of mitochondria in statin-induced myopathy. *Eur. J. Clin. Invest.* **45**, 745–754 (2015).
22. Bitzur, R., Cohen, H., Kamari, Y. & Harats, D. Intolerance to statins: Mechanisms and management. *Diabetes Care* **36**, (2013).
23. Hou, T., Li, Y., Chen, W., Heffner, R. R. & Vladutiu, G. D. Histopathologic and biochemical evidence for mitochondrial disease among 279 patients with severe statin myopathy. *J. Neuromusc. Dis.* **4**, 77–87 (2017).
24. Ramachandran, R. & Wierzbicki, A. S. Statins, muscle disease and mitochondria. *J. Clin. Med.* **6**, 75 (2017).
25. Baker, S. K. Molecular clues into the pathogenesis of statin-mediated muscle toxicity. *Muscle Nerve* https://doi.org/10.1002/mus.20291 (2005).
26. Hur, J., Liu, Z., Tong, W., Laaksonen, R. & Bai, J. P. F. Drug-induced rhabdomyolysis: From systems pharmacology analysis to biochemical flux. *Chem. Res. Toxicol.* **27**, 421–432 (2014).
27. Romanello, V. The Interplay between mitochondrial morphology and myomitokines in aging sarcopenia. *Int. J. Mol. Sci.* **22**, 91 (2020).

28. Pipinos, I. I. *et al.* Abnormal mitochondrial respiration in skeletal muscle in patients with peripheral arterial disease. *J. Vasc. Surg.* **38**, 827–832 (2003).
29. Pollock, N., Staunton, C. A., Vasilaki, A., McArdle, A. & Jackson, M. J. Denervated muscle fibers induce mitochondrial peroxide generation in neighboring innervated fibers: Role in muscle aging. *Free Radic. Biol. Med.* **112**, 84–92 (2017).
30. Lian, D., Chen, M.-M., Wu, H., Deng, S. & Hu, X. The role of oxidative stress in skeletal muscle myogenesis and muscle disease. *Antioxidants (Basel)* **11**, 755 (2022).
31. Peterson, C. M., Johannsen, D. L. & Ravussin, E. Skeletal muscle mitochondria and aging: A review. *J. Aging Res.* **2012**, e194821 (2012).
32. Camus, M. F., Rodriguez, E., Kotiadis, V., Carter, H. & Lane, N. Redox stress shortens lifespan through suppression of respiratory complex I in flies with mitonuclear incompatibilities. *Exp. Gerontol.* **175**, 112158 (2023).
33. Wall, J. M. *et al.* CRISPR/Cas9-engineered Drosophila knock-in models to study VCP diseases. *Dis. Model Mech.* **14**, 048603 (2021).
34. Avellaneda, J. *et al.* Myofibril and mitochondria morphogenesis are coordinated by a mechanical feedback mechanism in muscle. *Nat. Commun.* **12**, 1–18 (2021).
35. Hoppeler, H., Lüthi, P., Claassen, H., Weibel, E. R. & Howald, H. The ultrastructure of the normal human skeletal muscle. *Pflugers Arch.* **344**, 217–232 (1973).
36. Zhang, W., Wu, J., Zhou, L., Xie, H.-Y. & Zheng, S.-S. Fluvastatin, a lipophilic statin, induces apoptosis in human hepatocellular carcinoma cells through mitochondria-operated pathway. *Indian J. Exp. Biol.* **48**, 1167–1174 (2010).
37. Liu, A. *et al.* Statins: Adverse reactions, oxidative stress and metabolic interactions. *Pharmacol. Therap.* **195**, 54–84 (2019).
38. Vaughan, R. A., Garcia-Smith, R., Bisoffi, M., Conn, C. A. & Trujillo, K. A. Ubiquinol rescues simvastatin-suppression of mitochondrial content, function and metabolism: Implications for statin-induced rhabdomyolysis. *Eur. J. Pharmacol.* **711**, 1–9 (2013).
39. Stringer, H. A. J., Sohi, G. K., Maguire, J. A. & Côté, H. C. F. Decreased skeletal muscle mitochondrial DNA in patients with statin-induced myopathy. *J. Neurol. Sci.* **325**, 142–147 (2013).
40. Bennett, P. M., Ehler, E. & Wilson, A. J. Sarcoplasmic reticulum is an intermediary of mitochondrial and myofibrillar growth at the intercalated disc. *J. Muscle Res. Cell Motil.* **37**, 55–69 (2016).
41. Rossi, A. E., Boncompagni, S. & Dirksen, R. T. Sarcoplasmic reticulum-mitochondrial symbiosis: Bidirectional signaling in skeletal muscle. *Exerc. Sport Sci. Rev.* **37**, 29–35 (2009).
42. Lotteau, S. *et al.* A mechanism for statin-induced susceptibility to myopathy. *JACC Basic Transl. Sci.* **4**, 509–523 (2019).
43. Draeger, A. *et al.* Statin therapy and the expression of genes that regulate calcium homeostasis and membrane repair in skeletal muscle. *Am. J. Pathol.* **177**, 291–299 (2010).
44. Goodman, J. B. *et al.* Redox-resistant SERCA [sarco(endo)plasmic reticulum calcium ATPase] attenuates oxidant-stimulated mitochondrial calcium and apoptosis in cardiac myocytes and pressure overload-induced myocardial failure in mice. *Circulation* **142**, 2459–2469 (2020).
45. Liantonio, A. *et al.* Fluvastatin and atorvastatin affect calcium homeostasis of rat skeletal muscle fibers in vivo and in vitro by impairing the sarcoplasmic reticulum/mitochondria Ca2+-release system. *J. Pharmacol. Exp. Ther.* **321**, 626–634 (2007).
46. Dohlmann, T. L. *et al.* Statin treatment decreases mitochondrial respiration but muscle coenzyme Q10 levels are unaltered: The LIFESTAT study. *J. Clin. Endocrinol. Metab.* **104**, 2501–2508 (2019).
47. Mullen, P. J., Lüscher, B., Scharnagl, H., Krähenbühl, S. & Brecht, K. Effect of simvastatin on cholesterol metabolism in C2C12 myotubes and HepG2 cells, and consequences for statin-induced myopathy. *Biochem. Pharmacol.* **79**, 1200–1209 (2010).
48. Miettinen, T. P. & Björklund, M. Cellular allometry of mitochondrial functionality establishes the optimal cell size. *Dev. Cell* **39**, 370–370 (2016).
49. Banach, M. *et al.* Effects of coenzyme Q10 on statin-induced myopathy: A meta-analysis of randomized controlled trials. *Mayo Clin. Proc.* https://doi.org/10.1016/j.mayocp.2014.08.021 (2015).
50. Camerino, G. M. *et al.* Protein kinase C theta (PKCθ) modulates the ClC-1 chloride channel activity and skeletal muscle phenotype: A biophysical and gene expression study in mouse models lacking the PKCθ. *Pflugers Archiv Eur. J. Physiol.* **466**, 2215–2228 (2014).
51. Camerino, G. M. *et al.* Statin-induced myopathy: Translational studies from preclinical to clinical evidence. *Int. J. Mol. Sci.* **22**, 1–18 (2021).
52. Bieber, L. L. Carnitine. *Ann. Rev. Biochem.* **57**, 261–283 (1988).
53. Pereyra, A. S., Rajan, A., Ferreira, C. R. & Ellis, J. M. Loss of muscle carnitine palmitoyltransferase 2 prevents diet-induced obesity and insulin resistance despite long-chain acylcarnitine accumulation. *Cell Rep.* **33**, 108374 (2020).
54. Jones, P., Patel, K. & Rakheja, D. Chapter 26 - Disorder: Carnitine palmitoyltransferase 1 deficiency. In *A Quick Guide to Metabolic Disease Testing Interpretation (Second Edition)* (eds. Jones, P., Patel, K. & Rakheja, D.) 137–140 (Academic Press, 2020). https://doi.org/10.1016/B978-0-12-816926-1.00026-2.
55. Gempel, K. *et al.* Screening for carnitine palmitoyltransferase II deficiency by tandem mass spectrometry. *J. Inherit. Metab. Dis.* **25**, 17–27 (2002).
56. Ghatak, A., Faheem, O. & Thompson, P. D. The genetics of statin-induced myopathy. *Atherosclerosis* **210**, 337–343 (2010).
57. Bhuiyan, J. & Seccombe, D. W. The effects of 3-hydroxy-3-methylglutaryl-CoA reductase inhibition on tissue levels of carnitine and carnitine acyltransferase activity in the rabbit. *Lipids* **31**, 867–870 (1996).
58. Capel, F. *et al.* DHA at nutritional doses restores insulin sensitivity in skeletal muscle by preventing lipotoxicity and inflammation. *J. Nutr. Biochem.* **26**, 949–959 (2015).
59. Griffin, M. E. *et al.* Free fatty acid-induced insulin resistance is associated with activation of protein kinase C θ and alterations in the insulin signaling cascade. *Diabetes* **48**, 1270–1274 (2000).
60. Somers, T. *et al.* Mitochondrial complex III activity: From invasive muscle biopsies to patient-friendly buccal swab analysis. *Sci. Rep.* **13**, 9638 (2023).
61. Zhang, P., Verity, M. A. & Reue, K. Lipin-1 regulates autophagy clearance and intersects with statin drug effects in skeletal muscle. *Cell Metab.* **20**, 267–279 (2014).
62. Buemi, M. *et al.* Pro-apoptotic effect of fluvastatin on human smooth muscle cells. *Eur. J. Pharmacol.* **370**, 201–203 (1999).
63. Takahashi, M. *et al.* Fluvastatin enhances apoptosis in cytokine-stimulated vascular smooth muscle cells. *J. Cardiovasc. Pharmacol.* **39**, 310 (2002).
64. Alsehli, A. M. *et al.* The statin target HMG-coenzyme a reductase (HMGCR) regulates sleep homeostasis in drosophila. *Pharmaceuticals* **15**, 79–79 (2022).
65. Williams, M. J. *et al.* The statin target HMGCR regulates energy metabolism and food intake through central mechanisms. *Cells* **11**, 970–970 (2022).
66. Levine, B. D. & Cagan, R. L. Drosophila lung cancer models identify trametinib plus statin as candidate therapeutic. *Cell Rep.* **14**, 1477–1487 (2016).
67. Yi, P., Han, Z., Li, X. & Olson, E. H. The mevalonate pathway controls heart formation in Drosophila by isoprenylation of Gγ1. *Science* **313**, 1301–1303 (2006).
68. Hunt, L. C. & Demontis, F. Whole-mount immunostaining of Drosophila skeletal muscle. *Nat. Protoc.* **8**, 2496–2501 (2013).
69. Simard, C. J., Pelletier, G., Boudreau, L. H., Hebert-Chatelain, E. & Pichaud, N. Measurement of mitochondrial oxygen consumption in permeabilized fibers of drosophila using minimal amounts of tissue. *J. Vis. Exp.* https://doi.org/10.3791/57376 (2018).

Author contributions

The first draft was written by M.H.A.-S., N.A., and S.K. M.H.A.-S., H.B., H.B.S., contributed to conceptualization. M.H.A.-S., S.K., N.A., and H.B. contributed to experiments. Data analysis was performed by M.H.A.-S., S.K., N.A. Writing—review and editing were performed by M.H.A.-S., H.B., N.A., K.H., M.W., R.F., H.B.S. All authors read and approved the final manuscript.

Funding

Open access funding provided by Uppsala University. The studies were supported by the Swedish Research Council: 2019-01066. H.B. is also supported by the AFM-Telethon trampoline Grant 23108 and ATIP-Avenir. N.A. is supported by the AFM-Telethon PhD fellowship 23846.

Competing interests

The authors declare no competing interests.

Additional information

Supplementary Information The online version contains supplementary material available at https://doi.org/10.1038/s41598-024-53446-w.

Correspondence and requests for materials should be addressed to M.H.A.-S. or H.B.S.

Reprints and permissions information is available at www.nature.com/reprints.

Publisher's note Springer Nature remains neutral with regard to jurisdictional claims in published maps and institutional affiliations.

Open Access This article is licensed under a Creative Commons Attribution 4.0 International License, which permits use, sharing, adaptation, distribution and reproduction in any medium or format, as long as you give appropriate credit to the original author(s) and the source, provide a link to the Creative Commons licence, and indicate if changes were made. The images or other third party material in this article are included in the article's Creative Commons licence, unless indicated otherwise in a credit line to the material. If material is not included in the article's Creative Commons licence and your intended use is not permitted by statutory regulation or exceeds the permitted use, you will need to obtain permission directly from the copyright holder. To view a copy of this licence, visit http://creativecommons.org/licenses/by/4.0/.

© The Author(s) 2024

III. Discussion et perspectives

Interactions intercellulaires en réponse aux dommages musculaires

Du fait de son activité intense et de son exposition constante aux contraintes mécaniques, le muscle squelettique est particulièrement vulnérable aux lésions. La régénération de ce tissu repose sur une coordination synchronisée entre plusieurs types cellulaires qui assurent, de manière concertée, la réparation des fibres endommagées et le rétablissement de leur fonctionnalité. Chez les vertébrés, cette régénération implique notamment les MuSCs, macrophages, FAPs et les cellules endothéliales (Rodríguez et al. 2024). Une perturbation de communication entre ces différents types de cellules entraîne une réparation incomplète, pouvant se traduire par des phénomènes de fibrose, une perte de masse musculaire ou une altération durable des capacités contractiles. C'est dans ce cadre que s'inscrivent mes travaux de thèse, qui visaient à explorer et caractériser les mécanismes de communication intercellulaire en réponse aux dommages musculaires. **J'ai décrit un processus cellulaire et moléculaire impliquant une collaboration étroite entre les plasmatocytes, les cellules trachéales et les fibres musculaires dans le contexte de lésions des muscles du vol chez la *Drosophile*.** Ces travaux positionnent les plasmatocytes comme des acteurs centraux dans deux aspects complémentaires de la réponse aux dommages.

D'une part, j'ai montré que les plasmatocytes participent activement au remodelage de la trachée via l'activation de la voie de signalisation FGF Bnl-Btl. Cette signalisation favorise le recrutement et la ramification des branches trachéales vers les fibres lésées, assurant ainsi un apport optimal en oxygène. Ce mécanisme rappelle l'interaction entre macrophages et les cellules endothéliales observée chez les vertébrés. Néanmoins, l'existence réelle de cette interaction dans les modèles vertébrés est controversée (Rahat et al. 2014; Ochoa et al. 2007), soulignant les limites actuelles dans la caractérisation précise de l'interaction entre les macrophages et le système vasculaire impliquée dans la réparation musculaire. Cette difficulté est accentuée par la complexité de la néovascularisation chez les mammifères, qui mobilise une multitude de médiateurs, dont les principaux sont VEGF (Vascular Endothelial Growth Factor), PDGF (Platelet-derived Growth Factor), HGF (Hepatocyte

Growth Factor) et MCP-1 (Monocyte chemoattractant protein 1) (Murakami et Simons 2008). D'une manière intéressante, l'activité et la régulation de ces facteurs de croissance et chimiokines sont sous le contrôle de la voie FGF. Or, le rôle de la voie de signalisation FGF dans la régénération musculaire des mammifères n'a pas encore été clairement établi. Cette lacune pourrait s'expliquer par la redondance de cette famille, représentée par 22 gènes chez l'homme, contre seulement trois chez la *Drosophile* (Yun et al. 2010), et un unique FGF, Branchless (Bnl), qui assure à lui seul la régulation de la vascularisation chez cet organisme. Ainsi, l'insuffisance de connaissances sur l'implication des FGF dans la régulation de la vascularisation musculaire chez les mammifères pourrait découler de cette redondance fonctionnelle.

D'autre part, j'ai mis en évidence que les plasmatocytes produisent et sécrètent des composants essentiels de la matrice extracellulaire (ECM), tels que le collagène de type IV (Viking) et la glycoprotéine SPARC. Ces molécules assurent un support structurel indispensable au maintien de l'intégrité des fibres musculaires et participent à l'organisation du microenvironnement local.

L'ensemble de ces résultats mettent en lumière la polyvalence des hémocytes adultes dans la réponse aux blessures. Ils apparaissent comme des cellules multifonctionnelles capables d'assurer simultanément la régulation de l'oxygénation et la production de matrice extracellulaire. Cette double contribution souligne l'importance des interactions intercellulaires dans la coordination de la réparation musculaire et ouvre de nouvelles perspectives quant aux rôles des hémocytes dans d'autres contextes physiologiques, tels que le maintien de l'homéostasie tissulaire ou la réponse aux tumeurs.

Hémocytes, guidage trachéal et oxygénation tissulaire

Traditionnellement, les systèmes respiratoire et immunitaire de la *Drosophile* sont décrits comme remplissant des fonctions bien distinctes : La trachée garantit les échanges gazeux (Centanin et al. 2010), tandis que les hémocytes assurent la défense immunitaire (Lemaitre et Hoffmann 2007). Ce paradigme a toutefois été remis en question par des travaux révélant des interactions étroites entre ces deux systèmes, en particulier dans des contextes de stress tissulaire (Parvy et al. 2019).

Il a été en effet montré que la trachée ne joue pas un rôle purement respiratoire, mais elle peut également contribuer à la réponse immunitaire locale en produisant des peptides antimicrobiens (AMPs), tels que la Drosocin (Sanchez Bosch et al. 2019) ou Drosomycin (Bossen et al. 2024). De façon similaire, au cours du développement larvaire une sous-population d'hémocytes, les cellules à cristaux, quant à elles interviennent dans le transport d'oxygène fourni par les trachées (Shin et al. 2024). Cependant, cette fonction respiratoire potentielle des hémocytes reste inexplorée chez l'adulte, où les besoins métaboliques diffèrent.

Nous montrons que les hémocytes adultes régulent activement la réponse respiratoire locale. Cette régulation se fait indirectement via le remodelage trachéal en sécrétant Bnl, qui guide les branches trachéales par le biais de la voie de signalisation Bnl/Btl. Ainsi, les hémocytes, au-delà de leur rôle immunitaire classique, contribuent également à la restauration de l'homéostasie tissulaire en facilitant l'oxygénation des tissus adultes endommagés. Cette nouvelle fonction soulève toutefois une question intrigante : Pourquoi le muscle lésé, qui est pourtant la structure directement affectée par l'hypoxie ou la perte d'intégrité, ne produit-il pas lui-même Bnl ? Autrement dit, pourquoi confier aux cellules extrinsèques au tissu la capacité d'attirer les branches trachéales, alors que le besoin en oxygène et en réparation est intrinsèque au muscle ?

Une première explication pourrait résider dans une stratégie de prévention de l'activation inappropriée du guidage de la croissance trachéale. En effet, Bnl est un morphogène puissant et son expression diffuse dans le muscle pourrait induire une revascularisation aberrante, caractérisée par l'attraction de branches trachéales non spécifiques, perturbant ainsi l'architecture locale du réseau trachéal. Les cellules immunitaires, en revanche, sont moins abondantes que les noyaux des fibres (environ 1 000 noyaux par fibre) et, une fois localisées sur la fibre, elles pourraient déployer des quantités modérées de Bnl, de manière ciblée sur les zones nécessitant une oxygénation.

Une seconde possibilité est que la fibre endommagée limite la régulation transcriptionnelle de nouveaux gènes au profit d'une régulation post-transcriptionnelle, voire traductionnelle, de gènes déjà présents dans le syncytium, nécessaires à la consolidation rapide de la fibre (ex. MHC).

Au-delà de leur rôle indirect dans l'oxygénation, assuré par le guidage du réseau trachéal, il reste à déterminer si les hémocytes adultes pourraient également participer de manière directe au transport de l'oxygène, comme cela a été proposé lors de certaines étapes du développement larvaire (Shin et al. 2024). Pour tester cette hypothèse, plusieurs approches expérimentales sont envisageables. Tout d'abord, une analyse transcriptomique des hémocytes à l'échelle unicellulaire, en utilisant l'approche de smFISH (Single molécule fluorescence in situ hybridation) permettrait d'identifier l'expression des gènes codant pour des protéines capables de fixer ou transporter l'oxygène, tels que les protéines oxydables de type prophénoloxydase (PPO), dont une activité respiratoire primitive a été suggérée dans les cellules à cristaux (Shin et al. 2024). Une seconde approche complémentaire consisterait à mesurer l'état d'oxygénation des fibres musculaires lésées après ablation des hémocytes, et ceci à l'aide des indicateurs d'hypoxie tels que : la lignée rapportrice SyHREns (Zhao et al. 2024). Si l'élimination des hémocytes aggrave l'état d'hypoxie locale, cela fournirait une preuve fonctionnelle indirecte mais forte en faveur de leur rôle dans le transport ou la distribution de l'oxygène.

Si cette hypothèse se confirmait, elle ouvrirait une nouvelle perspective : celle d'une fonction respiratoire primitive assurée par les cellules immunitaires adultes, illustrant la plasticité fonctionnelle du système immunitaire chez les insectes. Dans un organisme dépourvu de globules rouges, les hémocytes pourraient donc assumer, de manière transitoire et localisée, une fonction d'adaptation respiratoire, essentielle à la réparation tissulaire dans des conditions extrêmes, telles que les lésions musculaires.

Les hémocytes comme substituts fonctionnels des FAPs ?

Nous avons montré que, dans le muscle adulte, les hémocytes produisent des composants essentiels de la ECM, tels que SPARC et Viking (Vkg, collagène de type IV), aussi bien en condition d'homéostasie qu'en réponse à des lésions musculaires. La délétion ciblée de ces gènes spécifiquement dans les hémocytes entraîne une désorganisation marquée de l'architecture musculaire, indiquant que ces cellules jouent un rôle clé dans le maintien de la structure et, potentiellement, de l'intégrité musculaire. Chez les mammifères, une fonction comparable est assurée par une population mésenchymateuse bien caractérisée : les FAPs. Ces cellules contribuent activement à la régénération musculaire en produisant des protéines de l'ECM, en

organisant le microenvironnement tissulaire et en modulant les interactions avec les cellules souches musculaires (Loomis et Smith 2023). Or, aucun équivalent des FAPs n'a été identifié à ce jour chez la *Drosophile*. Nos résultats suggèrent que les hémocytes adultes pourraient remplir une fonction analogue à celle des FAPs, en agissant comme producteurs et régulateurs de l'ECM dans le muscle adulte.

Signaux impliqués dans l'attraction des hémocytes en réponse aux lésions musculaires

Nous avons observé un recrutement d'hémocytes vers les fibres musculaires endommagées. Ce phénomène, qui survient dans un contexte stérile, soulève une question centrale : quels signaux orchestrent l'attraction des cellules immunitaires en l'absence de pathogènes ?

Classiquement, l'activation de la réponse immunitaire chez la *Drosophile* repose sur la détection de signaux microbiens exogènes, via les voies Toll et Imd (Voir chapitre 3). Or, dans notre modèle exempt d'infection, cette activation canonique peut être exclue, suggérant que le recrutement des hémocytes est déclenché par des signaux endogènes de dommage tissulaire. Cette hypothèse rejoint le concept des *Damage-Associated Molecular Patterns* (DAMPs), bien établi chez les vertébrés (Ma et al. 2024).

Parmi les candidats potentiels, les espèces réactives de l'oxygène (ROS) pourraient jouer un rôle (Chakrabarti et Visweswariah 2020). D'autres médiateurs plausibles incluent des cytokines de type interleukine, telles qu'Upd3, connue pour activer la voie JAK/STAT et favoriser le recrutement des cellules immunitaires (Yang et al. 2015).

Afin de tester ces hypothèses, il sera essentiel, dans un premier temps, de vérifier si les voies Toll et Imd ne sont pas activées dans le tissu musculaire endommagé, notamment en analysant l'expression de leurs cibles transcriptionnelles (par exemple, Drosomycin pour Toll (Lemaitre et al. 1996b) et Diptericin pour Imd (Foley et O'Farrell 2003)). Par la suite, il serait pertinent d'analyser le profil d'expression des ROS ainsi que celui de la voie JAK/STAT, dans les muscles contrôles et endommagés. En parallèle, il conviendrait d'interférer avec ces signaux et de déterminer si cela impacte le recrutement des hémocytes.

Cellules souches musculaires adultes de Drosophile : identification et limites méthodologiques

Une population résiduelle de MuSCs adulte a été identifiée à la périphérie des fibres des IFMs, elle dérive des AMPs larvaires qui ne rentrent pas en différenciation (Boukhatmi et Bray 2018; Chaturvedi et al. 2017). L'identification de ces cellules est basée sur l'expression du facteur de transcription Zfh1, considéré à ce jour comme un marqueur principal et unique des MuSCs chez la *Drosophile*. La perte de fonction de Zfh1 à l'âge adulte conduit à une atrophie musculaire progressive, suggérant que ce facteur est indispensable au maintien de l'homéostasie musculaire (Boukhatmi et Bray 2018). De plus, l'altération de certaines voies de signalisation telles que Notch dans ces cellules impacte négativement la régénération musculaire (Chaturvedi et al. 2017), ce qui renforce l'idée que les MuSCs participent activement au processus réparateur. Cependant, un biais majeur d'interprétation réside dans le fait que Zfh1 n'est pas exclusivement exprimé dans les MuSCs. Il est également présent dans d'autres lignages cellulaires, en particulier dans les plasmatocytes (Boukhatmi et Bray 2018; Ammar et al. 2025). Cette expression limite la spécificité des approches basées uniquement sur Zfh1, car les effets observés lors de sa déplétion ne peuvent pas être attribués de manière spécifique et unique aux MuSCs. Ceci constitue une lacune méthodologique importante. En effet, l'absence de marqueurs supplémentaires spécifiques des MuSCs chez la *Drosophile* restreint considérablement la capacité à caractériser cette population et à analyser son rôle dans la régénération. Une approche pour dépasser cette limite serait de mener des analyses transcriptomiques à l'échelle unicellulaire ciblant les IFMs lésés, afin de délimiter plus précisément la population de MuSCs adultes et identifier de nouveaux marqueurs co-exprimés spécifiquement dans ces cellules *(un projet en cours dans l'équipe)*.

Chez les vertébrés, l'homologue de Zfh1, Zeb1/2, est également exprimé à la fois dans les MuSCs et dans les macrophages (Siles et al. 2019b). Zeb1 joue un rôle déterminant dans la régénération, en modulant la transition des macrophages pro-inflammatoires vers un état anti-inflammatoire et en prévenant une activation prématurée des MuSCs, assurant ainsi une régénération coordonnée des muscles adultes (Siles et al. 2019b). Nous avons observé que, chez la *Drosophile*,

des plasmatocytes exprimant Zfh1 sont activement recrutés au site de la lésion musculaire. Toutefois, la fonction précise de Zfh1 dans cette population immunitaire reste largement inexplorée. Pour lever cette ambiguïté, il est nécessaire de réaliser des expériences de déplétion spécifique de Zfh1 dans les hémocytes, en utilisant des drivers restreints aux plasmatocytes tels que Pxn-Gal4 ou HmlΔ-Gal4. Cela permettrait de déterminer si Zfh1 régule dans ces cellules des fonctions analogues à celles observées chez les macrophages des vertébrés.

Surproduction de la MHC en réponse aux dommages musculaires

La régénération musculaire chez les mammifères s'appuie sur une reprogrammation transcriptionnelle qui reproduit, au moins en partie, les étapes du développement embryonnaire (Wang et Conboy 2010). Un des marqueurs les plus caractéristiques de ce processus est la réexpression transitoire des isoformes embryonnaires de la myosine lourde (MyHC-emb), marqueur classique d'un programme régénératif (Murphy et al. 2011b; Sartore et al. 1982), bien que sa fonction précise au cours de la régénération reste encore mal comprise.

Un processus analogue semble exister chez la *Drosophile*. Nos travaux montrent que la blessure des muscles du vol induit une régulation positive de la chaîne lourde de myosine (Mhc), un composant sarcomérique clé. Cette forte expression est également observée chez les mutants Naa30A, dont les IFMs présentent une fragilité intrinsèque et subissent des dommages en l'absence de toute manipulation physique. Cette observation exclut la possibilité d'un artefact expérimental lié à la procédure de lésion par aiguille et renforce l'idée qu'une atteinte intrinsèque du muscle suffit à déclencher cette réponse.

Cependant, le mécanisme régulant l'expression de la Mhc reste encore à déterminer. Nous avons exclu que cette régulation se fasse au niveau transcriptionnel, puisque la transcription est inactive dans la fibre endommagée *(données non présentées dans le manuscrit)*. Une autre possibilité serait une régulation traductionnelle intense de la MHC à partir ARNm abondamment présents dans la fibre. Récemment, le laboratoire de Frank Schnorrer a montré que les sarcomères des muscles du vol ont la capacité de se diviser au cours du développement en réponse à des tensions mécaniques (Rodier et al. 2025b). Nous pouvons donc spéculer que ce même processus de

division pourrait être mobilisé pour réparer les sarcomères endommagés, et que la forte production de MHC serait nécessaire pour structurer ces sarcomères néosynthétisés.

Réparation vs régénération des muscles adultes de la Drosophile

En réponse à des lésions externes ou à un dysfonctionnement physiologique, les organismes mettent en place divers processus et stratégies biologiques, tels que la cicatrisation, la réparation tissulaire, la régénération ou encore le renouvellement cellulaire, afin de préserver leur intégrité structurelle et de maintenir une stabilité fonctionnelle après un traumatisme (Arenas Gómez et al. 2020). Ces capacités de régénération et de réparation varient considérablement entre les espèces animales, en raison d'une combinaison de facteurs évolutifs, génétiques, développementaux et physiologiques (Alibardi 2024). En effet, bien que des capacités régénératives remarquables soient généralement observées chez les espèces aquatiques ou amphibies, les invertébrés et les vertébrés terrestres semblent limités à des processus réparateurs tels que la cicatrisation, la régénération partielle ou la cicatrisation (Alibardi 2024).

Nos résultats indiquent que, suite à une lésion, les IFMs de *Drosophile* subissent un processus de réparation mais ne régénèrent pas pleinement. Les MuSCs ne sont pas activées et le muscle ne retrouve pas son état initial, même après 20 jours. Cette capacité régénérative limitée contraste avec des tissus comme l'intestin, où la forte prolifération des cellules souches assure un remplacement efficace des cellules endommagées (Jiang et Edgar 2011; Perochon et al. 2021).

Par ailleurs, cette faible capacité régénérative pourrait être liée à la courte durée de vie de l'organisme. La *Drosophile* vit environs trois mois, ce qui pourrait ne pas avoir exercé de pression évolutive suffisante pour développer des mécanismes régénératifs performants ou des processus de maintenance tissulaire à long terme à l'âge adulte (Kirkwood 2005). Nos travaux révèlent que, si les cellules immunitaires contribuent au maintien de l'intégrité musculaire, le système immunitaire inné de la *Drosophile* ne dispose pas de la régulation complexe observée chez les mammifères ou les salamandres, qui soutient activement la régénération (Bolaños-Castro et al. 2021; Wang et Zhou 2022b). La réponse des cellules immunitaires favorise principalement

la consolidation du tissue musculaire par une forte production de protéines ECM, plutôt que la régénération musculaire complète.

IV. Références bibliographiques

« A Theory of Tracheal Respiration in Insects ». 1930. *Proceedings of the Royal Society of London. Series B, Containing Papers of a Biological Character* 106 (743): 229-50. https://doi.org/10.1098/rspb.1930.0024.

Affolter, Markus, et Emmanuel Caussinus. 2008. « Tracheal Branching Morphogenesis in *Drosophila* : New Insights into Cell Behaviour and Organ Architecture ». *Development* 135 (12): 2055-64. https://doi.org/10.1242/dev.014498.

Affolter, Markus, Jacques Montagne, Uwe Walldorf, et al. 1994. « The *Drosophila* SRF Homolog Is Expressed in a Subset of Tracheal Cells and Maps within a Genomic Region Required for Tracheal Development ». *Development* 120 (4): 743-53. https://doi.org/10.1242/dev.120.4.743.

Ahmad, Khurshid, Sibhghatulla Shaikh, Hee Jin Chun, et al. 2023. « Extracellular Matrix: The Critical Contributor to Skeletal Muscle Regeneration—a Comprehensive Review ». *Inflammation and Regeneration* 43 (1): 58. https://doi.org/10.1186/s41232-023-00308-z.

Akhouayri, Idir, Claire Turc, Julien Royet, et Bernard Charroux. 2011. « Toll-8/Tollo Negatively Regulates Antimicrobial Response in the Drosophila Respiratory Epithelium ». *PLoS Pathogens* 7 (10): e1002319. https://doi.org/10.1371/journal.ppat.1002319.

Al, Burcu, Tsz K. Suen, Katarzyna Placek, et Mihai G. Netea. 2023. « Innate (Learned) Memory ». *Journal of Allergy and Clinical Immunology* 152 (3): 551-66. https://doi.org/10.1016/j.jaci.2023.06.014.

Alibardi, Lorenzo. 2024. « Regeneration, Regengrow and Tissue Repair in Animals: Evolution Indicates That No Regeneration Occurs in Terrestrial Environments but Only Recovery Healing ». *Journal of Developmental Biology* 13 (1): 2. https://doi.org/10.3390/jdb13010002.

Allen, James, Mark Ramsden, et Sohail Nisar. 2024. « Skeletal Muscle Structure, Function and Pathology ». *Orthopaedics and Trauma* 38 (3): 137-44. https://doi.org/10.1016/j.mporth.2024.03.004.

Ammar, Nourhene, Olivier Josse, Aurélien Guillou, Jessica Perochon, et Hadi Boukhatmi. 2025. « Immune–Tracheal Intercellular Signalling Coordinates the Muscle Injury Response in *Drosophila* ». Prépublication, Developmental Biology, juin 25. https://doi.org/10.1101/2025.06.25.661466.

Anderl, Ines, Laura Vesala, Teemu O. Ihalainen, et al. 2016. « Transdifferentiation and Proliferation in Two Distinct Hemocyte Lineages in Drosophila Melanogaster Larvae after Wasp Infection ». *PLOS Pathogens* 12 (7): e1005746. https://doi.org/10.1371/journal.ppat.1005746.

Apidianakis, Yiorgos, Michael N. Mindrinos, Wenzhong Xiao, et al. 2007. « Involvement of Skeletal Muscle Gene Regulatory Network in Susceptibility to Wound Infection Following Trauma ». *PLoS ONE* 2 (12): e1356. https://doi.org/10.1371/journal.pone.0001356.

Arenas Gómez, Claudia M., Keith Z. Sabin, et Karen Echeverri. 2020. « Wound Healing across the Animal Kingdom: Crosstalk between the Immune System and the Extracellular Matrix ». *Developmental Dynamics* 249 (7): 834-46. https://doi.org/10.1002/dvdy.178.

Atreya, Krishan B., et Joyce J. Fernandes. 2008. « Founder Cells Regulate Fiber Number but Not Fiber Formation during Adult Myogenesis in Drosophila ». *Developmental Biology* 321 (1): 123-40. https://doi.org/10.1016/j.ydbio.2008.06.023.

Avellaneda, Jerome, Clement Rodier, Fabrice Daian, et al. 2021. « Myofibril and Mitochondria Morphogenesis Are Coordinated by a Mechanical Feedback Mechanism in Muscle ». *Nature Communications* 12 (1). https://doi.org/10.1038/s41467-021-22058-7.

Ayyaz, Arshad, Hongjie Li, et Heinrich Jasper. 2015. « Haemocytes Control Stem Cell Activity in the Drosophila Intestine ». *Nature Cell Biology* 17 (6): 736-48. https://doi.org/10.1038/ncb3174.

Aztekin, Can. 2024. « Mechanisms of Regeneration: To What Extent Do They Recapitulate Development? » *Development* 151 (14): dev202541. https://doi.org/10.1242/dev.202541.

Balakrishnan, Mridula, Shannon F. Yu, Samantha M. Chin, et al. 2020. « Cofilin Loss in Drosophila Muscles Contributes to Muscle Weakness through Defective Sarcomerogenesis during Muscle Growth ». *Cell Reports* 32 (3): 107893. https://doi.org/10.1016/j.celrep.2020.107893.

Balasubramanian, Krishnakumar, et Alan J. Schroit. 2003. « Aminophospholipid Asymmetry: A Matter of Life and Death ». *Annual Review of Physiology* 65 (1): 701-34. https://doi.org/10.1146/annurev.physiol.65.092101.142459.

Banerjee, Utpal, Juliet R Girard, Lauren M Goins, et Carrie M Spratford. 2019. « *Drosophila* as a Genetic Model for Hematopoiesis ». *Genetics* 211 (2): 367-417. https://doi.org/10.1534/genetics.118.300223.

Bate, Michael, et Kendal Broadie. 1995. « Wiring by Fly: The Neuromuscular System of the Drosophila Embryo ». *Neuron* 15 (3): 513-25. https://doi.org/10.1016/0896-6273(95)90141-8.

Beckett, Karen, et Mary K. Baylies. 2007. « 3D Analysis of Founder Cell and Fusion Competent Myoblast Arrangements Outlines a New Model of Myoblast Fusion ». *Developmental Biology* 309 (1): 113-25. https://doi.org/10.1016/j.ydbio.2007.06.024.

Bernard, Frédéric, Petar Kasherov, Sabrina Grenetier, et al. 2009. « Integration of Differentiation Signals during Indirect Flight Muscle Formation by a Novel Enhancer of Drosophila Vestigial Gene ». *Developmental Biology* 332 (2): 258-72. https://doi.org/10.1016/j.ydbio.2009.05.573.

Binggeli, Olivier, Claudine Neyen, Mickael Poidevin, et Bruno Lemaitre. 2014. « Prophenoloxidase Activation Is Required for Survival to Microbial Infections in Drosophila ». *PLoS Pathogens* 10 (5): e1004067. https://doi.org/10.1371/journal.ppat.1004067.

Bolaños-Castro, Lizbeth Airais, Hannah Elisabeth Walters, Rubén Octavio García Vázquez, et Maximina Hee Yun. 2021. « Immunity in Salamander Regeneration: Where Are We Standing and Where Are We Headed? » *Developmental Dynamics: An Official Publication of the American Association of Anatomists* 250 (6): 753-67. https://doi.org/10.1002/dvdy.251.

Bossen, Judith, Reshmi Raveendran, Jingjing He, et Thomas Roeder. 2024. « Terminal Tracheal Cells of *Drosophila* Are Immune Privileged to Maintain Their Foxo-Dependent Structural Plasticity ». Prépublication, août 23. https://doi.org/10.1101/2024.08.22.609264.

Boube, Muriel, Marta Llimargas, et Jordi Casanova. 2000. « Cross-Regulatory Interactions among Tracheal Genes Support a Co-Operative Model for the Induction of Tracheal Fates in the Drosophila Embryo ». *Mechanisms of Development* 91 (1-2): 271-78. https://doi.org/10.1016/S0925-4773(99)00315-9.

Boube, Muriel, Maria D. Martin-Bermudo, Nicholas H. Brown, et Jordi Casanova. 2001. « Specific Tracheal Migration Is Mediated by Complementary Expression of Cell Surface Proteins ». *Genes & Development* 15 (12): 1554-62. https://doi.org/10.1101/gad.195501.

Boukhatmi, Hadi. 2021. « Drosophila, an Integrative Model to Study the Features of Muscle Stem Cells in Development and Regeneration ». *Cells* 10 (8): 2112. https://doi.org/10.3390/cells10082112.

Boukhatmi, Hadi, et Sarah Bray. 2018. « A Population of Adult Satellite-like Cells in Drosophila Is Maintained through a Switch in RNA-Isoforms ». *eLife* 7 (avril). https://doi.org/10.7554/elife.35954.

Boukhatmi, Hadi, Torcato Martins, Zoe Pillidge, Tsveta Kamenova, et Sarah Bray. 2020. « Notch Mediates Inter-Tissue Communication to Promote Tumorigenesis ». *Current Biology* 30 (10): 1809-1820.e4. https://doi.org/10.1016/j.cub.2020.02.088.

Boulet, Manon, Yoan Renaud, François Lapraz, Billel Benmimoun, Laurence Vandel, et Lucas Waltzer. 2021. « Characterization of the Drosophila Adult Hematopoietic System Reveals a Rare Cell Population With Differentiation and Proliferation Potential ». *Frontiers in Cell and Developmental Biology* 9 (octobre): 739357. https://doi.org/10.3389/fcell.2021.739357.

Brennan, Keith, Mary Baylies, et Alfonso Martinez Arias. 1999. « Repression by Notch Is Required before Wingless Signalling during Muscle Progenitor Cell Development in Drosophila ». *Current Biology* 9 (13): 707-S1. https://doi.org/10.1016/s0960-9822(99)80313-3.

Broadie, Kendal, et Michael Bate. 1993. « Muscle Development Is Independent of Innervation during *Drosophila* Embryogenesis ». *Development* 119 (2): 533-43. https://doi.org/10.1242/dev.119.2.533.

Brodu, Véronique, et Jordi Casanova. 2006. « The RhoGAP *Crossveinless-c* Links *Trachealess* and EGFR Signaling to Cell Shape Remodeling in *Drosophila* Tracheal Invagination ». *Genes & Development* 20 (13): 1817-28. https://doi.org/10.1101/gad.375706.

Brooks, Elliot C., Martin P. Zeidler, Albert C. M. Ong, et Iwan R. Evans. 2024. « Macrophage subpopulation identity in Drosophila is modulated by apoptotic cell clearance and related signalling pathways ». *Frontiers in Immunology* 14 (janvier): 1310117. https://doi.org/10.3389/fimmu.2023.1310117.

Bryantsev, Anton L., Sandy Duong, Tonya M. Brunetti, et al. 2012. « Extradenticle and Homothorax Control Adult Muscle Fiber Identity in Drosophila ». *Developmental Cell* 23 (3): 664-73. https://doi.org/10.1016/j.devcel.2012.08.004.

Buchon, Nicolas, Neal Silverman, et Sara Cherry. 2014a. « Immunity in Drosophila Melanogaster — from Microbial Recognition to Whole-Organism Physiology ». *Nature Reviews Immunology* 14 (12): 796-810. https://doi.org/10.1038/nri3763.

Buchon, Nicolas, Neal Silverman, et Sara Cherry. 2014b. « Immunity in Drosophila Melanogaster — from Microbial Recognition to Whole-Organism Physiology ». *Nature Reviews Immunology* 14 (12): 796-810. https://doi.org/10.1038/nri3763.

Bunt, Stephanie, Clare Hooley, Nan Hu, Catherine Scahill, Helen Weavers, et Helen Skaer. 2010. « Hemocyte-Secreted Type IV Collagen Enhances BMP Signaling to Guide Renal Tubule Morphogenesis in Drosophila ». *Developmental Cell* 19 (2): 296-306. https://doi.org/10.1016/j.devcel.2010.07.019.

Cabernard, Clemens, et Markus Affolter. 2005. « Distinct Roles for Two Receptor Tyrosine Kinases in Epithelial Branching Morphogenesis in Drosophila ». *Developmental Cell* 9 (6): 831-42. https://doi.org/10.1016/j.devcel.2005.10.008.

Caine, Charlotte, Petar Kasherov, Joël Silber, et Alexis Lalouette. 2014. « Mef2 Interacts with the Notch Pathway during Adult Muscle Development in Drosophila Melanogaster ». *PLoS ONE* 9 (9): e108149. https://doi.org/10.1371/journal.pone.0108149.

Carmena, A, M Bate, et F Jiménez. 1995. « Lethal of Scute, a Proneural Gene, Participates in the Specification of Muscle Progenitors during Drosophila Embryogenesis. » *Genes & Development* 9 (19): 2373-83. https://doi.org/10.1101/gad.9.19.2373.

Carmena, A., B. Murugasu-Oei, D. Menon, F. Jimenez, et W. Chia. 1998. « Inscuteable and Numb Mediate Asymmetric Muscle Progenitor Cell Divisions during Drosophila Myogenesis ». *Genes & Development* 12 (3): 304-15. https://doi.org/10.1101/gad.12.3.304.

Carmena, Ana, Stephen Gisselbrecht, Jacob Harrison, Fernando Jiménez, et Alan M. Michelson. 1998. « Combinatorial Signaling Codes for the Progressive Determination of Cell Fates in the *Drosophila* Embryonic Mesoderm ». *Genes & Development* 12 (24): 3910-22. https://doi.org/10.1101/gad.12.24.3910.

Catalani, Elisabetta, Silvia Zecchini, Matteo Giovarelli, et al. 2022. « RACK1 Is Evolutionary Conserved in Satellite Stem Cell Activation and Adult Skeletal Muscle Regeneration ». *Cell Death Discovery* 8 (1). https://doi.org/10.1038/s41420-022-01250-8.

Cattenoz, Pierre B, Rosy Sakr, Alexia Pavlidaki, et al. 2020. « Temporal Specificity and Heterogeneity of *Drosophila* Immune Cells ». *The EMBO Journal* 39 (12): e104486. https://doi.org/10.15252/embj.2020104486.

Caussinus, Emmanuel, Julien Colombelli, et Markus Affolter. 2008. « Tip-Cell Migration Controls Stalk-Cell Intercalation during Drosophila Tracheal Tube Elongation ». *Current Biology* 18 (22): 1727-34. https://doi.org/10.1016/j.cub.2008.10.062.

Centanin, Lázaro, Andrés Dekanty, Nuria Romero, Maximiliano Irisarri, Thomas A. Gorr, et Pablo Wappner. 2008. « Cell Autonomy of HIF Effects in Drosophila: Tracheal Cells Sense Hypoxia and Induce Terminal Branch Sprouting ». *Developmental Cell* 14 (4): 547-58. https://doi.org/10.1016/j.devcel.2008.01.020.

Centanin, Lazaro, Thomas A. Gorr, et Pablo Wappner. 2010. « Tracheal Remodelling in Response to Hypoxia ». *Journal of Insect Physiology* 56 (5): 447-54. https://doi.org/10.1016/j.jinsphys.2009.05.008.

Chakrabarti, Sveta, et Sandhya S. Visweswariah. 2020. « Intramacrophage ROS Primes the Innate Immune System via JAK/STAT and Toll Activation ». *Cell Reports* 33 (6): 108368. https://doi.org/10.1016/j.celrep.2020.108368.

Chanana, Bhavna, Roland Graf, Tatyana Koledachkina, Ralf Pflanz, et Gerd Vorbrüggen. 2007. « αPS2 Integrin-Mediated Muscle Attachment in Drosophila Requires the ECM Protein Thrombospondin ». *Mechanisms of Development* 124 (6): 463-75. https://doi.org/10.1016/j.mod.2007.03.005.

Chatterjee, Nirmalya, et Norbert Perrimon. 2021. « What Fuels the Fly: Energy Metabolism in *Drosophila* and Its Application to the Study of Obesity and Diabetes ». *Science Advances* 7 (24). https://doi.org/10.1126/sciadv.abg4336.

Chaturvedi, Dhananjay, Heinrich Reichert, Rajesh D Gunage, et K VijayRaghavan. 2017. « Identification and Functional Characterization of Muscle Satellite Cells in Drosophila ». *eLife* 6 (octobre). https://doi.org/10.7554/elife.30107.

Chechenova, Maria, Lilla McLendon, Bracey Dallas, et al. 2024. « Muscle Degeneration in Aging Drosophila Flies: The Role of Mechanical Stress ». *Skeletal Muscle* 14 (1). https://doi.org/10.1186/s13395-024-00352-4.

Chen, Chao-Kung, Ronald P. Kühnlein, Karsten G. Eulenberg, Stéphane Vincent, Markus Affolter, et Reinhard Schuh. 1998. « The Transcription Factors KNIRPS and KNIRPS RELATED Control Cell Migration and Branch Morphogenesis during *Drosophila* Tracheal Development ». *Development* 125 (24): 4959-68. https://doi.org/10.1242/dev.125.24.4959.

Chen, Grace Y., et Gabriel Nuñez. 2010. « Sterile Inflammation: Sensing and Reacting to Damage ». *Nature Reviews Immunology* 10 (12): 826-37. https://doi.org/10.1038/nri2873.

Chihara, Takahiro, et Shigeo Hayashi. 2000. « Control of Tracheal Tubulogenesis by Wingless Signaling ». *Development* 127 (20): 4433-42. https://doi.org/10.1242/dev.127.20.4433.

Chu, Wei-Chen, et Shigeo Hayashi. 2021. « Mechano-Chemical Enforcement of Tendon Apical ECM into Nano-Filaments during Drosophila Flight Muscle Development ». *Current Biology* 31 (7): 1366-1378.e7. https://doi.org/10.1016/j.cub.2021.01.010.

Contreras, Osvaldo, Fabio M. V. Rossi, et Marine Theret. 2021. « Origins, Potency, and Heterogeneity of Skeletal Muscle Fibro-Adipogenic Progenitors—Time for New Definitions ». *Skeletal Muscle* 11 (1). https://doi.org/10.1186/s13395-021-00265-6.

Crozatier, Michèle, et Marie Meister. 2007. « Drosophila Haematopoiesis ». *Cellular Microbiology* 9 (5): 1117-26. https://doi.org/10.1111/j.1462-5822.2007.00930.x.

Cruz, Josefa, Neus Bota-Rabassedas, et Xavier Franch-Marro. 2015. « FGF Coordinates Air Sac Development by Activation of the EGF Ligand Vein through the Transcription Factor PntP2 ». *Scientific Reports* 5 (1). https://doi.org/10.1038/srep17806.

Currie, Douglas A., et Michael Bate. 1991. « The Development of Adult Abdominal Muscles in *Drosophila:* Myoblasts Express *Twist* and Are Associated with Nerves ». *Development* 113 (1): 91-102. https://doi.org/10.1242/dev.113.1.91.

Demontis, Fabio, et Norbert Perrimon. 2009. « Integration of Insulin Receptor/Foxo Signaling and dMyc Activity during Muscle Growth Regulates Body Size in*Drosophila* ». *Development* 136 (6): 983-93. https://doi.org/10.1242/dev.027466.

Demontis, Fabio, et Norbert Perrimon. 2010. « FOXO/4E-BP Signaling in Drosophila Muscles Regulates Organism-Wide Proteostasis during Aging ». *Cell* 143 (5): 813-25. https://doi.org/10.1016/j.cell.2010.10.007.

Dennis, Robert G., et Paul E. Kosnik, Ii. 2000. « EXCITABILITY AND ISOMETRIC CONTRACTILE PROPERTIES OF MAMMALIAN SKELETAL MUSCLE CONSTRUCTS ENGINEERED IN VITRO ». *In Vitro Cellular & Developmental Biology - Animal* 36 (5): 327. https://doi.org/10.1290/1071-2690(2000)036%253C0327:eaicpo%253E2.0.co;2.

Dobi, Krista C., Victoria K. Schulman, et Mary K. Baylies. 2015. « Specification of the Somatic Musculature in Drosophila ». *Wiley Interdisciplinary Reviews. Developmental Biology* 4 (4): 357-75. https://doi.org/10.1002/wdev.182.

Domsch, Katrin, Andreas Acs, Claudia Obermeier, Hanh T. Nguyen, et Ingolf Reim. 2017. « Identification of the Essential Protein Domains for Mib2 Function during the Development of the Drosophila Larval Musculature and Adult Flight Muscles ». *PLOS ONE* 12 (3): e0173733. https://doi.org/10.1371/journal.pone.0173733.

Dossenbach, Caroline, Salome Röck, et Markus Affolter. 2001. « Specificity of FGF Signaling in Cell Migration in *Drosophila* ». *Development* 128 (22): 4563-72. https://doi.org/10.1242/dev.128.22.4563.

Du, Hongqing, Chung-Hsuan Shih, Michael N. Wosczyna, et al. 2017. « Macrophage-Released ADAMTS1 Promotes Muscle Stem Cell Activation ». *Nature Communications* 8 (1). https://doi.org/10.1038/s41467-017-00522-7.

Du, Lijuan, Alex Sohr, Yujia Li, et Sougata Roy. 2022. « GPI-Anchored FGF Directs Cytoneme-Mediated Bidirectional Contacts to Regulate Its Tissue-Specific Dispersion ». *Nature Communications* 13 (1): 3482. https://doi.org/10.1038/s41467-022-30417-1.

Dudzic, Jan P., Shu Kondo, Ryu Ueda, Casey M. Bergman, et Bruno Lemaitre. 2015. « Drosophila Innate Immunity: Regional and Functional Specialization of Prophenoloxidases ». *BMC Biology* 13 (1): 81. https://doi.org/10.1186/s12915-015-0193-6.

Dutta, Devkanya, Sumita Anant, Mar Ruiz-Gomez, Michael Bate, et K. VijayRaghavan. 2004. « Founder Myoblasts and Fibre Number during Adult Myogenesis in*Drosophila* ». *Development* 131 (15): 3761-72. https://doi.org/10.1242/dev.01249.

Ellis, Ronald E., Junying Yuan, et H. Robert Horvitz. 1991. « Mechanisms and Functions of Cell Death ». *Annual Review of Cell Biology* 7 (1): 663-98. https://doi.org/10.1146/annurev.cb.07.110191.003311.

Etchegaray, Jon Iker, Emma J. Elguero, Jennifer A. Tran, Vincent Sinatra, Mel B. Feany, et Kimberly McCall. 2016. « Defective Phagocytic Corpse Processing Results in Neurodegeneration and Can Be Rescued by TORC1 Activation ». *The Journal of Neuroscience* 36 (11): 3170-83. https://doi.org/10.1523/jneurosci.1912-15.2016.

Everetts, Nicholas J, Melanie I Worley, Riku Yasutomi, Nir Yosef, et Iswar K Hariharan. 2021. « Single-Cell Transcriptomics of the Drosophila Wing Disc Reveals Instructive Epithelium-to-Myoblast Interactions ». *eLife* 10 (mars). https://doi.org/10.7554/elife.61276.

Fernandes, J. 1995. « Neuromuscular development in Drosophila: insights from embryos and pupae ». *Current Opinion in Neurobiology* 5 (1): 10-18. https://doi.org/10.1016/0959-4388(95)80081-6.

Fernandes, Joyce, Michael Bate, et K. Vijayraghavan. 1991. « Development of the Indirect Flight Muscles of *Drosophila* ». *Development* 113 (1): 67-77. https://doi.org/10.1242/dev.113.1.67.

Fernandes, Joyce J., Susan E. Celniker, et K. VijayRaghavan. 1996. « Development of the Indirect Flight Muscle Attachment Sites inDrosophila:Role of the PS Integrins and thestripeGene ». *Developmental Biology* 176 (2): 166-84. https://doi.org/10.1006/dbio.1996.0125.

Fernandes, Joyce J., et Haig Keshishian. 1996. « Patterning the Dorsal Longitudinal Flight Muscles (DLM) of *Drosophila*: Insights from the Ablation of Larval Scaffolds ». *Development* 122 (12): 3755-63. https://doi.org/10.1242/dev.122.12.3755.

Fernandes, Joyce J., et Haig Keshishian. 2005. « Motoneurons Regulate Myoblast Proliferation and Patterning in Drosophila ». *Developmental Biology* 277 (2): 493-505. https://doi.org/10.1016/j.ydbio.2004.09.038.

Fernandes, Joyce, et K. VijayRaghavan. 1993. « The Development of Indirect Flight Muscle Innervation in *Drosophila Melanogaster* ». *Development* 118 (1): 215-27. https://doi.org/10.1242/dev.118.1.215.

Ferrandon, D. 1998. « A drosomycin-GFP reporter transgene reveals a local immune response in Drosophila that is not dependent on the Toll pathway ». *The EMBO Journal* 17 (5): 1217-27. https://doi.org/10.1093/emboj/17.5.1217.

Fiore, Daniela, Robert N. Judson, Marcela Low, et al. 2016. « Pharmacological Blockage of Fibro/Adipogenic Progenitor Expansion and Suppression of Regenerative Fibrogenesis Is Associated with Impaired Skeletal Muscle Regeneration ». *Stem Cell Research* 17 (1): 161-69. https://doi.org/10.1016/j.scr.2016.06.007.

Fisher, Lucas A. B., Belén Carriquí-Madroñal, Tiara Mulder, Sven Huelsmann, Frieder Schöck, et Nicanor González-Morales. 2024. « Filamin Protects Myofibrils from Contractile Damage through Changes in Its Mechanosensory Region ». *PLOS Genetics* 20 (6): e1011101. https://doi.org/10.1371/journal.pgen.1011101.

Floriano, Juliana Ferreira, Costanza Emanueli, Sofia Vega, et al. 2022. « Pro-Angiogenic Approach for Skeletal Muscle Regeneration ». *Biochimica et Biophysica Acta (BBA) - General Subjects* 1866 (2): 130059. https://doi.org/10.1016/j.bbagen.2021.130059.

Foley, Edan, et Patrick H. O'Farrell. 2003. « Nitric Oxide Contributes to Induction of Innate Immune Responses to Gram-Negative Bacteria in *Drosophila* ». *Genes & Development* 17 (1): 115-25. https://doi.org/10.1101/gad.1018503.

Forcina, Laura, Marianna Cosentino, et Antonio Musarò. 2020. « Mechanisms Regulating Muscle Regeneration: Insights into the Interrelated and Time-Dependent Phases of Tissue Healing ». *Cells* 9 (5): 1297. https://doi.org/10.3390/cells9051297.

Fry, Christopher S, Jonah D Lee, Jyothi Mula, et al. 2015. « Inducible Depletion of Satellite Cells in Adult, Sedentary Mice Impairs Muscle Regenerative Capacity without Affecting Sarcopenia ». *Nature Medicine* 21 (1): 76-80. https://doi.org/10.1038/nm.3710.

Gervais, Louis, et Jordi Casanova. 2011. « The *Drosophila* Homologue of SRF Acts as a Boosting Mechanism to Sustain FGF-Induced Terminal Branching in the Tracheal System ». *Development* 138 (7): 1269-74. https://doi.org/10.1242/dev.059188.

Ghabrial, Amin, Stefan Luschnig, Mark M. Metzstein, et Mark A. Krasnow. 2003. « Branching Morphogenesis of the *Drosophila* Tracheal System ». *Annual Review of Cell and Developmental Biology* 19 (1): 623-47. https://doi.org/10.1146/annurev.cellbio.19.031403.160043.

Ghabrial, Amin S., et Mark A. Krasnow. 2006a. « Social Interactions among Epithelial Cells during Tracheal Branching Morphogenesis ». *Nature* 441 (7094): 746-49. https://doi.org/10.1038/nature04829.

Ghabrial, Amin S., et Mark A. Krasnow. 2006b. « Social Interactions among Epithelial Cells during Tracheal Branching Morphogenesis ». *Nature* 441 (7094): 746-49. https://doi.org/10.1038/nature04829.

Ghazi, Arjumand, Litty Paul, et K. VijayRaghavan. 2003. « Prepattern Genes and Signaling Molecules Regulate Stripe Expression to Specify Drosophila Flight Muscle Attachment Sites ». *Mechanisms of Development* 120 (5): 519-28. https://doi.org/10.1016/s0925-4773(03)00042-x.

Ghosh, Saikat, Sudip Mandal, et Lolitika Mandal. 2018. « Detecting Proliferation of Adult Hemocytes in Drosophila by BrdU Incorporation and PH3 Expression in Response to Bacterial Infection ». *Wellcome Open Research* 3 (août): 47. https://doi.org/10.12688/wellcomeopenres.14560.2.

Girardot, Fabrice, Christelle Lasbleiz, Véronique Monnier, et Hervé Tricoire. 2006. « Specific Age Related Signatures in Drosophila Body Parts Transcriptome ». *BMC Genomics* 7 (1). https://doi.org/10.1186/1471-2164-7-69.

Goh, Kah Yong, Wen Xing Lee, Sze Mun Choy, et al. 2024. « FOXO-Regulated DEAF1 Controls Muscle Regeneration through Autophagy ». *Autophagy* 20 (12): 2632-54. https://doi.org/10.1080/15548627.2024.2374693.

Gold, Katrina S., et Katja Brückner. 2015. « Macrophages and Cellular Immunity in Drosophila Melanogaster ». *Seminars in Immunology* 27 (6): 357-68. https://doi.org/10.1016/j.smim.2016.03.010.

Götz, Karl G. 1987. « Course-Control, Metabolism and Wing Interference During Ultralong Tethered Flight in *Drosophila Melanogaster* ». *Journal of Experimental Biology* 128 (1): 35-46. https://doi.org/10.1242/jeb.128.1.35.

Guha, Arjun, et Thomas B. Kornberg. 2005. « Tracheal Branch Repopulation Precedes Induction of the Drosophila Dorsal Air Sac Primordium ». *Developmental Biology* 287 (1): 192-200. https://doi.org/10.1016/j.ydbio.2005.09.005.

Guillemin, Karen, Jay Groppe, Klaus Dücker, et al. 1996. « The *Pruned* Gene Encodes the *Drosophila* Serum Response Factor and Regulates Cytoplasmic Outgrowth during Terminal Branching of the Tracheal System ». *Development* 122 (5): 1353-62. https://doi.org/10.1242/dev.122.5.1353.

Guillou, Aurélien, Katia Troha, Hui Wang, Nathalie C. Franc, et Nicolas Buchon. 2016. « The Drosophila CD36 Homologue Croquemort Is Required to Maintain Immune and Gut Homeostasis during Development and Aging ». *PLOS Pathogens* 12 (10): e1005961. https://doi.org/10.1371/journal.ppat.1005961.

Gunage, Rajesh D., Nagaraju Dhanyasi, Heinrich Reichert, et K. VijayRaghavan. 2017. « Drosophila Adult Muscle Development and Regeneration ». *Seminars in Cell & Developmental Biology* 72 (décembre): 56-66. https://doi.org/10.1016/j.semcdb.2017.11.017.

Gunage, Rajesh D, Heinrich Reichert, et K VijayRaghavan. 2014. « Identification of a New Stem Cell Population That Generates Drosophila Flight Muscles ». *eLife* 3 (août). https://doi.org/10.7554/elife.03126.

Hamer, P. W., J. M. McGeachie, M. J. Davies, et M. D. Grounds. 2002. « Evans Blue Dye as an *in Vivo* Marker of Myofibre Damage: Optimising Parameters for Detecting Initial Myofibre Membrane Permeability ». *Journal of Anatomy* 200 (1): 69-79. https://doi.org/10.1046/j.0021-8782.2001.00008.x.

Hanson, Mark Austin, Anna Dostálová, Camilla Ceroni, Mickael Poidevin, Shu Kondo, et Bruno Lemaitre. 2019. « Synergy and Remarkable Specificity of Antimicrobial Peptides in Vivo Using a Systematic Knockout Approach ». *eLife* 8 (février): e44341. https://doi.org/10.7554/eLife.44341.

Hanson, Mark Austin, et Bruno Lemaitre. 2020. « New Insights on Drosophila Antimicrobial Peptide Function in Host Defense and Beyond ». *Current Opinion in Immunology* 62 (février): 22-30. https://doi.org/10.1016/j.coi.2019.11.008.

Harrison, Jon F. 2009. « Tracheal System ». In *Encyclopedia of Insects*. Elsevier. https://doi.org/10.1016/B978-0-12-374144-8.00265-4.

Hayashi, Shigeo, et Takefumi Kondo. 2018. « Development and Function of the *Drosophila* Tracheal System ». *Genetics* 209 (2): 367-80. https://doi.org/10.1534/genetics.117.300167.

Henry, Joanna R., et Jon F. Harrison. 2004. « Plastic and Evolved Responses of Larval Tracheae and Mass to Varying Atmospheric Oxygen Content in*Drosophila Melanogaster* ». *Journal of Experimental Biology* 207 (20): 3559-67. https://doi.org/10.1242/jeb.01189.

Hirooka, Eri, Ryo Hattori, Keisuke Ikawa, et al. 2025. « Macrophages Promote Tumor Growth by Phagocytosis-Mediated Cytokine Amplification in Drosophila ». *Current Biology* 35 (13): 3209-3227.e6. https://doi.org/10.1016/j.cub.2025.05.068.

Honti, Viktor, Gábor Csordás, Róbert Márkus, Éva Kurucz, Ferenc Jankovics, et István Andó. 2010. « Cell Lineage Tracing Reveals the Plasticity of the Hemocyte Lineages and of the Hematopoietic Compartments in Drosophila Melanogaster ». *Molecular Immunology* 47 (11-12): 1997-2004. https://doi.org/10.1016/j.molimm.2010.04.017.

Hultmark, Dan, et István Andó. 2022. « Hematopoietic Plasticity Mapped in Drosophila and Other Insects ». *eLife* 11 (août): e78906. https://doi.org/10.7554/eLife.78906.

Ikeya, Tomoatsu, et Shigeo Hayashi. 1999. « Interplay of Notch and FGF Signaling Restricts Cell Fate and MAPK Activation in the *Drosophila* Trachea ». *Development* 126 (20): 4455-63. https://doi.org/10.1242/dev.126.20.4455.

Inaki, Mikiko, Makiko Shinza-Kameda, Afshan Ismat, Manfred Frasch, et Akinao Nose. 2010. « *Drosophila* Tey Represses Transcription of the Repulsive Cue Toll and Generates Neuromuscular Target Specificity ». *Development* 137 (13): 2139-46. https://doi.org/10.1242/dev.046672.

Jacobsen, Nicole L., Aaron B. Morton, et Steven S. Segal. 2023. « Angiogenesis Precedes Myogenesis during Regeneration Following Biopsy Injury of Skeletal Muscle ». *Skeletal Muscle* 13 (1). https://doi.org/10.1186/s13395-023-00313-3.

Jaramillo, MaryAnn S., Candice V. Lovato, Erica M. Baca, et Richard M. Cripps. 2009. « Crossveinless and the TGFβ Pathway Regulate Fiber Number in the*Drosophila*Adult Jump Muscle ». *Development* 136 (7): 1105-13. https://doi.org/10.1242/dev.031567.

Jarecki, Jill, Eric Johnson, et Mark A Krasnow. 1999. « Oxygen Regulation of Airway Branching in Drosophila Is Mediated by Branchless FGF ». *Cell* 99 (2): 211-20. https://doi.org/10.1016/S0092-8674(00)81652-9.

Jia, Xi-Xi, Michael Gorczyca, et Vivian Budnik. 1993. « Ultrastructure of Neuromuscular Junctions in *Drosophila*: Comparison of Wild Type and Mutants with Increased Excitability ». *Journal of Neurobiology* 24 (8): 1025-44. https://doi.org/10.1002/neu.480240804.

Jiang, Huaqi, et Bruce A. Edgar. 2011. « Intestinal Stem Cells in the Adult Drosophila Midgut ». *Experimental Cell Research* 317 (19): 2780-88. https://doi.org/10.1016/j.yexcr.2011.07.020.

Jiang, Lan, et Stephen T. Crews. 2003. « The *Drosophila Dysfusion* Basic Helix-Loop-Helix (bHLH)–PAS Gene Controls Tracheal Fusion and Levels of the Trachealess bHLH-PAS Protein ». *Molecular and Cellular Biology* 23 (16): 5625-37. https://doi.org/10.1128/MCB.23.16.5625-5637.2003.

Jiang, Lan, et Stephen T. Crews. 2006. « *Dysfusion* Transcriptional Control of *Drosophila* Tracheal Migration, Adhesion, and Fusion ». *Molecular and Cellular Biology* 26 (17): 6547-56. https://doi.org/10.1128/MCB.00284-06.

Jung, Seung-Hye, Cory J. Evans, Christine Uemura, et Utpal Banerjee. 2005. « The *Drosophila* Lymph Gland as a Developmental Model of Hematopoiesis ». *Development* 132 (11): 2521-33. https://doi.org/10.1242/dev.01837.

Junion, Guillaume, et Krzysztof Jagla. 2022. « Diversification of Muscle Types in Drosophila Embryos ». *Experimental Cell Research* 410 (1): 112950. https://doi.org/10.1016/j.yexcr.2021.112950.

Karunendiran, Abiramy, Christine T. Nguyen, Virginijus Barzda, et Bryan A. Stewart. 2021. « Disruption of Drosophila Larval Muscle Structure and Function by UNC45 Knockdown ». *BMC Molecular and Cell Biology* 22 (1). https://doi.org/10.1186/s12860-021-00373-7.

Kirkwood, Thomas B.L. 2005. « Understanding the Odd Science of Aging ». *Cell* 120 (4): 437-47. https://doi.org/10.1016/j.cell.2005.01.027.

Kolley, Francine, Clara Sidor, Benoit Dehapiot, Frank Schnorrer, et Benjamin M. Friedrich. 2024. « Mechanisms of Sarcomere Assembly in Muscle Cells Inferred from Sequential Ordering of Myofibril Components ». *PRX Life* 2 (1). https://doi.org/10.1103/prxlife.2.013002.

Kotsaris, Georgios, Taimoor H. Qazi, Christian H. Bucher, et al. 2023. « Odd Skipped-Related 1 Controls the pro-Regenerative Response of Fibro-Adipogenic Progenitors ». *Npj Regenerative Medicine* 8 (1). https://doi.org/10.1038/s41536-023-00291-6.

Landgraf, Matthias, Torsten Bossing, Gerd M. Technau, et Michael Bate. 1997. « The Origin, Location, and Projections of the Embryonic Abdominal Motorneurons of*Drosophila* ». *The Journal of Neuroscience* 17 (24): 9642-55. https://doi.org/10.1523/jneurosci.17-24-09642.1997.

Lanot, René, Daniel Zachary, François Holder, et Marie Meister. 2001. « Postembryonic Hematopoiesis in Drosophila ». *Developmental Biology* 230 (2): 243-57. https://doi.org/10.1006/dbio.2000.0123.

Latroche, Claire, Cyril Gitiaux, Fabrice Chrétien, Isabelle Desguerre, Rémi Mounier, et Bénédicte Chazaud. 2015. « Skeletal Muscle Microvasculature: A Highly Dynamic Lifeline ». *Physiology* 30 (6): 417-27. https://doi.org/10.1152/physiol.00026.2015.

Latroche, Claire, Michèle Weiss-Gayet, Laurent Muller, et al. 2017. « Coupling between Myogenesis and Angiogenesis during Skeletal Muscle Regeneration Is Stimulated by Restorative Macrophages ». *Stem Cell Reports* 9 (6): 2018-33. https://doi.org/10.1016/j.stemcr.2017.10.027.

Laurichesse, Quentin, et Cedric Soler. 2020. « Muscle Development : A View from Adult Myogenesis in Drosophila ». *Seminars in Cell & Developmental Biology* 104 (août): 39-50. https://doi.org/10.1016/j.semcdb.2020.02.009.

Lavergne, G., M. Zmojdzian, J. P. Da Ponte, G. Junion, et K. Jagla. 2020. « *Drosophila* Adult Muscle Precursor Cells Contribute to Motor Axon Pathfinding and Proper Innervation of Embryonic Muscles ». *Development*, publication en ligne anticipée, janvier 1. https://doi.org/10.1242/dev.183004.

Lee, Jun Hee, Andrei V. Budanov, Eek Joong Park, et al. 2010. « Sestrin as a Feedback Inhibitor of TOR That Prevents Age-Related Pathologies ». *Science* 327 (5970): 1223-28. https://doi.org/10.1126/science.1182228.

Leitão, Alexandre B, et Élio Sucena. 2015. « Drosophila Sessile Hemocyte Clusters Are True Hematopoietic Tissues That Regulate Larval Blood Cell Differentiation ». *eLife* 4 (février): e06166. https://doi.org/10.7554/eLife.06166.

Lemaitre, Bruno, et Jules Hoffmann. 2007. « The Host Defense of *Drosophila Melanogaster* ». *Annual Review of Immunology* 25 (1): 697-743. https://doi.org/10.1146/annurev.immunol.25.022106.141615.

Lemaitre, Bruno, Emmanuelle Nicolas, Lydia Michaut, Jean-Marc Reichhart, et Jules A Hoffmann. 1996a. « The Dorsoventral Regulatory Gene Cassette Spätzle/Toll/Cactus Controls the Potent Antifungal Response in Drosophila Adults ». *Cell* 86 (6): 973-83. https://doi.org/10.1016/S0092-8674(00)80172-5.

Lemaitre, Bruno, Emmanuelle Nicolas, Lydia Michaut, Jean-Marc Reichhart, et Jules A Hoffmann. 1996b. « The Dorsoventral Regulatory Gene Cassette Spätzle/Toll/Cactus Controls the Potent Antifungal Response in Drosophila Adults ». *Cell* 86 (6): 973-83. https://doi.org/10.1016/S0092-8674(00)80172-5.

Lemke, Sandra B., et Frank Schnorrer. 2017. « Mechanical Forces during Muscle Development ». *Mechanisms of Development* 144 (avril): 92-101. https://doi.org/10.1016/j.mod.2016.11.003.

Li, Bin, et James H.-C. Wang. 2011. « Fibroblasts and Myofibroblasts in Wound Healing: Force Generation and Measurement ». *Journal of Tissue Viability* 20 (4): 108-20. https://doi.org/10.1016/j.jtv.2009.11.004.

Li, Xiaoyan, Xiaomin Wang, Zhen Shang, Shan Yang, Yan Tang, et Wenhua Xu. 2025. « Non-Immune Functions of Innate Immunity Acting on Physiological Processes: Insights from Drosophila ». *International Journal of Molecular Sciences* 26 (3): 1087. https://doi.org/10.3390/ijms26031087.

Linneweber, Gerit A., Jake Jacobson, Karl Emanuel Busch, et al. 2014. « Neuronal Control of Metabolism through Nutrient-Dependent Modulation of Tracheal Branching ». *Cell* 156 (1-2): 69-83. https://doi.org/10.1016/j.cell.2013.12.008.

Liotta, David, Jun Han, Stuart Elgar, Clare Garvey, Zhe Han, et Michael V. Taylor. 2007. « The Him Gene Reveals a Balance of Inputs Controlling Muscle Differentiation in Drosophila ». *Current Biology* 17 (16): 1409-13. https://doi.org/10.1016/j.cub.2007.07.039.

Liu, Ze (Cindy), et Erika R. Geisbrecht. 2011. « Moleskin Is Essential for the Formation of the Myotendinous Junction in Drosophila ». *Developmental Biology* 359 (2): 176-89. https://doi.org/10.1016/j.ydbio.2011.08.028.

Llimargas, Marta. 1999. « The *Notch* Pathway Helps to Pattern the Tips of the *Drosophila* Tracheal Branches by Selecting Cell Fates ». *Development* 126 (11): 2355-64. https://doi.org/10.1242/dev.126.11.2355.

Llimargas, Marta. 2000. « Wingless and Its Signalling Pathway Have Common and Separable Functions during Tracheal Development ». *Development* 127 (20): 4407-17. https://doi.org/10.1242/dev.127.20.4407.

Lo, Arthur, Andrew J. Fuglevand, et Timothy W. Secomb. 2003. « Oxygen Delivery to Skeletal Muscle Fibers: Effects of Microvascular Unit Structure and Control Mechanisms ». *American Journal of Physiology-Heart and Circulatory Physiology* 285 (3): H955-63. https://doi.org/10.1152/ajpheart.00278.2003.

Loomis, Taryn, et Lucas R. Smith. 2023. « Thrown for a Loop: Fibro-Adipogenic Progenitors in Skeletal Muscle Fibrosis ». *American Journal of Physiology-Cell Physiology* 325 (4): C895-906. https://doi.org/10.1152/ajpcell.00245.2023.

Loreau, Vincent, Wouter H. Koolhaas, Eunice HoYee Chan, et al. 2025. « Titin-Dependent Biomechanical Feedback Tailors Sarcomeres to Specialized Muscle Functions in Insects ». *Science Advances* 11 (19). https://doi.org/10.1126/sciadv.ads8716.

Loreau, Vincent, Renate Rees, Eunice HoYee Chan, et al. 2023. « A Nanobody Toolbox to Investigate Localisation and Dynamics of Drosophila Titins and Other Key Sarcomeric Proteins ». *eLife* 12 (janvier). https://doi.org/10.7554/elife.79343.

Luschnig, Stefan, Tilmann Bätz, Kristina Armbruster, et Mark A. Krasnow. 2006. « Serpentine and Vermiform Encode Matrix Proteins with Chitin Binding and Deacetylation Domains That Limit Tracheal Tube Length in Drosophila ». *Current Biology* 16 (2): 186-94. https://doi.org/10.1016/j.cub.2005.11.072.

Ma, Ming, Wei Jiang, et Rongbin Zhou. 2024. « DAMPs and DAMP-Sensing Receptors in Inflammation and Diseases ». *Immunity* 57 (4): 752-71. https://doi.org/10.1016/j.immuni.2024.03.002.

Maartens, Aidan P., et Nicholas H. Brown. 2015. « Anchors and Signals ». In *Current Topics in Developmental Biology*, vol. 112. Elsevier. https://doi.org/10.1016/bs.ctdb.2014.11.020.

Mackenzie, Danielle K., Luc F. Bussière, et Matthew C. Tinsley. 2011. « Senescence of the Cellular Immune Response in Drosophila Melanogaster ». *Experimental Gerontology* 46 (11): 853-59. https://doi.org/10.1016/j.exger.2011.07.004.

Manaka, Junko, Takayuki Kuraishi, Akiko Shiratsuchi, et al. 2004. « Draper-Mediated and Phosphatidylserine-Independent Phagocytosis of Apoptotic Cells by Drosophila Hemocytes/Macrophages ». *Journal of Biological Chemistry* 279 (46): 48466-76. https://doi.org/10.1074/jbc.m408597200.

Marcetteau, Julien, Patrícia Duarte, Alexandre B Leitão, et Élio Sucena. 2025. « Transdifferentiation of Plasmatocytes to Crystal Cells in the Lymph Gland of Drosophila Melanogaster ». *EMBO Reports* 26 (8): 2077-97. https://doi.org/10.1038/s44319-025-00366-z.

Martinek, Nathalie, Jaffer Shahab, Manuela Saathoff, et Maurice Ringuette. 2008. « Haemocyte-Derived SPARC Is Required for Collagen-IV-Dependent Stability of Basal Laminae in *Drosophila* Embryos ». *Journal of Cell Science* 121 (10): 1671-80. https://doi.org/10.1242/jcs.021931.

Mauro, Alexander. 1961. « SATELLITE CELL OF SKELETAL MUSCLE FIBERS ». *The Journal of Cell Biology* 9 (2): 493-95. https://doi.org/10.1083/jcb.9.2.493.

McLennan, I. S. 1996. « Degenerating and Regenerating Skeletal Muscles Contain Several Subpopulations of Macrophages with Distinct Spatial and Temporal Distributions ». *Journal of Anatomy* 188 (Pt 1) (Pt 1): 17-28.

Melcarne, C., B. Lemaitre, et E. Kurant. 2019. « Phagocytosis in Drosophila: From Molecules and Cellular Machinery to Physiology ». *Insect Biochemistry and Molecular Biology* 109 (juin): 1-12. https://doi.org/10.1016/j.ibmb.2019.04.002.

Miller, Mark S., Panagiotis Lekkas, Joan M. Braddock, et al. 2008. « Aging Enhances Indirect Flight Muscle Fiber Performance yet Decreases Flight Ability in Drosophila ». *Biophysical Journal* 95 (5): 2391-401. https://doi.org/10.1529/biophysj.108.130005.

Mitchell-Gee, Robert, Robert Hoff, Kumar Vishal, et al. 2024. « The *Drosophila* Myogenic Inhibitor *Him* Gene Is Essential for Adult Muscle Function and Muscle Stem Cell Maintenance ». Prépublication, septembre 7. https://doi.org/10.1101/2024.09.06.611611.

Mofarrahi, Mahroo, Joseph M. McClung, Christopher D. Kontos, et al. 2015. « Angiopoietin-1 Enhances Skeletal Muscle Regeneration in Mice ». *American Journal of Physiology-Regulatory, Integrative and Comparative Physiology* 308 (7): R576-89. https://doi.org/10.1152/ajpregu.00267.2014.

Motohashi, Norio, et Atsushi Asakura. 2014. « Muscle satellite cell heterogeneity and self-renewal ». *Frontiers in Cell and Developmental Biology* 2. https://doi.org/10.3389/fcell.2014.00001.

Muñoz-Cánoves, Pura, Camilla Scheele, Bente K. Pedersen, et Antonio L. Serrano. 2013. « Interleukin-6 Myokine Signaling in Skeletal Muscle: A Double-edged Sword? » *The FEBS Journal* 280 (17): 4131-48. https://doi.org/10.1111/febs.12338.

Murakami, Masahiro, et Michael Simons. 2008. « Fibroblast Growth Factor Regulation of Neovascularization »: *Current Opinion in Hematology* 15 (3): 215-20. https://doi.org/10.1097/MOH.0b013e3282f97d98.

Murphy, Malea M., Jennifer A. Lawson, Sam J. Mathew, David A. Hutcheson, et Gabrielle Kardon. 2011a. « Satellite Cells, Connective Tissue Fibroblasts and Their Interactions Are Crucial for Muscle Regeneration ». *Development* 138 (17): 3625-37. https://doi.org/10.1242/dev.064162.

Murphy, Malea M., Jennifer A. Lawson, Sam J. Mathew, David A. Hutcheson, et Gabrielle Kardon. 2011b. « Satellite Cells, Connective Tissue Fibroblasts and Their Interactions Are Crucial for Muscle Regeneration ». *Development* 138 (17): 3625-37. https://doi.org/10.1242/dev.064162.

Musarò, Antonio. 2020. « Muscle Homeostasis and Regeneration: From Molecular Mechanisms to Therapeutic Opportunities ». *Cells* 9 (9): 2033. https://doi.org/10.3390/cells9092033.

Myat, Monn Monn, Harrell Lightfoot, Ping Wang, et Deborah J. Andrew. 2005. « A Molecular Link between FGF and Dpp Signaling in Branch-Specific Migration of the Drosophila Trachea ». *Developmental Biology* 281 (1): 38-52. https://doi.org/10.1016/j.ydbio.2005.02.005.

Nam, Hyuck-Jin, In-Hwan Jang, Tsunaki Asano, et Won-Jae Lee. 2008. « Involvement of Pro-Phenoloxidase 3 in Lamellocyte-Mediated Spontaneous Melanization in Drosophila ». *Molecules and Cells* 26 (6): 606-10.

Nawaz, Allah, Muhammad Bilal, Shiho Fujisaka, et al. 2022a. « Depletion of CD206+ M2-like Macrophages Induces Fibro-Adipogenic Progenitors Activation and Muscle Regeneration ». *Nature Communications* 13 (1). https://doi.org/10.1038/s41467-022-34191-y.

Nawaz, Allah, Muhammad Bilal, Shiho Fujisaka, et al. 2022b. « Depletion of CD206+ M2-like Macrophages Induces Fibro-Adipogenic Progenitors Activation and Muscle Regeneration ». *Nature Communications* 13 (1). https://doi.org/10.1038/s41467-022-34191-y.

Nelson, Kevin S, Mikio Furuse, et Greg J Beitel. 2010. « The Drosophila Claudin Kune-Kune Is Required for Septate Junction Organization and Tracheal Tube Size Control ». *Genetics* 185 (3): 831-39. https://doi.org/10.1534/genetics.110.114959.

Nelson, R.E., L.I. Fessler, Y. Takagi, et al. 1994. « Peroxidasin: A Novel Enzyme-Matrix Protein of Drosophila Development. » *The EMBO Journal* 13 (15): 3438-47. https://doi.org/10.1002/j.1460-2075.1994.tb06649.x.

Nongthomba, Upendra, Sam Clark, Mark Cummins, Maqsood Ansari, Meg Stark, et John C. Sparrow. 2004. « Troponin I Is Required for Myofibrillogenesis and Sarcomere Formation in*Drosophila*Flight Muscle ». *Journal of Cell Science* 117 (9): 1795-805. https://doi.org/10.1242/jcs.01024.

Ochoa, Oscar, Dongxu Sun, Sara M. Reyes-Reyna, et al. 2007. « Delayed Angiogenesis and VEGF Production in CCR2−/− Mice during Impaired Skeletal Muscle Regeneration ». *American Journal of Physiology-Regulatory, Integrative and Comparative Physiology* 293 (2): R651-61. https://doi.org/10.1152/ajpregu.00069.2007.

Ohshiro, Tomokazu, et Kaoru Saigo. 1997. « Transcriptional Regulation of *Breathless* FGF Receptor Gene by Binding of TRACHEALESS/dARNT Heterodimers to Three Central Midline Elements in *Drosophila* Developing Trachea ». *Development* 124 (20): 3975-86. https://doi.org/10.1242/dev.124.20.3975.

Ordan, Elly, et Talila Volk. 2015. « A Non-Signaling Role of Robo2 in Tendons Is Essential for Slit Processing and Muscle Patterning ». *Development*, publication en ligne anticipée, janvier 1. https://doi.org/10.1242/dev.128157.

Öztürk-Çolak, Arzu, Camille Stephan-Otto Attolini, Jordi Casanova, et Sofia J Araújo. 2018. « Blimp-1 Mediates Tracheal Lumen Maturation in *Drosophila Melanogaster* ». *Genetics* 210 (2): 653-63. https://doi.org/10.1534/genetics.118.301444.

Parvy, Jean-Philippe, Yachuan Yu, Anna Dostalova, et al. 2019. « The Antimicrobial Peptide Defensin Cooperates with Tumour Necrosis Factor to Drive Tumour Cell Death in Drosophila ». *eLife* 8 (juillet): e45061. https://doi.org/10.7554/eLife.45061.

Pastor-Pareja, José Carlos, Ming Wu, et Tian Xu. 2008. « An Innate Immune Response of Blood Cells to Tumors and Tissue Damage in Drosophila ». *Disease Models & Mechanisms* 1 (2-3): 144-54. https://doi.org/10.1242/dmm.000950.

Perochon, Jessica, Yachuan Yu, Gabriel N. Aughey, André B. Medina, Tony D. Southall, et Julia B. Cordero. 2021. « Dynamic Adult Tracheal Plasticity Drives Stem Cell Adaptation to Changes in Intestinal Homeostasis in Drosophila ». *Nature Cell Biology* 23 (5): 485-96. https://doi.org/10.1038/s41556-021-00676-z.

Peterson, Soren J., et Mark A. Krasnow. 2015. « Subcellular Trafficking of FGF Controls Tracheal Invasion of Drosophila Flight Muscle ». *Cell* 160 (1-2): 313-23. https://doi.org/10.1016/j.cell.2014.11.043.

Petrignani, Bianca, Samuel Rommelaere, Ketty Hakim-Mishnaevski, et al. 2021. « A Secreted Factor NimrodB4 Promotes the Elimination of Apoptotic Corpses by Phagocytes in *Drosophila* ». *EMBO Reports* 22 (9): e52262. https://doi.org/10.15252/embr.202052262.

Pitsouli, Chrysoula, et Norbert Perrimon. 2010. « Embryonic Multipotent Progenitors Remodel the*Drosophila*Airways during Metamorphosis ». *Development* 137 (21): 3615-24. https://doi.org/10.1242/dev.056408.

Poovathumkadavil, Preethi, et Krzysztof Jagla. 2020. « Genetic Control of Muscle Diversification and Homeostasis: Insights from Drosophila ». *Cells* 9 (6): 1543. https://doi.org/10.3390/cells9061543.

Pospisil, Dean A., Max J. Aragon, Sven Dorkenwald, et al. 2024. « The Fly Connectome Reveals a Path to the Effectome ». *Nature* 634 (8032): 201-9. https://doi.org/10.1038/s41586-024-07982-0.

Rahat, Michal A., Bernhard Hemmerlein, et Vijaya Iragavarapu-Charyulu. 2014. « The regulation of angiogenesis by tissue cell-macrophage interactions ». *Frontiers in Physiology* 5 (juillet). https://doi.org/10.3389/fphys.2014.00262.

Reedy, Mary C., Belinda Bullard, et Jim O. Vigoreaux. 2000. « Flightin Is Essential for Thick Filament Assembly and Sarcomere Stability in *Drosophila* Flight Muscles ». *The Journal of Cell Biology* 151 (7): 1483-500. https://doi.org/10.1083/jcb.151.7.1483.

Riera Romo, Mario, Dayana Pérez-Martínez, et Camila Castillo Ferrer. 2016. « Innate Immunity in Vertebrates: An Overview ». *Immunology* 148 (2): 125-39. https://doi.org/10.1111/imm.12597.

Rigamonti, Elena, Paola Zordan, Clara Sciorati, Patrizia Rovere-Querini, et Silvia Brunelli. 2014. « Macrophage Plasticity in Skeletal Muscle Repair ». *BioMed Research International* 2014: 560629. https://doi.org/10.1155/2014/560629.

Ritzenthaler, Sarah, et Akira Chiba. 2001. « Multiple Personalities: Synaptic Target Cells as Introverts and Extroverts ». *Development, Growth & Differentiation* 43 (5): 503-8. https://doi.org/10.1046/j.1440-169x.2001.00603.x.

Roberts, Edward W., Andrew Deonarine, James O. Jones, et al. 2013. « Depletion of Stromal Cells Expressing Fibroblast Activation Protein-α from Skeletal Muscle and Bone Marrow Results in Cachexia and Anemia ». *Journal of Experimental Medicine* 210 (6): 1137-51. https://doi.org/10.1084/jem.20122344.

Rodier, Clement, Ian D. Estabrook, Eunice HoYee Chan, et al. 2025a. « Muscle Growth by Sarcomere Divisions ». *Science Advances* 11 (28). https://doi.org/10.1126/sciadv.adw9445.

Rodier, Clement, Ian D. Estabrook, Eunice HoYee Chan, et al. 2025b. « Muscle Growth by Sarcomere Divisions ». *Science Advances* 11 (28). https://doi.org/10.1126/sciadv.adw9445.

Rodríguez, Cristina, Filipa Timóteo-Ferreira, Gabriella Minchiotti, Silvia Brunelli, et Ombretta Guardiola. 2024. « Cellular interactions and microenvironment dynamics in skeletal muscle regeneration and disease ». *Frontiers in Cell and Developmental Biology* 12 (mai). https://doi.org/10.3389/fcell.2024.1385399.

Rowe, Glenn C., Srilatha Raghuram, Cholsoon Jang, et al. 2014. « PGC-1α Induces SPP1 to Activate Macrophages and Orchestrate Functional Angiogenesis in Skeletal Muscle ». *Circulation Research* 115 (5): 504-17. https://doi.org/10.1161/circresaha.115.303829.

Saclier, Marielle, Sylvain Cuvellier, Mélanie Magnan, Rémi Mounier, et Bénédicte Chazaud. 2013. « Monocyte/Macrophage Interactions with Myogenic Precursor Cells during Skeletal Muscle Regeneration ». *The FEBS Journal* 280 (17): 4118-30. https://doi.org/10.1111/febs.12166.

Samakovlis, Christos, Nir Hacohen, Gerard Manning, David C. Sutherland, Karen Guillemin, et Mark A. Krasnow. 1996. « Development of the *Drosophila* Tracheal System Occurs by a Series of Morphologically Distinct but Genetically Coupled Branching Events ». *Development* 122 (5): 1395-407. https://doi.org/10.1242/dev.122.5.1395.

Sanchez Bosch, Pablo, Kalpana Makhijani, Leire Herboso, et al. 2019. « Adult Drosophila Lack Hematopoiesis but Rely on a Blood Cell Reservoir at the Respiratory Epithelia to Relay Infection Signals to Surrounding Tissues ». *Developmental Cell* 51 (6): 787-803.e5. https://doi.org/10.1016/j.devcel.2019.10.017.

Sandstrom, David J., Cynthia A. Bayer, James W. Fristrom, et Linda L. Restifo. 1997. « Broad-ComplexTranscription Factors Regulate Thoracic Muscle Attachment inDrosophila ». *Developmental Biology* 181 (2): 168-85. https://doi.org/10.1006/dbio.1996.8469.

Sandstrom, David J., et Linda L. Restifo. 1999. « Epidermal Tendon Cells Require Broad Complex Function for Correct Attachment of the Indirect Flight Muscles in Drosophila Melanogaster ». *Journal of Cell Science* 112 (22): 4051-65. https://doi.org/10.1242/jcs.112.22.4051.

Sartore, S., L. Gorza, et S. Schiaffino. 1982. « Fetal Myosin Heavy Chains in Regenerating Muscle ». *Nature* 298 (5871): 294-96. https://doi.org/10.1038/298294a0.

Sato, Makoto, et Thomas B. Kornberg. 2002. « FGF Is an Essential Mitogen and Chemoattractant for the Air Sacs of the Drosophila Tracheal System ». *Developmental Cell* 3 (2): 195-207. https://doi.org/10.1016/s1534-5807(02)00202-2.

Sauerwald, Julia, Wilko Backer, Till Matzat, Frank Schnorrer, et Stefan Luschnig. 2019. « Matrix Metalloproteinase 1 Modulates Invasive Behavior of Tracheal Branches during Entry into Drosophila Flight Muscles ». *eLife* 8 (octobre). https://doi.org/10.7554/elife.48857.

Schönbauer, Cornelia, Jutta Distler, Nina Jährling, et al. 2011. « Spalt Mediates an Evolutionarily Conserved Switch to Fibrillar Muscle Fate in Insects ». *Nature* 479 (7373): 406-9. https://doi.org/10.1038/nature10559.

Schulman, Victoria K., Krista C. Dobi, et Mary K. Baylies. 2015. « Morphogenesis of the Somatic Musculature in *Drosophila Melanogaster* ». *WIREs Developmental Biology* 4 (4): 313-34. https://doi.org/10.1002/wdev.180.

Schütze, Laura, Maria Jelena Musillo, Bilyana Popova, et al. 2025. « Gradient of Wnt Signaling Facilitates Mef2 Heterogeneity and Limits Commitment of the Developmental Muscle Progenitor Pool ». Prépublication, juillet 18. https://doi.org/10.1101/2025.07.17.665417.

Schwarze, Steven R., Richard Weindruch, et Judd M. Aiken. 1998. « Oxidative Stress and Aging Reduce COX I RNA and Cytochrome Oxidase Activity in Drosophila ». *Free Radical Biology and Medicine* 25 (6): 740-47. https://doi.org/10.1016/s0891-5849(98)00153-1.

Segal, Dagan. 2017. « Live Imaging of Myogenesis in Indirect Flight Muscles in Drosophila ». *BIO-PROTOCOL* 7 (13). https://doi.org/10.21769/BioProtoc.2377.

Segal, Dagan, Nagaraju Dhanyasi, Eyal D. Schejter, et Ben-Zion Shilo. 2016. « Adhesion and Fusion of Muscle Cells Are Promoted by Filopodia ». *Developmental Cell* 38 (3): 291-304. https://doi.org/10.1016/j.devcel.2016.07.010.

Shahab, Jaffer, Cristina Baratta, Bianca Scuric, Dorothea Godt, Koen J.T. Venken, et Maurice J. Ringuette. 2015. « Loss of SPARC Dysregulates Basal Lamina Assembly to Disrupt Larval Fat Body Homeostasis in *Drosophila Melanogaster* ». *Developmental Dynamics* 244 (4): 540-52. https://doi.org/10.1002/dvdy.24243.

Shin, Mingyu, Nuri Cha, Ferdinand Koranteng, Bumsik Cho, et Jiwon Shim. 2020. « Subpopulation of Macrophage-Like Plasmatocytes Attenuates Systemic Growth via JAK/STAT in the Drosophila Fat Body ». *Frontiers in Immunology* 11 (janvier): 63. https://doi.org/10.3389/fimmu.2020.00063.

Shin, Mingyu, Eunji Chang, Daewon Lee, et al. 2024. « Drosophila Immune Cells Transport Oxygen through PPO2 Protein Phase Transition ». *Nature* 631 (8020): 350-59. https://doi.org/10.1038/s41586-024-07583-x.

Sicherer, Sydnee T., Rashmi S. Venkatarama, et Jonathan M. Grasman. 2020. « Recent Trends in Injury Models to Study Skeletal Muscle Regeneration and Repair ». *Bioengineering* 7 (3): 76. https://doi.org/10.3390/bioengineering7030076.

Siles, Laura, Chiara Ninfali, Marlies Cortés, Douglas S. Darling, et Antonio Postigo. 2019a. « ZEB1 Protects Skeletal Muscle from Damage and Is Required for Its Regeneration ». *Nature Communications* 10 (1): 1364. https://doi.org/10.1038/s41467-019-08983-8.

Siles, Laura, Chiara Ninfali, Marlies Cortés, Douglas S. Darling, et Antonio Postigo. 2019b. « ZEB1 Protects Skeletal Muscle from Damage and Is Required for Its Regeneration ». *Nature Communications* 10 (1): 1364. https://doi.org/10.1038/s41467-019-08983-8.

Smith, David S. 1961. « THE STRUCTURE OF INSECT FIBRILLAR FLIGHT MUSCLE ». *The Journal of Cell Biology* 10 (4): 123-58. https://doi.org/10.1083/jcb.10.4.123.

Sohr, Alex, Lijuan Du, Ruofan Wang, Li Lin, et Sougata Roy. 2019. « *Drosophila* FGF Cleavage Is Required for Efficient Intracellular Sorting and Intercellular Dispersal ». *Journal of Cell Biology* 218 (5): 1653-69. https://doi.org/10.1083/jcb.201810138.

Soler, Cédric, Malgorzata Daczewska, Jean Philippe Da Ponte, Bernard Dastugue, et Krzysztof Jagla. 2004. « Coordinated Development of Muscles and Tendons of the *Drosophila* Leg ». *Development* 131 (24): 6041-51. https://doi.org/10.1242/dev.01527.

Soler, Cédric, et Michael V. Taylor. 2009. « The Him Gene Inhibits the Development of Drosophila Flight Muscles during Metamorphosis ». *Mechanisms of Development* 126 (7): 595-603. https://doi.org/10.1016/j.mod.2009.03.003.

Spletter, Maria L, Christiane Barz, Assa Yeroslaviz, et al. 2018. « A Transcriptomics Resource Reveals a Transcriptional Transition during Ordered Sarcomere Morphogenesis in Flight Muscle ». *eLife* 7 (mai): e34058. https://doi.org/10.7554/eLife.34058.

Steneberg, Pär, Johanna Hemphälä, et Christos Samakovlis. 1999. « Dpp and Notch Specify the Fusion Cell Fate in the Dorsal Branches of the Drosophila Trachea ». *Mechanisms of Development* 87 (1-2): 153-63. https://doi.org/10.1016/S0925-4773(99)00157-4.

Subasi, Bengisu S., Veit Grabe, Martin Kaltenpoth, Jens Rolff, et Sophie A. O. Armitage. 2024. « How Frequently Are Insects Wounded in the Wild? A Case Study Using *Drosophila Melanogaster* ». *Royal Society Open Science* 11 (6). https://doi.org/10.1098/rsos.240256.

Subramanian, Arul, Bess Wayburn, Thomas Bunch, et Talila Volk. 2007. « Thrombospondin-Mediated Adhesion Is Essential for the Formation of the Myotendinous Junction in*Drosophila* ». *Development* 134 (7): 1269-78. https://doi.org/10.1242/dev.000406.

Sudarsan, Vikram, Sumita Anant, Preeta Guptan, K. VijayRaghavan, et Helen Skaer. 2001. « Myoblast Diversification and Ectodermal Signaling in Drosophila ». *Developmental Cell* 1 (6): 829-39. https://doi.org/10.1016/s1534-5807(01)00089-2.

Sutherland, David, Christos Samakovlis, et Mark A Krasnow. 1996. « Branchless Encodes a Drosophila FGF Homolog That Controls Tracheal Cell Migration and the Pattern of Branching ». *Cell* 87 (6): 1091-101. https://doi.org/10.1016/S0092-8674(00)81803-6.

Suzuki, Nanoka, et Haruki Ochi. 2020. « Regeneration Enhancers: A Clue to Reactivation of Developmental Genes ». *Development, Growth & Differentiation* 62 (5): 343-54. https://doi.org/10.1111/dgd.12654.

Takahashi, A., D. E. Philpott, et J. Miquel. 1970. « Electron Microscope Studies on Aging Drosophila Melanogaster III. Flight Muscle ». *Journal of Gerontology* 25 (3): 222-28. https://doi.org/10.1093/geronj/25.3.222.

Tamamouna, Vasilia, M. Mahidur Rahman, Monika Petersson, et al. 2021. « Remodelling of Oxygen-Transporting Tracheoles Drives Intestinal Regeneration and Tumorigenesis in Drosophila ». *Nature Cell Biology* 23 (5): 497-510. https://doi.org/10.1038/s41556-021-00674-1.

Tidball, James G. 2011. « Mechanisms of Muscle Injury, Repair, and Regeneration ». *Comprehensive Physiology* 1 (4): 2029-62. https://doi.org/10.1002/j.2040-4603.2011.tb00387.x.

Tidball, James G., et Michelle Wehling-Henricks. 2007. « Macrophages Promote Muscle Membrane Repair and Muscle Fibre Growth and Regeneration during Modified Muscle Loading in Mice *in Vivo* ». *The Journal of Physiology* 578 (1): 327-36. https://doi.org/10.1113/jphysiol.2006.118265.

Tonning, Anna, Johanna Hemphälä, Erika Tång, Ulf Nannmark, Christos Samakovlis, et Anne Uv. 2005. « A Transient Luminal Chitinous Matrix Is Required to Model Epithelial Tube Diameter in the Drosophila Trachea ». *Developmental Cell* 9 (3): 423-30. https://doi.org/10.1016/j.devcel.2005.07.012.

Toumi, Hechmi, Sleem F'guyer, et Thomas M. Best. 2006. « The Role of Neutrophils in Injury and Repair Following Muscle Stretch ». *Journal of Anatomy* 208 (4): 459-70. https://doi.org/10.1111/j.1469-7580.2006.00543.x.

Tzou, Phoebe, Serge Ohresser, Dominique Ferrandon, et al. 2000. « Tissue-Specific Inducible Expression of Antimicrobial Peptide Genes in Drosophila Surface Epithelia ». *Immunity* 13 (5): 737-48. https://doi.org/10.1016/S1074-7613(00)00072-8.

Uezumi, Akiyoshi, So-ichiro Fukada, Naoki Yamamoto, Shin'ichi Takeda, et Kunihiro Tsuchida. 2010. « Mesenchymal Progenitors Distinct from Satellite Cells Contribute to Ectopic Fat Cell Formation in Skeletal Muscle ». *Nature Cell Biology* 12 (2): 143-52. https://doi.org/10.1038/ncb2014.

Van De Bor, Véronique, Geordie Zimniak, Lise Papone, et al. 2015. « Companion Blood Cells Control Ovarian Stem Cell Niche Microenvironment and Homeostasis ». *Cell Reports* 13 (3): 546-60. https://doi.org/10.1016/j.celrep.2015.09.008.

Varga, Virginia, Janka Szinyákovics, Anikó Bebes, Fanni Szikszai, et Tibor Kovács. 2025. « Role of Hemocytes in the Aging of Drosophila Male Germline ». *Cells* 14 (4): 315. https://doi.org/10.3390/cells14040315.

Varland, Sylvia, Rui Duarte Silva, Ine Kjosås, et al. 2023. « N-Terminal Acetylation Shields Proteins from Degradation and Promotes Age-Dependent Motility and Longevity ». *Nature Communications* 14 (1). https://doi.org/10.1038/s41467-023-42342-y.

Vincent, Stéphane, Esther Ruberte, Nicole C. Grieder, et al. 1997. « DPP Controls Tracheal Cell Migration along the Dorsoventral Body Axis of the *Drosophila* Embryo ». *Development* 124 (14): 2741-50. https://doi.org/10.1242/dev.124.14.2741.

Vishal, Kumar, David S Brooks, Simranjot Bawa, Samantha Gameros, Marta Stetsiv, et Erika R Geisbrecht. 2017. « Adult Muscle Formation Requires *Drosophila* Moleskin for Proliferation of Wing Disc-Associated Muscle Precursors ». *Genetics* 206 (1): 199-213. https://doi.org/10.1534/genetics.116.193813.

Volk, T. 1999. « Singling out Drosophila tendon cells: a dialogue between two distinct cell types ». *Trends in Genetics* 15 (11): 448-53. https://doi.org/10.1016/s0168-9525(99)01862-4.

Vorbrüggen, Gerd, et Herbert Jäckle. 1997. « Epidermal Muscle Attachment Site-Specific Target Gene Expression and Interference with Myotube Guidance in Response to Ectopic *Stripe* Expression in the Developing *Drosophila* Epidermis ». *Proceedings of the National Academy of Sciences* 94 (16): 8606-11. https://doi.org/10.1073/pnas.94.16.8606.

Wang, J., et I. Conboy. 2010. « Embryonic vs. Adult Myogenesis: Challenging the "Regeneration Recapitulates Development" Paradigm ». *Journal of Molecular Cell Biology* 2 (1): 1-4. https://doi.org/10.1093/jmcb/mjp027.

Wang, Ruyuan, Caini Lan, Kamel Benlagha, et al. 2024. « The Interaction of Innate Immune and Adaptive Immune System ». *MedComm* 5 (10): e714. https://doi.org/10.1002/mco2.714.

Wang, Shenqiu, Satish Arcot Jayaram, Johanna Hemphälä, et al. 2006. « Septate-Junction-Dependent Luminal Deposition of Chitin Deacetylases Restricts Tube Elongation in the Drosophila Trachea ». *Current Biology* 16 (2): 180-85. https://doi.org/10.1016/j.cub.2005.11.074.

Wang, Xingyu, et Lan Zhou. 2022a. « The Many Roles of Macrophages in Skeletal Muscle Injury and Repair ». *Frontiers in Cell and Developmental Biology* 10 (juillet): 952249. https://doi.org/10.3389/fcell.2022.952249.

Wang, Xingyu, et Lan Zhou. 2022b. « The Many Roles of Macrophages in Skeletal Muscle Injury and Repair ». *Frontiers in Cell and Developmental Biology* 10 (juillet): 952249. https://doi.org/10.3389/fcell.2022.952249.

Webster, Micah T., Uri Manor, Jennifer Lippincott-Schwartz, et Chen-Ming Fan. 2016. « Intravital Imaging Reveals Ghost Fibers as Architectural Units Guiding Myogenic Progenitors during Regeneration ». *Cell Stem Cell* 18 (2): 243-52. https://doi.org/10.1016/j.stem.2015.11.005.

Weitkunat, Manuela, Aynur Kaya-Çopur, Stephan W. Grill, et Frank Schnorrer. 2014. « Tension and Force-Resistant Attachment Are Essential for Myofibrillogenesis in Drosophila Flight Muscle ». *Current Biology* 24 (7): 705-16. https://doi.org/10.1016/j.cub.2014.02.032.

Wilk, R, I Weizman, et B Z Shilo. 1996. « Trachealess Encodes a bHLH-PAS Protein That Is an Inducer of Tracheal Cell Fates in Drosophila. » *Genes & Development* 10 (1): 93-102. https://doi.org/10.1101/gad.10.1.93.

Wood, Brent M., Valentina Baena, Hai Huang, Danielle M. Jorgens, Mark Terasaki, et Thomas B. Kornberg. 2021. « Cytonemes with Complex Geometries and Composition Extend into Invaginations of Target Cells ». *Journal of Cell Biology* 220 (5): e202101116. https://doi.org/10.1083/jcb.202101116.

Wosczyna, Michael N., Colin T. Konishi, Edgar E. Perez Carbajal, et al. 2019a. « Mesenchymal Stromal Cells Are Required for Regeneration and Homeostatic Maintenance of Skeletal Muscle ». *Cell Reports* 27 (7): 2029-2035.e5. https://doi.org/10.1016/j.celrep.2019.04.074.

Wosczyna, Michael N., Colin T. Konishi, Edgar E. Perez Carbajal, et al. 2019b. « Mesenchymal Stromal Cells Are Required for Regeneration and Homeostatic Maintenance of Skeletal Muscle ». *Cell Reports* 27 (7): 2029-2035.e5. https://doi.org/10.1016/j.celrep.2019.04.074.

Yang, Hairu, Jesper Kronhamn, Jens-Ola Ekström, Gül Gizem Korkut, et Dan Hultmark. 2015. « JAK / STAT Signaling in *D Rosophila* Muscles Controls the Cellular Immune Response against Parasitoid Infection ». *EMBO Reports* 16 (12): 1664-72. https://doi.org/10.15252/embr.201540277.

Yang, Shuo, Allison Weske, Yingqiu Du, Juliana M. Valera, Kenneth L. Jones, et Aaron N. Johnson. 2020. « FGF Signaling Directs Myotube Guidance by Regulating Rac Activity ». *Development* 147 (3): dev183624. https://doi.org/10.1242/dev.183624.

Younossi-Hartenstein, Amelia, et Volker Hartenstein. 1993. « The Role of the Tracheae and Musculature during Pathfinding of Drosophila Embryonic Sensory Axons ». *Developmental Biology* 158 (2): 430-47. https://doi.org/10.1006/dbio.1993.1201.

Yu, Shichao, Fangzhou Luo, Yongyi Xu, Yan Zhang, et Li Hua Jin. 2022a. « Drosophila Innate Immunity Involves Multiple Signaling Pathways and Coordinated Communication Between Different Tissues ». *Frontiers in Immunology* 13 (juillet): 905370. https://doi.org/10.3389/fimmu.2022.905370.

Yu, Shichao, Fangzhou Luo, Yongyi Xu, Yan Zhang, et Li Hua Jin. 2022b. « Drosophila Innate Immunity Involves Multiple Signaling Pathways and Coordinated Communication Between Different Tissues ». *Frontiers in Immunology* 13 (juillet): 905370. https://doi.org/10.3389/fimmu.2022.905370.

Yun, Ye-Rang, Jong Eun Won, Eunyi Jeon, et al. 2010. « Fibroblast Growth Factors: Biology, Function, and Application for Tissue Regeneration ». *Journal of Tissue Engineering* 1 (1): 218142. https://doi.org/10.4061/2010/218142.

Zappia, Maria Paula, Lucia De Castro, Majd M Ariss, Holly Jefferson, Abul Bmmk Islam, et Maxim V Frolov. 2020. « A Cell Atlas of Adult Muscle Precursors Uncovers Early Events in Fibre-type Divergence in *Drosophila* ». *EMBO Reports* 21 (10). https://doi.org/10.15252/embr.201949555.

Zappia, Maria Paula, Alice Rogers, Abul B.M.M.K. Islam, et Maxim V. Frolov. 2019. « Rbf Activates the Myogenic Transcriptional Program to Promote Skeletal Muscle Differentiation ». *Cell Reports* 26 (3): 702-719.e6. https://doi.org/10.1016/j.celrep.2018.12.080.

Zelzer, Elazar, et Ben-Zion Shilo. 2000. « Interaction between the bHLH-PAS Protein Trachealess and the POU-Domain Protein Drifter, Specifies Tracheal Cell Fates ». *Mechanisms of Development* 91 (1-2): 163-73. https://doi.org/10.1016/S0925-4773(99)00295-6.

Zhang, Min, Kaz Nagaosa, Yuji Nakai, et al. 2020. « Role for Phagocytosis in the Prevention of Neoplastic Transformation in *Drosophila* ». *Genes to Cells* 25 (10): 675-84. https://doi.org/10.1111/gtc.12804.

Zhao, Yifan, Cyrille Alexandre, Gavin Kelly, Gantas Perez-Mockus, et Jean-Paul Vincent. 2024. « Growth-Induced Physiological Hypoxia Correlates with Growth Deceleration during Normal Development ». Prépublication, juin 5. https://doi.org/10.1101/2024.06.04.597345.

Zhao, Yu, Yujie Wang, Ayibota Tulehalede, et al. 2025. « Drosophila Melanogaster: A Model Organism in Muscular Dystrophy Studies ». *International Journal of Molecular Sciences* 26 (4): 1459. https://doi.org/10.3390/ijms26041459.

Zindel, Joel, et Paul Kubes. 2020. « DAMPs, PAMPs, and LAMPs in Immunity and Sterile Inflammation ». *Annual Review of Pathology: Mechanisms of Disease* 15 (1): 493-518. https://doi.org/10.1146/annurev-pathmechdis-012419-032847.

COLLEGE SCIENCES DOCTORAL DE LA VIE BRETAGNE ET DE LA SANTE

Université de Rennes

Titre : Communication cellulaire dans le maintien de l'intégrité musculaire chez la *Drosophile*

Mots clés : *Drosophile, Muscle, Régénération, Cellules immunitaires, Matrice extracellulaire, Système respiratoire*

Résumé : Le muscle squelettique assure des fonctions vitales telles que le mouvement, le maintien de la posture et la régulation du métabolisme. Sa forte sollicitation au cours de la vie adulte en fait un tissu particulièrement vulnérable, dont le maintien repose sur une remarquable capacité de régénération. Ce processus dépend d'une synchronisation précise entre plusieurs types cellulaires. Si la fonction de ces différentes cellules a été largement étudiée, les mécanismes de communication qui les coordonnent restent encore à élucider. Au cours de ma thèse, j'ai caractérisé les mécanismes cellulaires et moléculaires qui régissent la réponse précoce des muscles aux dommages, en utilisant les muscles du vol de la drosophile comme modèle. Mes travaux ont révélé que cette réponse repose sur une communication intercellulaire active. Plus particulièrement, j'ai montré que les plasmatocytes, équivalents fonctionnels des macrophages, sont recrutées rapidement au niveau des fibres endommagées et jouent un rôle central et polyvalent dans l'adaptation des muscles aux dommages. D'une part, elles déposent sur la fibre lésée le chemoattractant FGF/Bnl, permettant de recruter les branches trachéales (système respiratoire) spécifiquement vers le site de dommage et d'assurer ainsi un apport optimal en oxygène. D'autre part, elles produisent et sécrètent des composants de la matrice extracellulaire, tels que le collagène de type IV et la glycoprotéine SPARC, qui participent à la fois au soutien structurel et à l'organisation du microenvironnement musculaire.

Mes travaux révèlent que la réponse musculaire aux dommages repose sur une coopération étroite entre cellules immunitaires, système respiratoire et fibres musculaires et ouvrent de nouvelles perspectives pour identifier d'autres signaux coordonnant ce processus.

Title: Cellular crosstalk in preserving muscle integrity in *Drosophila*

Keywords : *Drosophila, Muscle, Regeneration, Immune Cells, Extracellular Matrix, Respiratory system*

Abstract: Skeletal muscle is essential for movement, posture, and metabolic regulation. Its heavy use during adulthood makes it particularly vulnerable, and its maintenance relies on a remarkable capacity for regeneration. This process depends on precise coordination between multiple cell types. While the roles of these different cells have been extensively studied, the mechanisms that coordinate them remain largely unknown. I investigated the early cellular and molecular response of Drosophila flight muscles to damage. My work revealed that this response relies on active intercellular communication. Specifically, I showed that plasmatocytes, the functional equivalent of macrophages, are rapidly recruited to damaged fibers and play a central, multifunctional role in muscle adaptation to damage. On one hand, they deposit the chemoattractant factor FGF/Bnl on the injured fibers, which recruits tracheal branches (the respiratory system) specifically to the damage site, ensuring optimal oxygen supply. On the other hand, they produce and secrete extracellular matrix components, such as type IV collagen and the glycoprotein SPARC, which contribute both to structural support and to the organization of the muscle microenvironment.

Overall, my work described the mechanisms underlying the response to the muscle damage. I showed that it depends on close cooperation between immune cells, the respiratory system, and muscle fibers. This work opens new avenues for identifying additional signals that coordinate this process.